Integral Bridge Abutment-to-Approach Slab Connection



Final Report
June 2008

Sponsored by
the Iowa Department of Transportation (Projects 05-197 & 05-219)
and
the Iowa Highway Research Board (Projects TR-530 & TR-539)

ctre
Center for Transportation Research and Education

IOWA STATE UNIVERSITY

Iowa State University's Center for Transportation Research and Education is the umbrella organization for the following centers and programs: Bridge Engineering Center • Center for Weather Impacts on Mobility and Safety • Construction Management & Technology • Iowa Local Technical Assistance Program • Iowa Traffic Safety Data Service • Midwest Transportation Consortium • National Concrete Pavement Technology Center • Partnership for Geotechnical Advancement • Roadway Infrastructure Management and Operations Systems • Statewide Urban Design and Specifications • Traffic Safety and Operations

About the Bridge Engineering Center

The mission of the Bridge Engineering Center is to conduct research on bridge technologies to help bridge designers/owners design, build, and maintain long-lasting bridges.

Disclaimer Notice

The contents of this report reflect the views of the authors, who are responsible for the facts and the accuracy of the information presented herein. The opinions, findings and conclusions expressed in this publication are those of the authors and not necessarily those of the sponsors.

The sponsors assume no liability for the contents or use of the information contained in this document. This report does not constitute a standard, specification, or regulation.

The sponsors do not endorse products or manufacturers. Trademarks or manufacturers' names appear in this report only because they are considered essential to the objective of the document.

Nondiscrimination Statement

Iowa State University does not discriminate on the basis of race, color, age, religion, national origin, sexual orientation, gender identity, sex, marital status, disability, or status as a U.S. veteran. Inquiries can be directed to the Director of Equal Opportunity and Diversity, (515) 294-7612.

Federal and state laws prohibit employment and/or public accommodation discrimination on the basis of age, color, creed, disability, gender identity, national origin, pregnancy, race, religion, sex, sexual orientation or veteran's status. If you believe you have been discriminated against, please contact the Iowa Civil Rights Commission at 800-457-4416 or Iowa Department of Transportation's affirmative action officer. If you need accommodations because of a disability to access the Iowa Department of Transportation's services, contact the agency's affirmative action officer at 800-262-0003.

Technical Report Documentation Page

1. Report No. IHRB Project TR-530 & TR-539 CTRE Project 05-197 & 05-219	**2. Government Accession No.**	**3. Recipient's Catalog No.**	
4. Title and Subtitle Integral Bridge Abutment-to-Approach Slab Connection		**5. Report Date** June 2008	
		6. Performing Organization Code	
7. Author(s) Lowell Greimann, Brent Phares, Adam Faris, and Jake Bigelow		**8. Performing Organization Report No.**	
9. Performing Organization Name and Address Center for Transportation Research and Education Iowa State University 2711 South Loop Drive, Suite 4700 Ames, IA 50010-8664		**10. Work Unit No. (TRAIS)**	
		11. Contract or Grant No.	
12. Sponsoring Organization Name and Address Iowa Department of Transportation 800 Lincoln Way Ames, IA 50010		**13. Type of Report and Period Covered** Final Report	
		14. Sponsoring Agency Code	
15. Supplementary Notes Visit www.ctre.iastate.edu for color PDF files of this and other research reports.			

16. Abstract

The Iowa Department of Transportation has long recognized that approach slab pavements of integral abutment bridges are prone to settlement and cracking, which manifests as the "bump at the end of the bridge". A commonly recommended solution is to integrally attach the approach slab to the bridge abutment. Two different approach slabs, one being precast concrete and the other being cast-in-place concrete, were integrally connected to side-by-side bridges and investigated. The primary objective of this investigation was to evaluate the approach slab performance and the impacts the approach slabs have on the bridge. To satisfy the research needs, the project scope involved a literature review, survey of Midwest Department of Transportation current practices, implementing a health monitoring system on the bridge and approach slab, interpreting the data obtained during the evaluation, and conducting periodic visual inspections. Based on the information obtained from the testing the following general conclusions were made: The integral connection between the approach slabs and the bridges appear to function well with no observed distress at this location and no relative longitudinal movement measured between the two components; Tying the approach slab to the bridge appears to impact the bridge; The two different approach slabs, the longer precast slab and the shorter cast-in-place slab, appear to impact the bridge differently; The measured strains in the approach slabs indicate a force exists at the expansion joint and should be taken into consideration when designing both the approach slab and the bridge; The observed responses generally followed an annual cyclic and/or short term cyclic pattern over time.

17. Key Words Slab pavements—abutment bridges—approach slab		**18. Distribution Statement** No restrictions.	
19. Security Classification (of this report) Unclassified.	**20. Security Classification (of this page)** Unclassified.	**21. No. of Pages** 166	**22. Price** NA

INSTRUMENTATION AND MONITORING OF INTEGRAL BRIDGE ABUTMENT-TO-APPROACH SLAB CONNECTION

Final Report
June 2008

Co-Principal Investigators
Brent Phares
Associate Director
Bridge Engineering Center
Iowa State University

Dean Bierwagen
Methods Engineer
Iowa Department of Transportation

Michael D. LaViolette
Former Bridge Engineer
Iowa State University

Research Assistant
Adam Faris

Authors
Lowell Greimann, Brent Phares, Adam Faris, and Jake Bigelow

Sponsored by the Iowa Highway Research Board
(IHRB Projects TR-530 & TR-539)

Preparation of this report was financed in part
through funds provided by the Iowa Department of Transportation
through its research management agreement with the
Center for Transportation Research and Education.
CTRE Projects 05-197 & 05-218

Center for Transportation Research and Education
Iowa State University
2711 South Loop Drive, Suite 4700
Ames, IA 50010-8664
Phone: 515-294-8103
Fax: 515-294-0467
www.ctre.iastate.edu

TABLE OF CONTENTS

ACKNOWLEDGMENTS XIII

EXECUTIVE SUMMARY XV

INTRODUCTION 1

1.1. Background 1
1.2. Scope and Objectives 1
1.3. Report Content 2

2. LITERATURE REVIEW 3

2.1. Bump Problem 3
2.2. Approach Slabs 6
2.3. Specific Practices 9

3. PROJECT DESCRIPTION 17

3.1. Bridge Description 17
3.2. Approach Slab Description 21
3.2.1. Precast Approach Slab – Northbound Bridge 21
3.2.2. Cast-In-Place Approach Slab – Southbound Bridge 23
3.3. Instrumentation 24
3.3.1. Temperature 28
3.3.2. Abutments 28
3.3.3. Girders 31
3.3.4. Approach Slabs 32
3.3.5. Post-Tensioning Strands 33
3.3.6. Joints 34
3.3.7. Piles 35

4. NORTHBOUND BRIDGE RESULTS 37

4.1. Temperature 37
4.1.1. Approach Slab Temperatures 37
4.1.2. Bridge Superstructure Temperatures 37
4.2. Bridge Superstructure 43
4.2.1. Abutment Displacement 43
4.2.2 Girder Strain Gauges 53
4.3. Approach Slab 64
4.3.1 Embedded Strain Gauges 64
4.3.1. Post-Tensioning Strandmeters 72
4.3.2. Crackmeters 75
4.3.3. Comparison of Expansion Joint Movement and Abutment Movement 77
4.4. Bridge Substructure 80

4.4.1. Pile Gauges 80
4.5. Visual Inspection 90

5. SOUTHBOUND BRIDGE RESULTS 91

5.1. Temperature 91
5.1.1. Approach Slab Temperatures 91
5.1.2. Bridge Superstructure Temperature 93
5.2. Bridge Superstructure 97
5.2.1. Abutment Displacement 97
5.2.2. Girder Strain Gauges 104
5.3. Approach Slab 113
5.3.1. Embedded Strain Gauges 113
5.3.2. Crackmeters 118
5.3.3. Comparison of Expansion Joint Movement and Abutment Movement 120
5.4. Bridge Substructure 123
5.4.1. Pile Gauges 123
5.5. Visual Inspection 126

6. COMPARISONS, CONCLUSIONS, AND RECOMMENDATIONS 128

6.1. Temperatures 128
6.2. Bridge Superstructure 128
6.2.1. Abutment Displacements 128
6.2.2. Girder Forces 130
6.3. Approach Slab 131
6.4. Bridge Substructure 133
6.5. Visual Inspection 133
6.6. General Conclusions 134
6.7. Recommendations for Further Study 135

7. REFERENCES 136

APPENDIX A A-1

A.1. A Simple Model A-2
A.2. Some Numerical Results with Bridge Parameters A-5

LIST OF FIGURES

Figure 2.1. Simplified elevation view of a typical integral abutment bridge 3
Figure 2.2. Problems leading to the formation of the bump (Briaud et al. 1997) 4
Figure 2.3. Temperature induced movement of an integral abutment bridge 5
Figure 2.4. Deck steel extension connection (standard Nevada detail) 7
Figure 2.5. Abutment steel connection (standard Ohio detail) 7
Figure 2.6. Abutment with no connection (standard Iowa detail) 8
Figure 2.7. Typical New York detail 10
Figure 2.8. Typical Illinois detail 11
Figure 2.9. Typical Kansas detail 12
Figure 2.10. Typical Minnesota detail 13
Figure 2.11. Typical Missouri detail 13
Figure 2.12. Typical Nebraska detail 14
Figure 2.13. Typical North Dakota detail 15
Figure 2.14. Typical South Dakota detail 16
Figure 3.1. Plan view of bridges 17
Figure 3.2. Elevation view of bridges 17
Figure 3.3. Typical LXD beam cross section 18
Figure 3.4. Plan view of a typical abutment 19
Figure 3.5. Elevation view of a typical abutment 20
Figure 3.6. Typical pier plan view (top) and elevation view (bottom 20
Figure 3.7. Plan view of precast approach slab (northbound bridge) 21
Figure 3.8. Connection detail for the precast approach slab to abutment 22
Figure 3.9. Precast panel detail along longitudinal edge 22
Figure 3.10. Precast panel detail along transverse edge 23
Figure 3.11. Plan view of cast-in-place approach slab (southbound bridge) 23
Figure 3.12. Elevation view of approach slab with connection detail 24
Figure 3.13. Typical vibrating wire gauge 25
Figure 3.14. Instrumentation layout (a) southbound (b) northbound 26
Figure 3.15. Typical displacement meter installation 30
Figure 3.16. Photograph of a displacement gauge and tiltmeter 30
Figure 3.17. Photograph of a tiltmeter 31
Figure 3.18. Typical girder strain gauge installation positions 32
Figure 3.19. Photograph of installed girder gauge 32
Figure 3.20. Photograph of an installed embedded strain gauge 33
Figure 3.21. Photograph of an installed strandmeter 34
Figure 3.22. A crackmeter installed across the bridge-to-approach slab joint 34
Figure 3.23. Instrumented pile plan 35
Figure 3.24. Pile strain gauge layout 36
Figure 3.25. Photograph of an instrumented pile 36
Figure 4.1. Temperature variation in the northbound bridge precast approach slab 38
Figure 4.2. Average northbound bridge approach slab temperature versus time 38
Figure 4.3. Temperature variation at the top of the northbound bridge girders 39
Figure 4.4. Temperature variation at bottom of the northbound bridge girders 39
Figure 4.5. Average northbound bridge temperature variations with position 40
Figure 4.6. Average northbound bridge temperature over time 41

Figure 4.7. Average northbound bridge and Sheldon, IA air temperatures over time.....41
Figure 4.8. Correlation of daily high and low Sheldon, IA air to northbound bridge temperatures42
Figure 4.9. Drawing showing displacement and rotation of a typical abutment 43
Figure 4.10. Typical recorded northbound bridge displacement transducer temperatures and air temperature versus time 44
Figure 4.11. Typical northbound bridge abutment displacement (Δ_{abut}) over time 45
Figure 4.12. Typical displacement of the northbound bridge abutment due to abutment rotation over time 46
Figure 4.13. Total northbound bridge abutment displacement at slab mid-depth over time at west end.....46
Figure 4.14. Total northbound bridge abutment displacement at slab mid-depth over time at east end.....47
Figure 4.15. Average total northbound bridge abutment displacement at slab mid-depth over time47
Figure 4.16. Theoretical abutment displacement.....48
Figure 4.17. Theoretical and average actual abutment displacement of the northbound bridge over time (combinded Figure 4.15 and Figure 4.16) 49
Figure 4.18. Northbound bridge abutment displacement versus change in bridge temperature ...50
Figure 4.19. Northbound abutment transverse displacement over time 51
Figure 4.20. Illustration of (a) total displacement, (b) longitudinal expansion, and (c) horizontal rotation based on work by Abendroth and Greimann (2005) 52
Figure 4.21. Northbound transverse abutment displacement versus average longitudinal displacement 53
Figure 4.22. Typical northbound bridge girder load strain behavior over time as recorded by gauge GNWT2 55
Figure 4.23. Load strain variation at the top of the northbound bridge girders with respect to position.....56
Figure 4.24. Load strain variation at the bottom of the northbound bridge girders with respect to position.....56
Figure 4.25. Typical composite bridge deck and girder section.....57
Figure 4.26. Average northbound bridge girder moment with respect to position.....58
Figure 4.27. Free body diagram of bridge 59
Figure 4.28. Average northbound bridge mid-span moment over time.....60
Figure 4.29. Average northbound bridge mid-span moment versus average bridge temperature.60
Figure 4.30. Average northbound bridge mid-span moment versus average longitudinal abutment displacement 61
Figure 4.31. Northbound bridge girder moment envelope 61
Figure 4.32. Average northbound bridge axial load versus girder position 62
Figure 4.33. Average northbound bridge girder axial load over time 63
Figure 4.34. Average axial load versus external girder temperature.....63
Figure 4.35. Average axial load versus average longitudinal abutment displacement.....64
Figure 4.36. Representative strain reading obtained from embedded northbound bridge approach slab strain gauge EN4BE 65
Figure 4.37. Northbound bridge embedded strain gauge ENB1E discarded due to large amount of outlier data 65
Figure 4.38. Hot and cold day northbound bridge load strain comparison with respect to location66
Figure 4.39. Average load strain of 15 northbound bridge embedded working gauges.....67
Figure 4.40. Northbound bridge approach slab load strain with respect to temperature.....67

Figure 4.41. Northbound bridge approach slab average force with respect to slab temperature ..68
Figure 4.42. Hot and cold load force comparison with respect to location for the northbound bridge approach slab 69
Figure 4.43. Free body diagram of friction force in slab 70
Figure 4.44. Bottom of slab friction over time – northbound bridge 70
Figure 4.45. Comparison of northbound expansion joint, average, and abutment force 71
Figure 4.46. Northbound bridge approach slab average force relative to the average abutment movement 71
Figure 4.47. Load strain of post tensioning strand in the northbound bridge approach slab with respect to transverse position 73
Figure 4.48. Average change in strand strain due to load over time – northbound bridge 74
Figure 4.49. Change in prestress average force for a strand – northbound bridge 74
Figure 4.50. Change in post tensioning strain relative to average slab temperature 75
Figure 4.51. Northbound bridge precast approach slab joint movements 76
Figure 4.52. Northbound bridge expansion joint movement relative to average slab temperature 77
Figure 4.53. Total movement of south end of northbound bridge approach slab 78
Figure 4.54. Comparison of northbound bridge abutment movement and expansion joint movement 79
Figure 4.55. Northbound bridge expansion joint movement related to the load force in the approach slab 80
Figure 4.56. Gauge location and orientation of local axis (HP 10x57 pile) 81
Figure 4.57. Pile location and global axis orientation 81
Figure 4.58. Northbound bridge west pile strains obtained at tips of flanges 82
Figure 4.59. Northbound bridge middle pile strains obtained at tips of flanges 82
Figure 4.60. Northbound bridge west pile axial and bending strains 85
Figure 4.61. Northbound bridge middle pile axial and bending strains 86
Figure 4.62. Forces in northbound bridge west pile 86
Figure 4.63. Northbound bridge middle pile forces 87
Figure 4.64. Northbound bridge west pile y-axis movement compared to strong axis bending 88
Figure 4.65. Northbound bridge west pile x-axis movement compared to weak axis bending 88
Figure 4.66. Northbound bridge middle pile y-axis movement compared to strong axis bending 89
Figure 4.67. Northbound bridge middle pile x-axis movement compared to weak axis bending 89
Figure 4.68. Transverse crack in precast approach slab 90
Figure 5.1. Temperature variation across the southbound bridge cast-in-place approach slab 92
Figure 5.2. Average southbound and northbound bridge approach slab temperatures over time 92
Figure 5.3. Temperature variation of the top of the southbound bridge girders 93
Figure 5.4. Temperature variation of the bottom of the southbound bridge girders 94
Figure 5.5. Average temperature variation along the southbound bridge girders 94
Figure 5.6. Southbound bridge temperature over time 95
Figure 5.7. Northbound and southbound bridge temperatures over time 96
Figure 5.8. Southbound bridge and air temperature over time 96
Figure 5.9. Correlation of daily high and low air to southbound bridge temperatures 97
Figure 5.10. Typical southbound bridge abutment displacement at abutment base over time (Δ_{abut}) 98
Figure 5.11. Typical displacement of the southbound bridge abutment due to abutment rotation over time 98
Figure 5.12. Total southbound bridge abutment displacement at the west end at slab mid-depth

over time 99
Figure 5.13. Total southbound bridge abutment displacement at the east end at slab mid-depth over time 100
Figure 5.14. Average total southbound bridge abutment displacement at slab mid-depth over time 100
Figure 5.15. Theoretical and average actual abutment displacement of the southbound bridge over time 101
Figure 5.16. Southbound bridge abutment displacement versus change in bridge temperature .102
Figure 5.17. Southbound bridge transverse abutment displacement over time 103
Figure 5.18. Southbound bridge transverse abutment displacement versus average longitudinal abutment displacement....103
Figure 5.19. Typical southbound bridge girder load strain behavior over time 104
Figure 5.20. Southbound bridge girder load strain over time from gauge GSWT2 105
Figure 5.21. Load strain over time from gauge GSEB3 105
Figure 5.22. Load strain variation at the top of the girders with respect to position....106
Figure 5.23. Load strain variation at the bottom of the girders with respect to position....107
Figure 5.24. Southbound bridge average girder moment with respect to position....108
Figure 5.25. Southbound bridge average mid-span moment over time....109
Figure 5.26. Southbound bridge average mid-span moment versus bridge temperature 109
Figure 5.27. Southbound bridge average mid-span moment versus average longitudinal abutment displacement 110
Figure 5.28. Southbound bridge girder moment envelope 110
Figure 5.29. Southbound bridge average axial load with respect to position....111
Figure 5.30. Southbound bridge average girder axial load over time....112
Figure 5.31. Average axial load versus bridge temperature 112
Figure 5.32. Southbound bridge average axial load versus average longitudinal abutment displacement 113
Figure 5.33. Representative strain reading obtained from southbound bridge embedded approach slab strain gauge ESEW....114
Figure 5.34. Southbound bridge hot and cold day load strain comparison with respect to location115
Figure 5.35. Average load strain of the southbound bridge embedded gauges 115
Figure 5.36. Southbound bridge approach slab load strain with respect to temperature....116
Figure 5.37. Southbound bridge approach slab average force with respect to change in slab temperature 117
Figure 5.38. Southbound bridge approach slab average force relative to the movement at the abutment....117
Figure 5.39. Southbound bridge hot and cold day load force comparison with respect to location118
Figure 5.40. Southbound bridge cast in place approach slab joint opening 119
Figure 5.41. Movement of east and west edge of the southbound bridge expansion joint....119
Figure 5.42. Southbound bridge expansion joint opening relative to temperature....120
Figure 5.43. Total movement of south end of southbound bridge approach slab....121
Figure 5.44. Comparison of southbound bridge abutment movement and expansion joint movement....122
Figure 5.45. Expansion joint opening related to the load force in the southbound bridge approach slab 122
Figure 5.46. Southbound bridge west pile strains obtained at tip of flanges....123
Figure 5.47. Southbound bridge middle pile strains obtained at flange tips 124
Figure 5.48. Southbound bridge east pile strains obtained at flange tips 124

Figure 5.49. Southbound and northbound strain at W2 location 125
Figure 5.50. PSW2 load strain compared to average bridge temperature 126
Figure 5.51. Transverse cracking of the doubly reinforced approach slab at the south end starting at the east shoulder 127
Figure 5.52. Void under the west edge of the approach slab at the bridge abutment 127
Figure 6.1. Longitudinal abutment displacements (south end) for both bridges 130
Figure 6.2. Illustration of approach slab crack positions 134
Figure A.1. Elevation view of northbound bridge A-2
Figure A.2. Simple analytical model A-2
Figure A.3. Simulated annual temperature variation for sample model A-6
Figure A.4. Annual Movement at expansion joint from simple model A-6
Figure A.5. Annual movement at abutment from simple model A-7
Figure A.6. Annual frictional force from simple model A-7
Figure A.7. Abutment Displacement versus temperature from simple model A-8
Figure A.8. Typical temperature loop A-9
Figure A.9. Slab force versus temperature from simple model A-11
Figure A.10. Slab force versus movement at expansion joint from simple model A-11

LIST OF TABLES

Table 2.1. Summary of DOT responses 16
Table 3.1. Instrumentation description, location, and quantity 25
Table 3.2. Northbound bridge gauge labels and location 27
Table 3.3. Southbound bridge gauge labels and location 28
Table 4.1. Experimentally measured and recommended average bridge temperatures 42
Table 6.1. Displacement results 129
Table 6.2. Girder force results 131
Table 6.3. Approach slab results 133
Table A.1 Behavior of slab analytical model along various paths A-12

ACKNOWLEDGMENTS

This research was sponsored by the Iowa Department of Transportation and the Iowa Highway Research Board. The authors would like to thank Doug Wood, Travis Hosteng, and the many students that were involved in the project for there help with completing much of the instrumentation field installation. The authors would like to thank the Iowa DOT Office of Bridges and Structures for their assistance in contacting other Department of Transportation agencies. Special thanks to the Illinois, Kansas, Minnesota, Missouri, Nebraska, North Dakota, South Dakota, and Wisconsin Departments of Transportation bridge offices for sharing their specific bridge practices pertaining to integral abutments and approach slab systems.

EXECUTIVE SUMMARY

The Iowa Department of Transportation has long recognized that approach slab pavements of integral abutment bridges are prone to settlement and cracking, which manifests itself as the "bump at the end of the bridge". The bump is not a significant safety problem; rather it is an expensive maintenance issue. A commonly recommended solution is to integrally attach the approach slab to the bridge abutment, which moves the expansion joint typically found at the approach slab/abutment interface to a location further from the bridge where soil settlement is less of a concern and maintenance is easier. Two different approach slabs, one being precast concrete and the other being cast-in-place concrete, were integrally connected to side-by-side bridges on Iowa Highway 60. The primary objective of this investigation was to evaluate the approach slab performance and the impacts the approach slabs have on the bridge.

The Iowa State University Bridge Engineering Center installed a health monitoring system on both bridges and the two different approach slab systems. To encompass all aspects of the system and to obtain meaningful conclusions, several behaviors were studied and monitored during the evaluation period including abutment movement, bridge girder strain changes, approach slab strain changes, approach slab joint displacements, post-tensioning strain, and abutment pile strain changes. The project scope also involved a literature review, survey of midwest Department of Transportation current practices, and periodic visual inspection of the bridges.

Based on the information obtained from the 12 month long monitoring period the following general conclusions were made in regards to the integral approach slab system. The integral connection between the approach slabs and the bridges appear to function well with no observed distress at this location and no relative longitudinal movement measured between the two components. Tying the approach slab to the bridge appears to impact the bridge abutment displacements and girder forces. The source of the impact may be the manner in which the approach slab is attached to the main line pavement. The two different approach slabs, the longer precast slab and the shorter cast-in-place slab, appear to impact the bridge differently. This impact was clear in the differences in the mid-span moments and the slab strain patterns over time. It is not clear, however, whether it was the type of approach slab or the size of the approach slab that has the greatest impact. The measured strains in the approach slabs indicate a force exists at the expansion joint and should be taken into consideration when designing both the approach slab and the bridge. The observed responses generally followed an annual cyclic and/or short term cyclic pattern over time. The annual cyclic pattern had summer responses at one extreme, a transition through the fall to the other extreme response in the winter, followed by a transition in the spring back to the summer responses. A linear relationship of the transitions between the extreme responses was typically observed. Seasonal and short term cycles were evident in most data, probably caused by friction ratcheting.

INTRODUCTION

1.1. Background

The Iowa Department of Transportation (Iowa DOT) has long recognized that approach slab pavements at integral abutment bridges are prone to settlement and cracking, which is manifested as the "bump at the end of the bridge". The bump is not a significant safety problem; rather it is an expensive maintenance issue. Further, public perception is negatively affected by the presence of the bump. The formation of the bump is typically attributed to settlement of backfill soil under the approach slab, deterioration of the corbel or paving notch, and poorly functioning expansion joints. Integral abutment (I-A) bridges are believed by many engineers to worsen the bump; although it is recognized that I-A bridges have many other highly desirable attributes. A commonly recommended solution is to attach the approach slab to the bridge abutment, which moves the expansion joint typically found at the approach slab/abutment interface to a location further from the bridge where soil settlement is less of a concern and maintenance is easier. Other states in the Midwest utilize this type of connection.

Two new side-by-side bridges on new Iowa Highway 60 bypass of Sheldon, IA in O'Brien County were chosen as test bridges for testing such a connection detail. The integral approach slab to abutment connection detail was implemented on both bridges. These are the first bridges in Iowa to tie the approach slab to an I-A abutment bridge. One bridge utilized a cast-in-place approach slab system while the other utilized a precast approach slab system.

1.2. Scope and Objectives

A literature review and informal phone survey of other Midwest DOTs were conducted to find current practices and ideologies on integrally connecting the approach slab to the bridge abutment. This further emphasized the thought that the impact of attaching the approach slab is not quantifiably known. As such, a health monitoring system was installed to monitor bridge abutment movement (displacement and rotation), bridge girder strain changes, approach slab strain changes, approach slab joint relative displacements, post-tensioning losses (in the precast post-tensioned approach slab), and abutment pile strain changes on the two bridges. The objectives of this work are:

1. Determine the impact attaching two different approach slabs have on bridge performance.
2. Evaluate the performance of the two different approach slabs.
3. Determine the range of forces that should be considered when designing integral abutment bridges with integrally connected approach slabs.

1.3. Report Content

Chapter 2 presents the findings of a formal literature review that was focused on the problem of the "bump" and approach slab to integral bridge abutment connections. Also included in Chapter 2 are summaries of informal phone interviews with the bridge engineers of the north central states DOTs with respect to current practices involving approach slabs. Descriptions of the two bridges monitored as well as the information on the instrumentation are provided in Chapter 3. The data and results of the monitoring program for the bridges are discussed in Chapters 4 and 5 for the two bridges. Comparisons of the two bridges are given in Chapter 6 along with the conclusions formed. Recommendations for future studies are given at the end of Chapter 6.

2. LITERATURE REVIEW

I-A bridges, which are conceptually depicted in Figure 2.1, have become well known and widely used across the country. A study of current practices in the U.S. and Canada was performed by Kunin and Alampalli (2000). The authors reported the results of a 1996 survey of which 31 agencies responded to having experience with I-A bridges. Additionally, they found that by 1996 over 9,770 I-A bridges had been built. The popularity of I-A bridges stems from the many advantages they offer (Brena et. al. 2007; Burke 1993; Lawver et. al. 2000; Kunin and Alampalli 2000). Cost, both initial construction and long-term maintenance, is the biggest benefit derived from I-A designs due to the elimination of expansion joints and bearings. Generally I-A bridges experience less deterioration from de-icing chemicals and snowplows, decreased impact loads, improved ride quality, are simpler to construct, and have improved structural resistance to seismic events. Burke (1993) concludes that I-A bridges should be used whenever applicable because of the many advantages over the few disadvantages. One problem facing bridges nationwide is bump development at the end of the bridge. The bump problem appears to be a consistent problem with I-A bridges (Briaud et al. 1997).

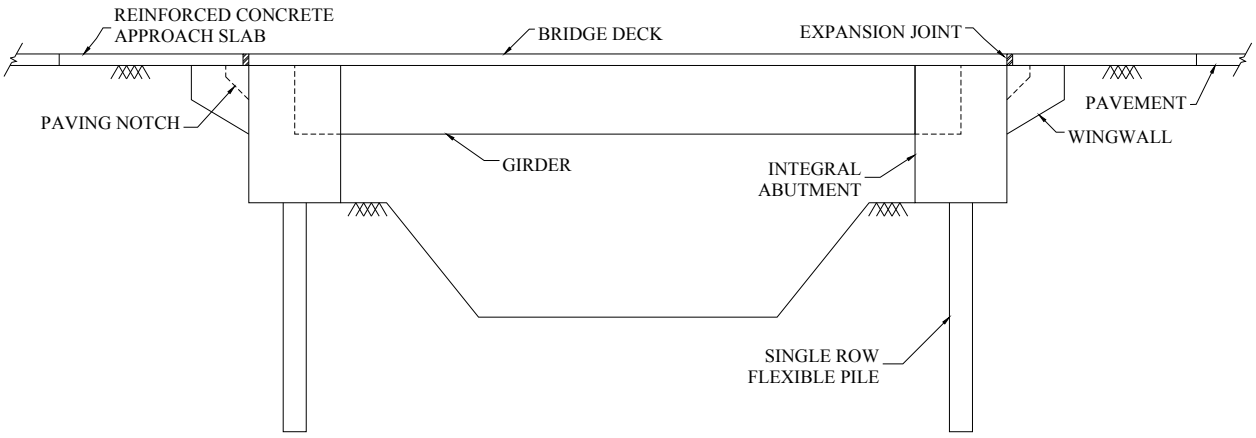


Figure 2.1. Simplified elevation view of a typical integral abutment bridge

2.1. Bump Problem

In a literature review and survey of various state DOTs, Briaud et al (1997) summarized causes of the bump and offered potential solutions. According to the report "the bump develops when there is a differential settlement or movements between the bridge abutment and the pavement of the approach embankment." This problem was estimated to impact 25% of the bridges in the country. Typically the bump is not a significant safety problem: rather it is an expensive maintenance issue. Three main causes for the bump can be taken from Briaud's report. Figure 2.2 conceptually shows the causes which are summarized below:

1. Differential settlement between the top of the embankment and the abutment due to the different loads on the natural soil and compression of embankment soils, typically because of insufficient compaction.
2. Void development under the pavement due to erosion of embankment fill because of poor drainage.
3. Abutment displacement due to pavement growth, embankment slope instability, and temperature cycles on integral abutments.

While the above items seem to suggest that the problem is geotechnical and construction in nature, there is actually a structural issue present. Integral abutment bridges are called out as a distinct issue, with "many engineers responding to the survey believing the bump worsens with integral abutment bridges" (Briaud et. al 1997 pp. 25). Thermal cycles are a key behavior with I-A bridges since they do not have expansion joints and expand/contract with the thermal cycles. When I-A bridges expand, the fill material is compacted, creating a void that increases when the bridge contracts.

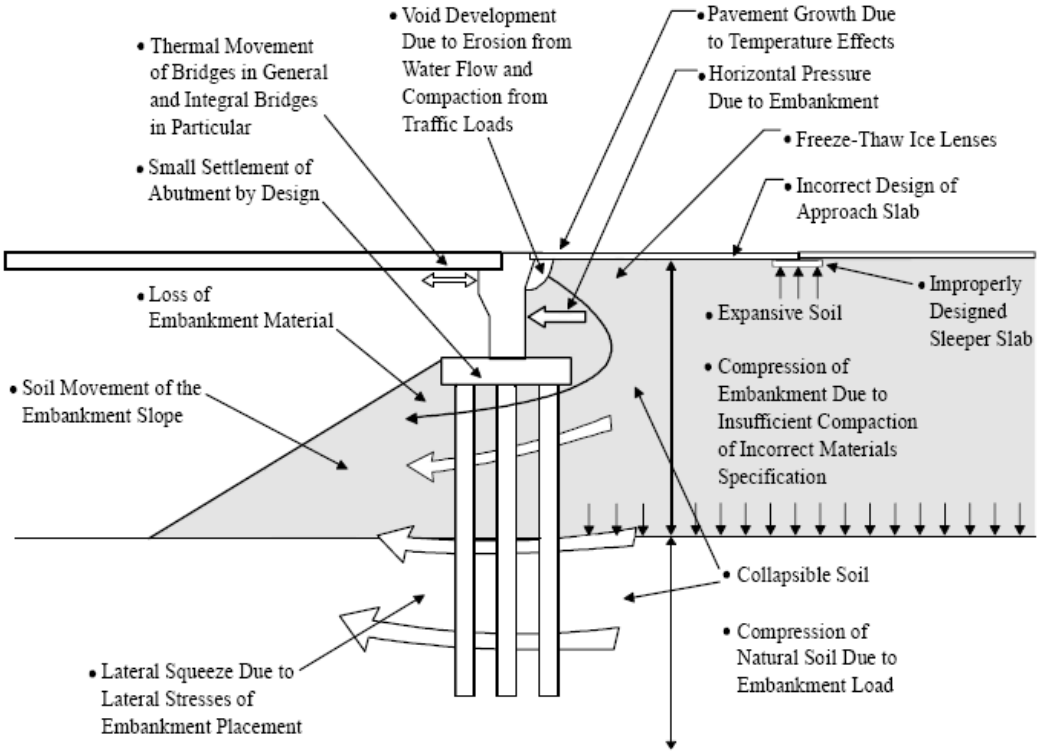
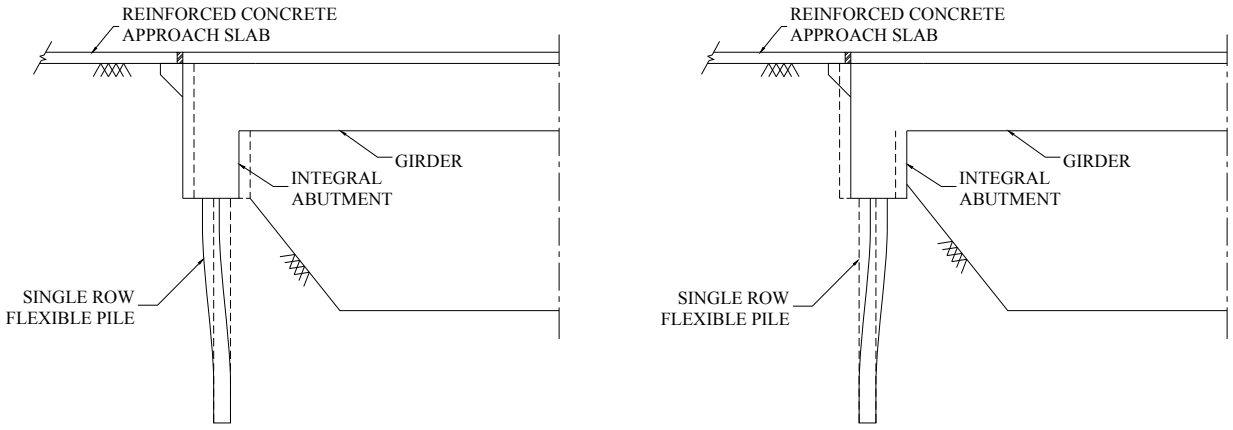


Figure 2.2. Problems leading to the formation of the bump (Briaud et al. 1997)

Schaefer and Koch (1992) also reported on the longitudinal movement of I-A bridges and the cyclic loading they impose on the backfill and foundation. As the temperature increases the superstructure and abutment move outward, toward the soil causing lateral earth pressures, and compacting the soil. As the temperature decreases, the bridge abutments move away from the compressed soil and a void forms (Figure 2.3). The creation of this void may lead to soil erosion that further increases the size of the void (White et al. 2005).



a) Expansion of bridge **b) Contraction of bridge**

Figure 2.3. Temperature induced movement of an integral abutment bridge

White et al. (2005 and 2007) investigated general bridge approach settlement in Iowa. At 25% of the 74 bridge sites (13 were I-A bridges) severe void development problems were observed. The authors indicate that void development commonly occurs within the first year after bridge approach pavement construction. Voids, and the erosion associated with void formation, lead to problems such as (1) exposing H-piles which potentially leads to accelerated corrosion and a reduction in capacity; (2) failure of slope protection; and (3) severe faulting in the approach slab caused by the loss of support. During observation of new I-A bridges under construction, White et al. found that poor construction practices may be another source of settlement of the approach pavement. The construction practices identified by the authors included poor approach pavement and paving notch construction, use of non-specified backfill material, and placing granular backfill in too thick of layers at the incorrect moisture for compaction. White et al. concluded that approach pavement systems were performing poorly because of poor backfill properties, inadequate subsurface drainage, and poor construction practices. They also reported that void development was more pronounced with I-A bridges.

In their 2005 report White et al. tested a variety of backfill soil types and geocomposite configurations. Some of the results were:

- Granular backfill, placed at bulking moisture content, undergoes 6% collapse compared to no collapse at 8% or higher moisture content.
- Granular backfill specified is highly erodible.
- Granular backfill can lead to large void development due to erodibility and compressibility at bulking moisture.
- Porous backfill does not experience collapse nor is it highly erodible.
- Porous backfill usage prevented approach settlement, void development, and increased drainage.

In a similar way, Briaud et al. (1997) gives several recommendations for best current practices associated with minimizing bridge approach ride issues. The recommendations are:

1. Make the bump a design issue with prevention as the goal.
2. Assign the design issue to an engineer.
3. Encourage teamwork and open-mindedness between geotechnical, structural, pavement, construction, and maintenance engineers.
4. Carry out proper settlement vs. time calculations.
5. Design an approach pavement slab for excessive settlement.
6. Provide for expansion/contraction between the structure and the approach roadway.
7. Design a proper drainage and erosion protection system.
8. Use and enforce proper specifications.
9. Choose knowledgeable inspectors, particularly on geotechnical aspects.
10. Perform inspections including joints, grade specifications, and drainage.

Of particular interest to this project is what Briaud et al. (1997) had to say about approach slabs (#5 in their best practice list). The report states that approach slabs are used by many states, with several states installing them on all bridges. Also reported was that "the use of reinforced approach slabs minimizes the bump or eliminates it all together," and that "suggestions have been made to tie the approach slab to the abutment."

In addition to recommending better backfill systems White et al. (2005) also recommended connecting the approach slab to either the abutment or the bridge deck. This eliminates the expansion joint at the bridge/approach slab interface. Both Briaud et al. (1997) and White et al. (2005 and 2007) made recommendations with regard to using approach slabs and the possibility of tying or integrally connecting them to the bridge as a way to minimize or eliminate the bump problem.

2.2. Approach Slabs

White et al. (2005) described approach slabs as being designed to be supported on the bridge abutment at one end and the fill or a sleeper slab (or beam) at the other. The purpose of the approach slab is to minimize differential settlement effects and to provide a transition from the pavement to the bridge deck. The level of performance of the approach slab is based upon many factors, including: (1) approach slab dimensions, (2) steel reinforcement, (3) the use of a sleeper slab, and (4) the type of connection between the approach slab and bridge.

Kunin and Alampalli (2000) found that there are two main approach slab to bridge connections. The first technique is to connect the slab reinforcement to the bridge through extension of the deck steel (see Figure 2.4). The second technique uses reinforcing steel to connect the slab to the corbel or abutment (see Figure 2.5). Another option to the two cited by Kunin and Alampalli is to have the approach slab rest on the paving notch of the abutment (see Figure 2.6). Hoppe (1999) reports that 71% of the state DOT's using I-A bridges use a mechanical connection between the approach slab and bridge.

A more recent survey conducted by Maruri and Petro (2005) found practices similar to those found by Kunin and Alampalli. Maruri and Petro suggest that standardization and guidelines would be beneficial for abutment/approach slab connections. They also found that 31% of the respondents use sleeper slabs, 26% do nothing but float the slab on the fill, and 30% do both.

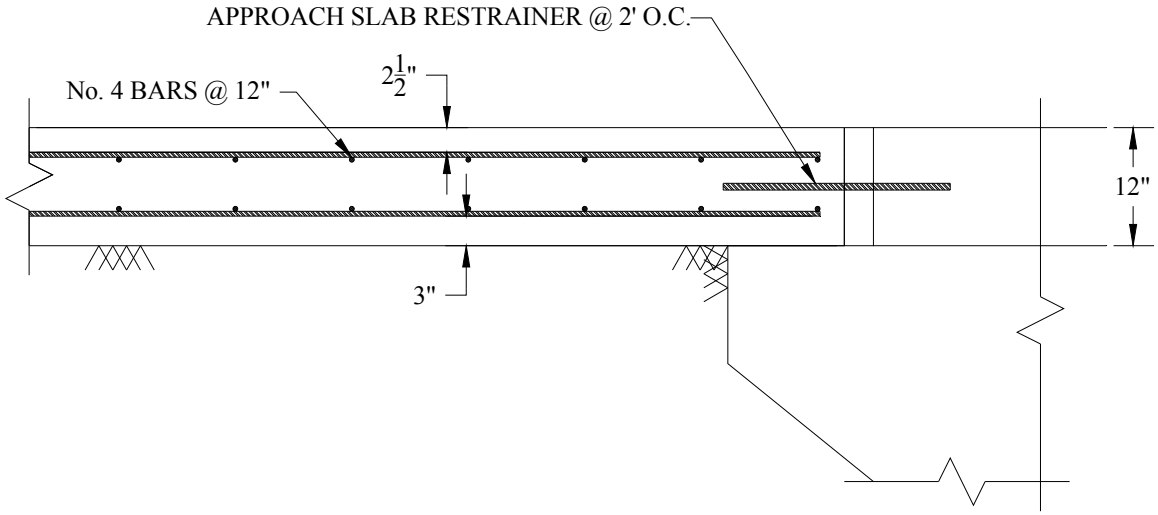


Figure 2.4. Deck steel extension connection (standard Nevada detail)

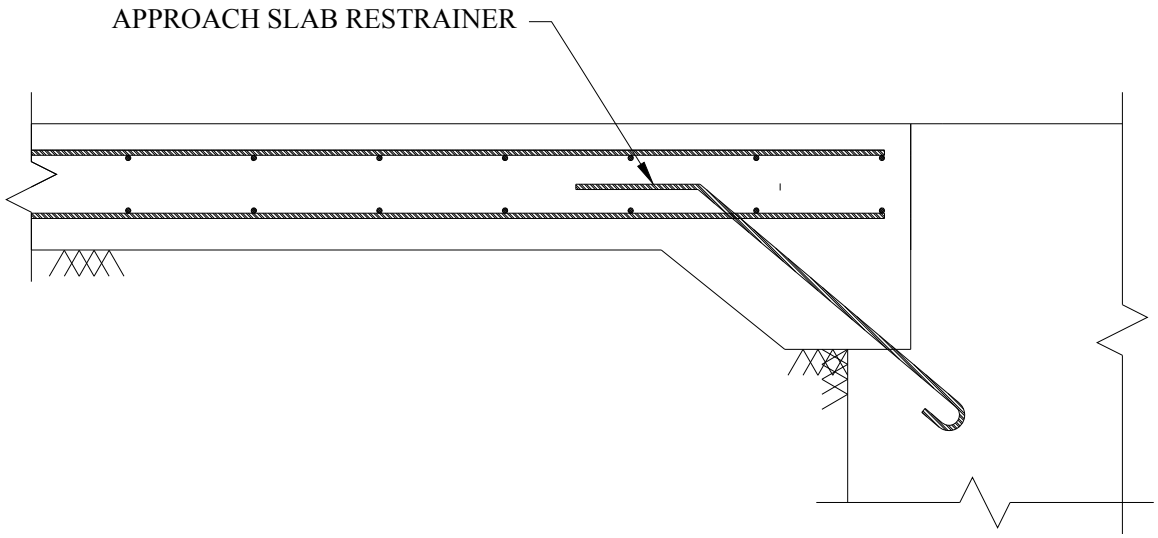


Figure 2.5. Abutment steel connection (standard Ohio detail)

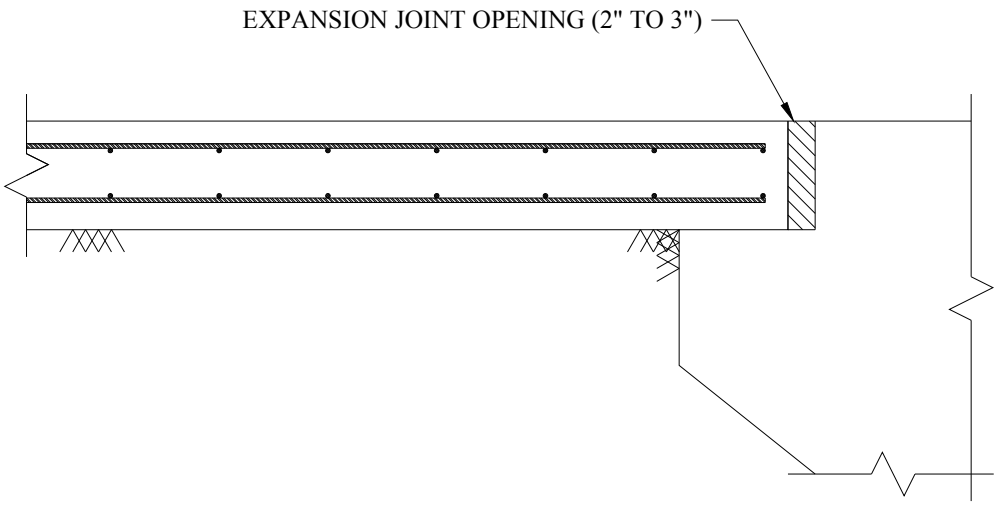


Figure 2.6. Abutment with no connection (standard Iowa detail)

Burke (1993) indicates that "full width approach slabs should be provided for most integral abutments and should be tied to the bridge to avoid being shoved off their seat by the horizontal cycle action of the bridge as it responds to daily temperature changes." He also indicates with regards to approach slab to bridge connections that "approach slabs tied to bridges become part of the bridge, responding to moisture and temperature changes. They increase the overall structure length and require cycle control joints with greater ranges." The cycle control joints are important because they relieve resistance pressures that are a result of the lengthening/shortening of the bridge. As the bridge moves, it is resisted by the approach slab in the form of a pressure. That pressure is distributed to both the slab and the bridge, but is a much greater problem for the pavement which has a smaller area. As a result, fracturing and buckling (i.e., blowouts) can occur in the approach pavement. Therefore cycle control joints must be designed and used. Burke also suggests another method to minimize the force required to move the approach slabs: "They should be cast on smooth, low-friction surfaces such as polyethylene or filter fabric."

Similar to the above, Mistry (2005) recommends the following:

- Make installation of the approach slab a joint decision between the Bridge/Structures group and the Geotechnical group.
- Standardize the practice of using sleeper slabs, as cracking and settlement typically develops at the slab/pavement joint.
- Use well drained granular backfill to accommodate the expansion/contraction.
- Tie approach slabs to abutments with hinge type reinforcing.
- Provide layers of polyethylene sheets or fabric under approach slabs to minimize friction against horizontal movement.
- Limit skew to less than 30 degrees to minimize the magnitude and lateral eccentricity of longitudinal forces

The above recommendations reinforce the emphasis to use proper backfill and friction reducing material under the approach slab. More importantly, Mistry's recommendations reinforce the importance of integrally connecting approach slabs to the bridge.

A report by Cai et al. (2005) noted the problem of the bump at the end of the bridge, repeating the causes previously discussed. They also recommended designing approach slabs to "span" the resulting voids. Designing the slabs as simply supported beams between the abutment and pavement ends is very conservative, and uneconomical. They also point out that the AASHTO code (AASHTO 2004) has no guidelines for designing approach slabs.

Due to the lack of guidelines, Cai et al. (2005) performed finite analysis on approach slabs loaded with a HS20 load while varying the amount of soil settlement. The resulting deflections and internal moments were recorded. Using the results of the finite element analysis and the parameters of the slab, formulas were developed to provide information for structural analysis and design of approach slabs for a given settlement. Cai et al. concluded that despite improving the approach slab design, the bump is still a function of settlement. They noted that even if minimal settlement is allowed in the embankment soil through construction and geotechnical practices, there will always be a bump. A more rigid slab will have less deflection and change of slope but may increase soil pressures under the contact areas which are smaller due to spanning of any voids resulting in increasing faulting deflections.

There was very little literature found that investigates or discusses the effects that attaching the approach slabs to the I-A bridge has on the bridge itself. One report by Lawver et al. (2000) covers the instrumentation and study of an integral abutment bridge with tied approach pavement near Rochester, MN. The conclusion was that the bridge performed well during the reporting period, but that backfill material loss and void formation still occurred. There was no discussion directly on the effect the pavement may or may not have had.

2.3. Specific Practices

The reports on current practices, by Kunin and Alampalli (2000) and Maruri and Petro (2005), provide statistical summaries as to what many states do. They do not report many details and specifics on what individual states do, why they do it, or how they do it. In fact, there are only a few reports that go into detail on the specific practices.

The report by Yannotti, Alampalli, and White (2005) discussed the New York DOT experience with I-A bridges and presented specific practices. Of particular interest was the modification made to the approach slab to abutment connection after a 1996 study (similar to Figure 2.4). The older detail involved the extension of bridge deck steel horizontally into the approach slab. This detail was found to be unsatisfactory because the approach slab was unable to accommodate any settlement. This settlement typically caused transverse cracking in the bridge deck and transverse and longitudinal cracking of the approach slab. A new detail, shown in Figure 2.7, was developed using reinforcing bars at 45° into the bridge deck and the approach slab. This connection allows rotation of the slab by minimizing the moment capacity if the fill settles.

Harry White of the New York State DOT (NYSDOT) was contacted for further information. He added that the horizontal bar detail mentioned above provided negative moment capacity so that when the fill and slab settled, rotation was restrained leading to the cracking discussed above. He also indicated that the new detail (see Figure 2.7) is performing adequately and no notable problems have arisen. A requirement of NYSDOT and other states is the use of a polyethylene sheet under the full width of the slab to reduce sliding friction.

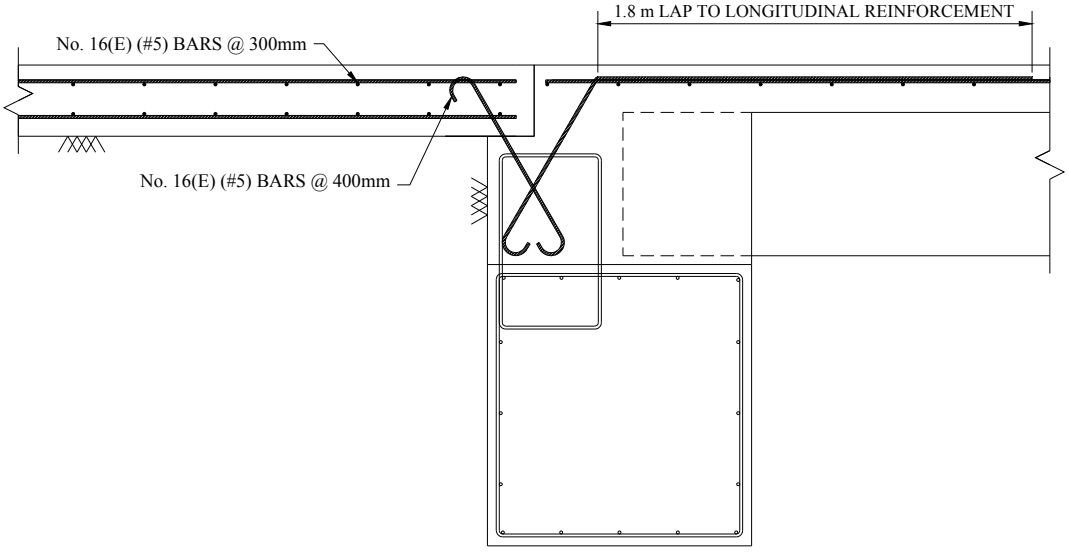


Figure 2.7. Typical New York detail

Since the New York report was one of only a few to discuss specific practices, bridge engineers at other DOTs were contacted for more information. With the assistance of the Iowa DOT nine other departments were contacted including those from Illinois, Kansas, Michigan, Minnesota, Missouri, Nebraska, North Dakota, South Dakota, and Wisconsin. Along with Iowa, these states make up the north central states. Engineers in each state were contacted first by email, followed by a phone conversation asking about specific practices regarding I-A bridges and approach slabs. The basic questions were:

- Do you typically connect the approach slab to the bridge? If so, how and why?
- How have the connections performed (any problems or good reports)?
- Has research or a study been performed?
- Is anything used beneath the slab to reduce friction?
- What is the backfill criterion in your state?

All the states, with the exception of Michigan participated. A summary of the practices of each state can be found at the end of this section in Table 2.1. Wisconsin was the only state that does not use a connection between the approach slab and the bridge. The contact, Lee Schuchardt, responded that the only change he would make would be to attach the slab to the abutment backwall with reinforcing bars because of the separation that happens between the abutment backwall and the approach slab.

Kevin Riechers of Illinois indicated that they have been building I-A bridges since the early 1980's and began connecting the approach slab approximately five years after that. The typical detail used by Illinois is shown in Figure 2.8. This detail consists of #5 reinforcing bars spaced every 12 in. that are extended horizontally from the bridge deck into the approach slab with 4 ft in the bridge deck and 6 ft in the approach slab. In addition, vertical #5 reinforcing bars are extended from the corbel into the approach slab every 12 in. The reason cited for connecting the slab and bridge was to keep the joint closed in order to keep water and debris out and the pavement moving with bridge. Transverse cracking of the slab was reported to be a problem. Mr. Riechers also reported that another problem is the settlement of the sleeper slab at the other end of the approach slab and that a new design is being considered. No research has been performed on approach slab to bridge connections. Also, nothing is apparently done to reduce surface friction under the approach slab except bond breaker between the slab and wing-walls of U-Back abutments. The soil is backfilled at the abutment with no compaction to avoid additional lateral earth pressures that may restrain thermal expansion of the bridge.

From Kansas, John Jones reported that approach slabs have been connected to the bridge for the last 12 years. The connection is made by extending #5 reinforcing bars horizontally from the bridge deck into the approach slab and ending in a standard hook (see Figure 2.9). The approach slab rests on a corbel at the bridge end and a sleeper slab at the other end, typically 13 ft away. The reason behind the connection was to remove the bump that formed at the end of the bridge. Though the bump was removed from the bridge end, it now appears between the slab and pavement. Mr. Jones reported that the connection has performed reasonably well and that public perception has been positive. Problems may arise if the sleeper slab settles, causing negative moments at the abutment. A solution to this is carefully mud-jacking the slab being mindful to avoid clogging the drain behind the abutment. No research as been performed and nothing is used to reduce friction. The backfill criteria used is the same as the road criteria (18 in. lifts at 90% compaction) with a strip drain installed behind the abutment.

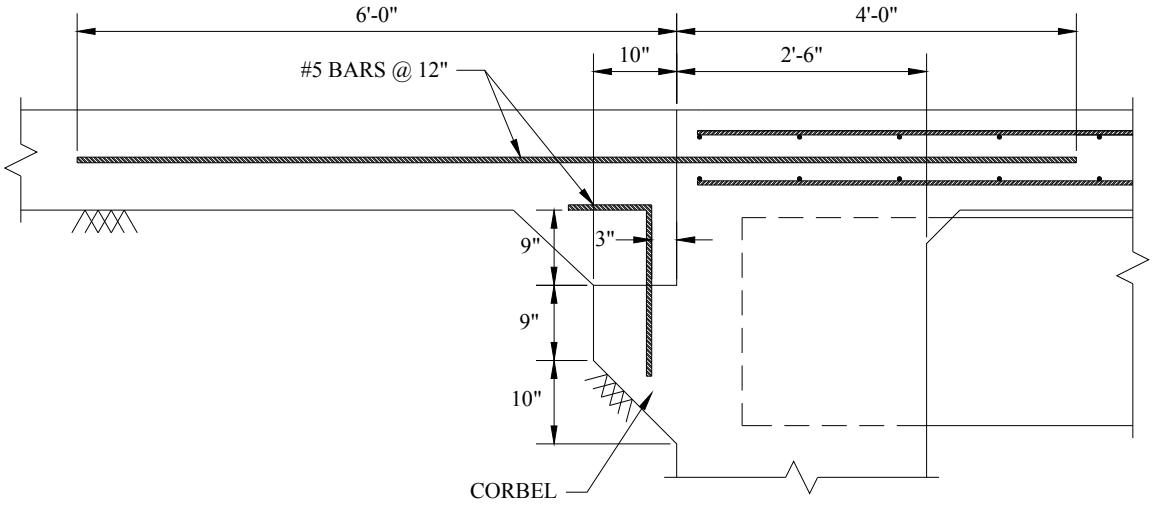


Figure 2.8. Typical Illinois detail

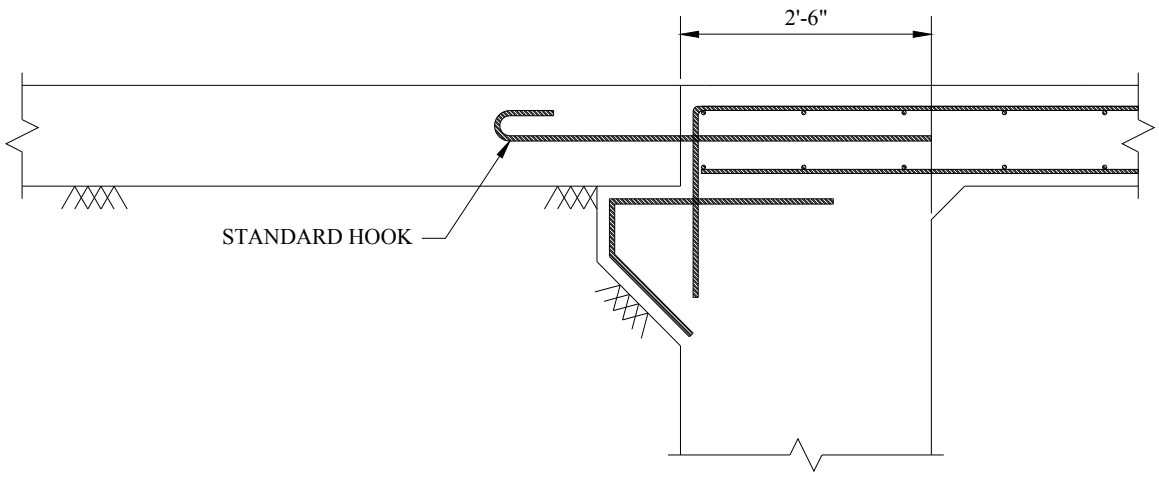


Figure 2.9. Typical Kansas detail

Paul Rowekamp provided information on the practices in Minnesota. He reported that Minnesota has been building I-A bridges for approximately five to six years and connecting the approach slabs to the bridge for the last three years. The standard detail, shown in Figure 2.10, is to extend a #16 (metric, #5 U.S.) reinforcing bar diagonally from the abutment into the approach slab. This connection was implemented because of maintenance concerns pertaining to the opening of the joint between the slab and bridge. He explained that after the bridge has expanded to its limits, and begins to contract, the slab may not move with the bridge immediately because of friction with soil and lack of friction between the slab and the paving notch. Thus the joint opens slightly, filling with debris. The next season the same thing happens, filling the joint with more debris. The slab now has less to rest on, and water can now flow in and beneath the slab. As the slab approaches the edge of the paving seat, it may eventually fall completely off. Mr. Rowekamp reported that the initial connection design used an 8 ft horizontal bar extending 4 ft each way into the slab and bridge deck. Transverse cracking across the entire approach slab appeared approximately where the horizontal bar ended, possibly caused by rotation of the slab being restrained. Two years ago a change was made to the current detail, and no problems have been reported thus far. No research has been performed on the connection. Minnesota standard details do not call for any friction reducing material. Backfill of the abutment is specified as modified select granular material (having no fines) and is installed in typical lifts and compacted.

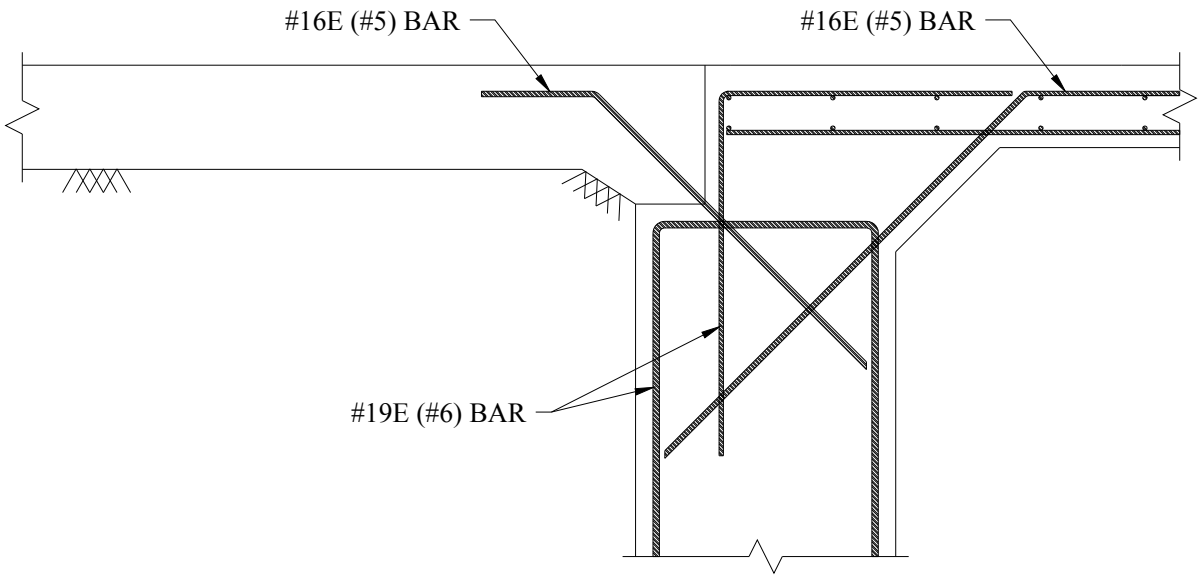


Figure 2.10. Typical Minnesota detail

David Straatmann, with the Missouri DOT, indicated that connecting the approach slab to the bridge has been standard practice for some time. The standard connection method, shown in Figure 2.11., is made by extending #5 reinforcing bars, spaced at 12 in., horizontally between the bridge deck and approach slab. Two layers of polyethylene sheeting are used between the approach slab and construction base. No information was given in regards to the reason why this connection is used, performance of this connection, research performed, and backfill criteria.

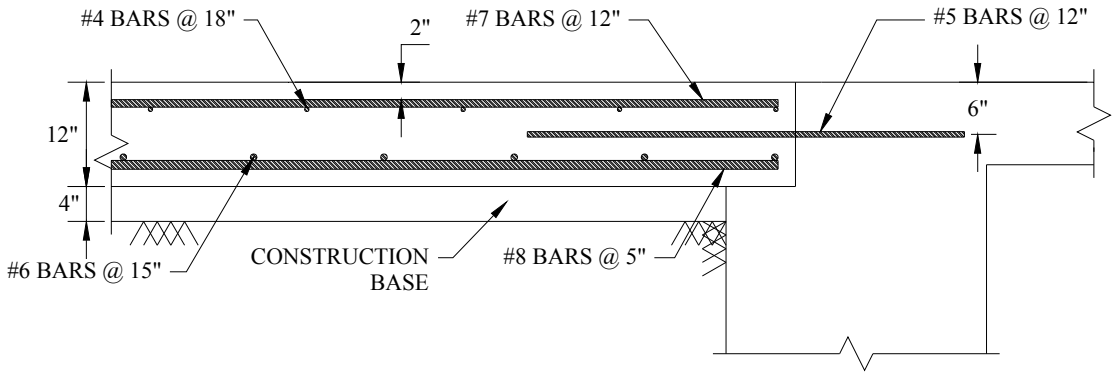


Figure 2.11. Typical Missouri detail

In Nebraska, according to Scott Milliken, approach slabs have been used for the last 15 years, with connecting the slab to the bridge being the standard practice for at least the last 10 years. The standard connection method, shown in Figure 2.12., is made by #6 reinforcing bars that extend vertically from the abutment, then bent at 45° into the approach slab. Nebraska refers to

the approach slab as an approach section, which rests on a grade beam supported by piles at the end opposite the bridge. From the grade beam to the pavement, another transition section, called the pavement section is used. According to Mr. Milliken, the reason for the connection was to eliminate, or at the least, move the bump from the end of the bridge to a location that is more easily maintained. This methodology also eliminated water from infiltrating the bearing of the bridge. A problem arising from the approach slabs was settlement of the sleeper slabs in the original design, leading to the use of grade beams as described above. Recently, hairline cracks, perpendicular to the grade beams on bridges with severe skews, were discovered. A top mat of steel was added in the approach slab, but no feedback was yet available. Overall, management is pleased with the performance thus far. No research has been performed on the approach slabs and connection. There is nothing done to reduce the friction between the slab and the ground. Fill behind the abutment is considered only necessary until the concrete in the approach section reaches strength, at which time it acts like a bridge between the abutment and grade beam. Granular backfill is used, with drainage provided by drainage fabric. The material is installed in lifts and compacted with smaller equipment to avoid damaging the wing-walls.

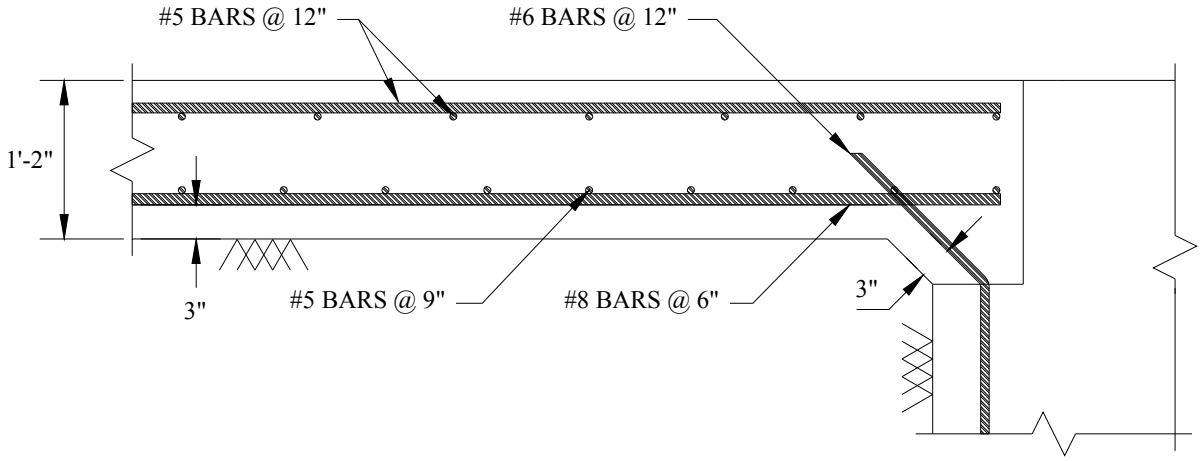


Figure 2.12. Typical Nebraska detail

According to Tim Schwagler of the North Dakota DOT, for approximately the last five years the practice in North Dakota has been to connect the approach slab to the bridge. This is accomplished by mechanically splicing a horizontal extension of #5 reinforcement from the bridge deck to the approach slab every 12 in. with joint filler (polystyrene), as shown in Figure 2.13. Two different types of approach slabs are used. On newer sites and newer embankments the far end of the approach slab is supported on piles. When approach slabs are used on older sites where settlement is assumed to have already occurred in the embankment soil, the far end of the approach slab rests on the base course. This connection was implemented to improve joint performance between the approach slab and bridge. One-inch joints were installed with filler and joint sealant. The North Dakota DOT found that the joints were opening and tearing the sealant. The connected joints have performed very well and no adjustments have been made. No research has been performed, and there is nothing done to reduce friction between the slab and the ground. When the abutments are backfilled a trench at the bottom 2 ft – 6 in. deep is filled with

rock wrapped in fabric with a drain pipe. Granular material ND Class 3 or 5 is then placed in 6 in. lifts and compacted.

According to Steve Johnson of the South Dakota DOT, the standard practice is to almost always connect the approach slab to the bridge deck on I-A bridges. This has been the practice for approximately the last 25 years. The connection is made by extending a #7 reinforcing bar that is embedded horizontally 2 ft into the bridge deck into the approach slab for 2 ft every 9 in. as shown in Figure 2.14. A mechanical splice is used to make construction easier. After backfilling of the abutment is complete, the horizontal reinforcement is spliced. The connection is used to keep water from flowing into the backfill and to provide a smoother transition while driving, because the "bump" is at least moved to the end of the approach slab. According to Mr. Johnson, the connection has performed relatively well over the years. One change was made after transverse cracking was noticed 4 to 5 ft. from the bridge. It was determined that the reinforcement was "too high" in the slab, so the design was changed to have the connection steel deeper in the slab. The only other problem reported is that the far end of the approach slab sometimes settles. No research has been performed on the connection. Plastic sheeting is required beneath the approach slab, not to reduce sliding friction, but to create a mud-jack barrier, so that mud is not lost into the voids of the base course, if it must be performed. When the abutment is backfilled, drains are installed along the backside of the abutment. The first 3 ft from the abutment is free draining granular material. After that typical fill (unspecified) is brought up in 8 to 12 in. lifts and compacted as best as possible.

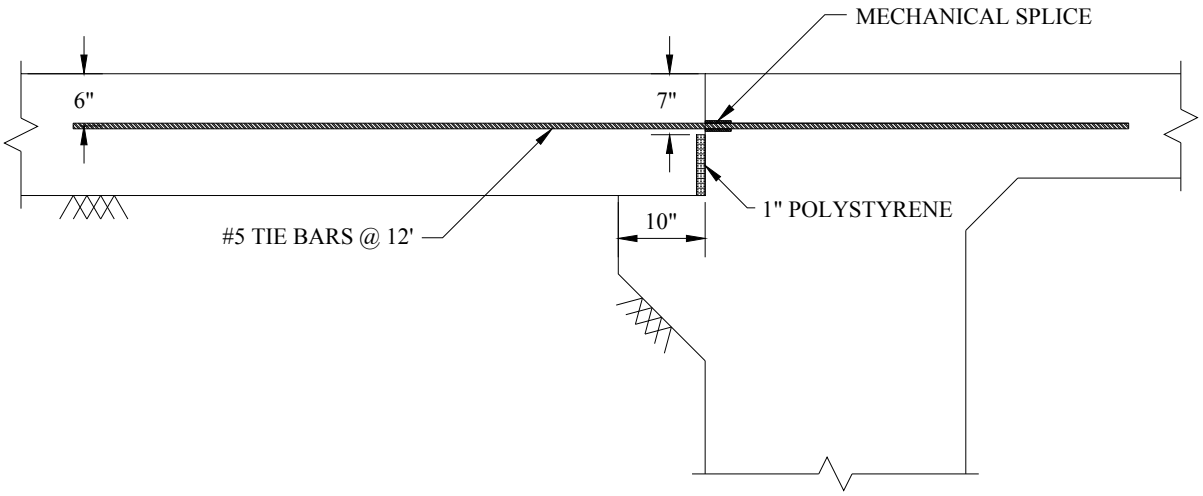


Figure 2.13. Typical North Dakota detail

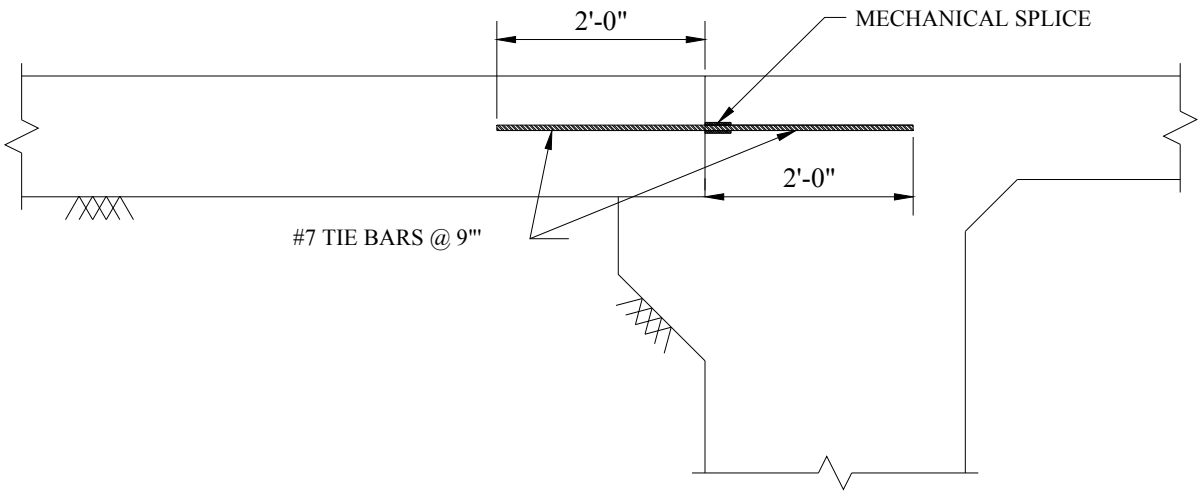


Figure 2.14. Typical South Dakota detail

Table 2.1. Summary of DOT responses

State	Connection	Performance	Research	Friction Reduction	Backfill Criteria
Illinois	Yes - Horizontal	Transverse cracking problem	No	No	Uncompacted
Kansas	Yes - Horizontal	Reasonably well	No	No	18 in. lifts, 90%
Minnesota	Yes – Diagonal	No problems reported	No	No	Modified select granular material compacted in lifts
Missouri	Yes - Horizontal	N/A	No	Yes	N/A
Nebraska	Yes – Diagonal	Management is pleased	No	No	Compacted granular material
North Dakota	Yes - Horizontal	Very well	No	No	Granular material compacted in 6 in. lifts
South Dakota	Yes - Horizontal	Pretty well	No	No	Granular fill for drainage, then typical fill compacted in 8 to 12 in. lifts
Wisconsin	No	N/A	No	N/A	N/A

N/A = Not applicable

3. PROJECT DESCRIPTION

3.1. Bridge Description

The two bridges selected for this project are located on the newly constructed Iowa highway 60 bypass, northeast of Sheldon Iowa, at the crossing of the Floyd River. The bridges are twin three-span-continuous prestressed concrete girder bridges, 303 ft x 40 ft, with a right-hand-ahead 30 degree skew angle. The end spans are 90 ft - 9 in. and the interior span measures 121 ft - 6 in. The bridges are inclined with a change in elevation from the south abutment to the north abutment of -1 ft – $2^1/_2$ in. A general plan view of the global geometry of each bridge is shown in Figure 3.1 and a general elevation view is shown in Figure 3.2. It should be noted that the bridges are identical except for the type of approach slab used. The bridges were designed to carry a HS20-44 live load plus an additional 20 psf for a future wearing surface.

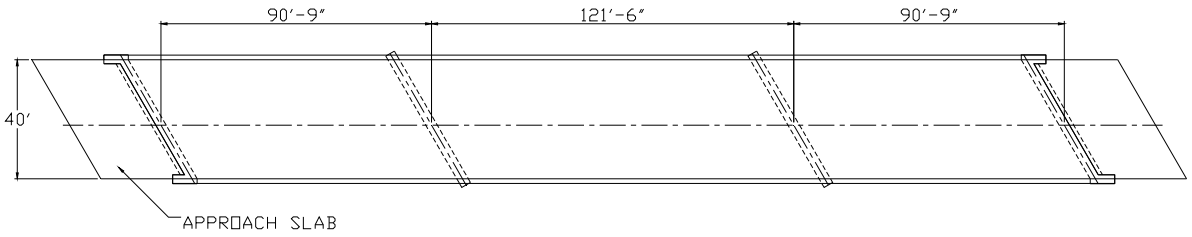


Figure 3.1. Plan view of bridges

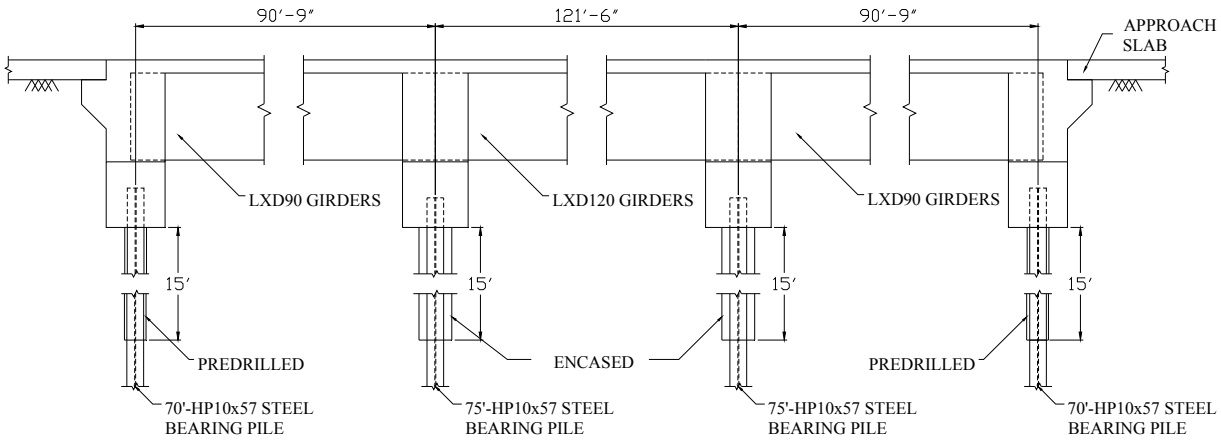


Figure 3.2. Elevation view of bridges

The superstructures consist of a 42 ft –2 in. wide, 8 in. thick cast-in-place deck that acts compositely with seven prestressed concrete girders. The girders are standard Iowa DOT LXD90 and LXD120 shapes depending on the span length. The girders measure 4 ft – 6 in. tall with 1 ft -

10 in. wide bottom flanges and 1 ft - 8 in. wide top flanges (see Figure 3.3). Spacing of the girders is 6 ft - 2in. center to center. The girders are integrally cast at the abutments and piers. Span-to-span live load continuity at the piers is achieved by cast-in-place diaphragms.

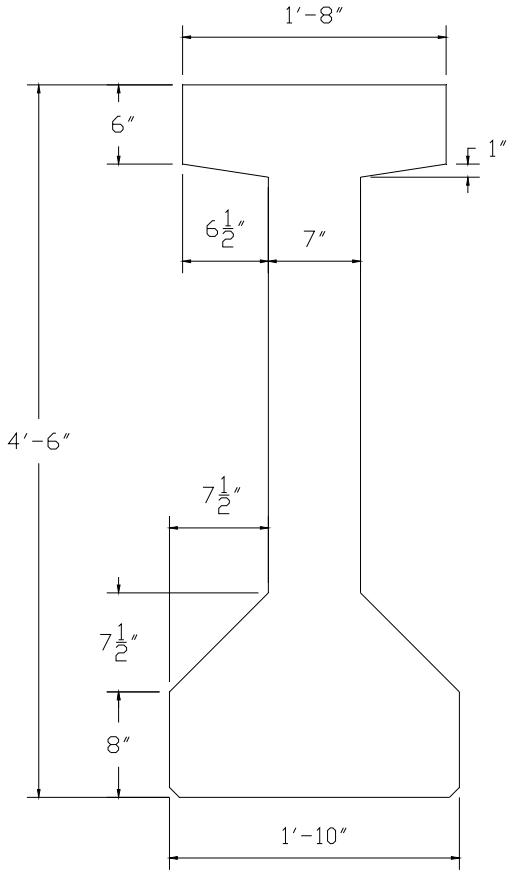


Figure 3.3. Typical LXD beam cross section

The bridge abutments are founded on a single row of nine nominal 70 ft long HP10x57 piles with an additional HP10x57 pile under each wing wall for a total of eleven piles (see Figure 3.4 and Figure 3.5). The piles are aligned with the web parallel to the face of the abutment and wing walls. The piles were driven the entire 70 ft length, with the top 15 ft predrilled. Design bearing of the piles is 50 tons. The piers consist of rectangular reinforced concrete (RC) pile caps 3 ft - 4in. x 3 ft- 4 in. at the lowest step, founded atop a line of 17 - 75 ft HP10x57 piles (see Figure 3.6). The exterior piles are battered transversely at a ratio of 1:12 horizontal to vertical. The upper 15 ft of all piles are encased in a 20 in. diameter reinforced concrete shell.

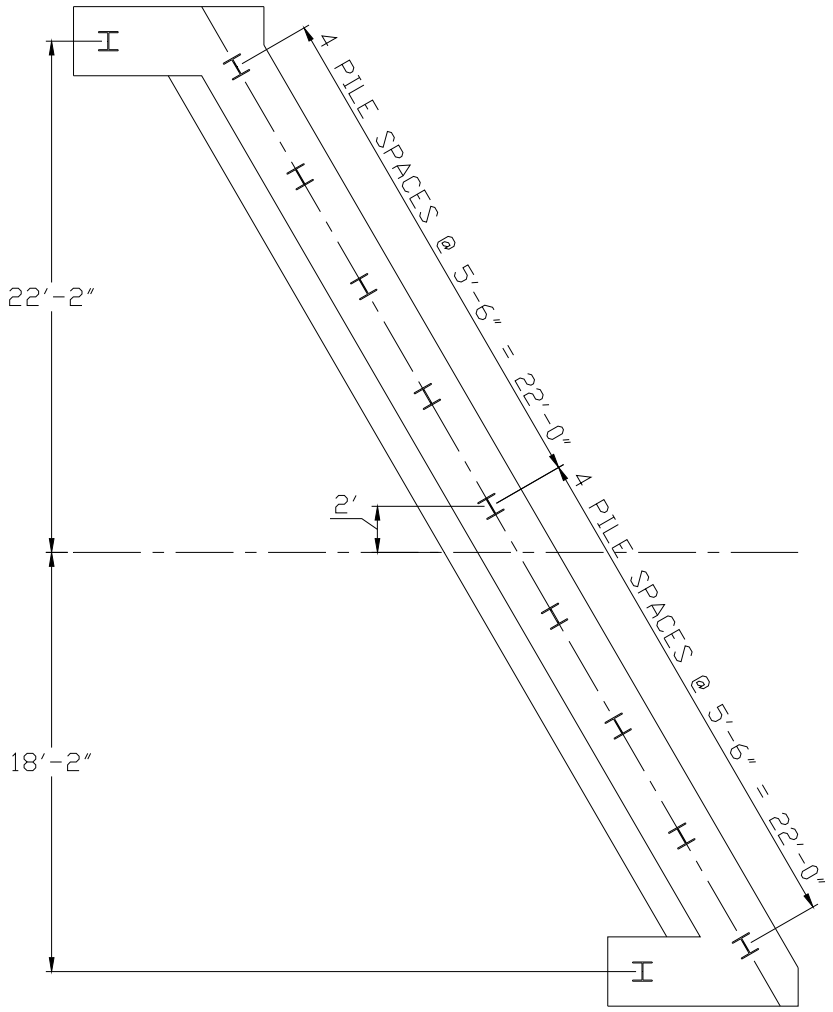


Figure 3.4. Plan view of a typical abutment

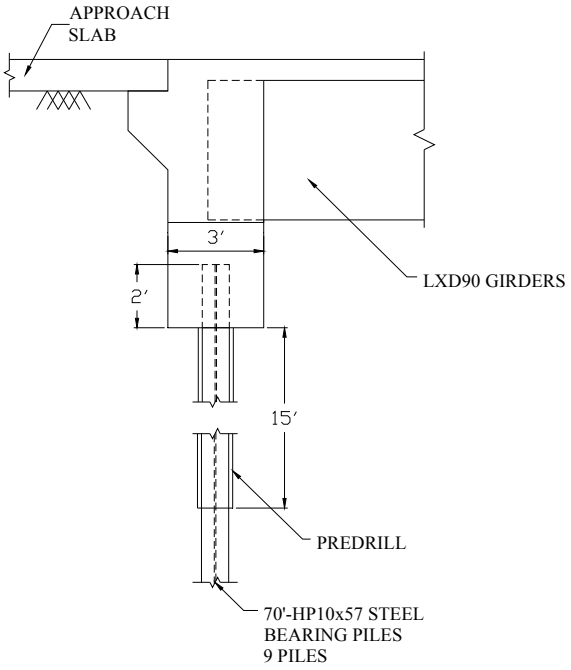


Figure 3.5. Elevation view of a typical abutment

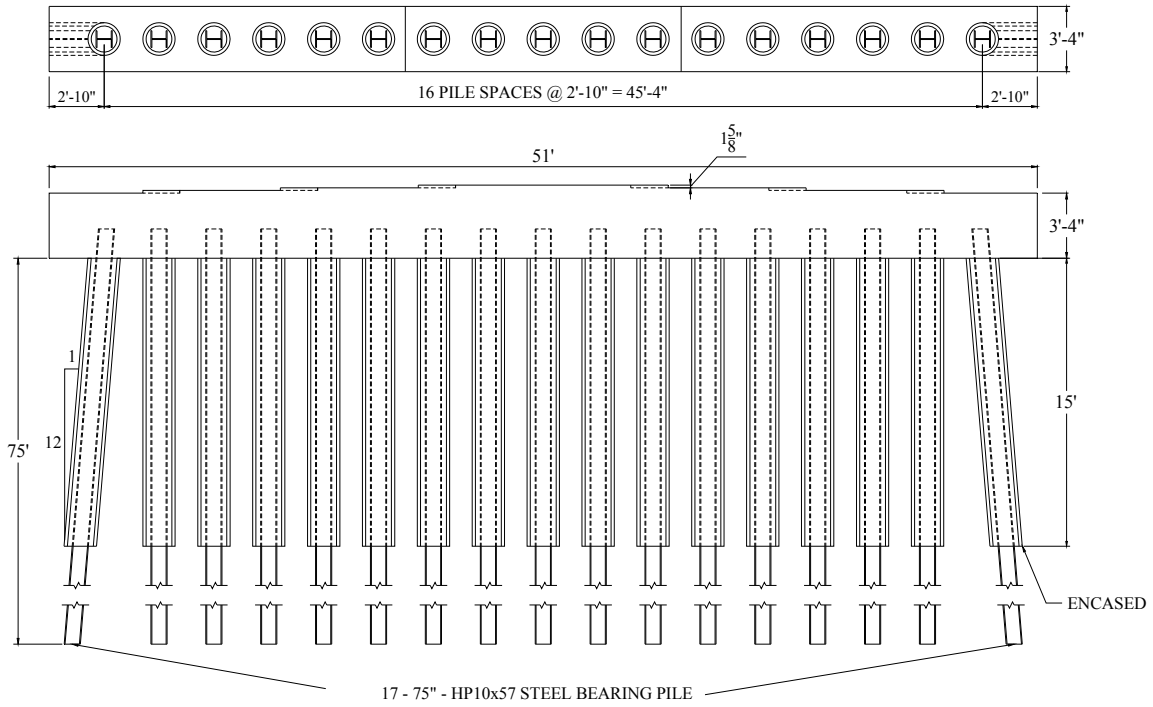


Figure 3.6. Typical pier plan view (top) and elevation view (bottom)

3.2. Approach Slab Description

While the bridges themselves are identical, the approach slabs differ from the northbound bridge to the southbound bridge. In both cases, however, the approach slabs are tied to the bridges. In the northbound direction, precast prestressed panels are used, while in the southbound direction a standard cast-in-place approach slab is used.

3.2.1. Precast Approach Slab – Northbound Bridge

The precast approach slab panels, shown in Figure 3.7, were designed by Dean Bierwagen of the Iowa DOT and Dave Merritt of The Transtec Group and were fabricated by Iowa Prestressed Concrete, Iowa Falls, Iowa. Each approach consists of eight panels that are nominally 12 in. thick. Six panels are rectangular panels 20 ft long by 14 ft wide. The remaining two panels are trapezoidal panels 14 ft wide with a 30 degree skew at the bridge end to match the bridge (see Figure 3.7). The approach slab is connected to the bridge by a vertical anchor bar drilled and grouted into the paving notch (see Figure 3.8). The holes in the panels were then filled with non-shrink grout. At the other end of the approach slab an IADOT standard EF expansion joint was used. A friction reducing polyethylene sheeting was used under the approach slab.

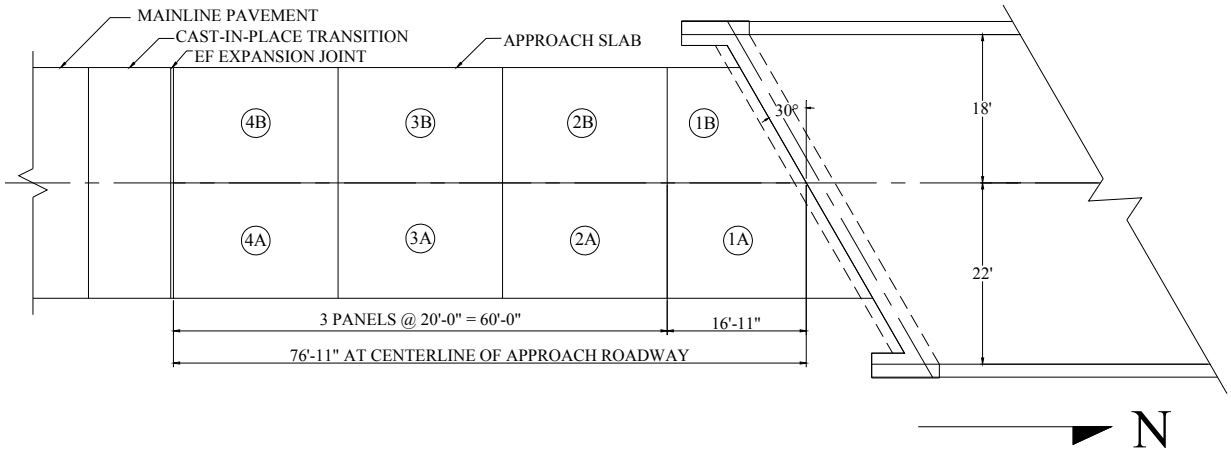


Figure 3.7. Plan view of precast approach slab (northbound bridge)

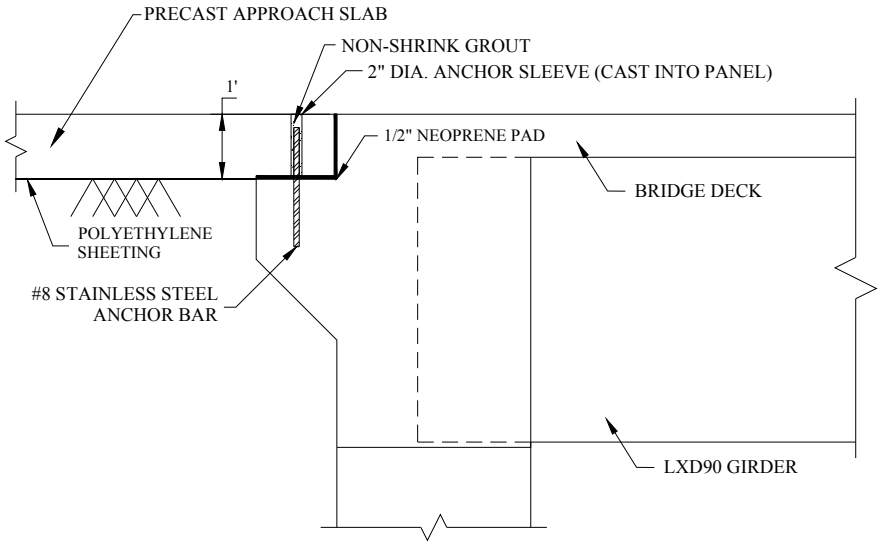


Figure 3.8. Connection detail for the precast approach slab to abutment

The transverse construction joint between panels is a male-female connection made by continuous shear keys cast into the panels (Figure 3.9). The shear keys help to ensure proper vertical alignment and load transfer of the longitudinal post-tensioning (PT). The longitudinal joint was and open joint in order to accommodate the crown of the roadway (see Figure 3.10). The resulting open joint was filled with grout after placement of the panels. One-inch diameter plastic post-tensioning ducts were used and spaced at approximately two feet on center in both the transverse and longitudinal direction to tie the panels together. All strands were stressed to 75% of the guaranteed ultimate stress. Additional panel details can be found in Merritt et. al (2007).

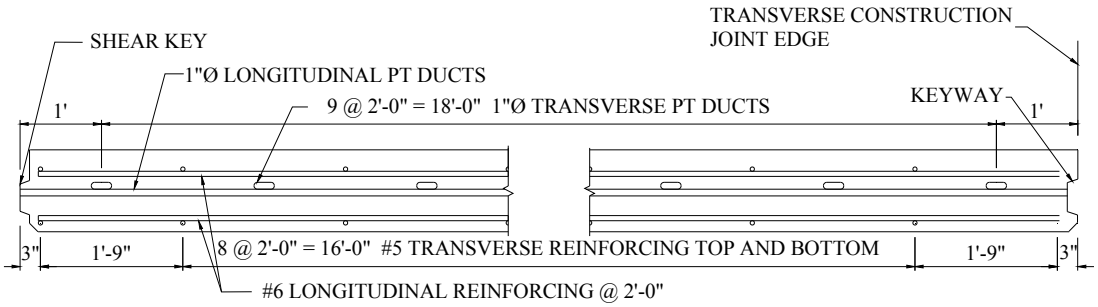


Figure 3.9. Precast panel detail along longitudinal edge

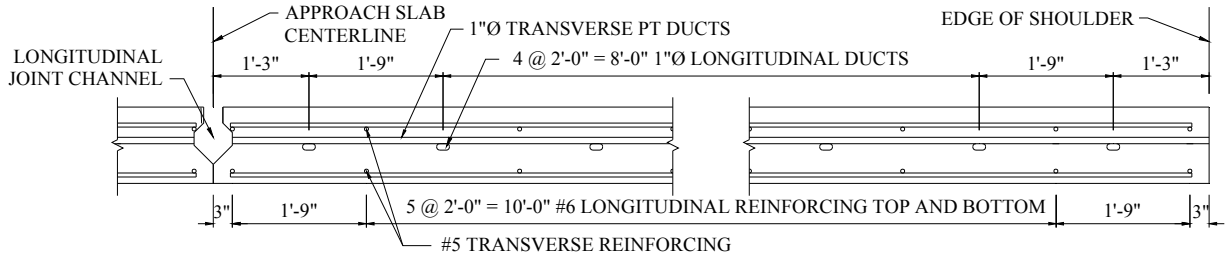


Figure 3.10. Precast panel detail along transverse edge

3.2.2. Cast-In-Place Approach Slab – Southbound Bridge

The cast-in-place approach slabs used for the southbound bridge are typical Iowa DOT approach slabs consisting of a 12 in. thick, doubly reinforced section from the bridge to the sleeper slab. The sleeper slab supports the end of the double reinforced section away from the bridge, as well as the next section of pavement which is a 12 in. thick single reinforced slab that terminates at tae non-reinforced approach slab. A standard 3 in. IADOT CF expansion joint is used between the approach slab and the sleeper slab. A typical "main pavement" configuration (see Figure 3.11) continues beyond the approach slab. This bridge differs from other typical Iowa bridges only in the fact that the approach slab was connected to the bridge and a sleeper slab was used. Similar to the northbound bridge a vertical anchor bar is used to connect the cast-in-place approach slab to the paving notch (see Figure 3.12).

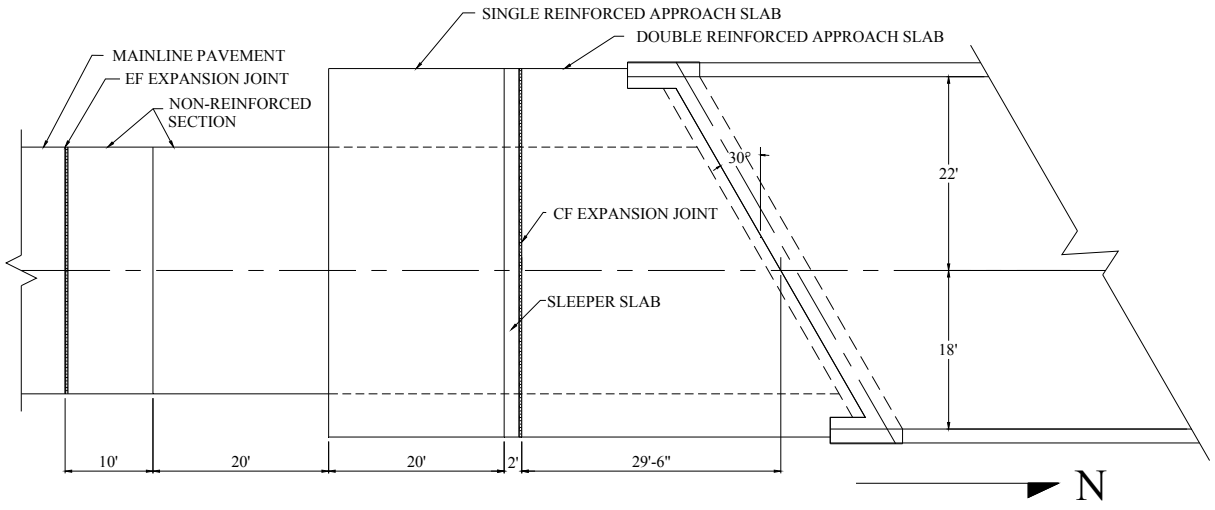


Figure 3.11. Plan view of cast-in-place approach slab (southbound bridge)

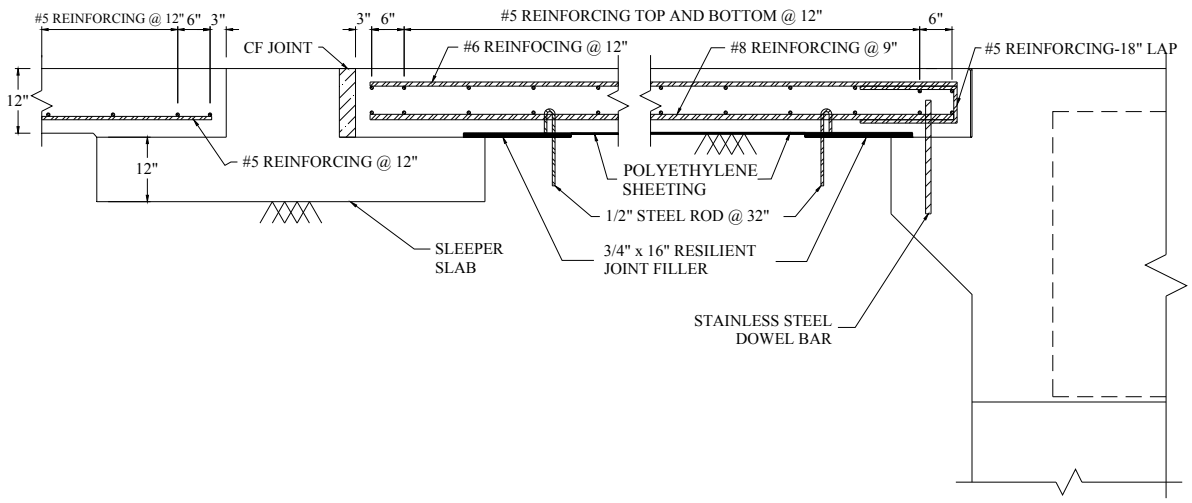


Figure 3.12. Elevation view of approach slab with connection detail

3.3. Instrumentation

All of the instrumentation used on this project consists of vibrating wire sensors manufactured by Geokon (see Figure 3.13). These sensors operate on the principle that a given wire will vibrate at a certain frequency dependent on the wire length and wire tension. As the length of the wire changes, so does the frequency. This is analogous to an electric guitar. Readings are taken by "plucking" the wire and measuring the frequency with an electromagnetic coil. These readings were collected by a Cambell 3000 data logger. The data logger contained a program which converted the readings to either strain, displacement, or tilt data and store the data on a memory card that was changed regularly. A wide variety of sensors (see Table 3.1) were installed on the bridge and the approach pavement, as shown in Figure 3.14 and listed in Table 3.2 and Table 3.3, to monitor the following behaviors:

- Temperature
- Bridge abutment movement (translation and rotation)
- Bridge girder strain changes
- Approach slab strain changes
- Post-tensioning strand losses
- Approach slab joint relative displacement
- Bridge abutment pile strain changes

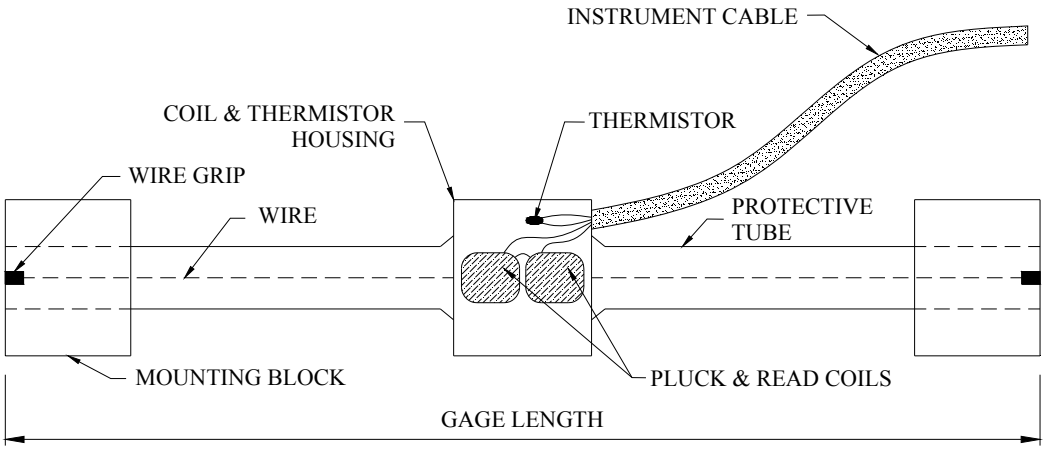


Figure 3.13. Typical vibrating wire gauge

Table 3.1. Instrumentation description, location, and quantity

		Location		Number of Gages	
Measurment	**Instrumentation**	**Northbound Bridge**	**Southbound Bridge**	**NB Bridge**	**SB Bridge**
Longitudinal abutment displacement	Displacement Tranducer	South abutment	South abutment	2	2
Transverse abutment displacement	Displacement Tranducer	South abutment	South abutment	1	1
Longitudinal abutment rotation	Tiltmeter	South abutment	South abutment	2	2
Strains in girders	Vibrating wire strain gauge	South span girders	South span girders	18	18
Strains in piles	Vibrating wire strain gauge	South abutment piles	South abutment piles	12	12
Joint movements	Vibrating wire crackmeters	South approach pavement joints	South approach pavement joints	10	4
Longitudinal post-tensioning strand losses	Vibrating wire strain gauge	Approach pavement	-	3	0
Transverse post-tensioning strand losses	Vibrating wire strain gauge	Approach pavement	-	4	0
Approach pavement strains	Vibrating wire strain gauge	Approach pavement	Approach Pavement	16	6
			Sub Total	68	45
			Total	113	

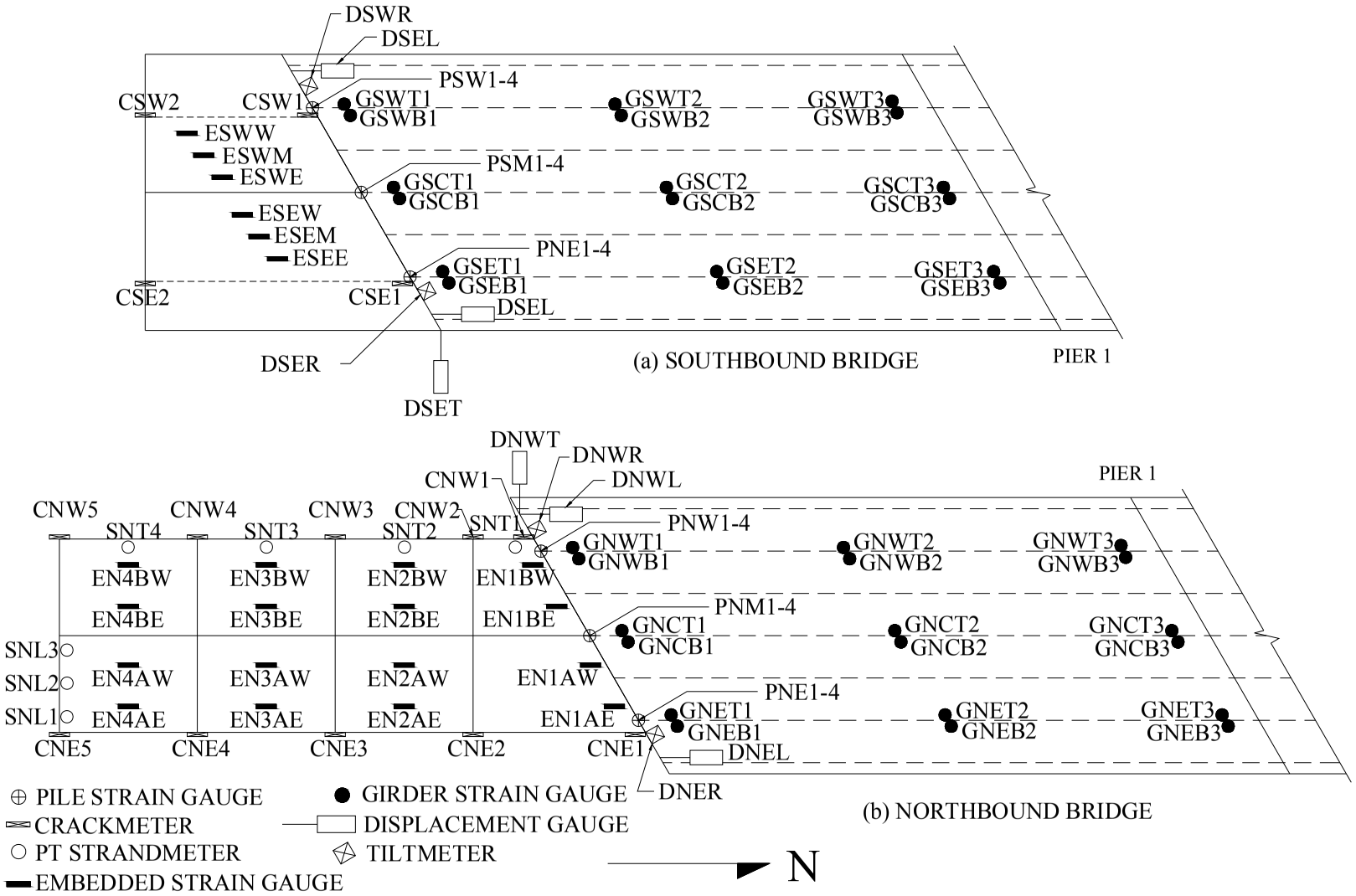


Figure 3.14. Instrumentation layout (a) southbound (b) northbound

Table 3.2. Northbound bridge gauge labels and location

Northbound Bridge			
Gauge No	**Gauge Label**	**Location**	**Measurement**
1 MP1	GNWT3	South span, west girder, top flange,pier end	Girder strain
2 MP1	GNWB3	South span, west girder, bottom flange, pier end	Girder strain
3 MP1	GNCT3	South span, center girder, top flange, pier end	Girder strain
4 MP1	GNCB3	South span, center girder, bottom flange, pier end	Girder strain
5 MP1	GNET3	South span, east girder, top flange, pier end	Girder strain
6 MP1	GNEB3	South span, east girder, bottom flange, pier end	Girder strain
7 MP1	GNWT2	South span, west girder, top flange, center span	Girder strain
8 MP1	GNWB2	South span, west girder, bottom flange, center span	Girder strain
9 MP1	GNCT2	South span, center girder, top flange, center span	Girder strain
10 MP1	GNCB2	South span, center girder, bottom flange, center span	Girder strain
11 MP1	GNET2	South span, east girder, top flange, center span	Girder strain
12 MP1	GNEB2	South span, east girder, bottom flange, center span	Girder strain
13 MP1	GNWT1	South span, west girder, top flange, abutment end	Girder strain
14 MP1	GNWB1	South span, west girder, bottom flange, abutment end	Girder strain
15 MP1	GNCT1	South span, center girder, top flange, abutment end	Girder strain
16 MP1	GNCB1	South span, center girder, bottom flange, abutment end	Girder strain
17 MP2	GNET1	South span, east girder, top flange, abutment end	Girder strain
18 MP2	GNEB1	South span, east girder, bottom flange, abutment end	Girder strain
19 MP2	DNWL	Southwest abutment corner	Longitudinal abutment displacement
20 MP2	DNWT	Southwest abutment corner	Transverse abutment displacement
21 MP2	DNWR	Southwest abutment corner	Longitudinal abutment rotation
22 MP2	PNW1	NW corner, west pile, south abutment	Pile strain
23 MP2	PNW3	NE corner, west pile, south abutment	Pile strain
24 MP2	PNW4	SE corner, west pile, south abutment	Pile strain
25 MP2	PNW2	SW corner, west pile, south abutment	Pile strain
26 MP2	PNM1	NW corner, middle pile, south abutment	Pile strain
27 MP2	PNM3	SE corner, middle pile, south abutment	Pile strain
28 MP2	PNM2	SW corner, middle pile, south abutment	Pile strain
29 MP2	PNM4	NE corner, middle pile, south abutment	Pile strain
30 MP2	PNE2	SW corner, east pile, south abutment	Pile strain
31 MP2	PNE1	NW corner, east pile, south abutment	Pile strain
32 MP2	PNE3	NE corner, east pile, south abutment	Pile strain
33 MP3	SNL1	Panel 4 east, east PT strand, near south end	Longitudinal PT strand losses
34 MP3	SNL2	Panel 4 east, middle PT strand, near south end	Longitudinal PT strand losses
35 MP3	SNL3	Panel 4 east, west Pt strand, near south end	Longitudinal PT strand losses
36 MP3	CNE1	East side, bridge to panel 1	Joint movement
37 MP3	CNE2	East side, panel 1 to panel 2	Joint movement
38 MP3	CNE3	East side, panel 2 to panel 3	Joint movement
39 MP3	CNE4	East side, panel 3 to panel 4	Joint movement
40 MP3	CNE5	East side, panel 4 to mainline pavement	Joint movement
41 MP3	EN1AE	Panel 1 east, east embedment	Pavement Strains
42 MP3	EN1AW	Panel 1 east, west embedment	Pavement Strains
43 MP3	EN2AE	Panel 2 east, east embedment	Pavement Strains
44 MP3	EN2AW	Panel 2 east, west embedment	Pavement Strains
45 MP3	EN3AE	Panel 3 east, east embedment	Pavement Strains
46 MP3	EN3AW	Panel 3 east, west embedment	Pavement Strains
47 MP3	EN4AE	Panel 4 east, east embedment	Pavement Strains
48 MP3	EN4AW	Panel 4 east, west embedment	Pavement Strains
49 MP4	EN1BW	Panel 1 west, west embedment	Pavement Strains
50 MP4	EN1BE	Panel 1 west, east embedment	Pavement Strains
51 MP4	EN2BW	Panel 2 west, west embedment	Pavement Strains
52 MP4	EN2BE	Panel 2 west, east embedment	Pavement Strains
53 MP4	EN3BW	Panel 3 west, west embedment	Pavement Strains
54 MP4	EN3BE	Panel 3 west, east embedment	Pavement Strains
55 MP4	EN4BW	Panel 4 west, west embedment	Pavement Strains
56 MP4	EN4BE	Panel 4 west, east embedment	Pavement Strains
57 MP4	SNT1	Panel 1, transverse PT strand at center of panel	Transverse PT strand losses
58 MP4	SNT2	Panel 2, transverse PT strand at center of panel	Transverse PT strand losses
59 MP4	SNT3	Panel 3, transverse PT strand at center of panel	Transverse PT strand losses
60 MP4	SNT3	Panel 4, transverse PT strand at center of panel	Transverse PT strand losses
61 MP4	PNE4	SE corner, east pile, south abutment	Pile strain
62 MP4	DNEL	Southeast abutment corner	Longitudinal abutment displacement
63 MP4	DNER	Southeast abutment corner	Longitudinal abutment rotation
64 MP4	CNW1	West side, bridge to panel 1	Joint movement
65 AVW4	CNW2	West side, panel 1 to panel 2	Joint movement
66 AVW4	CNW3	West side, panel 2 to panel 3	Joint movement
67 AVW4	CNW4	West side, panel 3 to panel 4	Joint movement
68 AVW4	CNW5	West side, panel 4 to mainline pavement	Joint movement

Table 3.3. Southbound bridge gauge labels and location

Southbound Bridge			
Gauge No	**Gauge Label**	**Location**	**Measurement**
69 MP5	GSWT3	South span, west girder, top flange,pier end	Girder Strain
70 MP5	GSWB3	South span, west girder, bottom flange, pier end	Girder Strain
71 MP5	GSCT3	South span, center girder, top flange, pier end	Girder Strain
72 MP5	GSCB3	South span, center girder, bottom flange, pier end	Girder Strain
73 MP5	GSET3	South span, east girder, top flange, pier end	Girder Strain
74 MP5	GSEB3	South span, east girder, bottom flange, pier end	Girder Strain
75 MP5	GSWT2	South span, west girder, top flange, center span	Girder Strain
76 MP5	GSWB2	South span, west girder, bottom flange, center span	Girder Strain
77 MP5	GSCT2	South span, center girder, top flange, center span	Girder Strain
78 MP5	GSCB2	South span, center girder, bottom flange, center span	Girder Strain
79 MP5	GSET2	South span, east girder, top flange, center span	Girder Strain
80 MP5	GSEB2	South span, east girder, bottom flange, center span	Girder Strain
81 MP5	GSWT1	South span, west girder, top flange, abutment end	Girder Strain
82 MP5	GSWB1	South span, west girder, bottom flange, abutment end	Girder Strain
83 MP5	GSCT1	South span, center girder, top flange, abutment end	Girder Strain
84 MP5	GSCB1	South span, center girder, bottom flange, abutment end	Girder Strain
85 MP6	GSET1	South span, east girder, top flange, abutment end	Girder Strain
86 MP6	GSEB1	South span, east girder, bottom flange, abutment end	Girder Strain
87 MP6	PSW2	SW corner, west pile, south abutment	Pile Strain
88 MP6	PSW1	NW corner, west pile, south abutment	Pile Strain
89 MP6	PSW4	SE corner, west pile, south abutment	Pile Strain
90 MP6	PSW3	NE corner, west pile, south abutment	Pile Strain
91 MP6	PSM4	SE corner, middle pile, south abutment	Pile Strain
92 MP6	PSM3	NE corner, middle pile, south abutment	Pile Strain
93 MP6	PSM2	SW corner, middle pile, south abutment	Pile Strain
94 MP6	PSM1	NW corner, middle pile, south abutment	Pile Strain
95 MP6	PSE1	NW corner, east pile, south abutment	Pile Strain
96 MP6	PSE4	SE corner, east pile, south abutment	Pile Strain
97 MP6	PSE3	NE corner, east pile, south abutment	Pile Strain
98 MP6	PSE2	SW corner, east pile, south abutment	Pile Strain
99 MP6	DSER	Southeast abutment corner	Longitudinal abutment rotation
100 MP6	DSWR	Southwest abutment corner	Longitudinal abutment rotation
101 MP7	DSWL	Southwest abutment corner	Longitudinal abutment displacement
102 MP7	DSEL	Southeast abutment corner	Longitudinal abutment displacement
103 MP7	DSWT	Southwest abutment corner	Transverse abutment displacement
104 MP7	CSW1	West edge, approach pavement to bridge	Joint Movement
105 MP7	CSW2	West edge, mainline pavement to approach pavement	Joint Movement
106 MP7	CSE1	East edge, approach pavement to bridge	Joint Movement
107 MP7	CSE2	East edge, mainline pavement to approach pavement	Joint Movement
108 MP7	ESWW	West lane, west embedment	Pavement Strains
109 MP7	ESWM	West lane, middle embedment	Pavement Strains
110 MP7	ESWE	West lane, east embedment	Pavement Strains
111 MP7	ESEW	East lane, west embedment	Pavement Strains
112 MP7	ESEM	East lane, middle embedment	Pavement Strains
113 MP7	ESEE	East lane, east embedment	Pavement Strains

3.3.1. Temperature

A thermistor encapsulated in the coil of each sensor (see Figure 3.13) records the temperature at the gauge at the same time the frequency of the wire is recorded. Since every gauge contains a thermistor, the temperatures in the approach slabs, the exterior temperature of the girders, and the temperature underground near the piles were recorded. Ambient temperature data were also collected from the archives of the National Climate Data Center (NCDC) and The Weather Channel website for the local community of Sheldon, IA.

3.3.2. Abutments

As a bridge heats and cools with the change in temperature and exposure to the sun, the superstructure expands and contracts. For an integral abutment bridge, the superstructure and abutment become one element, so that the abutment will be pushed and pulled accordingly.

Geokon Model 4427 Long Range Displacement Meters were used to measure these longitudinal and transverse movements of the bridge abutments. Displacement meters were installed at each end of the south abutments to measure the longitudinal displacement and a single transducer was installed on each south abutment to measure transverse displacement (see Figure 3.14).

A cable was extended from the displacement meter and attached to a reference post that is assumed not to move (see Figure 3.15). The cable is wound around a spring loaded drum in the displacement meter that keeps the cable taut. As the abutment displaces in relation to the post, rotation of the drum is converted into linear motion that is recorded by a vibrating wire transducer.

The reference posts, 3 in. diameter steel pipes, were initially installed near the toe of the embankment under the bridge. Four foot deep holes were drilled, the pipes were placed, and the hole and pipe were filled with concrete. Several months into the project, the initial longitudinal displacement reference posts were replaced with 2 in. diameter steel pipes because post movement was suspected. These new posts were installed 7 to 8 ft into the ground (see Figure 3.15). The bottom 3 to 4 ft of the holes were filled with concrete. In the top 3 to 4 ft of the holes a 6 in. diameter PVC pipe was used as casing to isolate the reference post from the soil. The cable running from the displacement meter to the reference post was enclosed in a PVC pipe to protect it from build up of snow, ice, and animals. Figure 3.16 shows a photograph of the installed displacement gauge.

In addition to the displacement meters, Geokon Vibrating Wire Tiltmeters were attached to the front abutment face as shown in Figure 3.15 to measure longitudinal rotation. As the bridge abutment rotates the effect of gravity on the mass inside the tiltmeter changes the force on an internal elastic hinge, changing the frequency of the vibrating wire in the elastic hinge. One tiltmeter was attached to each corner of the south abutment of each bridge (see Figure 3.14). Figure 3.16 is a photograph of an installed displacement gauge and tiltmeter and Figure 3.17 is a close up photograph of an installed tiltmeter.

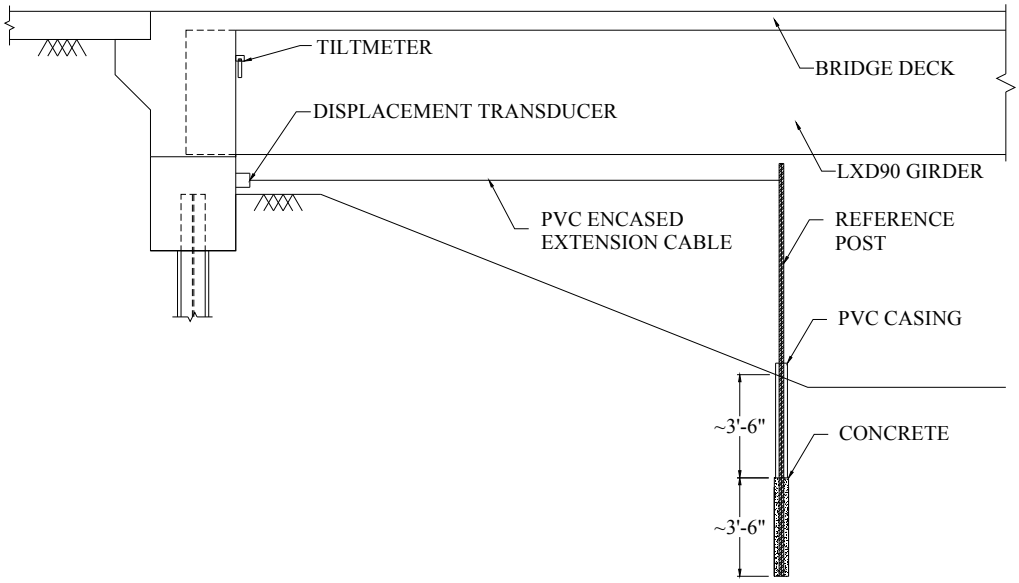


Figure 3.15. Typical displacement meter installation



Figure 3.16. Photograph of a displacement gauge and tiltmeter



Figure 3.17. Photograph of a tiltmeter

3.3.3. Girders

Geokon Model 4000 Vibrating Wire Strain Gauges were installed on the south span of each bridge along girders two, four, and six (see Figure 3.14). Gauges were placed on the top and bottom flanges as shown in Figure 3.18 at locations 5 ft from the abutment, mid-span, and 5 ft from the pier. Figure 3.19 is a photograph of an installed girder strain gauge.

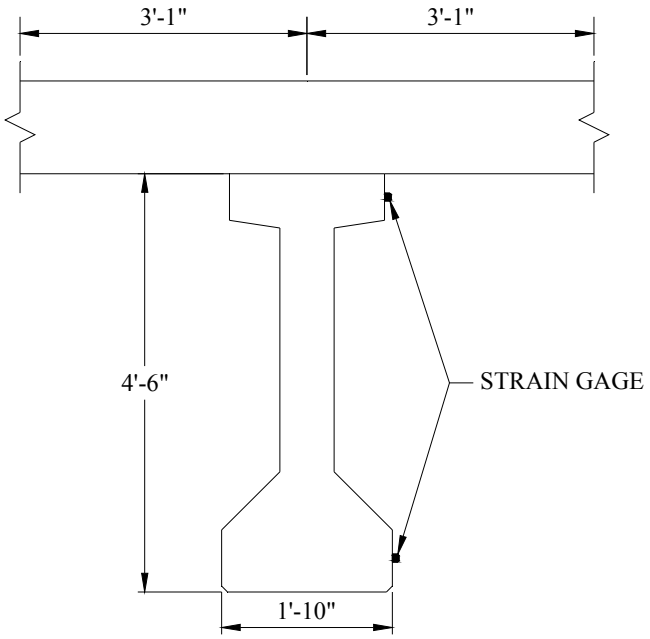


Figure 3.18. Typical girder strain gauge installation positions



Figure 3.19. Photograph of installed girder gauge

3.3.4. Approach Slabs

Embedded in the approach slabs were Geokon Model VCE-4200 Vibrating Wire Strain Gauges. For the cast-in-place approach slab, the sensors were installed mid-length of the doubly

reinforced section at mid-depth of the slab (see Figure 3.14). Three sensors were placed across each lane to measure longitudinal strain changes. In the precast panels, two sensors were installed across the panels at mid-length and mid-depth of each slab (see Figure 3.14).

The sensors were installed by placing blocks of wood between the sensor and a longitudinal reinforcing bar, and wire tying them together. Figure 3.20 is a photograph of an installed embedded strain gauge prior to concrete placement. Concrete was placed, leaving the sensors cast in the concrete.

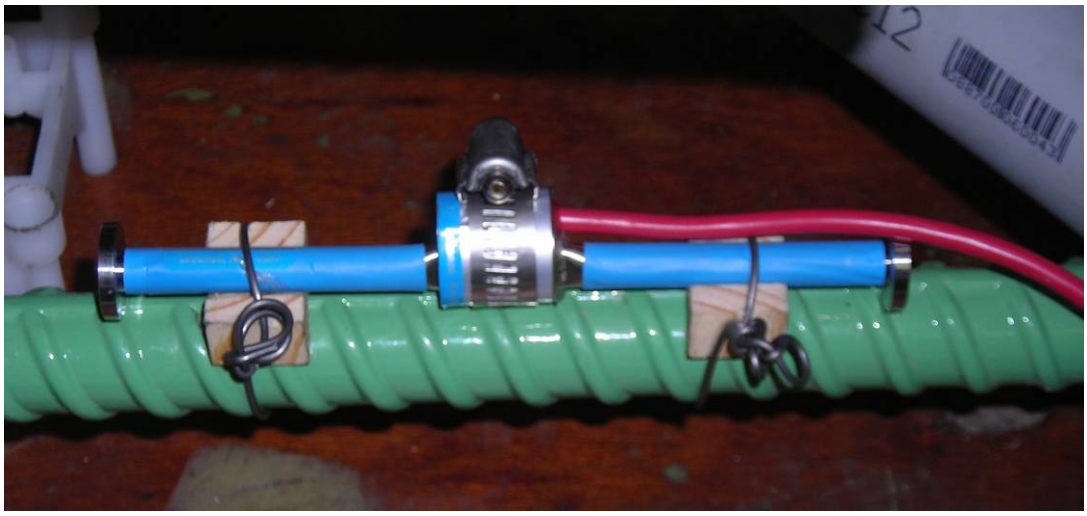


Figure 3.20. Photograph of an installed embedded strain gauge

3.3.5. Post-Tensioning Strands

Pre-formed block-outs in the precast panels allowed access to the post-tensioning strands. After the strands were tensioned and grouted, the duct was removed and the grout chipped away from the strands. Geokon Model 4410 Vibrating Wire Strandmeters, which are 8 in. long, were then installed on the strands. The sensor was covered by a protective PVC casing and the block-out filled with concrete. Figure 3.21 is a photograph showing an installed strandmeter prior to attaching the top half of the casing and filling the block out with concrete.

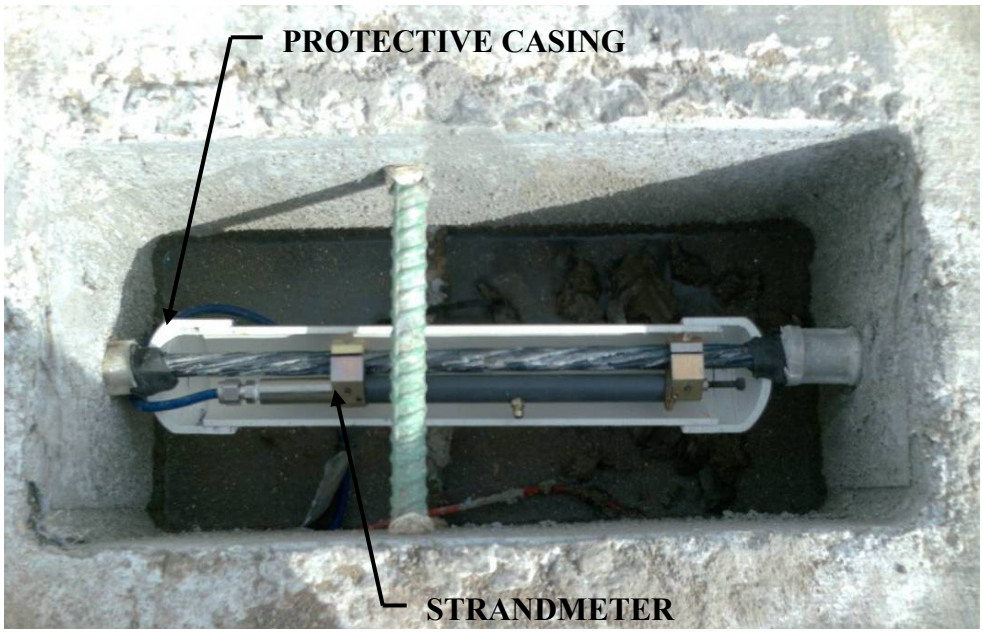


Figure 3.21. Photograph of an installed strandmeter

3.3.6. Joints

Across the transverse approach slab precast panel joints, the expansion joints, and the bridge to approach slab joints , Geokon Model 4420 Vibrating Wire Crackmeters were installed (see Figure 3.14). Special block-outs were cast into the approach slabs at the joint to accommodate the sensors. An installed crackmeter is shown in the photograph in Figure 3.22. As the joint opens and closes, the relative movement of the crackemeter ends is recorded.

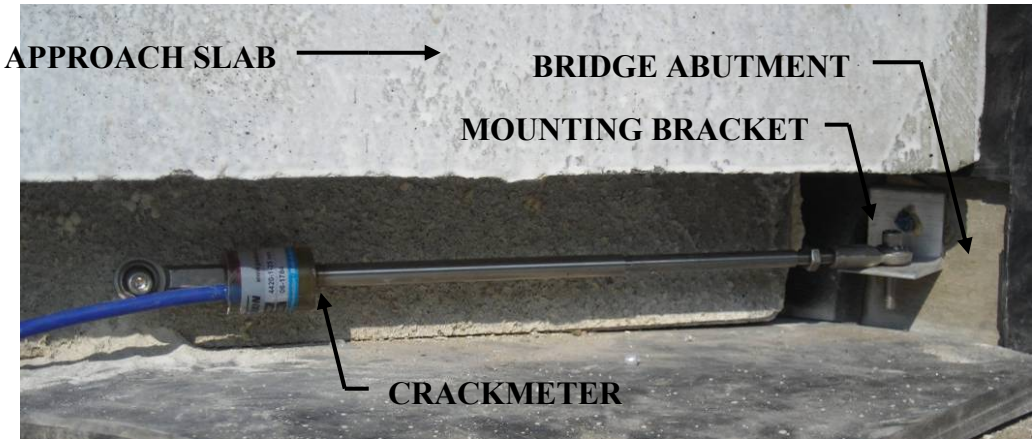


Figure 3.22. A crackmeter installed across the bridge-to-approach slab joint

3.3.7. Piles

Geokon Model 4150 Spot-Weldable Vibrating Wire Strain Gauges were epoxied to the flanges of piles two, five, and eight beneath the south bridge abutments on both bridges (see Figure 3.23). Four sensors were installed per pile, 1 in. from the flange tips (see Figure 3.24) and 1 ft below the bottom of the abutment. Figure 3.25 is a photograph showing an instrumented pile.

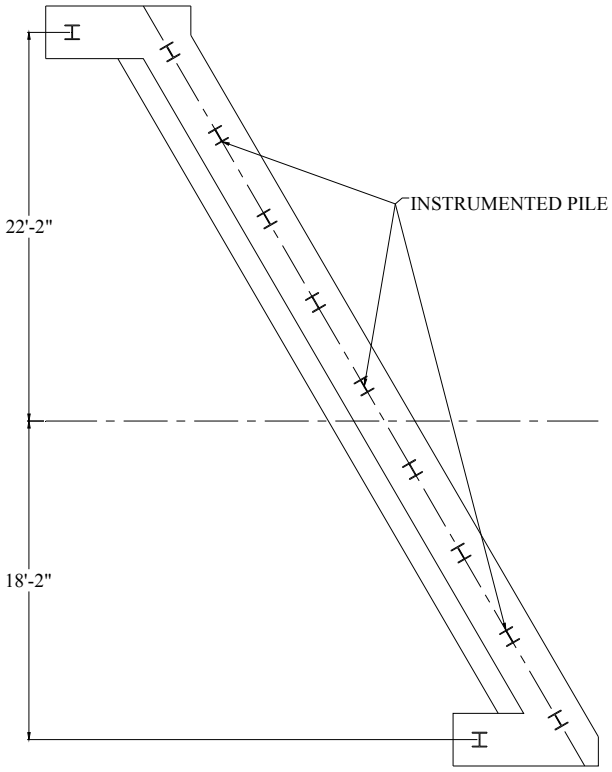


Figure 3.23. Instrumented pile plan

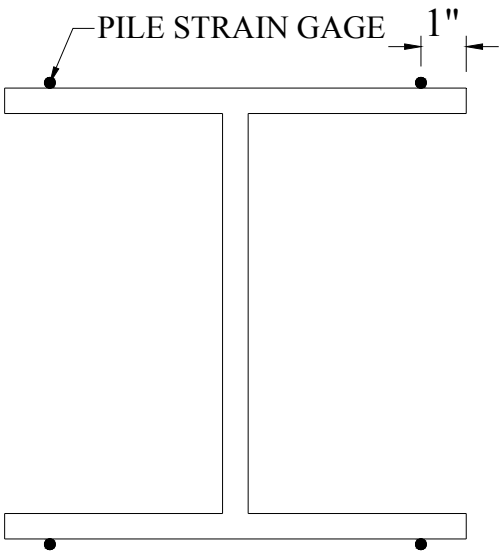


Figure 3.24. Pile strain gauge layout



Figure 3.25. Photograph of an instrumented pile

4. NORTHBOUND BRIDGE RESULTS

4.1. Temperature

4.1.1. Approach Slab Temperatures

The internal temperature of the precast concrete approach slab is measured by the thermistor on each embedded approach slab strain gauge. As described in Section 3.3.4 the embedded gauges are located along and across the approach slab as shown in Figure 3.14 at the mid-depth of the approach slab and, as such, the temperature gradients that occur through the slab thickness can not to be measured. These gradients occur because the top surface is exposed to the air temperature and solar radiation which cause the concrete to heat and cool faster than the bottom of the slab which is in contact with the ground causing slower heating and cooling.

The temperature recorded by the thermistors is shown in Figure 4.1 plotted with respect to the position of the gauge along the slab. Note that the typical "hot" temperature data were from August 1st at 5:00 pm and the typical "cold" temperature data are from January 20th at 6:00 am. Also note that these "hot" and "cold" times will be used throughout this report, unless otherwise specified, and are not necessarily the extreme hot and cold temperatures for the testing period. Figure 4.1 shows that the temperature across and along the slab is relatively uniform. Along the slab the temperature remains very consistent through the first three panels (0 to 50 ft). At the panel where the slab meets the bridge (70 to 80 ft) the temperatures tend to be slightly warmer during the hot days and slightly cooler during the cold days. Because the temperature variation is small, (5 to 10 °F), the results from all 16 gauges have been averaged together and are shown with time in Figure 4.2.

4.1.2. Bridge Superstructure Temperatures

The temperature of the bridge superstructure is not measured directly but is, most likely, close to the temperatures measured by the thermistors on the girder strain gauges. As described in Section 3.3.3 the girder strain gauges are located along the girder top and bottom flanges as shown in Figure 3.14 and Figure 3.18. Because the gauges are located on the exterior of the girders and not embedded, the deck temperature gradients and the effect of solar radiation on the bridge deck can not be studied.

The temperatures recorded by the girder strain gauges are shown in Figure 4.3 and Figure 4.4 for the top and bottom girder flanges, respectively, for the hot and cold days identified in Section 4.1.1. Variation across the bridge is shown by the different series for each girder. Unlike the approach slab when only a single gauge was used, temperature variation between the top and the bottom of the girder can be observed. As can be seen, the temperature remains almost constant both across the bridge and along the girders for both the top and bottom girder gauges.

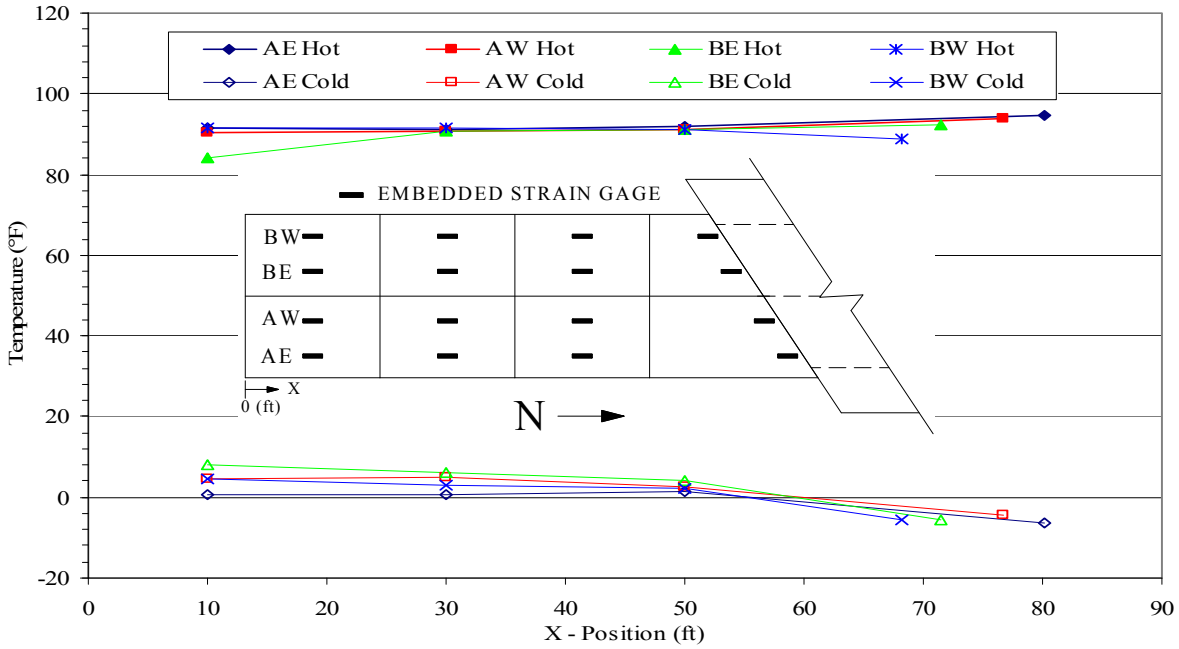


Figure 4.1. Temperature variation in the northbound bridge precast approach slab

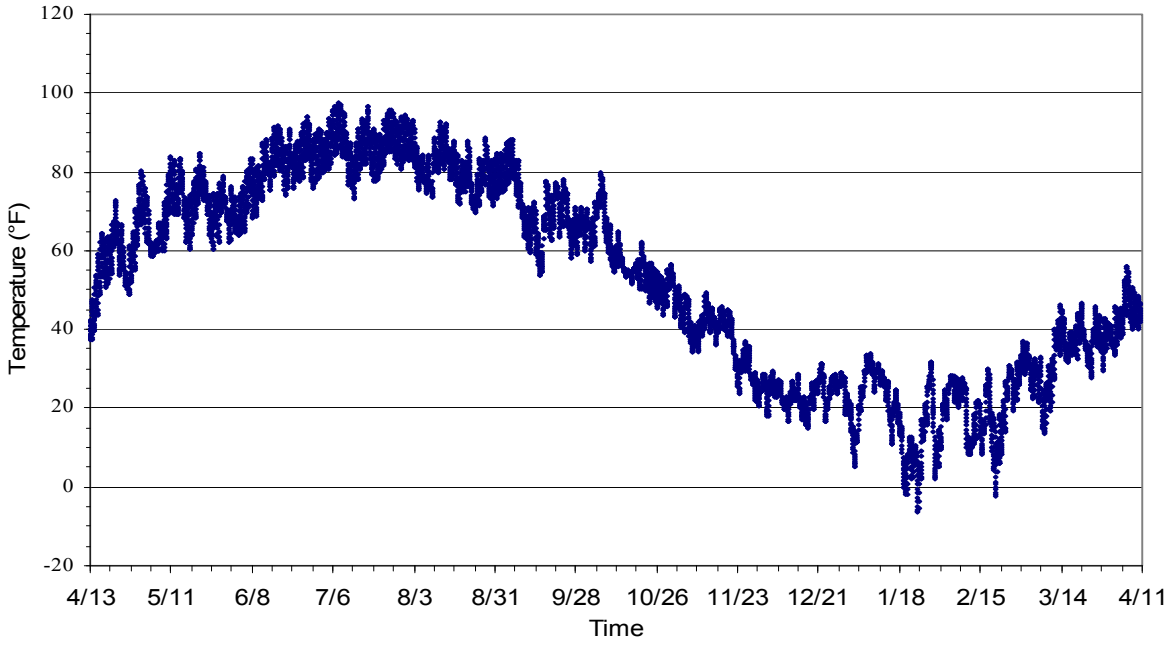


Figure 4.2. Average northbound bridge approach slab temperature versus time

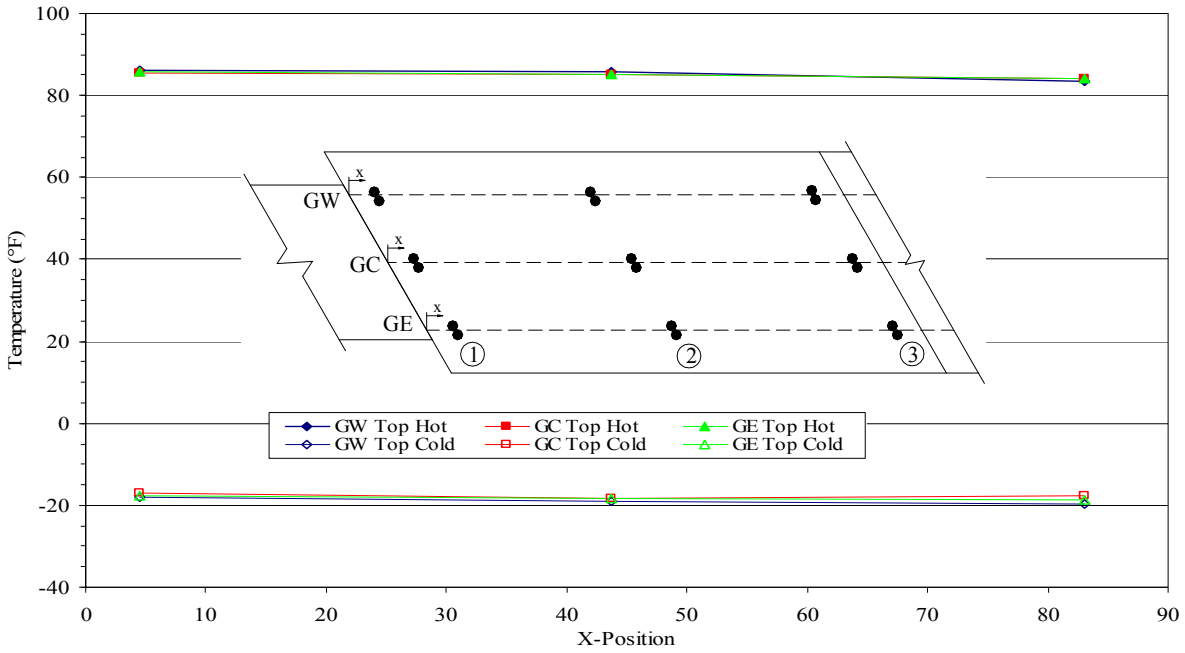


Figure 4.3. Temperature variation at the top of the northbound bridge girders

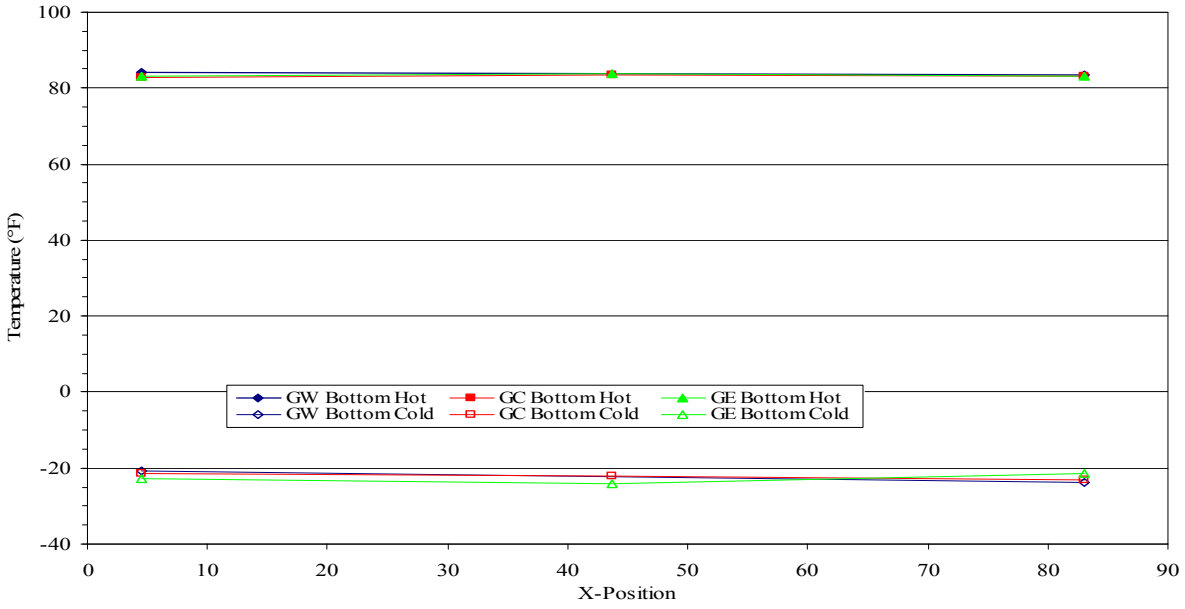


Figure 4.4. Temperature variation at bottom of the northbound bridge girders

Because of the small variation in the temperatures for the top and bottom flanges, the temperatures were averaged transversely across the bridge and the results of this averaging are plotted relative to their positions along the girders and shown in Figure 4.5.

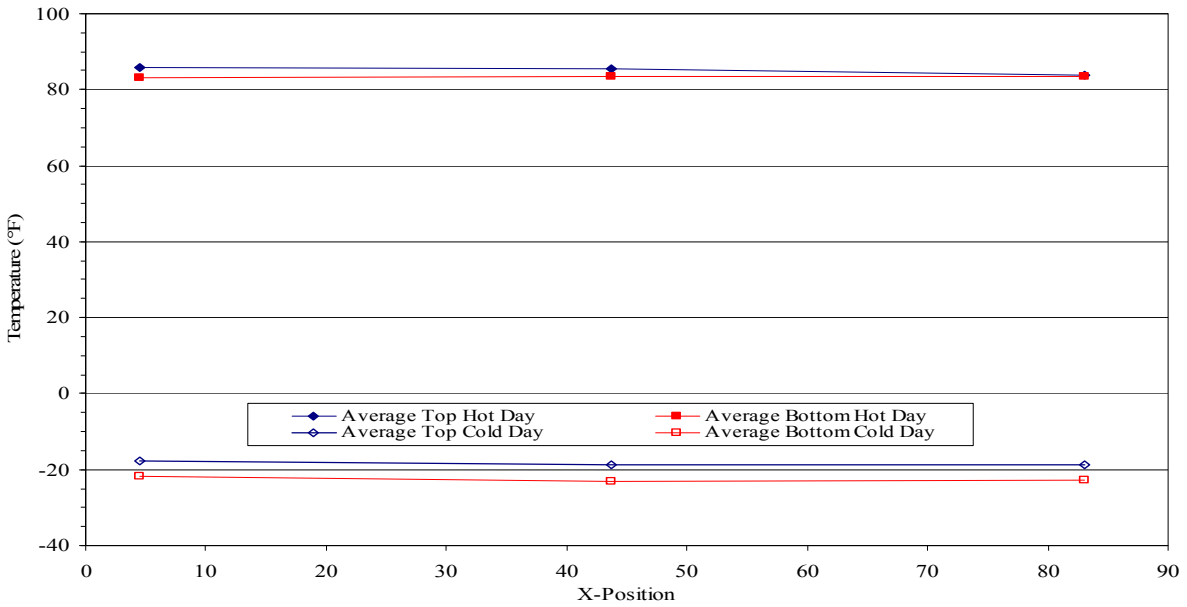


Figure 4.5. Average northbound bridge temperature variations with position

Figure 4.5 shows that there is only a few degrees difference in temperature between the top and bottom of the girders. Therefore it appears reasonable to average the 8 gauges on the top flanges and the 8 gauges on the bottom flanges together (GNWB2 thermistor did not work, so neither GNWB2 nor GNWT2 were used in the average). The resulting average temperature (referred to herein as the "average bridge temperature") is plotted against time in Figure 4.6.

The average bridge temperature in Figure 4.6 was compared to the observed Sheldon, IA ambient air temperature (referred to herein as the "air temperature") daily highs and lows gathered from the Weather Channel website for Sheldon, IA. The resulting comparison is shown in Figure 4.7. Weather Channel data were not gathered in July and are unavailable at this time. While the air temperatures do not exactly match the bridge temperatures, the two correlate well, with the exception of the extreme cold temperatures. The correlation between bridge and air temperature can be seen in Figure 4.8 where the daily high and low air temperatures are plotted against the daily high and low average bridge temperatures. A linear regression analysis was performed and indicates that a correlation with an R^2 greater than 0.95 existed for both the high and low values. The average high bridge temperature is about 3.86°F below the high air temperature. The average low bridge temperature was above the low air temperature on hot days, both of which tended to occur just before sunrise. On these days, the thermal mass of the bridge was retaining the heat of the previous day during the night while the air cooled more. On cold days (December to March), the average low bridge temperature was lower than the air temperature, which could not be explained.

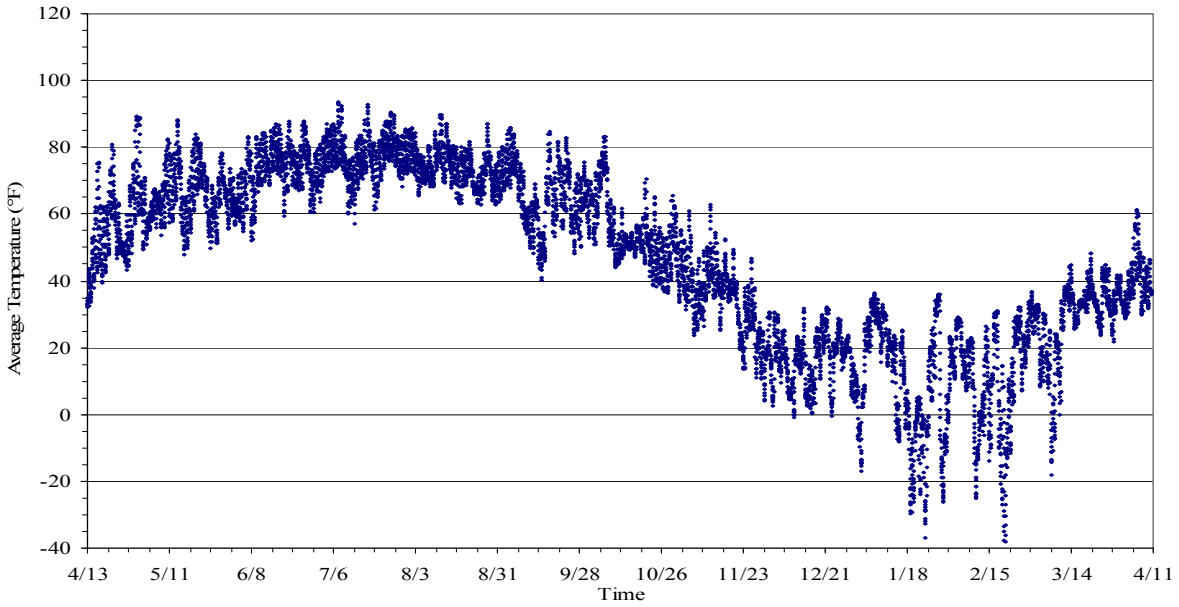


Figure 4.6. Average northbound bridge temperature over time

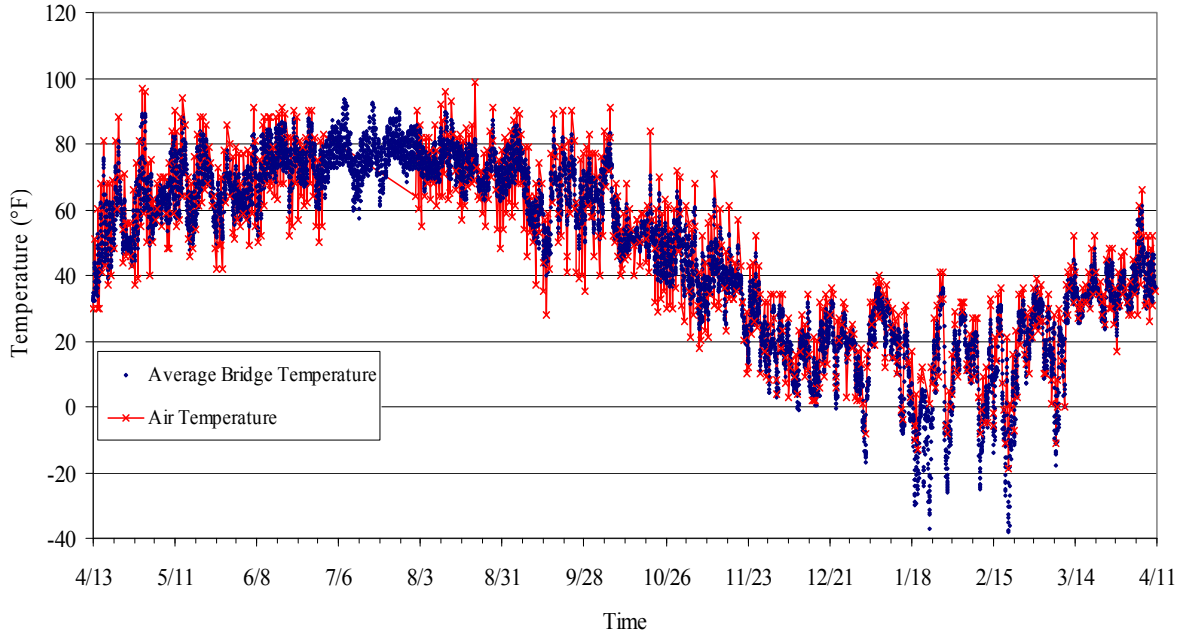


Figure 4.7. Average northbound bridge and Sheldon, IA air temperatures over time

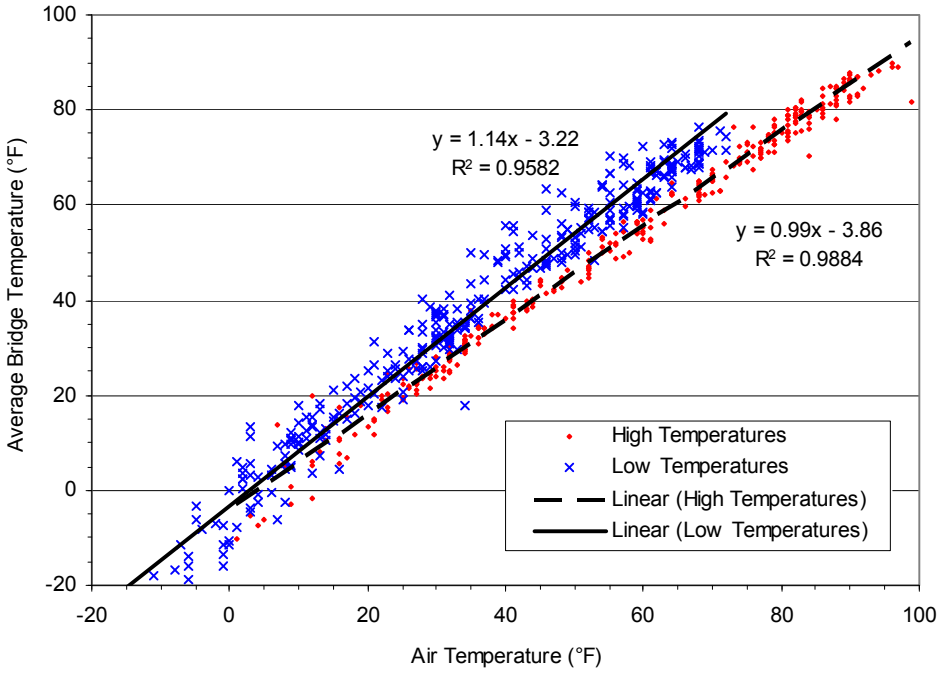


Figure 4.8. Correlation of daily high and low Sheldon, IA air to northbound bridge temperatures

The average bridge temperature range was compared to bridge temperature ranges previously found by Abendroth and Greimann (2005) and their recommended design temperature range, as well as the temperature range recommended by AASHTO Article 3.12.2.2 Procedure B in Table 4.1.

Table 4.1. Experimentally measured and recommended average bridge temperatures

Source	Average Bridge Temperatures (°F)		
	Minimum	Maximum	Range
Guthrie County Bridge (Abendroth and Greimann 2005)	-12	101	113
Story County Bridge (Abendroth and Greimann 2005)	-11	104	115
Boone River Bridge (Girton, etal. 1989)	-15	100	115
O'Brien County Bridge	-41	93	134
AASHTO - LRFD Specification (2006) Procedure B Article 3.12.2.2	-10	110	120
Abendroth and Greimann (2005)	-6	109	115

4.2. Bridge Superstructure

4.2.1. Abutment Displacement

As previously discussed, the south abutments of the bridges were instrumented to measure displacement (i.e., longitudinal and transverse translation and rotation of the abutment in the longitudinal direction (see Figure 3.15 and Figure 4.9)). The displacement transducer measures the longitudinal displacement, referred to as $\Delta_{abut,}$ of the abutment near the base. Displacement caused by rotation of the abutment is referred to as $\Delta_{\theta.}$ Positive displacement due to both sources is illustrated in Figure 4.9.

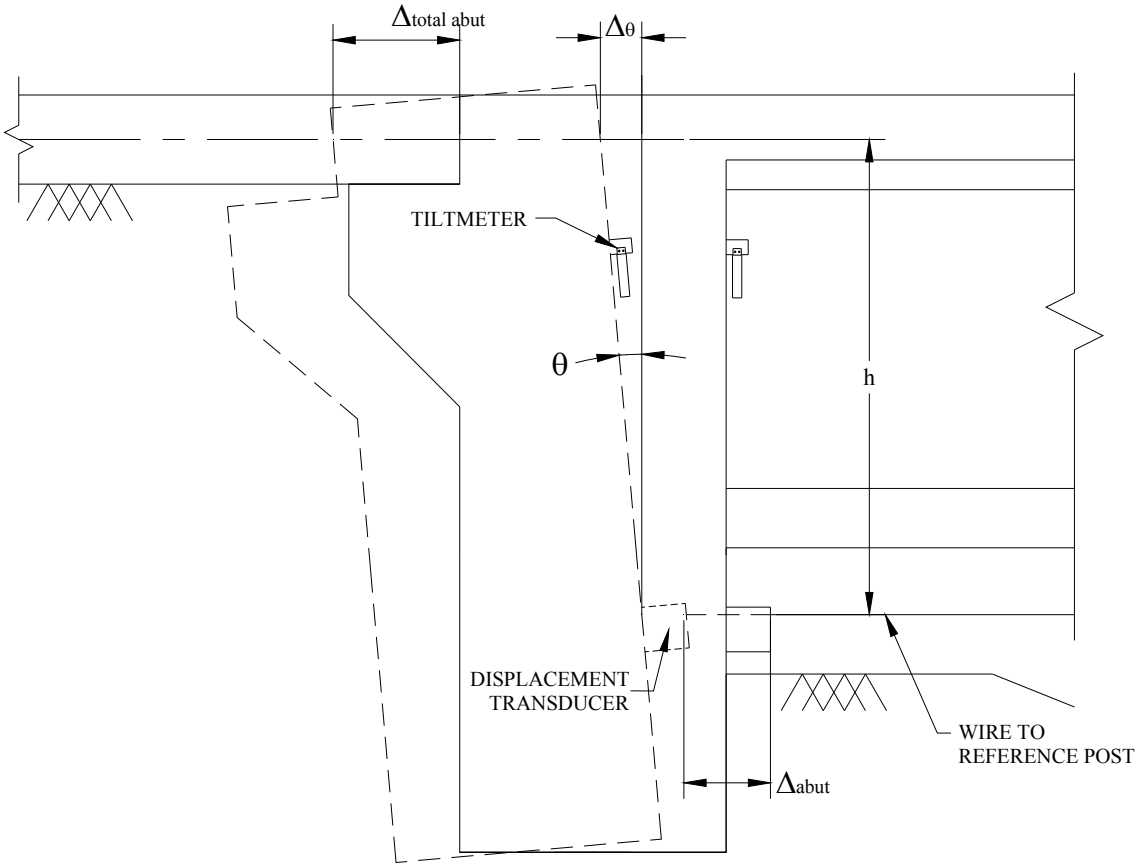


Figure 4.9. Drawing showing displacement and rotation of a typical abutment

As the temperature changes, the extension wire from the transducer to the reference post also expands and contracts. To compensate for this, the change in wire length must be added to the displacement reading (see Equation 4.1).

$$\Delta_{abut} = \Delta R * G + \alpha_w * \Delta T_w * L_w \tag{4.1}$$

Where:
ΔR = Change in recorded displacement
G = Gauge calibration factor
α = Coefficient of thermal expansion
L = Length
ΔT = Change in temperature
w = Properties or changes of the extension wire

Here the wire temperature has been assumed to be equal to the average of the recorded temperatures at the displacement gauges because they correlate well with the air temperature (refer to Section 4.1.2 for explanation on temperatures) as shown for a typical period in Figure 4.10. A representative plot of the corrected actual abutment displacement relative to initial readings taken April 13, 2007 versus time is shown in Figure 4.11. As can be seen the typical displacement range is approximately -0.45 in. to 0.4 in. for a total movement of 0.85 in. (Note that here, and in subsequent sections, that data felt to be "noise" are not considered when stating maximums, minimums, and ranges).

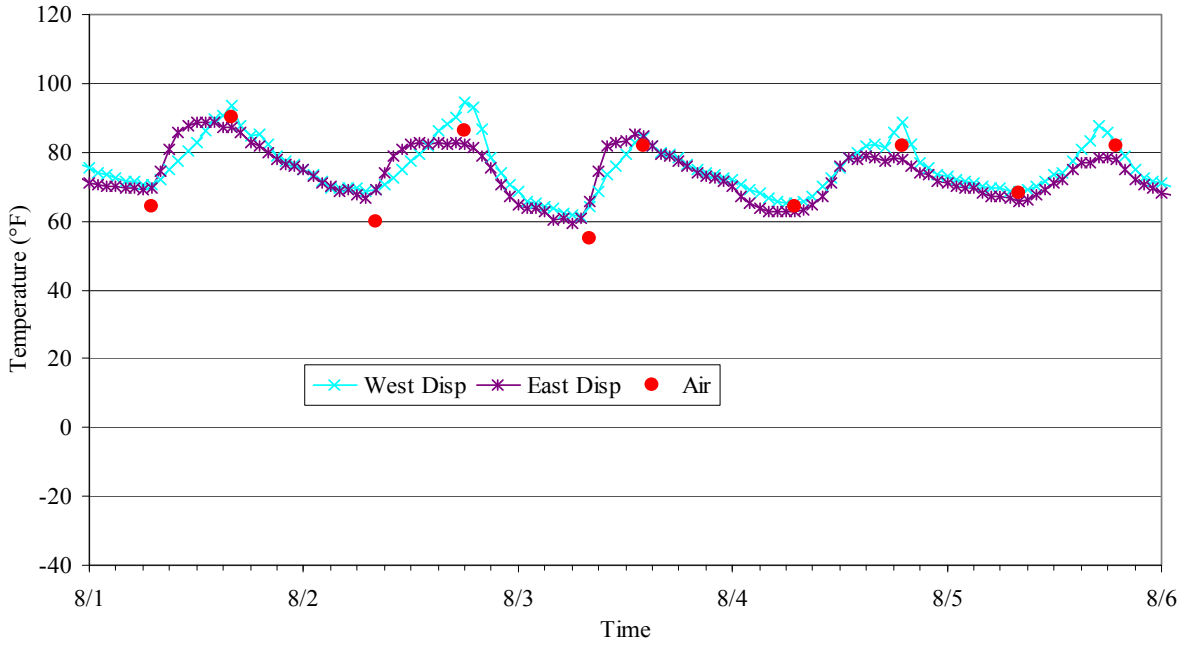


Figure 4.10. Typical recorded northbound bridge displacement transducer temperatures and air temperature versus time

As the abutment rotates in the longitudinal bridge direction by an angle, θ, the total displacement at a point above or below the transducer a distance h differs from the measured displacement by the rotation induced displacement, Δ_{θ}. Figure 4.9 illustrates the positive directions for Δ_{abut}, θ, and Δ_{θ}. At the mid-depth of the approach slab the total displacement of the abutment in the longitudinal direction, $\Delta_{total\ abut}$, given by:

$$\Delta_{totalabut} = \Delta_{abut} + \Delta_{\theta} \tag{4.2}$$

$$\Delta_{\theta} = h * \theta \text{ (for small angles)} \tag{4.3}$$

Typical displacement at the approach slab mid-depth due to abutment rotation alone is shown in Figure 4.12. As it turns out, the abutments rotate very little, approximately only 0.05 degrees on average. This results in an almost negligible difference in displacement between the location of the displacement transducers and the mid-depth of the approach slab.

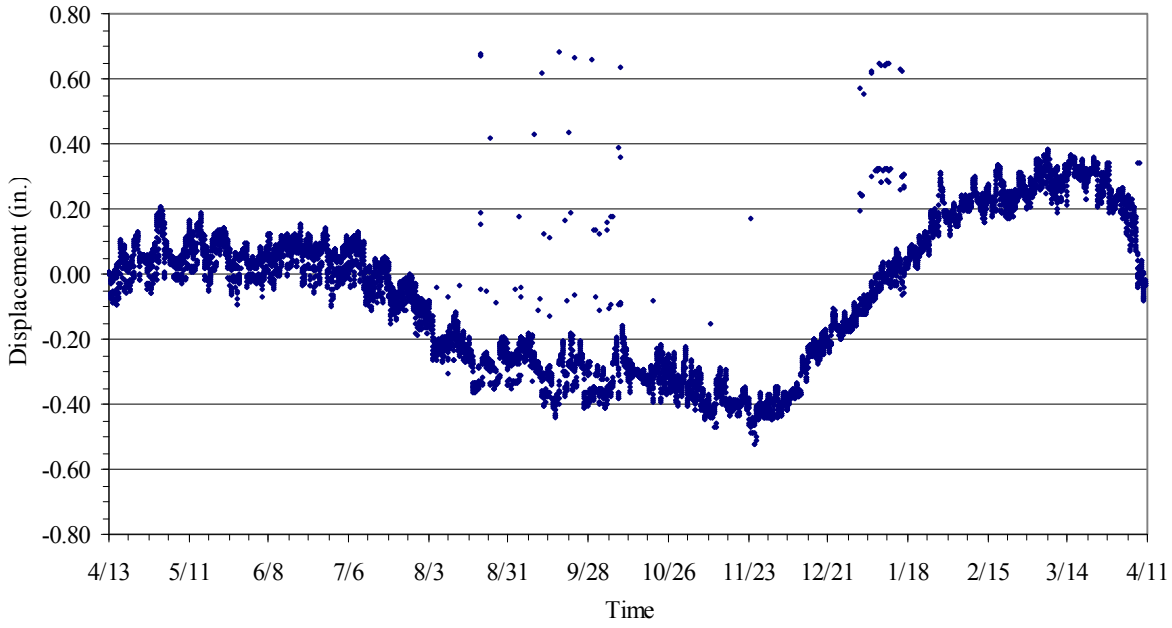


Figure 4.11. Typical northbound bridge abutment displacement (Δ_{abut}) over time

Even though the displacement due to abutment rotation was very small, for completeness it was taken into account for this work. Figure 4.13 shows the total displacement at the approach slab mid-depth at the west end of the abutment. Similarily, Figure 4.14 shows the total displacement at the approach slab mid-depth at the east end of the abutment. The west end displacement ranges from -0.45 in. to 0.35 in. while the east end displacement ranges from -0.7 to 0.1 in. The difference in displacement between the west and the east end of the abutment may be a result of the bridge skew. The displacement at the center of the bridge was estimated by averaging the east and west displacements, which is shown in Figure 4.15 to range from -0.6 in. to 0.2 in. for a total range of 0.8 in.

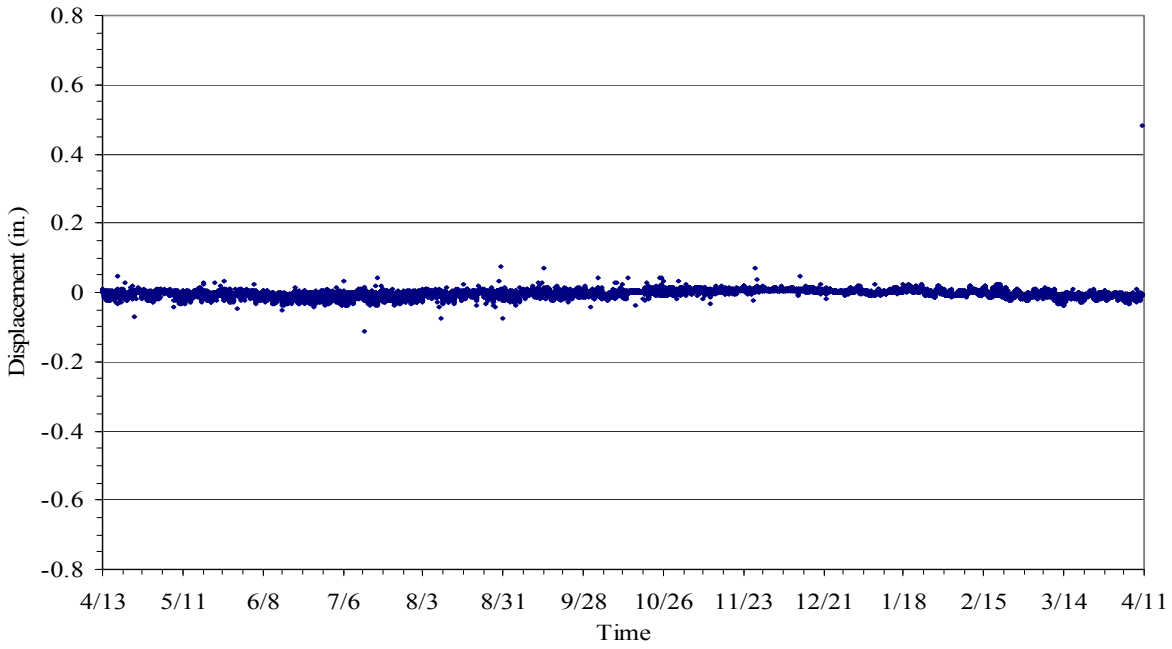


Figure 4.12. Typical displacement of the northbound bridge abutment due to abutment rotation over time

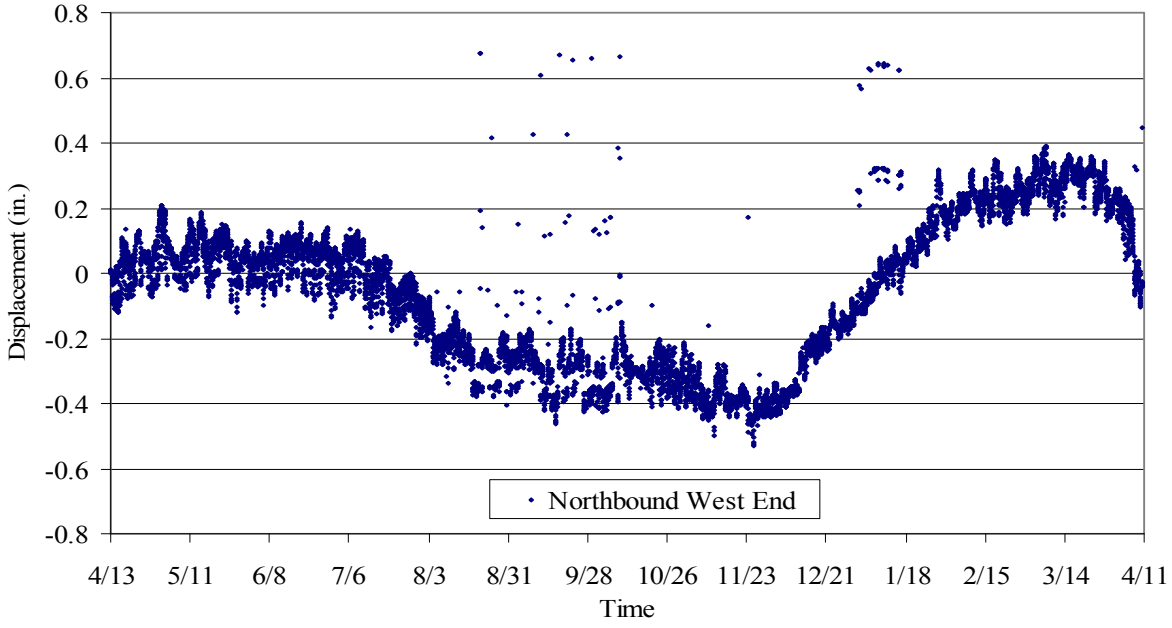


Figure 4.13. Total northbound bridge abutment displacement at slab mid-depth over time at west end

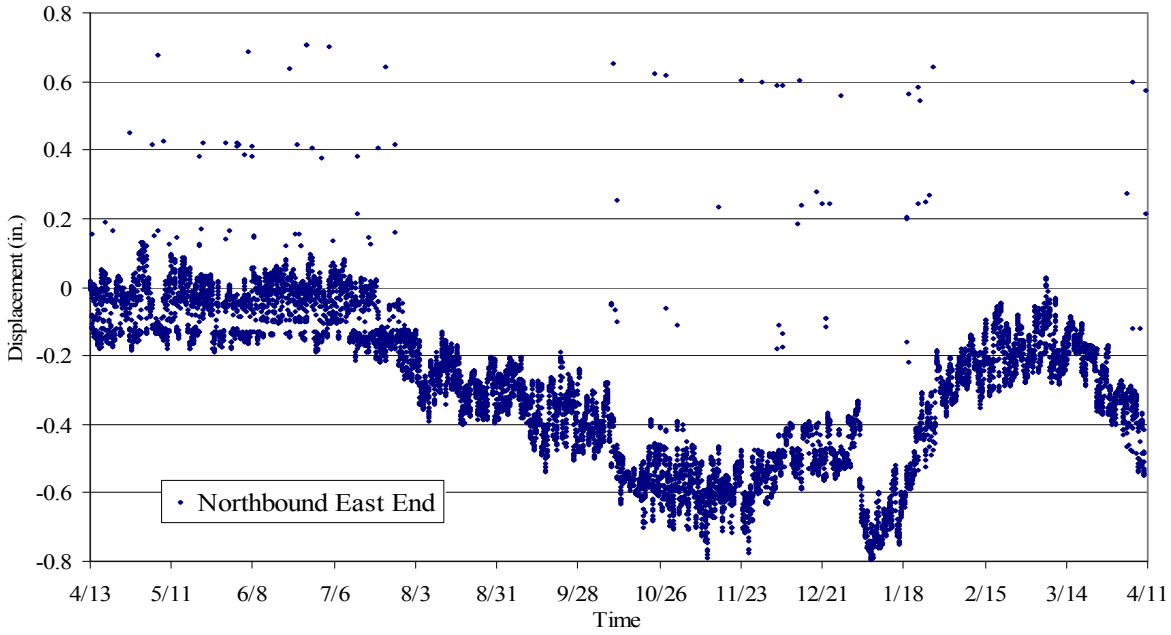


Figure 4.14. Total northbound bridge abutment displacement at slab mid-depth over time at east end

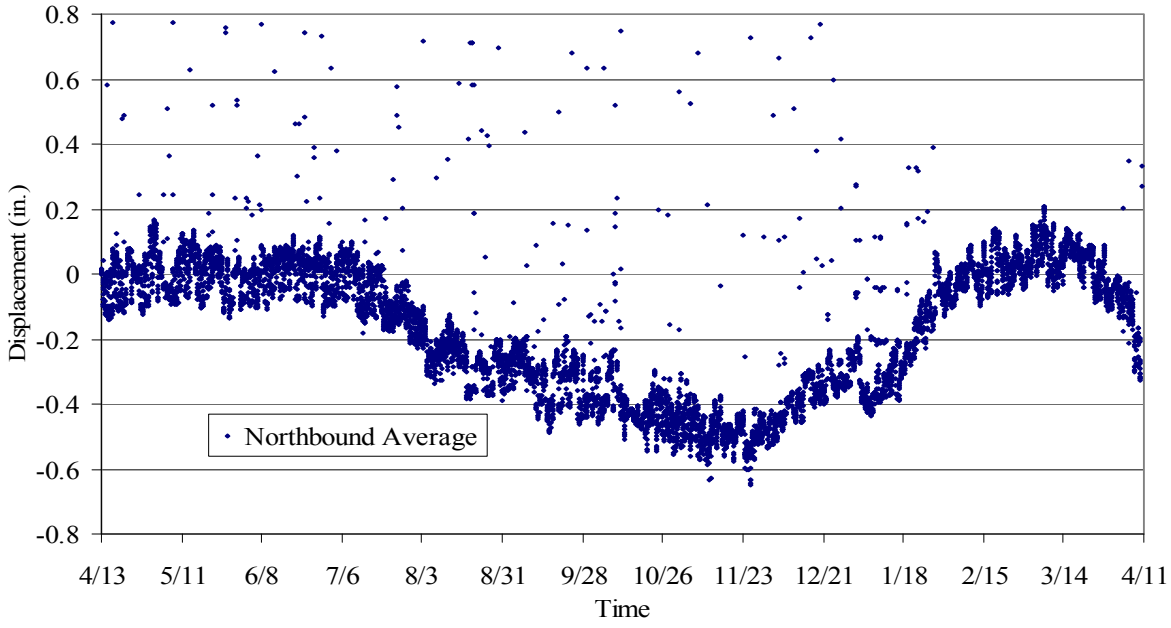


Figure 4.15. Average total northbound bridge abutment displacement at slab mid-depth over time

Because the displacement of the abutment is caused by the thermal expansion and contraction of the bridge superstructure, a theoretical or expected displacement can be calculated. A change in length from the center of the bridge to the end can be found by assuming the bridge thermally expands like an unrestrained bar from the center by:

$$\Delta = \alpha * \Delta T * \frac{L}{2} \tag{4.4}$$

Where:

α = Coefficient of thermal expansion for the bridge girders and deck
ΔT = Change in bridge temperature (refer to Section 4.1.2)
L = Length of the bridge

The coefficient of thermal expansion for concrete was calculated by the method presented by Abendroth and Greimann (Abendroth and Greimann 2005), which is based on the site specific concrete mix ingredients and proportions. Using the mix proportions furnished by Andrews Prestressed Concrete, the coefficient of thermal expansion (α) for the bridge girders was found to be on the order of 4.6 to 5.3x10^{-6}in./in./°F. In this work an α equal to 5.0x10^{-6}in./in./°F was used. The theoretical abutment displacement over time using the average bridge temperatures shown in Figure 4.6 can be seen in Figure 4.16. The range of theoretical displacement is near 1.0 in. which is greater than the observed 0.8 in. displacement of the abutment.

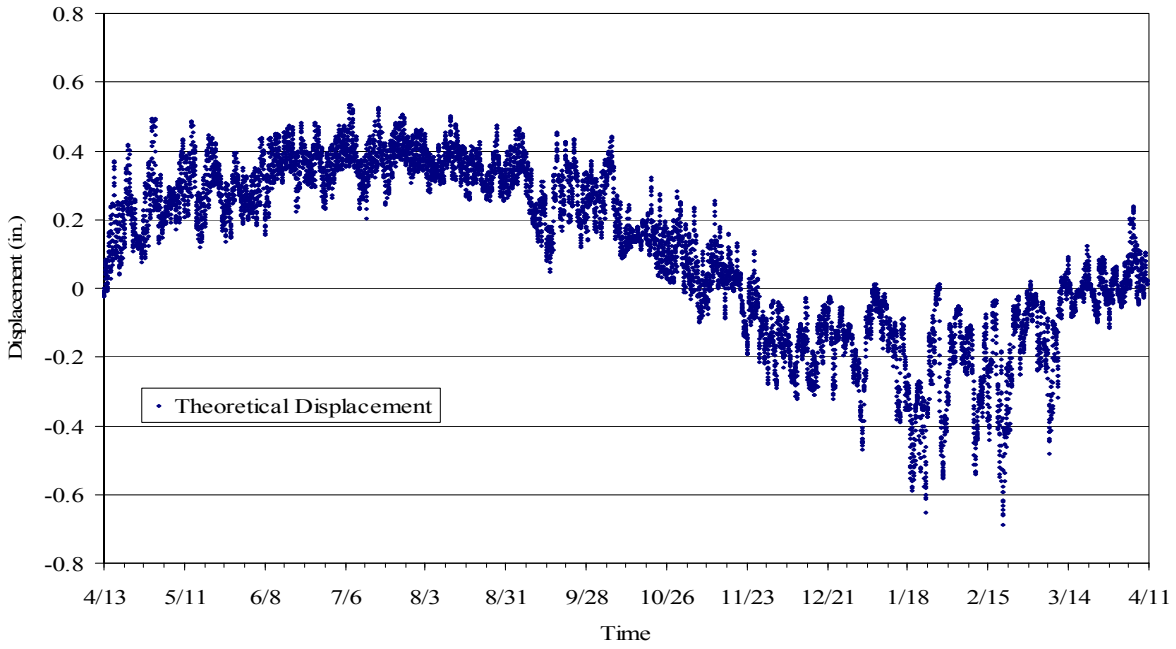


Figure 4.16. Theoretical abutment displacement

A comparison of the theoretical and average measured abutment displacement can be seen in Figure 4.17. From July to the beginning of December the theoretical and actual displacement follow the same trend (i.e., the abutment displaces to the north as the temperature cools). Beginning in December the abutment displaces to the south while the theoretical displacement predicts continued displacement to the north corresponding to reduced temperatures. Others (Hassiotis,2005) have observed somewhat similar behavior during the winter months and concluded that the behavior might be caused by (1) the bridge pushing against frozen soil as it warms in the spring and (2) soil filling the gap behind the abutment as the bridge contracts during the winter. Hassiotis also observed "strain-ratcheting" of the soil behind the abutment. In the current case with a long approach slab that is attached directly to the abutment a phenomena that produces a similar ratcheting behavior is observed. As the bridge expands, it pushes against the approach slab. Initially, the friction beneath the approach slab and forces at the approach slab/pavement expansion joint resist this motion. If the bridge expansion is sufficiently large, eventually the friction forces will be overcome and the slab will slide. As the bridge cools, the bridge will eventually slide the slab in the opposite direction. Appendix A presents a simple analytical model that helps to understand this phenomenon.

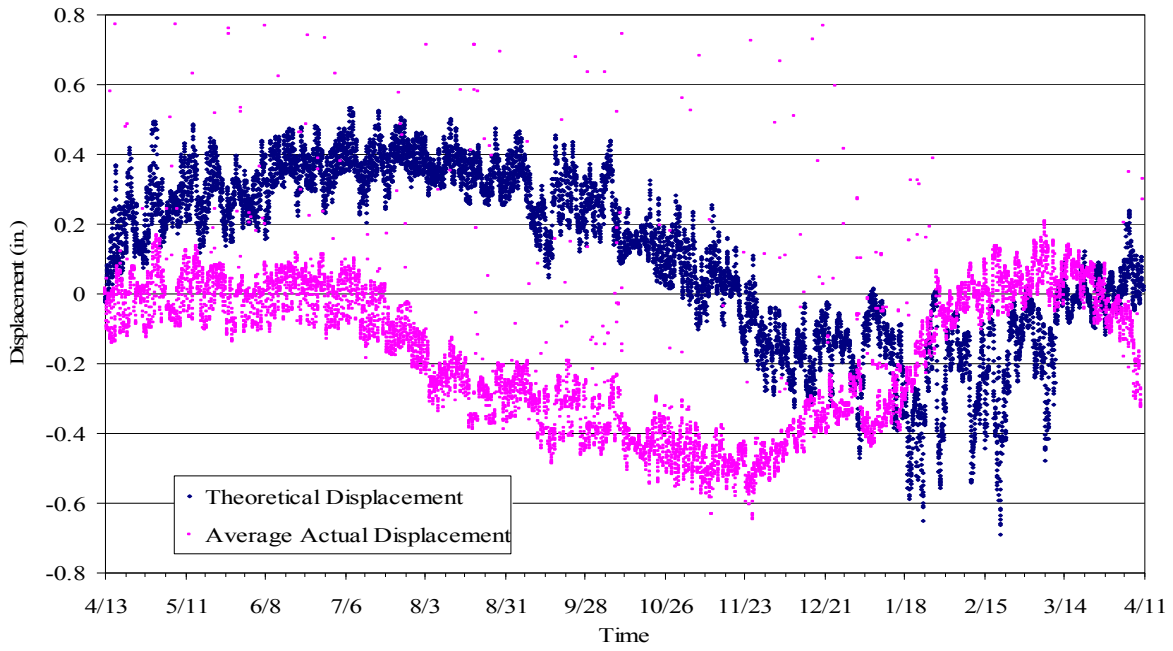


Figure 4.17. Theoretical and average actual abutment displacement of the northbound bridge over time (combinded Figure 4.15 and Figure 4.16)

The abutment mid-slab displacement is plotted against the average bridge temperature from Section 4.1.2 in Figure 4.18 (different colors were used to represent different seasons). During the summer and fall (July to December) the relationship between abutment displacement and temperature is generally positive (see Line A). However, short term cycles with a negative slope are also evident (Line B). These short term cycles occur for short term temperature variations and are probably due to the friction-ratcheting described above. During a short term cycle, the

frictional resistance under the slab may not be overcome and the bridge is pushed back and forth by the expanding and contracting slab. Eventually, however, as the temperatures continue their seasonal trend, the slab friction is overcome and the slab slides to a new position where again, for a period of time, the bridge and slab cycle without sliding. During the winter and spring period, the short term cycles with a negative slope are still evident (Line C). The simple analytical model in Appendix A helps to explain some of this.

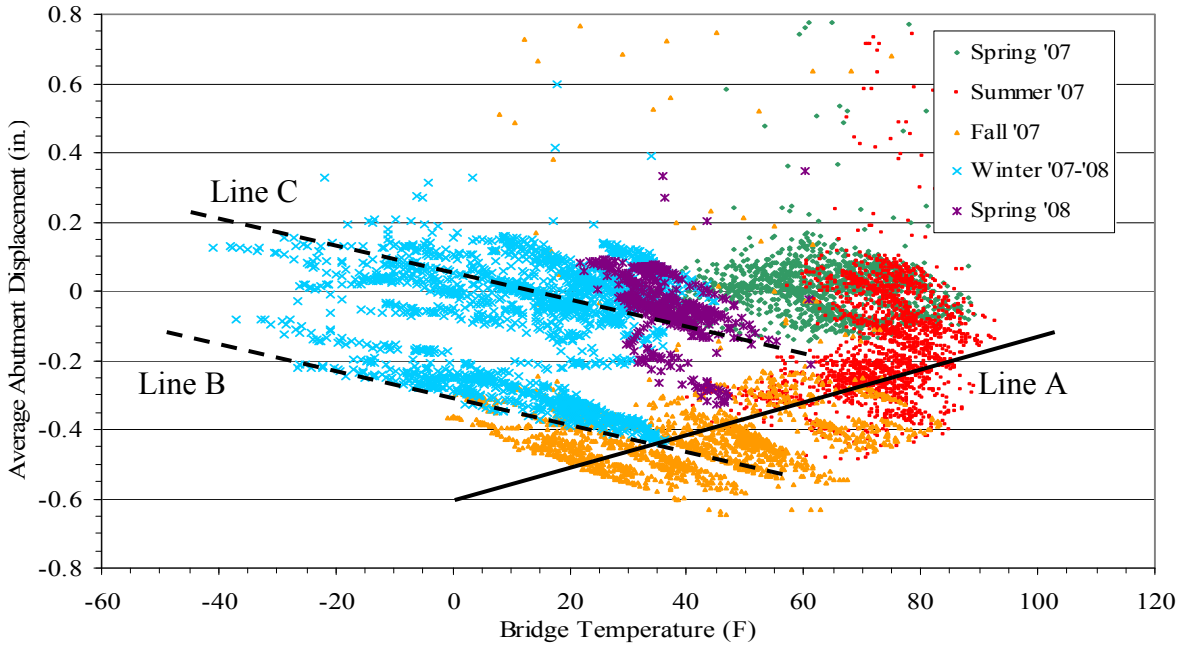


Figure 4.18. Northbound bridge abutment displacement versus change in bridge temperature

A displacement transducer was placed at the west end of the abutment (refer to Figure 3.14) to measure transverse displacement. Transverse abutment displacement over time is shown in Figure 4.19. As the temperature decreases displacement to the east occurs (counter clockwise rotation in Figure 4.20). From Figure 4.19 one can observe that the range of displacement is from -0.65 in. to 0.25 in. In this orientation positive displacements represent abutment displacement to the east as illustrated in Figure 4.20. Figure 4.20, from work by Abendroth and Greimann (2005), indicates that as a skewed bridge expands longitudinally, it will also rotate in the horizontal plane (Figure 4.20(c)). The $\Delta_{ABUT\ (WEST)}$ and $\Delta_{ABUT\ (EAST)}$ shown in Figure 4.20(a) are the displacements in Figure 4.13 and Figure 4.14 and $\Delta_{TRANSVERSE}$ in Figure 4.19. One can observe that the displacements in Figure 4.13 ($\Delta_{ABUT\ (WEST)}$) are greater than those of Figure 4.14 ($\Delta_{ABUT\ (EAST)}$) which is consistent with Figure 4.20 and the summation of Figure 4.20(c) and Figure 4.20(b).

The transverse displacement is compared to the average longitudinal displacement in Figure 4.21. There appears to be an annual cyclic relationship of the transverse displacement to the longitudinal displacement from the Spring ‘07 through Spring ’08. A linear trend (solid line)

with a slope of -0.57 is apparent from Summer ‘07 to Fall ’07. At that time the abutment is displacing to the north (longitudinally) and to the east (transversely).

Short term linear relationships (highlighted by the dashed trend lines) are also apparent. The slopes of the short term trends are positive at approximately 1.1 meaning that as the abutment displaces to the south (bridge expansion in Figure 4.13, Figure 4.14, and Figure 4.15) the abutment also displaces to the east (positive transverse displacement) an almost equal amount which correlates to counter clockwise rotation of the bridge (refer to Figure 4.20).

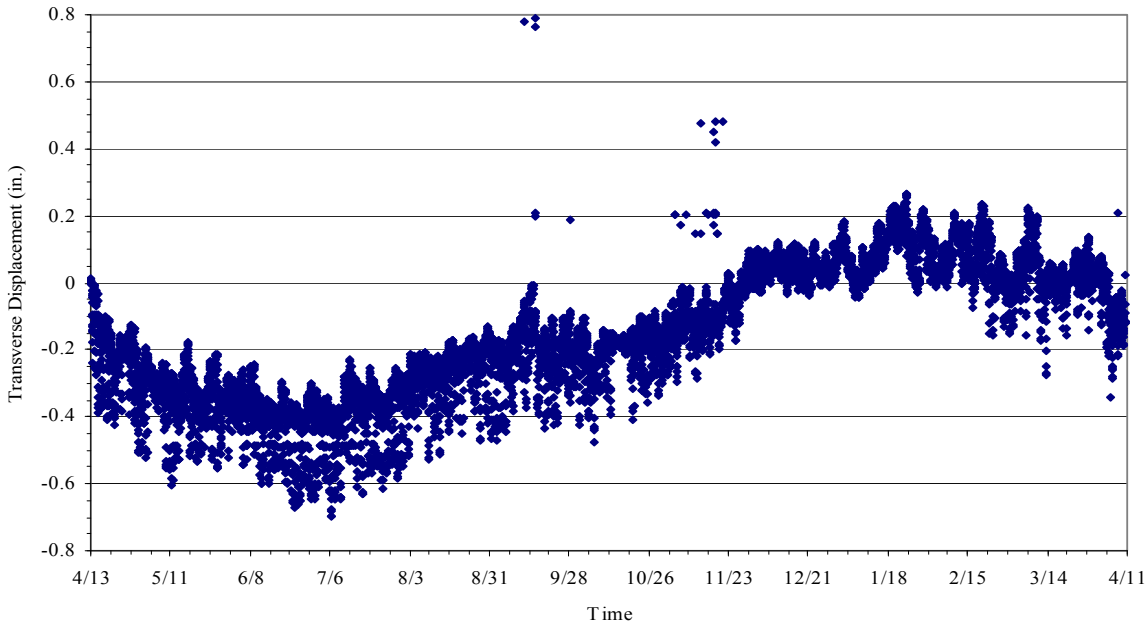


Figure 4.19. Northbound abutment transverse displacement over time

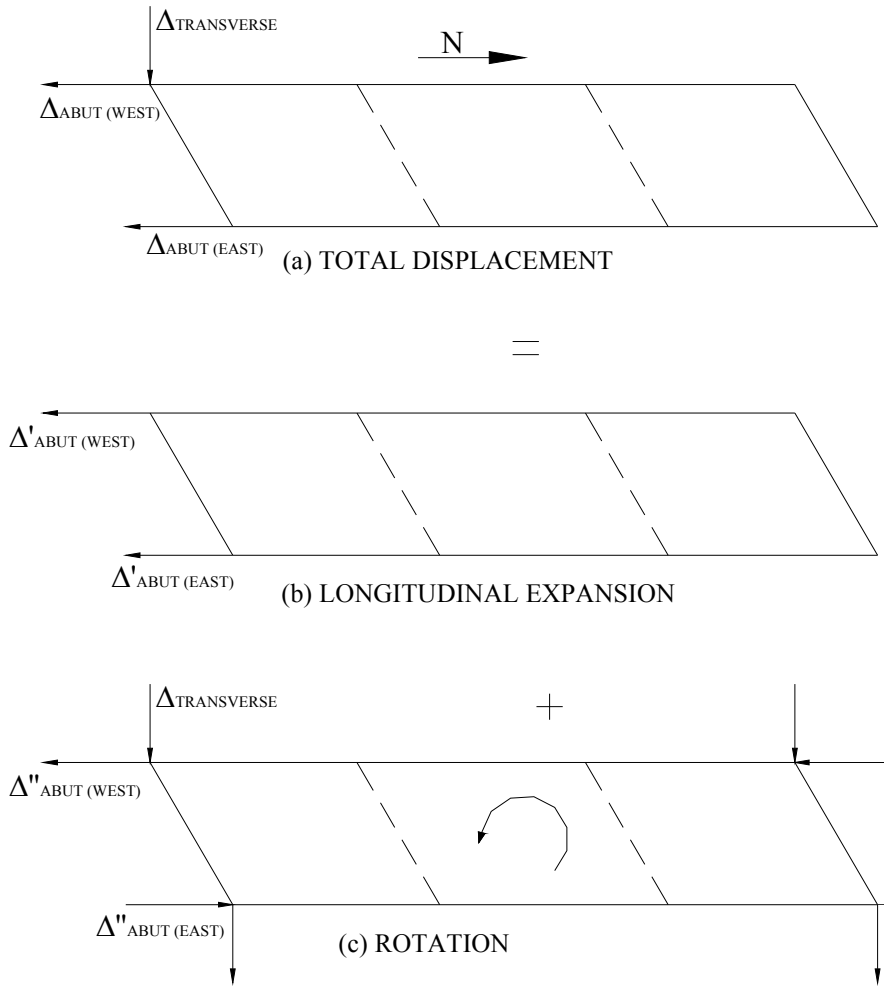


Figure 4.20. Illustration of (a) total displacement, (b) longitudinal expansion, and (c) horizontal rotation based on work by Abendroth and Greimann (2005)

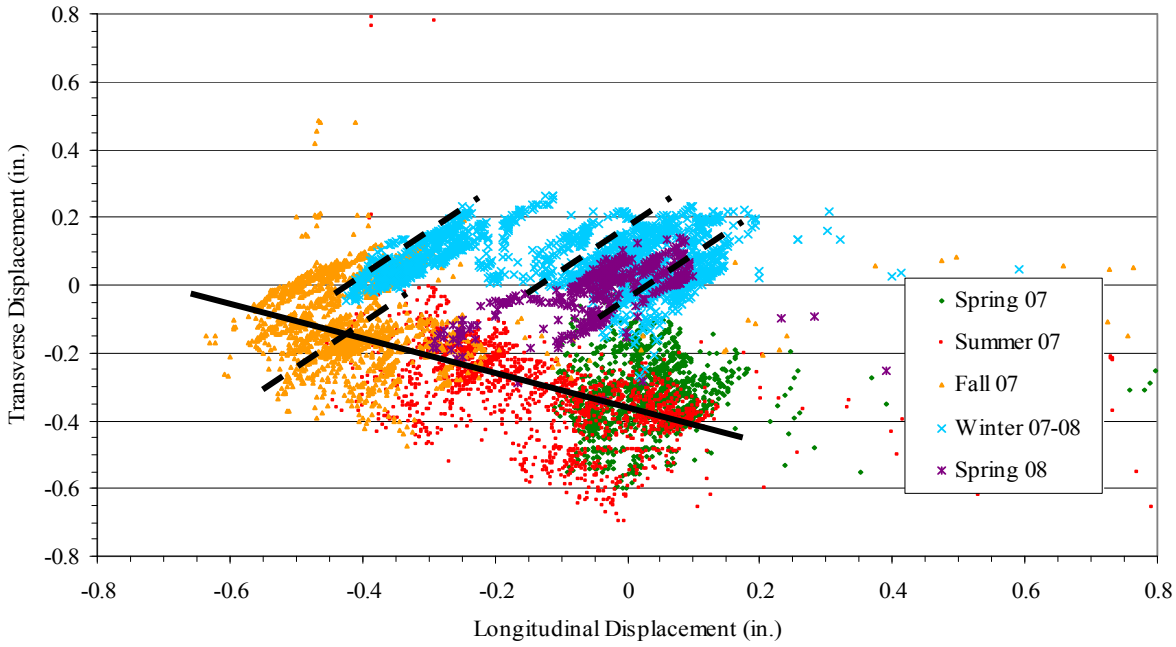


Figure 4.21. Northbound transverse abutment displacement versus average longitudinal displacement

4.2.2 Girder Strain Gauges

The girders were instrumented with 18 vibrating wire strain gauges as described in Section 3.3. Note that the readings obtained from the gauges are relative to initial readings taken April 13, 2007 (i.e., it is not the actual strain but rather a change in strain from that time). Each strain gauge is internally equipped with a thermistor for reading temperature. The temperature information obtained from the thermistor was used to correct the strain gauge readings due to elongation and shortening of the vibrating wire and to determine the load strain (strain caused by an applied load or a restraining force). The value of the coefficient of thermal expansion of the bridge superstructure used was 5×10^{-6} in./in./^{o}F. The total strains in the gauge and concrete are given by:

$$\Delta\varepsilon_{gauge} = \Delta R * B + \alpha_{gauge} * \Delta T \tag{4.5}$$

$$\Delta\varepsilon_{concrete} = \Delta\varepsilon_{load} + \alpha_{concrete} * \Delta T \tag{4.6}$$

Where:

$\Delta\varepsilon$ = Change in total strain
ΔR = Change in readout of the gauge
ΔT = Change in temperature
B = Batch gauge factor supplied by manufacturer

α = Coefficient of thermal expansion
$_{gauge}$ = properties or changes in the gauge
$_{concrete}$ = properties or changes within the concrete slab
$_{load}$ = changes caused by load

Because the gauge is installed on concrete, the total strain of the gauge and concrete must be the same. The load strain ($\Delta\varepsilon_{load}$) can then be found by equating Equations 4.5 and 4.6, and solving for load strain (Equation 4.7).

$$\Delta\varepsilon_{load} = \Delta R * B + (\alpha_{gauge} - \alpha_{concrete}) * \Delta T \tag{4.7}$$

A typical load strain over time is shown in Figure 4.22. As the temperature decreases (July to January) the load strain decreases. Since the girders are initially prestressed the decrease in load strain causes an increase in compression. In the same way, as the temperature increases the load strain increases, which is a decrease in compression.

The recorded girder load strains are shown in Figure 4.23 and Figure 4.24, top and bottom respectively, plotted against gauge position along the girder for the hot and cold days identified in Section 4.1.1. Variation across the bridge is shown by the different series for each girder. Similar strains might be expected for each girder for each case (top, bottom, hot, cold), but this is not always the case. On the cold day the load strains of each girder compared fairly well at all 3 positions. However, but on the hot day the mid-span load strains of the center girder, GC, and west girder, GW, did not compare as well. To study the overall, general behavior of the bridge, the load strains for the top and bottom of the bridge were averaged and are shown in Figure 4.23 and Figure 4.24, respectively.

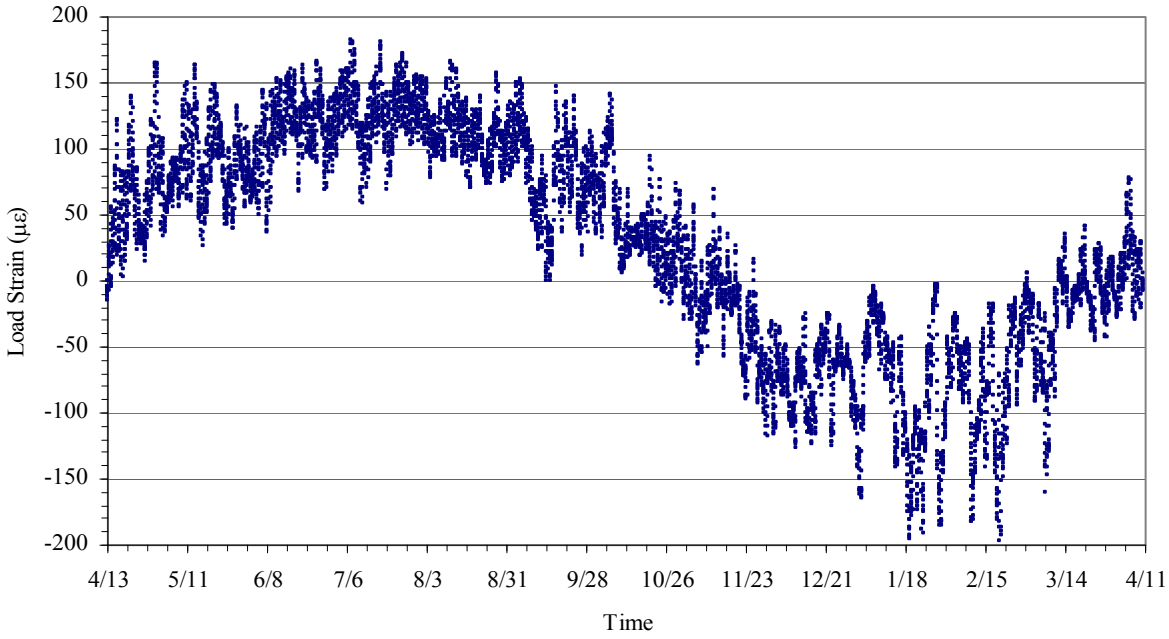


Figure 4.22. Typical northbound bridge girder load strain behavior over time as recorded by gauge GNWT2

Knowing the load strains in the top and bottom flanges of a section, the distance to the gauge location (y_1 and y_2), section properties (area, A, and moment-of-inertia, I,) and assuming a modulus of elasticity, E, the moment and axial load on the composite section (shown in Figure 4.25) can be found. Note that in this discussion axial force that cause tension is positive and moment that causes tension in the bottom fiber is positive.

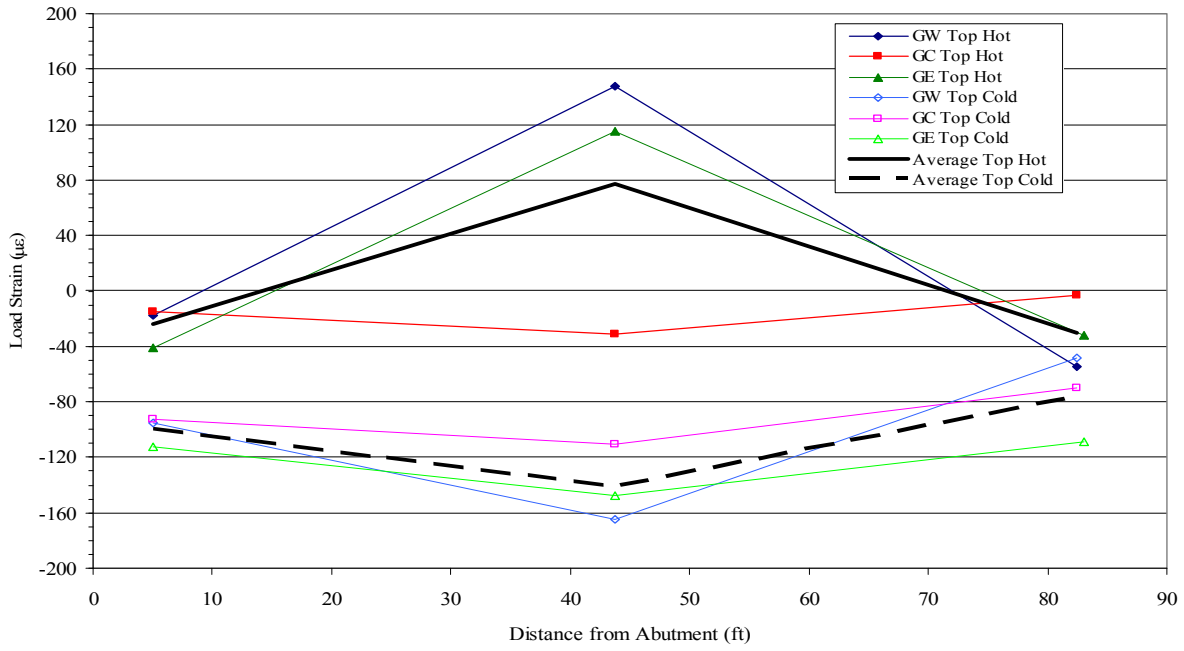


Figure 4.23. Load strain variation at the top of the northbound bridge girders with respect to position

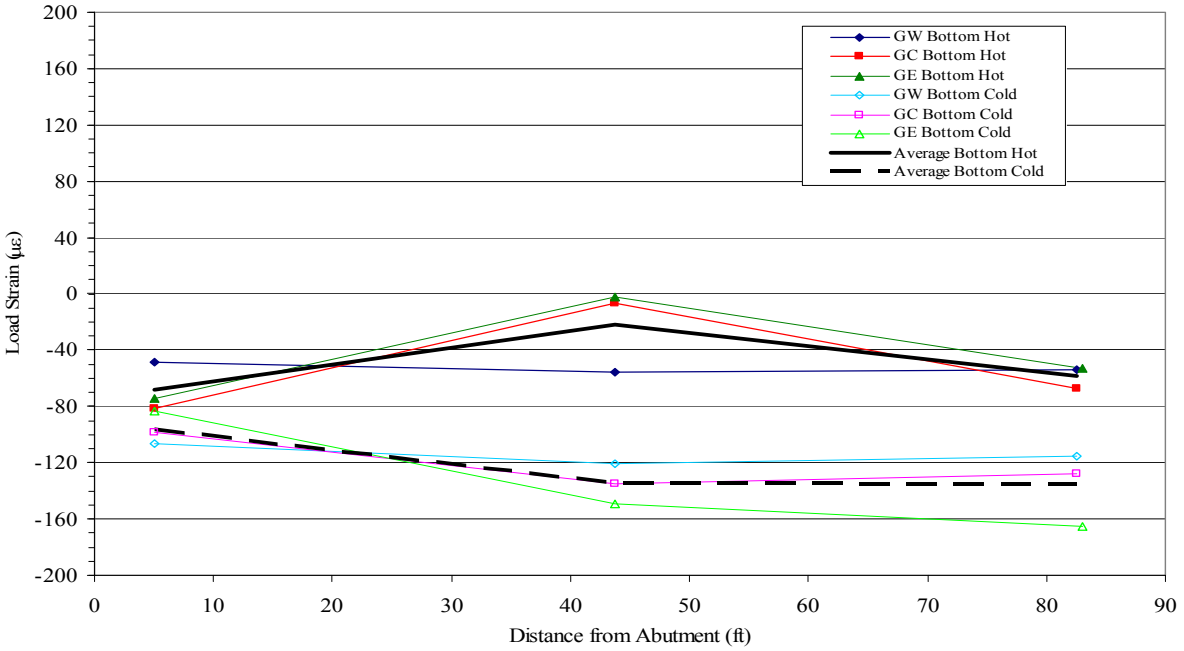


Figure 4.24. Load strain variation at the bottom of the northbound bridge girders with respect to position

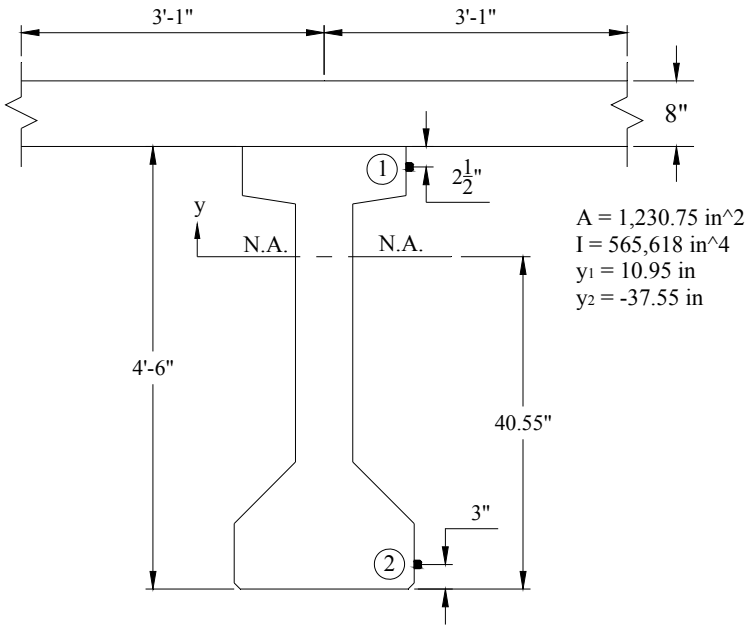


Figure 4.25. Typical composite bridge deck and girder section

The equation to find moment and axial force from strain are:

$$M = \frac{I * E_{concrete} * (\varepsilon_1 - \varepsilon_2)}{(y_2 - y_1)} \tag{4.8}$$

$$P = A * E_{concrete} * (\frac{\varepsilon_1 \cdot y_2 - \varepsilon_2 \cdot y_1}{y_2 - y_1}) \tag{4.9}$$

Where:

M = Moment acting on the section
P = Axial load acting on the section
A = Area of the composite section (A = 1231in.^{2})
E = Modulus of elasticity of the concrete (E = 4200ksi
I = Moment-of-inertia of the composite section (I = 565618in.^{4})
$\varepsilon_1, \varepsilon_2$ = Load strain at points 1 and 2 respectively
y_1, y_2 = Distance to points 1 and 2 respectively

Figure 4.26 shows the average girder moment relative to position along the girder for the typical hot and cold day. The moments were found by using the average load strains shown in Figure 4.23 and Figure 4.24 in Equation 4.8. For the typical hot day, which was reported as partly sunny, the moment is negative and decreases from either end of the girder to a maximum negative moment of -400 kip*ft.

As the bridge is heated both by the changing air temperature and solar radiation, it expands longitudinally and the top deck fibers are hotter than the shaded bottom girder fibers. Conceptually, the thermally induced forces at the abutment/girder joint include forces from the approach slab passive soil on the abutment back wall, piles, and girders (see Figure 4.27). The moment in the girder in Figure 4.27 is arbitrarily drawn as negative (causing tension on top), but is dependent on the magnitudes of the slab force, pile forces, and the soil pressure resultant force. If the slab force is greater than the soil pressure resultant force and pile forces, the reaction moment of the girder could become positive.

In addition, when viewed as a two-dimensional structure, the moments are expected to vary linearly between the girder ends since there is no vertical load applied during heating. Figure 4.26 shows that the moment varies non-uniformly which implies changing shear and, hence, a vertical load on the girder. However, when viewed as a three-dimensional structure the non-uniformity could be attributed to the bridge skew, which creates variable girder support due to transverse deck effects.

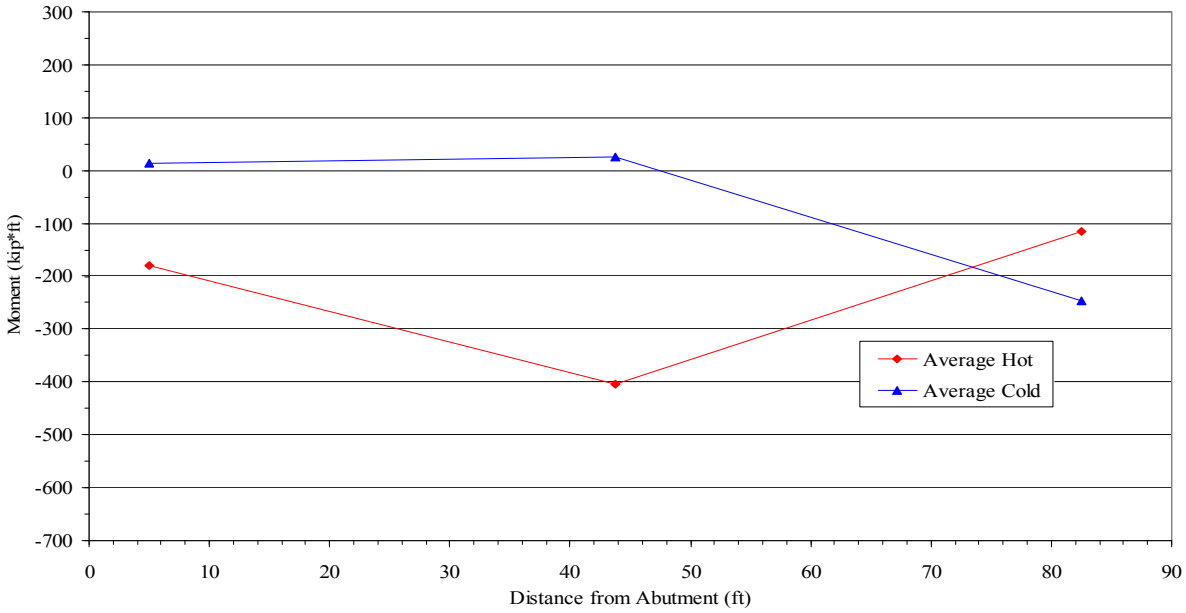


Figure 4.26. Average northbound bridge girder moment with respect to position

The average mid-span moment is plotted against time in Figure 4.28. A cyclic pattern of change from negative to positive to negative moments as the bridge is heated, cooled, and heated is evident. The average mid-span moment ranges from -600 kip*ft to 200 kip*ft (relative to a zero moment in April).

Figure 4.29 shows a plot of the average mid-span moment versus average bridge temperature from Section 4.1.2. Different colors were used to denote the different seasons highlighting the relationship of moment to temperature over time. Again, two trends are visible. The first trend is a short term trend highlighted by the dashed lines that show a linear relationship between the

moment and the temperature, at a slope of approximately -13.9 kip*ft/°F. The second trend is the annual trend, which is delineated with a bold solid line, with a slope of -5 kip*ft/°F. Note that the coldest part of Winter 07-08 is of a different shape than the rest of the seasons which may affect the annual trend. As noted in Section 4.2.1, the friction ratcheting of the attached approach slab are the primary cause of the different slopes of the annual and short term cycles that are evident in Figure 4.29. (See also Appendix A.)

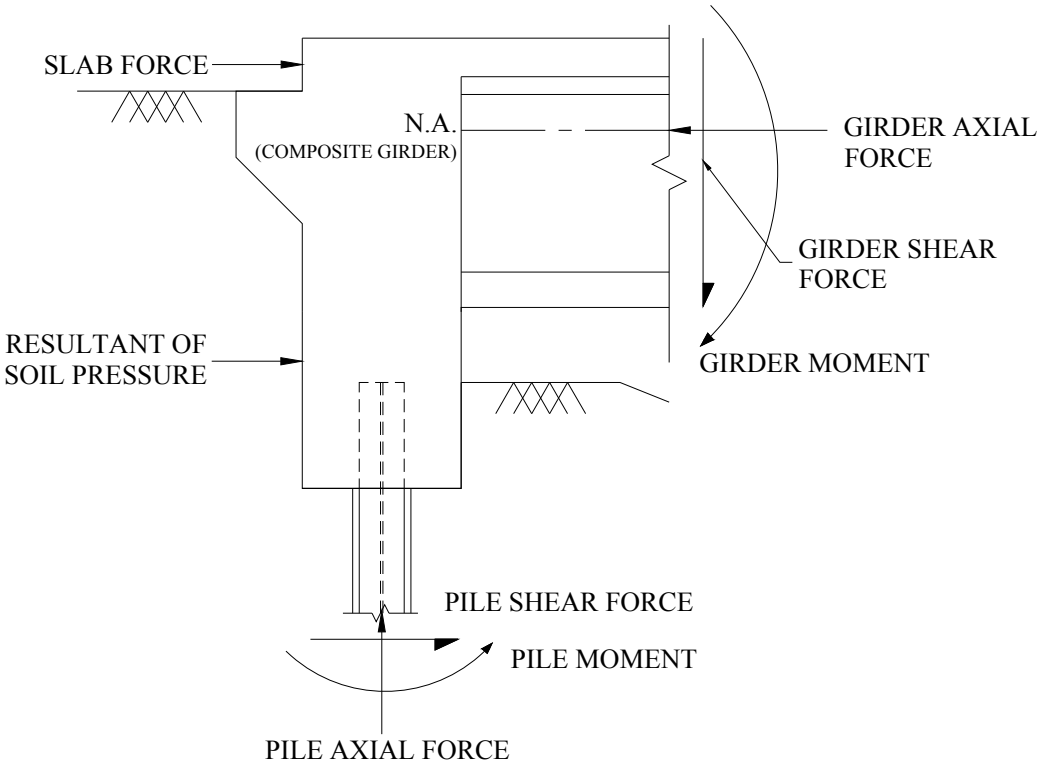


Figure 4.27. Free body diagram of bridge

Figure 4.30 is a plot of the average mid-span moment versus the average longitudinal abutment displacement from Section 4.2.1. Like Figure 4.29, different colors were used to highlight the different seasons. Again, there appears to be small groupings of data that have a consistent linear relation, shown by dashed lines, similar to the short term trends in Figure 4.29 and discussed in Section 4.2.1. The overall trend appears to have a zero slope.

The annual moment envelope, which is obtained from the absolute maximum and minimum average moments at the three gauge positions, is shown in Figure 4.31. The lower bound tends to follow the trend of the average hot day moment shown in Figure 4.26.

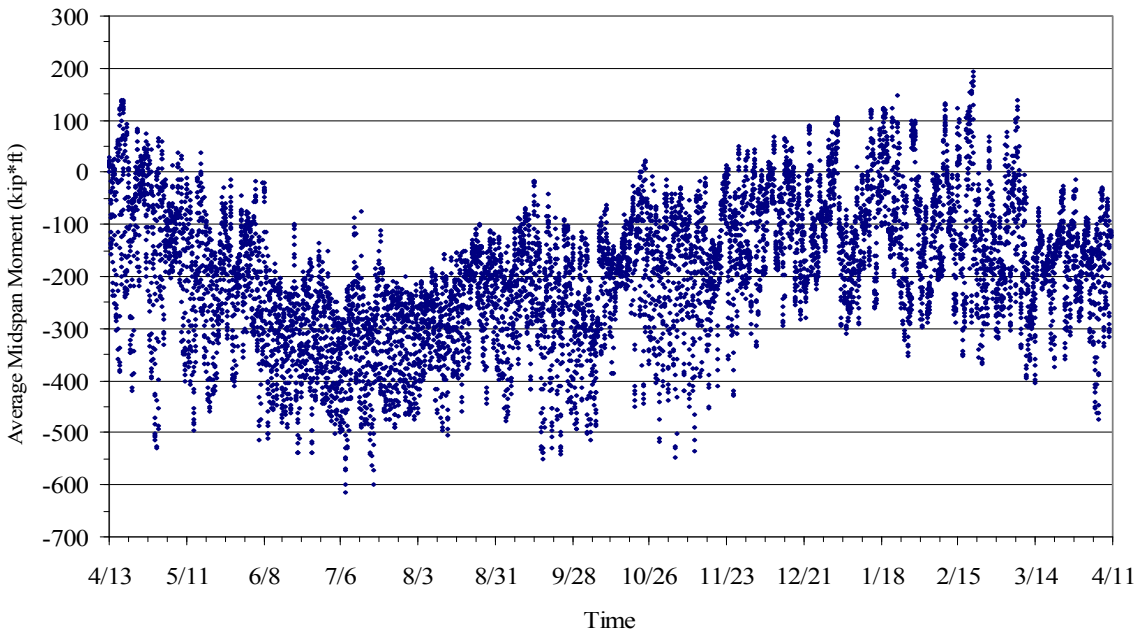


Figure 4.28. Average northbound bridge mid-span moment over time

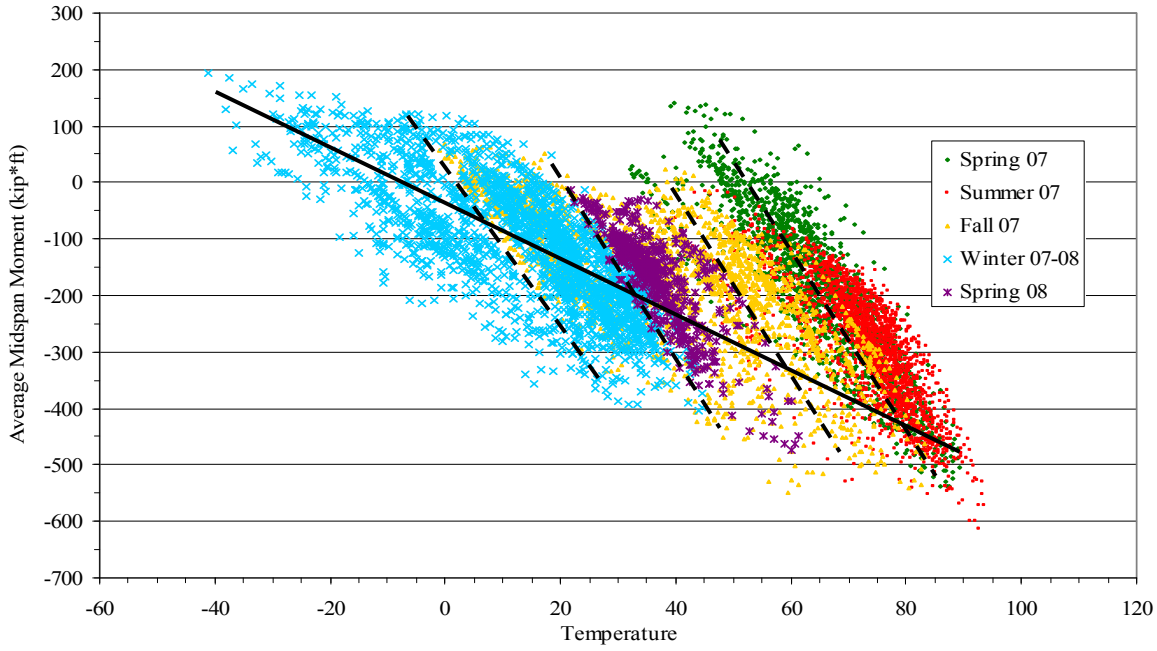


Figure 4.29. Average northbound bridge mid-span moment versus average bridge temperature

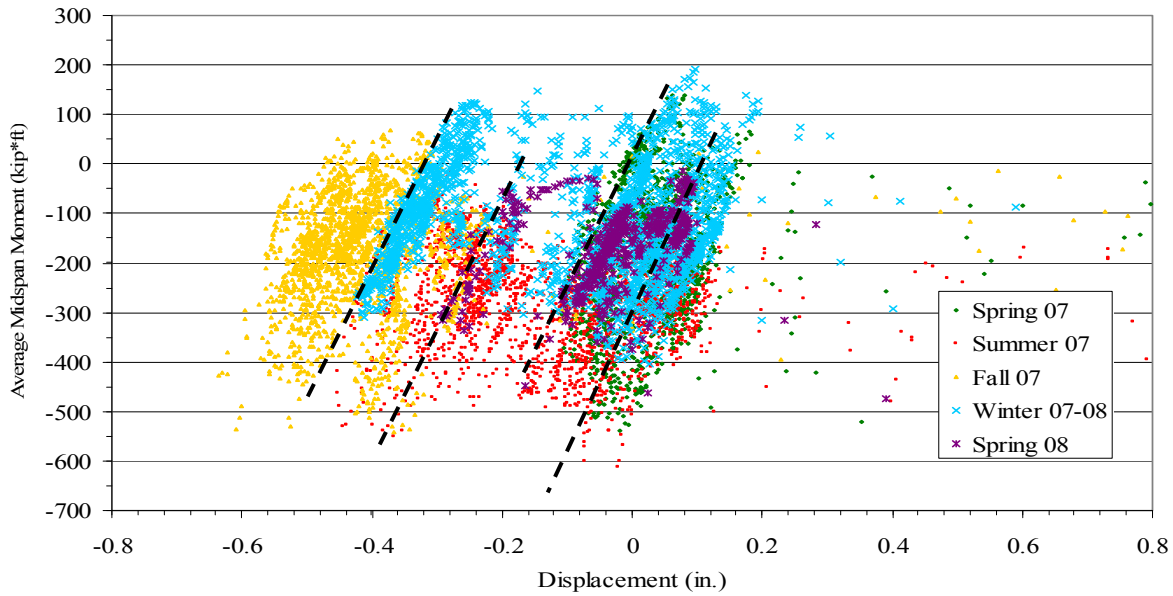


Figure 4.30. Average northbound bridge mid-span moment versus average longitudinal abutment displacement

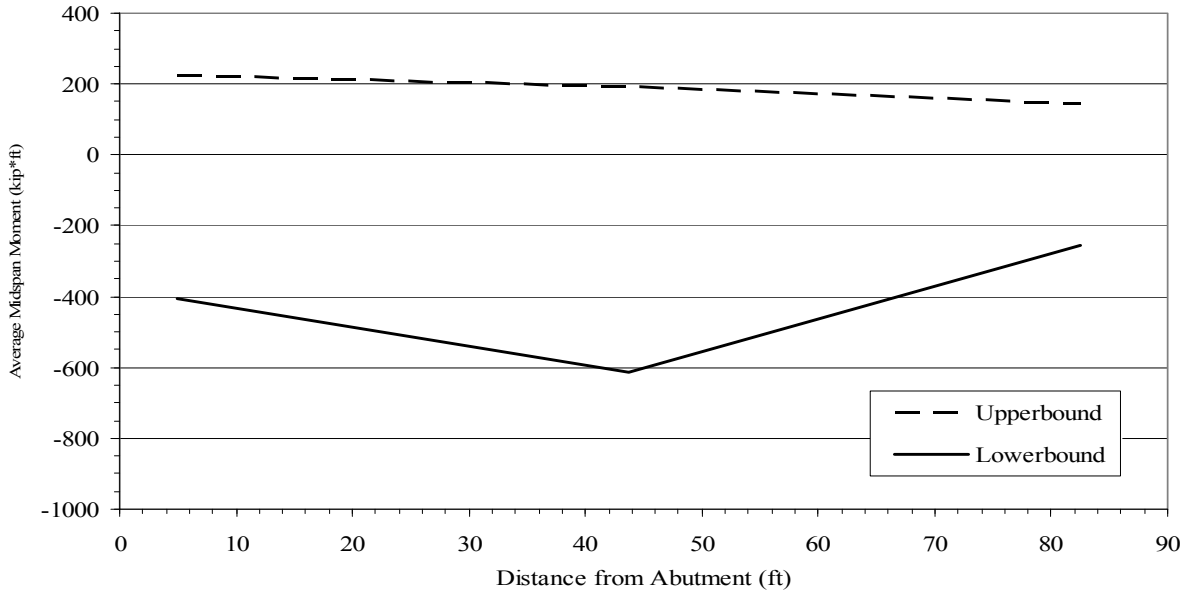


Figure 4.31. Northbound bridge girder moment envelope

Using the average load strains shown in Figure 4.23 and Figure 4.24 and Equation 4.9, the average change in axial loads at hot and cold times were found and are shown in Figure 4.32. For a two-dimensional structure, one would expect the axial force in the girders to be constant, but

the results in Figure 4.32 show that the axial loads vary along the girder length. The skew of the bridge introduces three-dimensional effects which will affect the axial load distribution.

To observe the behavior of the overall bridge span, the axial load along the girders were averaged and are shown versus time in Figure 4.33. The average axial load ranges from 100 kips to -650 kips. As the temperature decreases (July to January) the axial load decreases, or becomes more compressive.

When the average axial load is plotted versus the bridge temperature (found in Section 4.1.2), as it is in Figure 4.34, the linear relation of the axial load to temperature is clear. As the temperature increases, the axial load increases, which is a reduction in compression. The slope of the linear relation is 5.8 kips/°F, having a range of -600 kips to 100 kips.

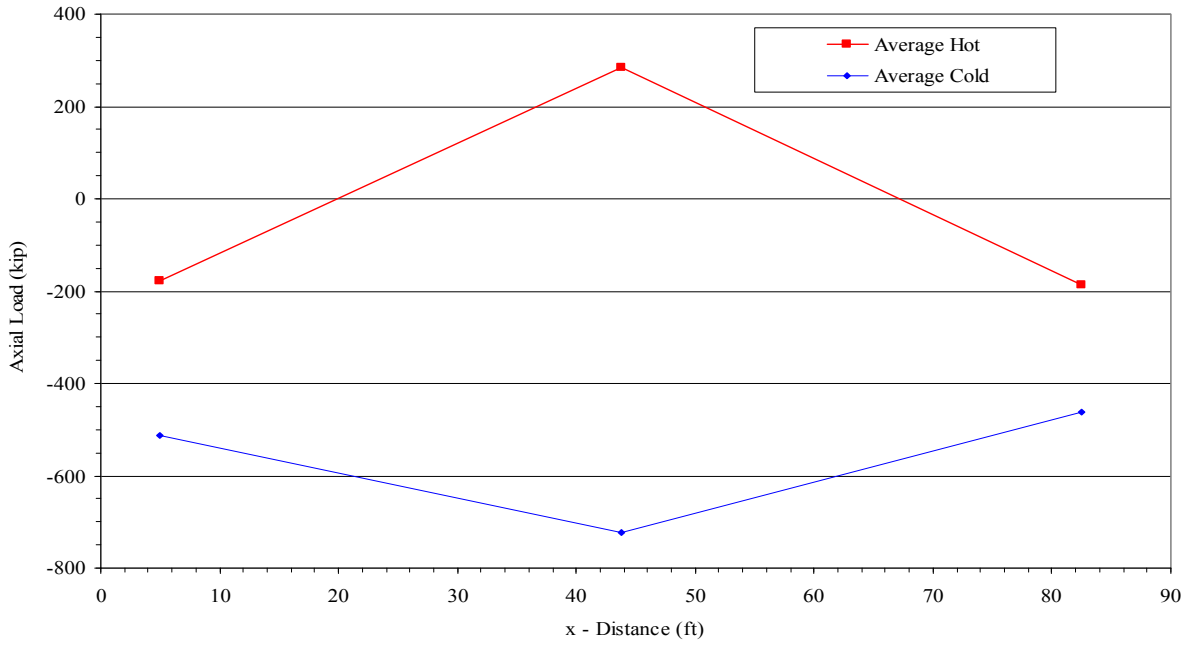


Figure 4.32. Average northbound bridge axial load versus girder position

The average axial load is plotted versus the average longitudinal abutment displacement found in Section 4.2.1 in Figure 4.35. There is no clear relationship between axial load and abutment displacement, although some cyclic short term behavior again seems evident as in the case of the movements.

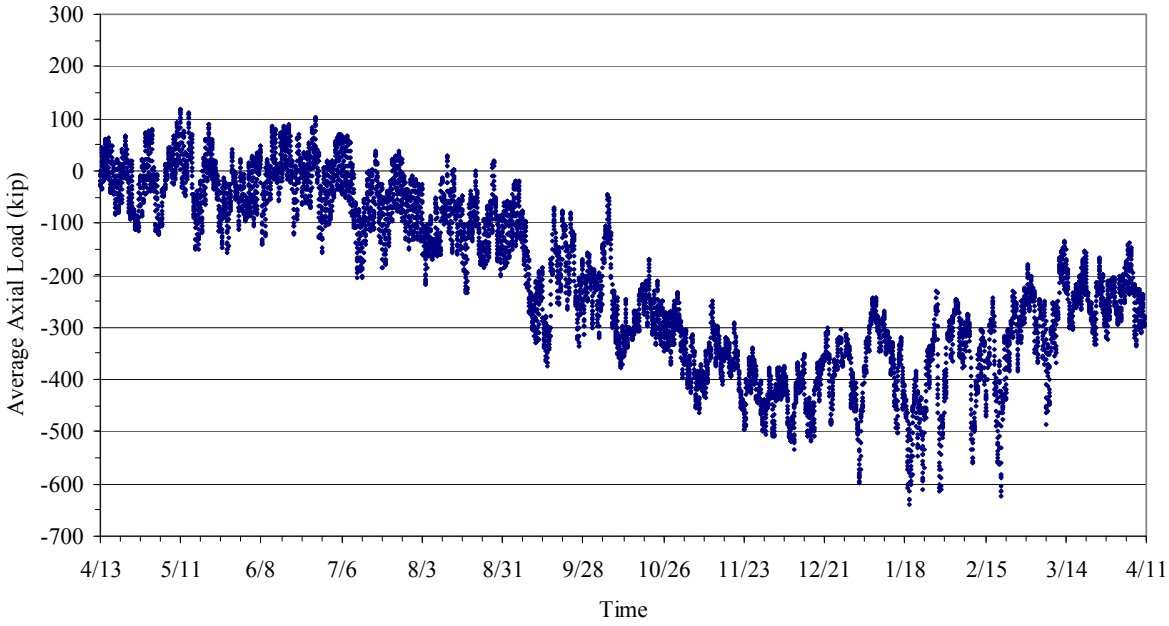


Figure 4.33. Average northbound bridge girder axial load over time

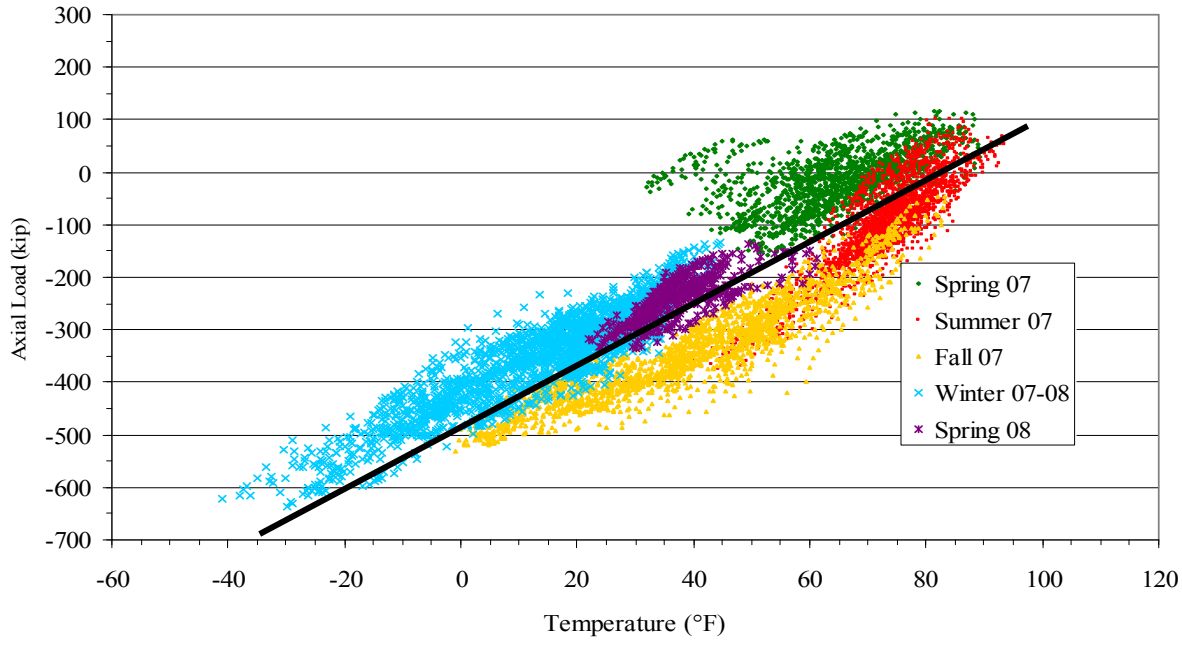


Figure 4.34. Average axial load versus external girder temperature

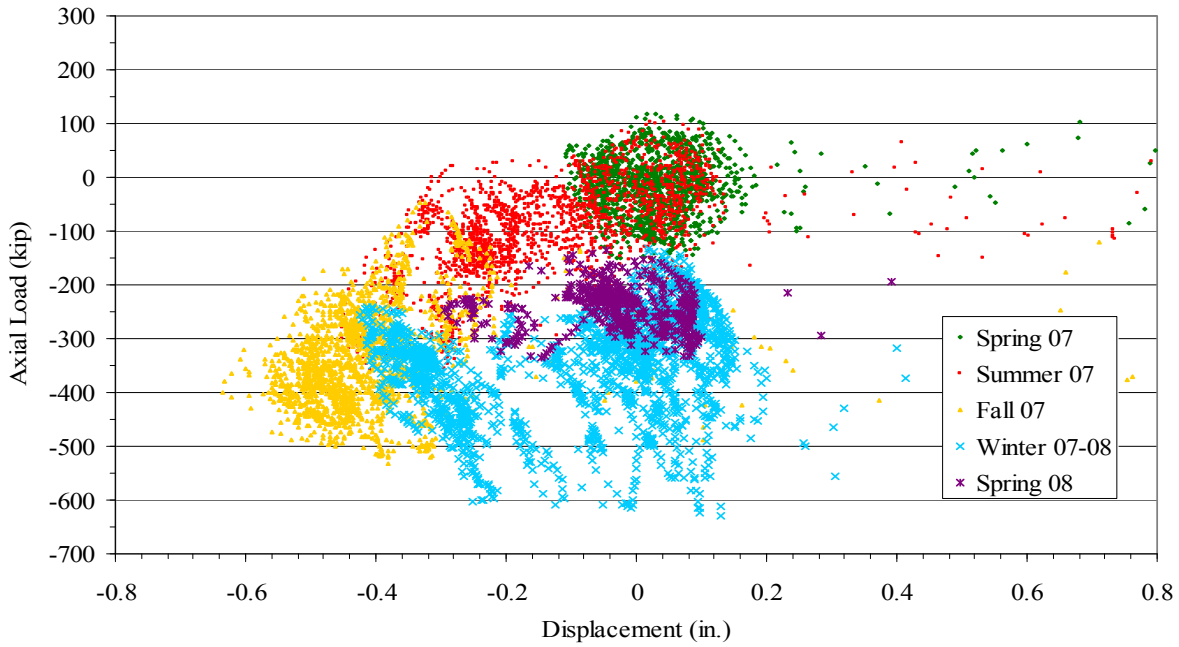


Figure 4.35. Average axial load versus average longitudinal abutment displacement

4.3. Approach Slab

4.3.1 Embedded Strain Gauges

The approach slab was instrumented with 16 vibrating wire strain gauges as described in Section 3.3. The strain gauges installed in the pavement are essentially the same as the strain gauges installed on the bridge girders with the exception that they can be embedded in concrete. Refer to the beginning of Section 4.2.2 for strain calculations, temperature corrections, etc. The value used for the coefficient of thermal expansion of the concrete for the precast approach slab was $5x10^{-6}$ in./in./°F.

A typical strain time history for an embedded strain transducer is shown in Figure 4.36. In general, as the temperature increased the load strain within the slab decreased indicating an increase in compression in the slab. The opposite behavior took place as the temperature decreased.

During the data reduction process, readings from gauge EN1BE, shown in Figure 4.37, were found to be very scattered. Although all of the gauges had some outlier data, the extent of outliers for gauge EN1BE was judged to be excessive and it was not used for further averaging and comparison purposes.

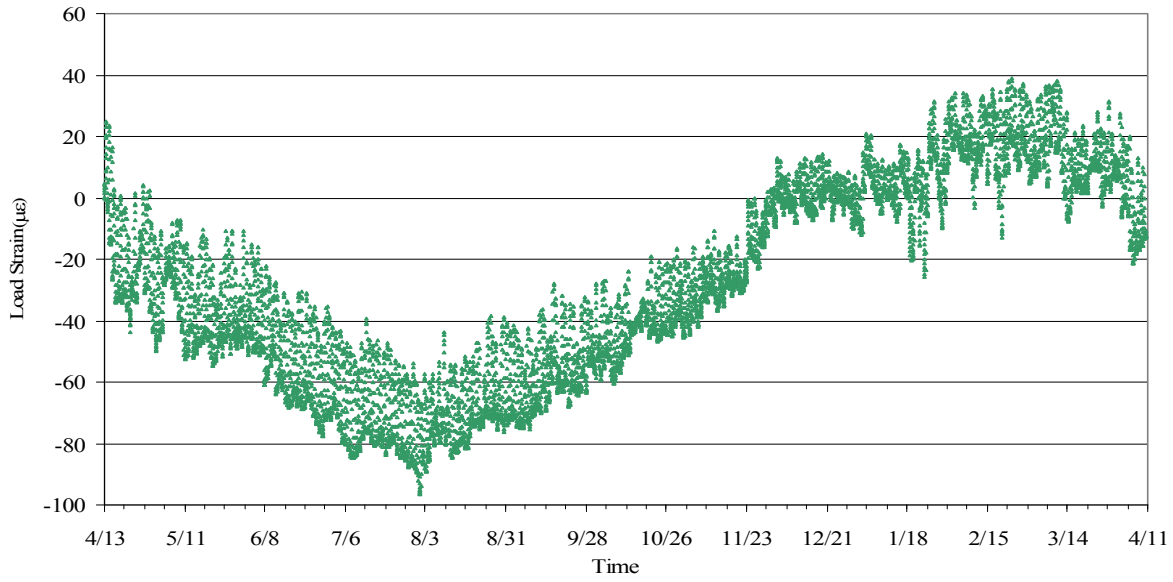


Figure 4.36. Representative strain reading obtained from embedded northbound bridge approach slab strain gauge EN4BE

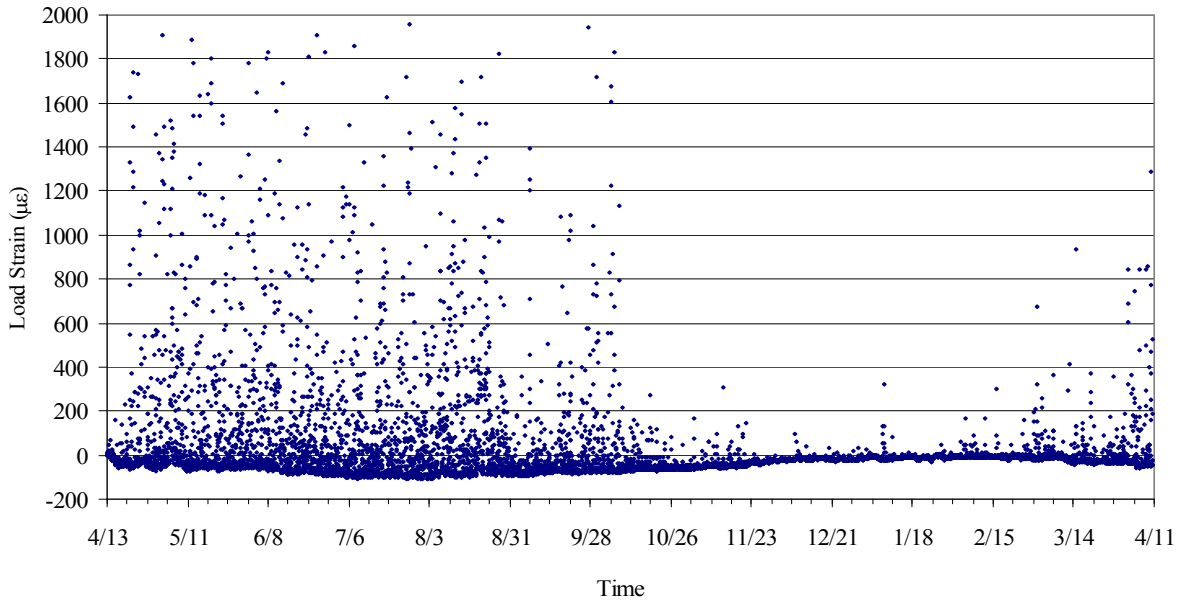


Figure 4.37. Northbound bridge embedded strain gauge ENB1E discarded due to large amount of outlier data

In order to compare longitudinal and transverse variations of the strain in the slab, a hot day (August 23rd at 5:00 pm) and a cold day (February 23rd at 4:00 am) were chosen. Note, these

hot and cold days are different than those previously mentioned in order to obtain the extreme load strain values. The strains for the 15 gauges are plotted in Figure 4.38 against longitudinal position for both the hot and cold days. For both days, the strains varied little between longitudinal and transverse location with the exception of the gauges in slab 3 (30ft location), which ranged over 40με and 70με for the cold and hot days, respectively.

To study the overall general behavior of the slab the data from the 15 usable gauges were averaged together to obtain the total average load strain in the slab as shown in Figure 4.39.

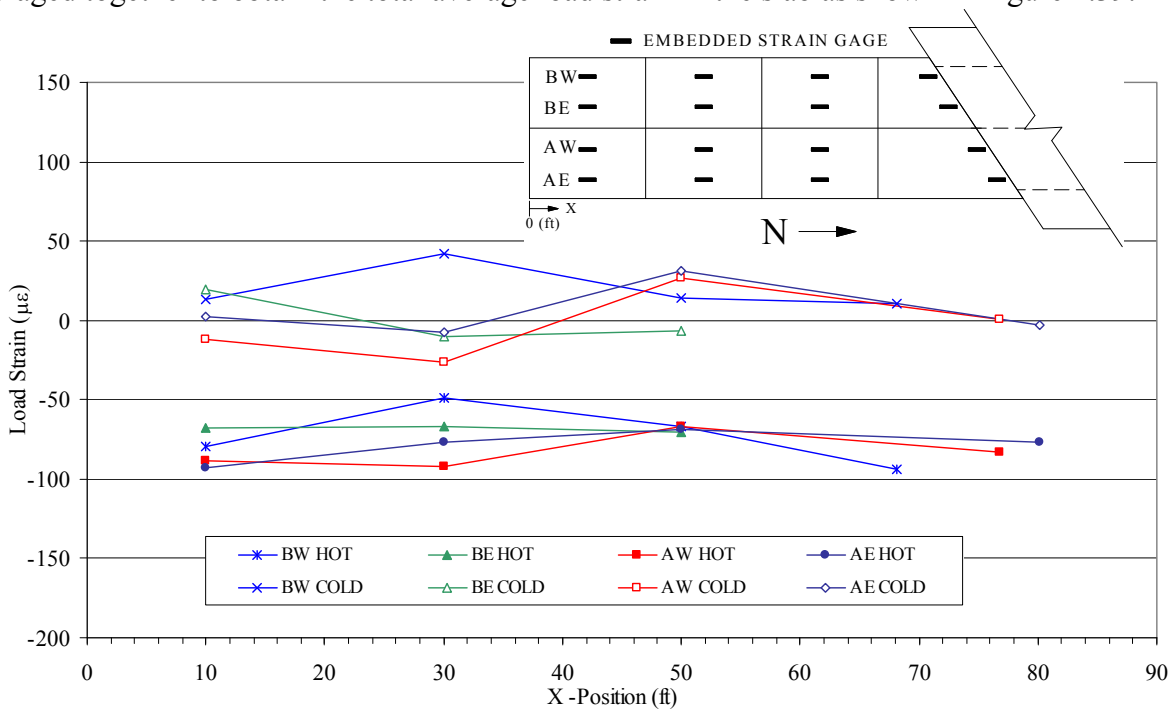


Figure 4.38. Hot and cold day northbound bridge load strain comparison with respect to location

The average load strain is plotted with respect to temperature in Figure 4.40. The relationship between the strain in the slab and temperature is nearly linear with a moderately small band width. The slope of the band is approximately -1.3με/^{o}F and has a range of approximately 120με. As before, different colors are used in Figure 4.40 to illustrate the seasonal effects. A cyclical pattern emerges with the winter and summer having the maximum and minimum load strain, respectively, while the spring and fall are seen as the transition periods. When Figure 4.40 is investigated at a smaller scale (i.e., short term), a clockwise looping cyclical pattern also emerges. In Section 4.2.1, the friction ratcheting is further discussed.

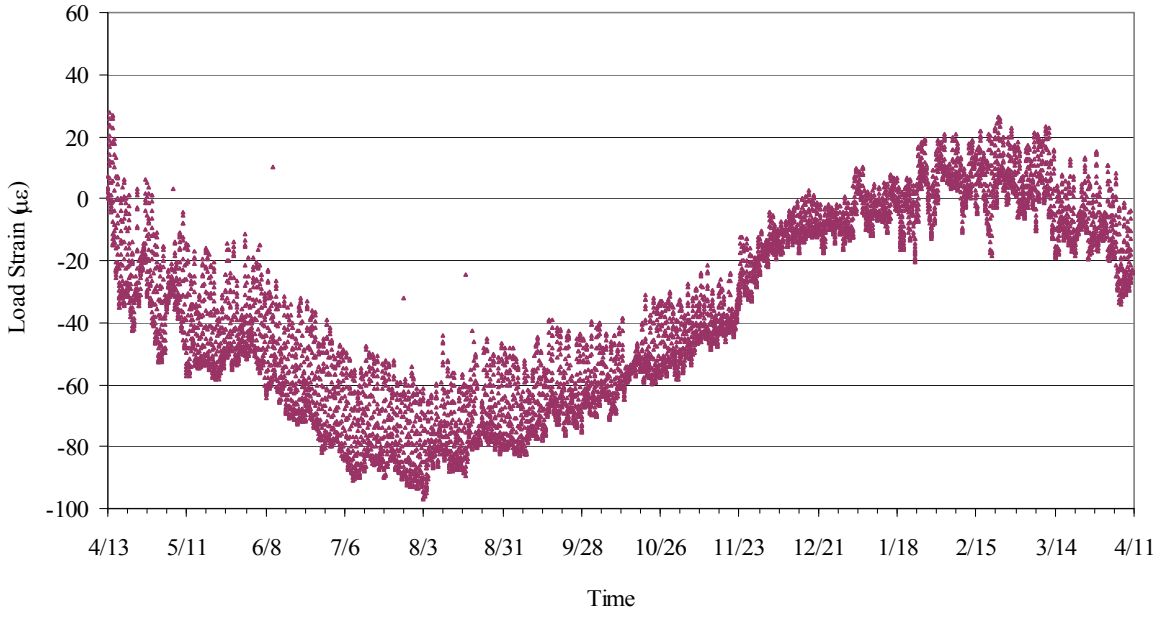


Figure 4.39. Average load strain of 15 northbound bridge embedded working gauges

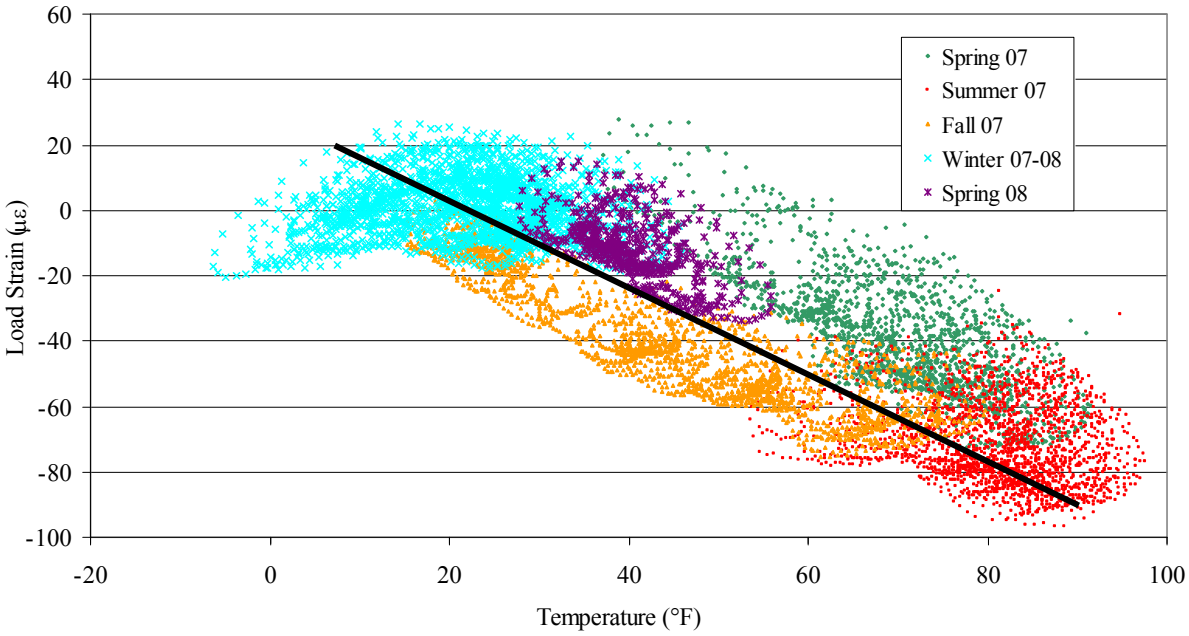


Figure 4.40. Northbound bridge approach slab load strain with respect to temperature

Knowing the change in load strain, the area of the slab, and the modulus of elasticity, the change in the approach slab longitudinal force was calculated by the equation:

$$\Delta P_{concrete} = \Delta \varepsilon_{load} * E_{concrete} * A_{concrete} \quad (4.10)$$

Where:
ΔP = change in the approach slab force
A = Cross-sectional area (A = 4,032in.^{2})

The force in the slab was plotted versus temperature and is shown in Figure 4.41. Figure 4.41 and Figure 4.40 yield similar observations with the same cyclical pattern found during the seasonal and short term changes over time (see Section 4.2.1) toward compression in the summer and tension in the winter. The slope of the data is approximately -24 kips/°F. The force in the slab ranged from -1860 kips in the summer to 480 kips in the winter. The total range of approximately 2300 kips relates to a 580 psi stress change in the slab from winter to summer.

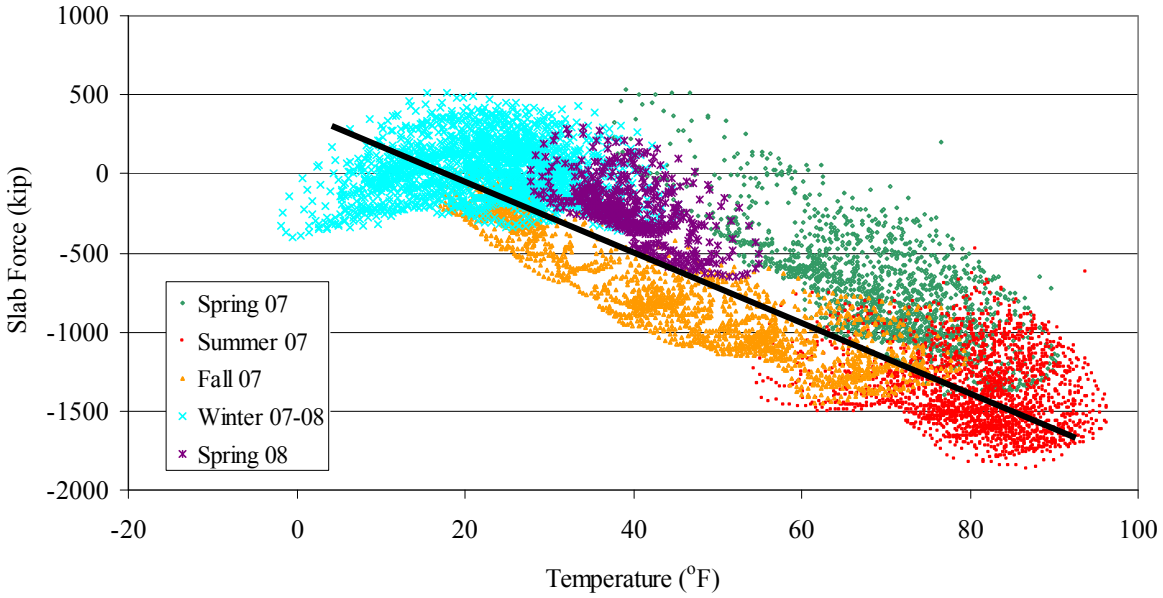


Figure 4.41. Northbound bridge approach slab average force with respect to slab temperature

Figure 4.42 shows the force in the slab versus location on the same hot and cold day as presented in Figure 4.38. In general, the longitudinal slope of the plotted force was very close to zero. Inspection of a large number of these data indicate that, in fact, the slope is not zero. In order to find the slope, as well as the force at the expansion joint and abutment, the method of least squares was used to determine a best fit line from the 15 force measurements. Figure 4.43 shows a free body diagram indicating a positive friction force orientation and a conceptual extrapolation of the best fit line to determine the forces at the expansion joint and abutment. Figure 4.44 shows the friction per unit slab length, f, of the slab on the base material for the

entire testing period. A positive or negative friction value simply represents the direction of the friction force as indicated in Figure 4.43. The maximum friction ranged from 8 to -8 kip/ft (coefficient of friction equal to the friction force/slab weight of 1.9 to -1.9), however, the majority of the friction ranged from 4 to -4 kip/ft (coefficient of friction of 0.95 to -0.95). The lower coefficient of friction range of 0.95 to -0.95 corresponds to a friction angle of approximately 43°, which is slightly higher than the upper limit presented by Das (1998) of 38° for friction between sand and concrete.

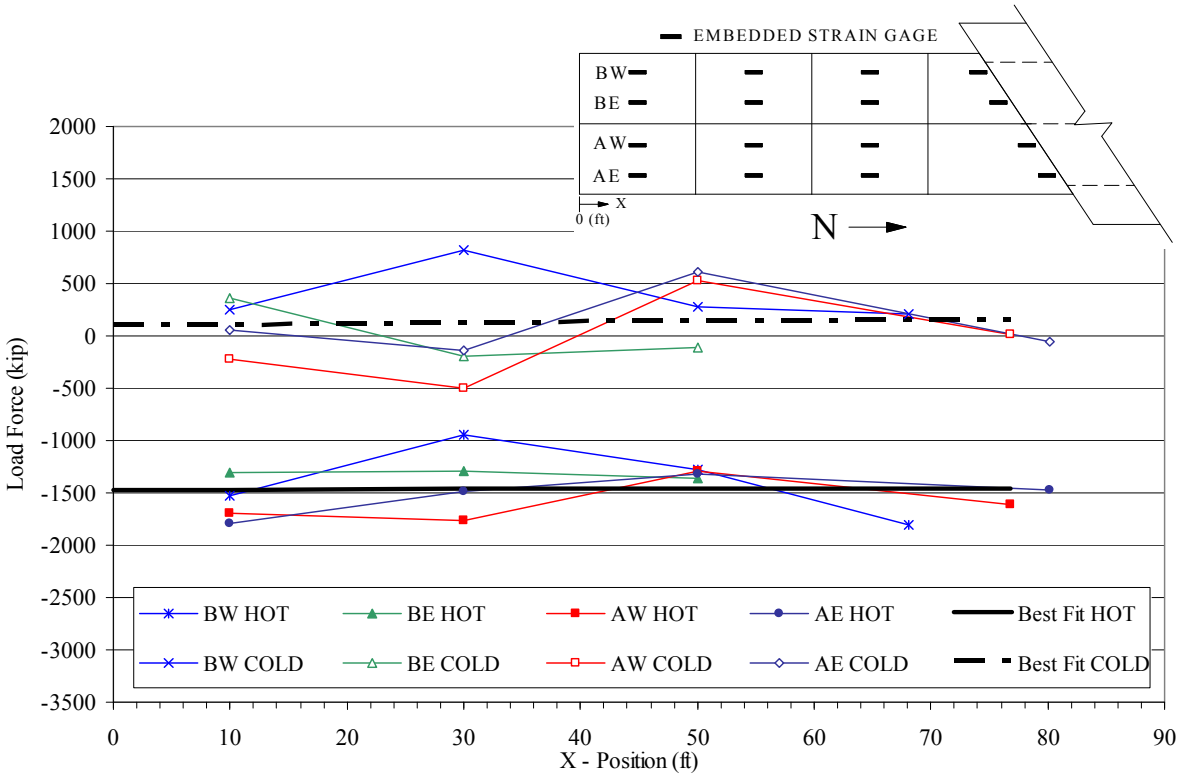


Figure 4.42. Hot and cold load force comparison with respect to location for the northbound bridge approach slab

The force at the expansion joint and abutment were calculated using the best fit procedure illustrated in Figure 4.43 and are shown in Figure 4.45. The expansion joint shows slightly larger negative forces (i.e., indicating a larger increase in compression) than the abutment, except during the spring and latter part of winter. The average force from the 15 strain gauges is also shown in Figure 4.45, and again shows a similar response. Since the three forces shown in Figure 4.45 are all very similar, the average slab force will be used in several plots to follow. When the expansion joint and abutment forces are plotted against temperature, abutment displacement, and expansion joint movement the results are nearly identical to the average slab force plots seen herein.

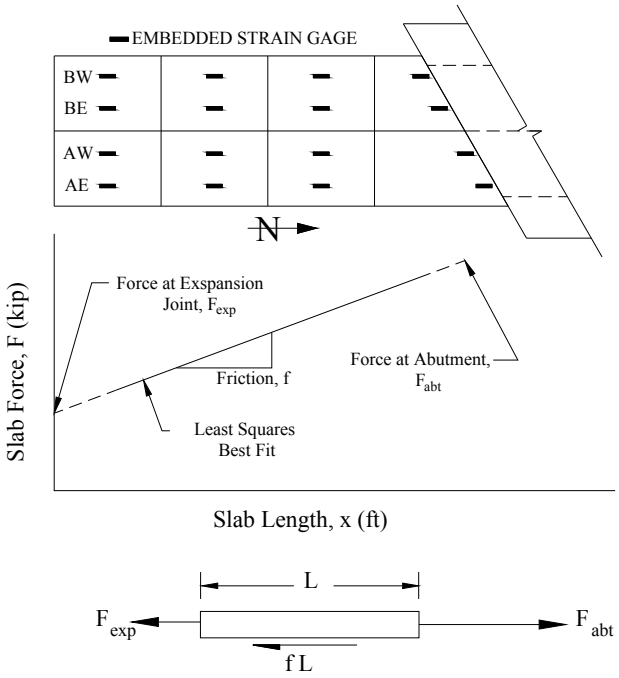


Figure 4.43. Free body diagram of friction force in slab

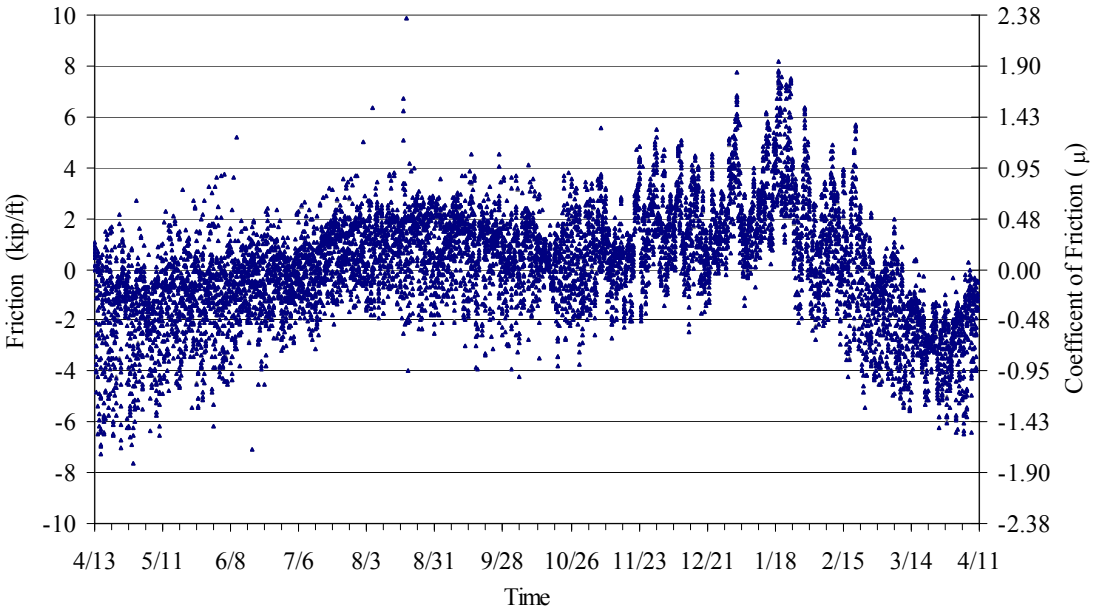


Figure 4.44. Bottom of slab friction over time – northbound bridge

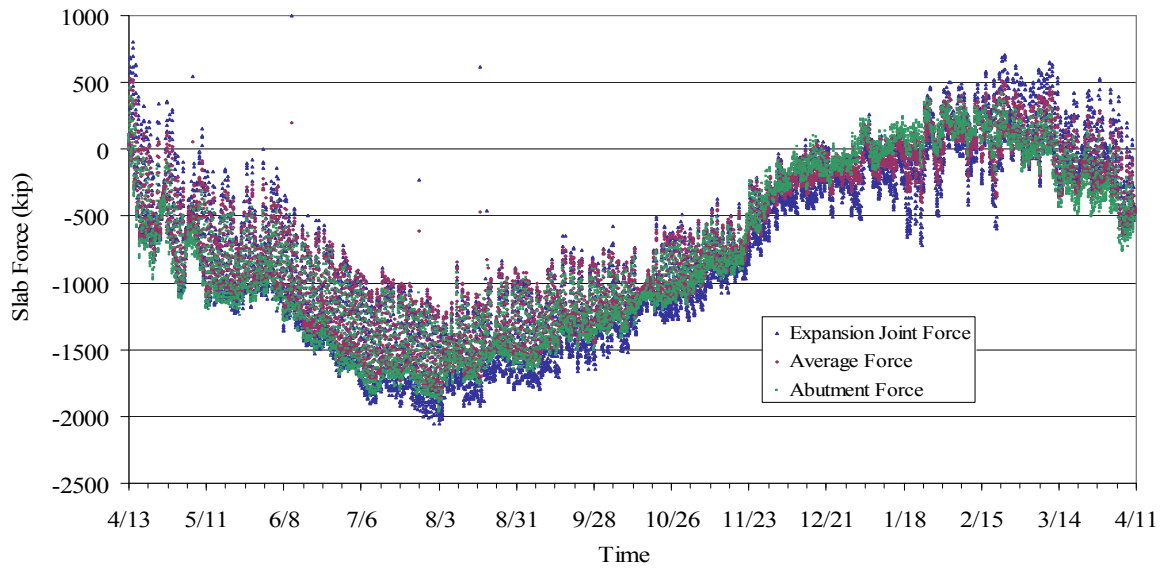


Figure 4.45. Comparison of northbound expansion joint, average, and abutment force

Figure 4.46 shows average slab force verse the change in average abutment movement from Figure 4.15 in Section 4.2.1. Once again, an annual cyclical behavior can be observed.

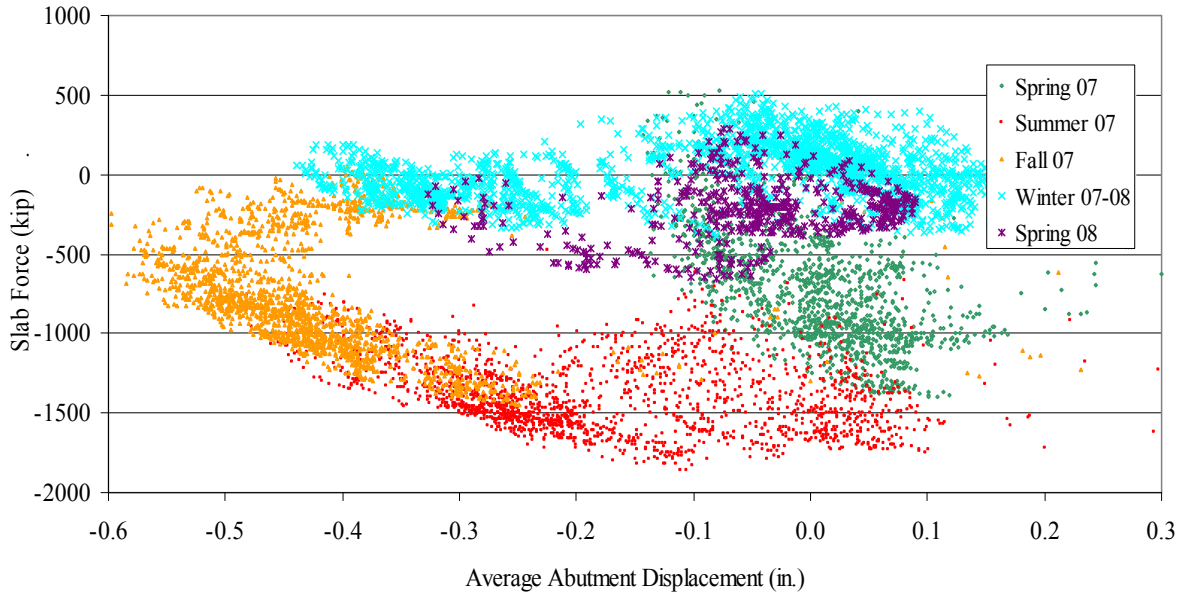


Figure 4.46. Northbound bridge approach slab average force relative to the average abutment movement

4.3.1. Post-Tensioning Strandmeters

Three longitudinal postensioned strands located in the slab were equipped with strandmeters (see Figure 3.14). The strandmeters measured the change in deformation of the strand relative to the initial instrument reading. The following equations were used to obtain the total strain from the strand meter:

$$\Delta D_{strandmeter} = \Delta R + \Delta T * K \tag{4.11}$$

$$\Delta \varepsilon_{strand} = \frac{\Delta D_{strandmeter}}{L} \tag{4.12}$$

Where:

ΔD = Change in deformation of strandmeter

L = Length of strandmeter (L = 8in. for the strandmeter)

K = Thermal correction factor for the strandmeter provided by suppler

$_{strandmeter}$ = properties or changes in the strandmeter

$_{strand}$ = properties or changes within the post-tensioning strand

The total strain in the strand is also given by Equation 4.13 in terms of load strain and thermal strain.

$$\Delta \varepsilon_{strand} = \Delta \varepsilon_{load} + \alpha_{strand} * \Delta T \tag{4.13}$$

Setting Equation 4.13 and the Equation 4.12 equal to each other the strain due to load can be obtained by Equation 4.14.

$$\Delta \varepsilon_{Load} = \frac{\Delta D_{strandmeter}}{L} - \alpha_{strand} * \Delta T \tag{4.14}$$

$$\Delta \sigma = \Delta \varepsilon_{strand} * E_{Strand} \tag{4.15}$$

Where:

E= Modulus of elasticity (E_{strand} = 28500ksi)

Figure 4.47 shows the variation in strain for the three transducers on the previously mentioned hot and cold days relative to transverse position. In general the three strains were found to be relatively uniform. Given this, the strains were averaged together to obtain an average change in strain of the strands over time, shown in Figure 4.48.

The strain, as shown in Figure 4.48, decreases during the spring and summer months when the temperatures are increasing and increases during the fall and winter months when the

temperatures are decreasing. The strand load strain does not completely return to the initial readings during the winter months suggesting that there are losses present in the postensioning system. The increase and decrease in strand strain, however, occur due to both the forces induced by bridge movement and the difference in the coefficient of thermal expansion of the concrete and steel. For example, since the steel has a higher value of the coefficient of thermal expansion the strand retracted more than the concrete as the temperature progressed from hot to cold, which increases the strand load stress and, hence, the strand tension.

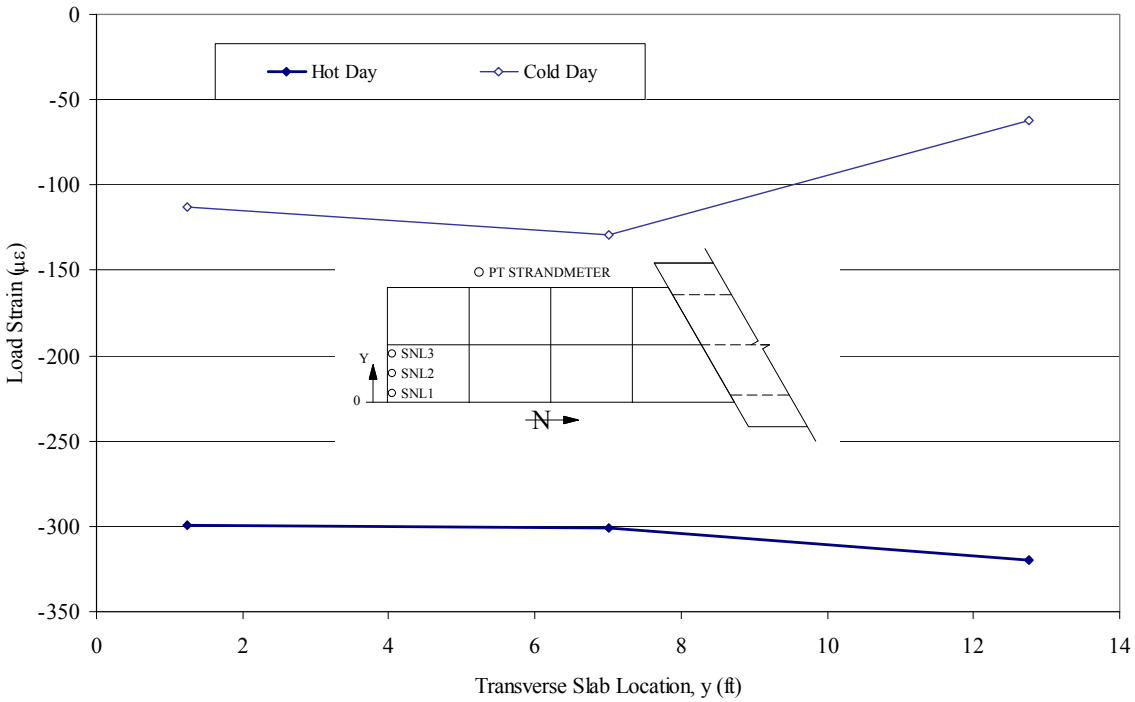


Figure 4.47. Load strain of post tensioning strand in the northbound bridge approach slab with respect to transverse position

The change of force in a strand was determined by multiplying the change in stress from Equation 4.15 by the strand area of 0.217 in^2. Figure 4.49 shows the change in average force over time for the strands. The strands were initially tensioned to 75% of their ultimate strength, or approximately 44 kips per strand. The range of change in average force was approximately 2.1 kips. The post-tensioning losses are illustrated by the change in postensioning force on November 14, 2007 and April 08, 2008 when the temperatures for both days were similar to April 13, 2007. Figure 4.49 shows that from April 13, 2007 to November 14, 2007 the force only rebounded to -1.1 kips, which represents the loss in each strand. The loss is less than 2.5% of the total initial stress within the strands. Similar results were found when comparing the change in force from April 13, 2007 to April 8, 2008.

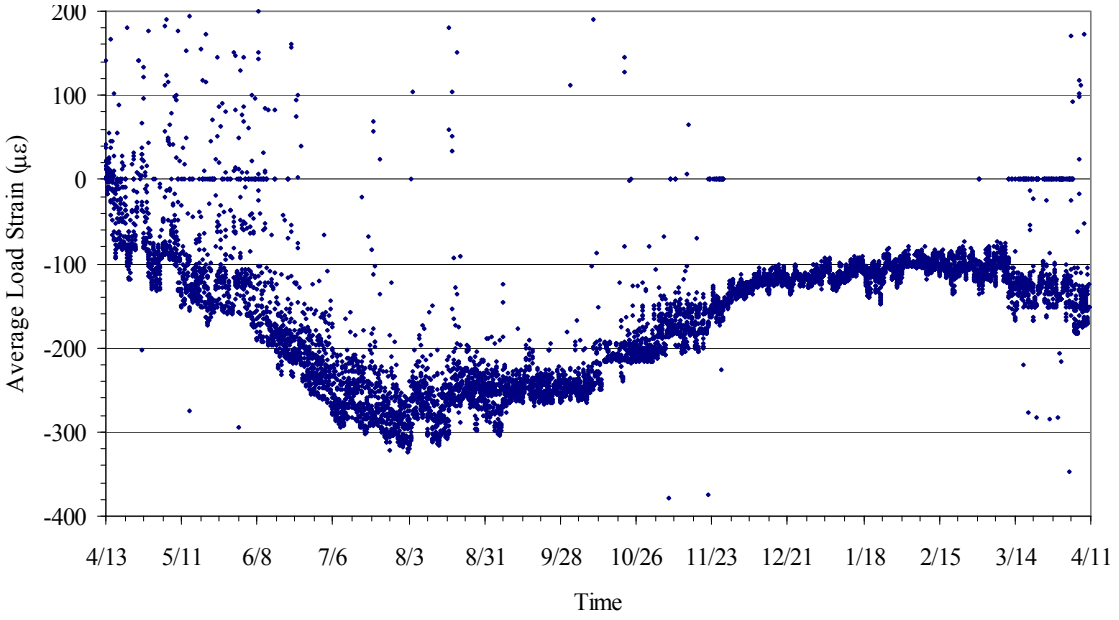


Figure 4.48. Average change in strand strain due to load over time – northbound bridge

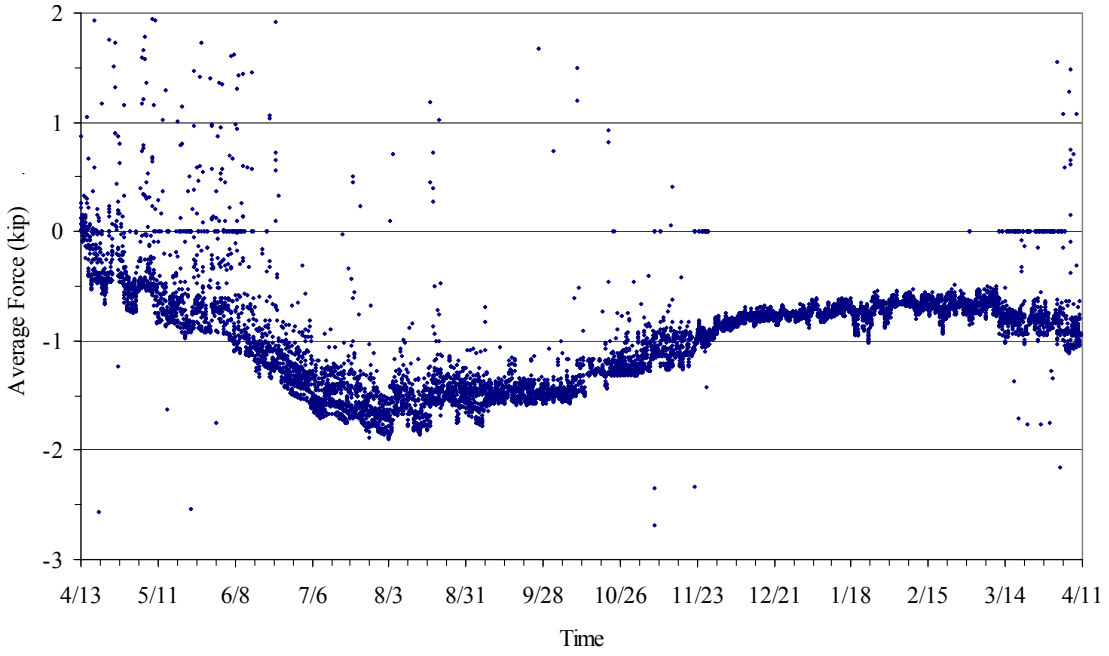


Figure 4.49. Change in prestress average force for a strand – northbound bridge

Figure 4.50 shows the load strain of a strand with respect to the average temperature of the slab. The load strain in the strand is illustrated by the two different sloping portions during the testing period. The change in slope of the fall 2007/winter 2007-2008 data compared to the spring 2007/ summer 2007 data indicates that most of the post tension losses occurred before September 2007.

After the post-tensioning losses took place, which appears to be around September 2007, the change of strain follows a linear path.

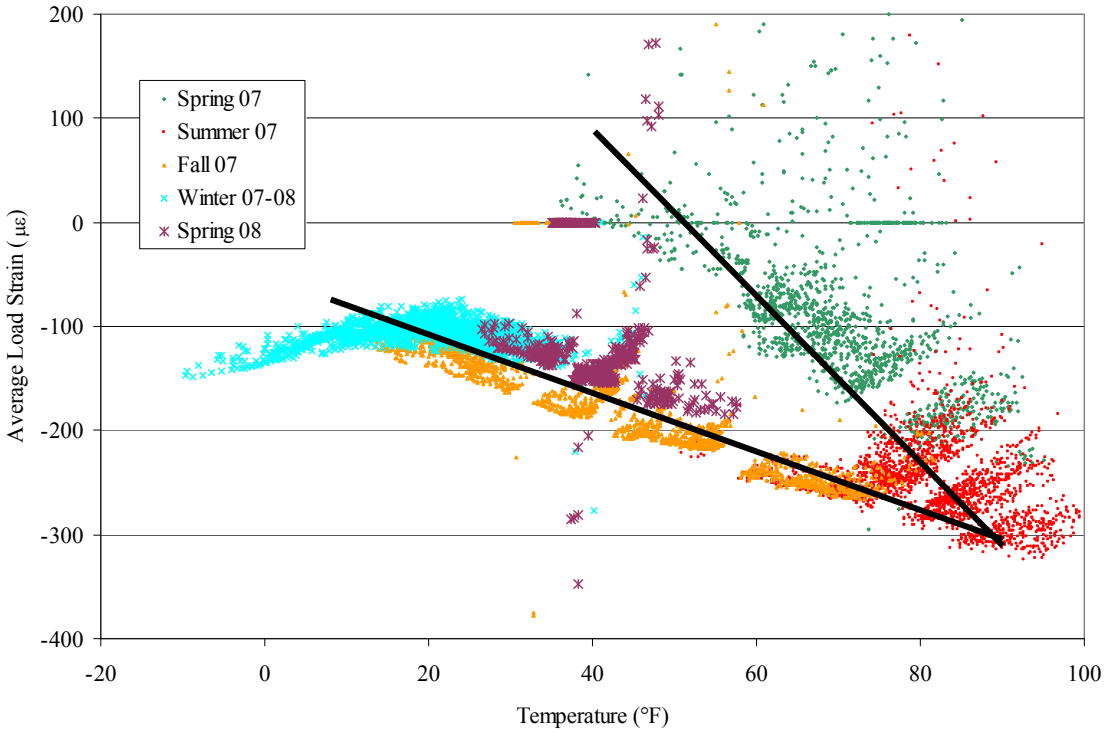


Figure 4.50. Change in post tensioning strain relative to average slab temperature

4.3.2. Crackmeters

The approach slab joints were equipped with crackmeters on the east and west faces of the slab to monitor joint opening and closing over time (see Figure 3.14). Similar equations were used for crackmeters as were used for the strandmeters. The measurement at the crackmeters is related to the change in readings by Equation 4.16.

$$\Delta D_{crackmeter} = \Delta R + \Delta T * K \tag{4.16}$$

Where:

K = Crackmeter thermal correction factor supplied by supplier

$_{crackmeter}$ = properties or changes in the crackmeter

To find the actual movement of the precast slab joints the concrete temperature and load effects must be accounted for over the length of the crackmeter.

$$\Delta\delta_{joint} = \Delta D_{crackmeter} - \alpha_{concrete} * \Delta T * L - \Delta\varepsilon_{load} * L \quad (4.17)$$

Where:

L = Length of crackmeter (L = 13.1in. for crackmeter)

$_{joint}$ = properties or changes precast slab joint

The crackmeters located on the west side of the of the approach slab, numbered CNW1 through CNW5, were damaged at some point after installation and the data obtained from these crackmeters were deemed to be unusable. The crackmeters located on the east side of the slab, denoted CNE1 through CNE5 in Figure 3.14, provided usable data during the duration of the project. Figure 4.51 shows the joint movement data for the east side of the precast slab. A positive movement indicates that the joint is opening. Joints CNE1 through CNE4, as shown in Figure 4.51, had less than 0.03 in. of movement during the test period. Crackmeter CNE5, which is located at the expansion joint of the approach slab and pavement, had a movement range of over 0.9 in. The change in the expansion joint, however, was less than that predicted by The Transtec Group and the Iowa DOT, who predicted a range of 1.70 in., with the bridge contributing 1.30 in. and the approach slab contributing 0.40 in.

The crackmeter at the expansion joint was connected to the pavement and to the precast approach slab. Therefore, the measurement obtained from crackmeter CNE5 is the relative movement of the approach slab and the pavement. No instrumentation was installed to monitor the actual movement of the pavement. The opening of the expansion joint has an inverse relationship with average slab temperatures, as shown in Figure 4.52. As the temperature increases the joint opening size decreases, as expected.

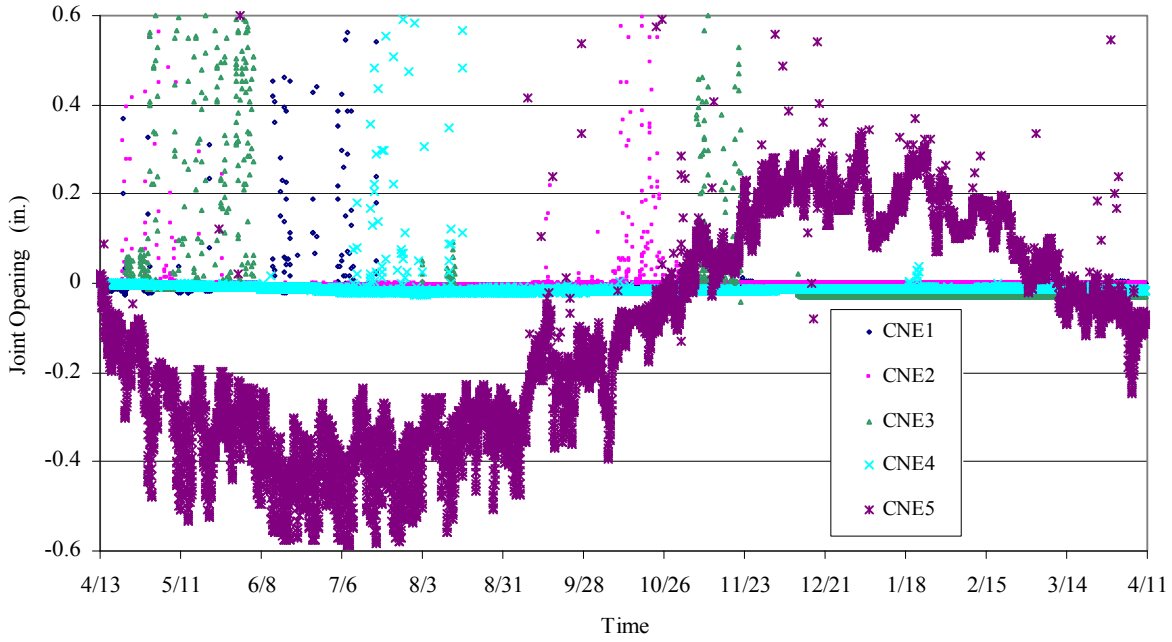


Figure 4.51. Northbound bridge precast approach slab joint movements

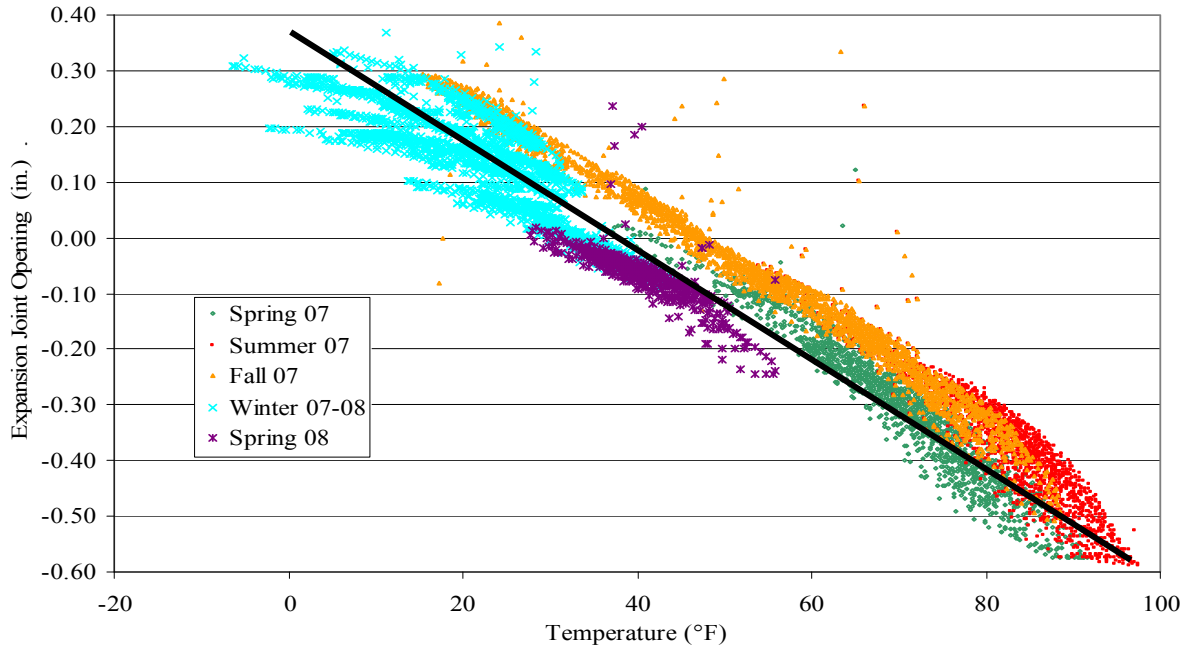


Figure 4.52. Northbound bridge expansion joint movement relative to average slab temperature

4.3.3. Comparison of Expansion Joint Movement and Abutment Movement

The total accumulated movement at the southern edge of the approach slab is shown in Figure 4.53. The south edge movement was calculated by summing the abutment movement (Section 4.2.1), change in slab length due to temperature and load strains (Section 4.3.1), and joint movement of CNE1 through CNE2 (Section 4.3.3). The joint movements, temperature, and stress effects contributed about 15% of the total movement of the slab. The maximum movement obtained during the test period was approximately 0.90 in. to the south, which is approximately a 0.15 in. increase from the abutment movement presented in Section 4.2.1.

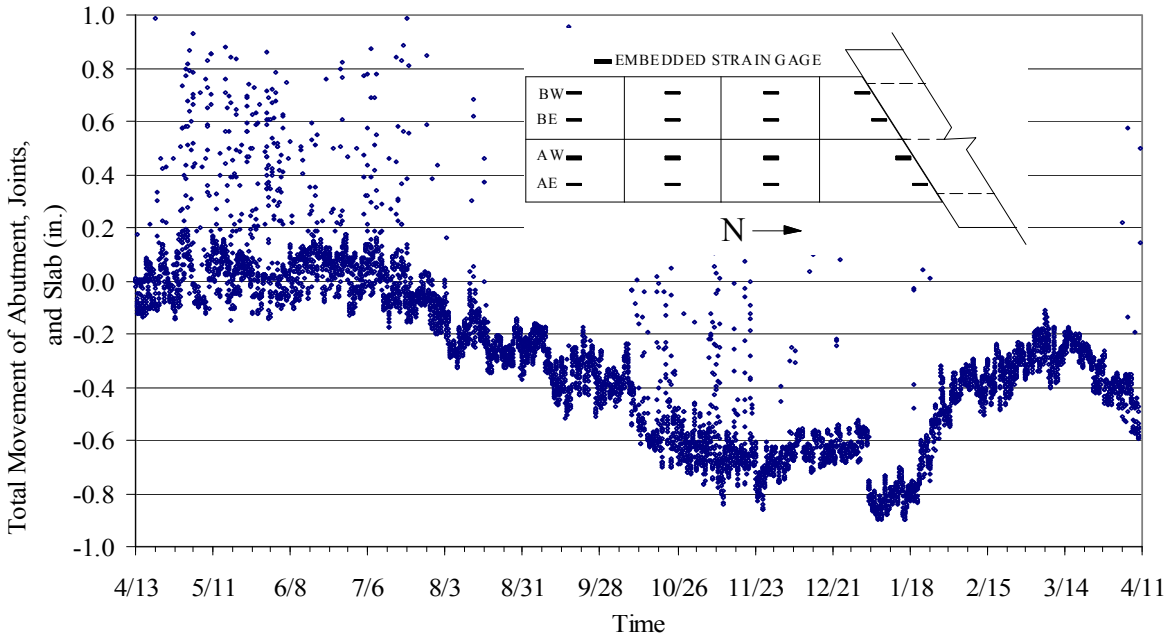


Figure 4.53. Total movement of south end of northbound bridge approach slab

Figure 4.54 shows the abutment movement (Section 4.2.1) with respect to the expansion joint opening. During the fall, the abutment moved to the north (negative) as the temperatures decreased and the expansion joint size increased as expected. However, this same pattern was not seen during the other seasons. The abutment had less than 0.2 in. of movement during spring 07, leading one to believe that the expansion joint would see very nearly the same amount of closure (if the pavement had not moved) and the joint was functioning as expected. The expansion joint during spring 07 closed 0.6 in., which is nearly three times the movement of the abutment.

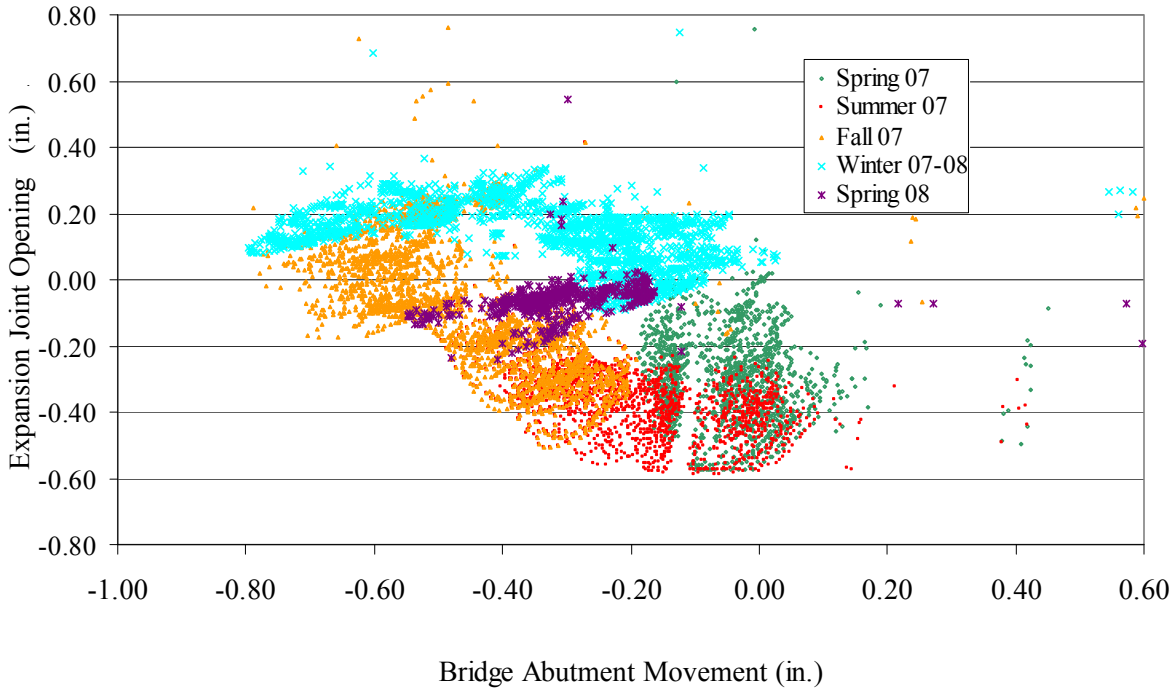


Figure 4.54. Comparison of northbound bridge abutment movement and expansion joint movement

When the expansion joint opening is compared with the force in the slab, as shown in Figure 4.55, the force in the slab increases as the expansion joint contracts. Similar to Figure 4.40 and Figure 4.41 the spring and fall seasons were transition periods where the change in force increased or decreased, respectively, with the temperature change of that season. During the summer, the maximum increase in compression occurred along with the maximum contraction of the expansion joint. The opposite was observed during the winter. In addition, a short term looping cyclical pattern discussed in Section 4.2.1 is very evident.

The expansion joint should allow free movement of the slab relative to the pavement, however, improper working dowel bars and/or foreign matter within the expansion joint could cause a build up of stress. The large force in the summer leads one to believe that the expansion joint or the dowel bars are not working properly causing an increase in the compression force in the slab as the pavement and approach slab move closer together. A portion of the build up or reduction of force within the slab can be attributed to differences in the coefficient of thermal expansion of the strand and the concrete.

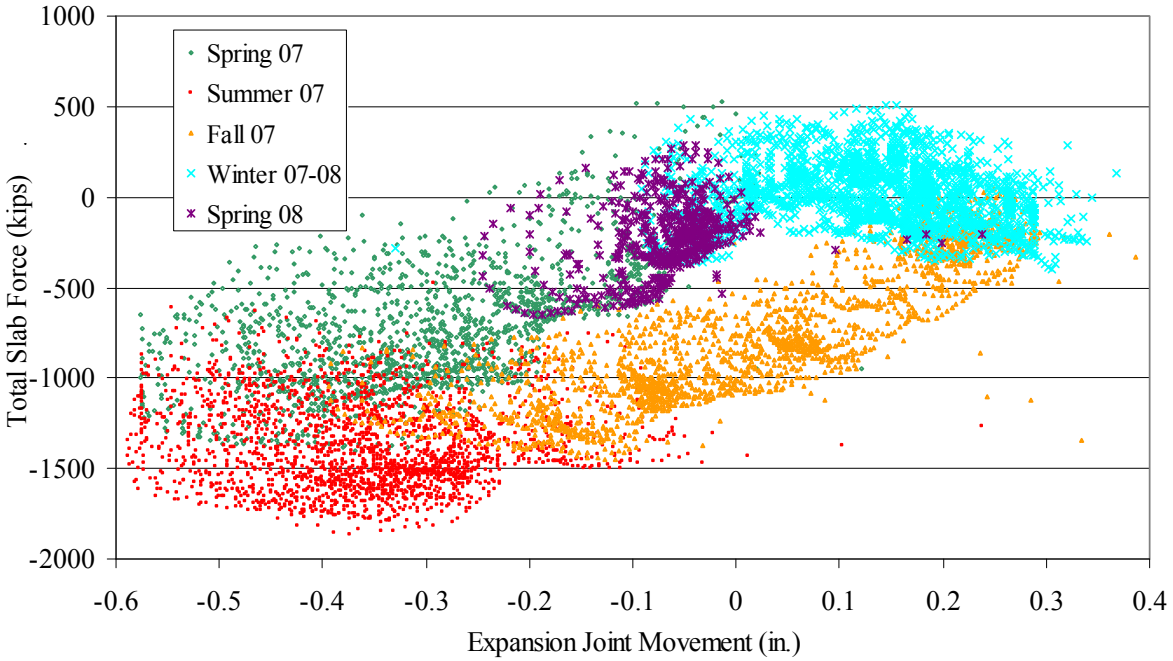


Figure 4.55. Northbound bridge expansion joint movement related to the load force in the approach slab

4.4. Bridge Substructure

4.4.1. Pile Gauges

Three HP 10x57 piles located in the south abutment of the northbound bridge were monitored with four strain gauges located on each pile. The location of the strain gauges and positive local axis orientation of the piles is shown in Figure 4.56. The pile orientation and location with respect to the abutment is shown in Figure 4.57. Of the 12 pile gauges installed on the northbound bridge only six stayed operational during the test period. Figure 4.58 and Figure 4.59 show the west and middle pile strain responses, respectively, for the test duration. The strain response from gauge PNW1 and PNM1 were not used due to the gauge only working properly for the first three months and data scatter. No usable data were obtained from the east pile strain gauges.

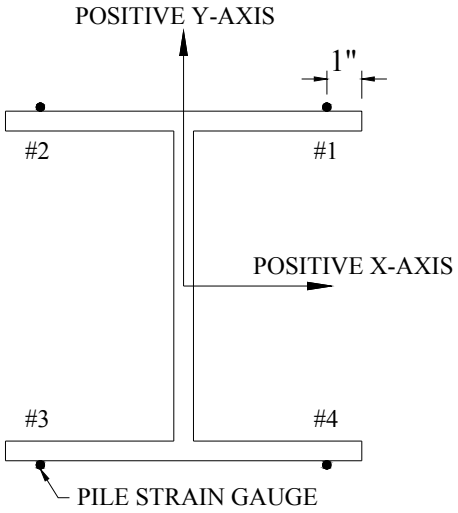


Figure 4.56. Gauge location and orientation of local axis (HP 10x57 pile)

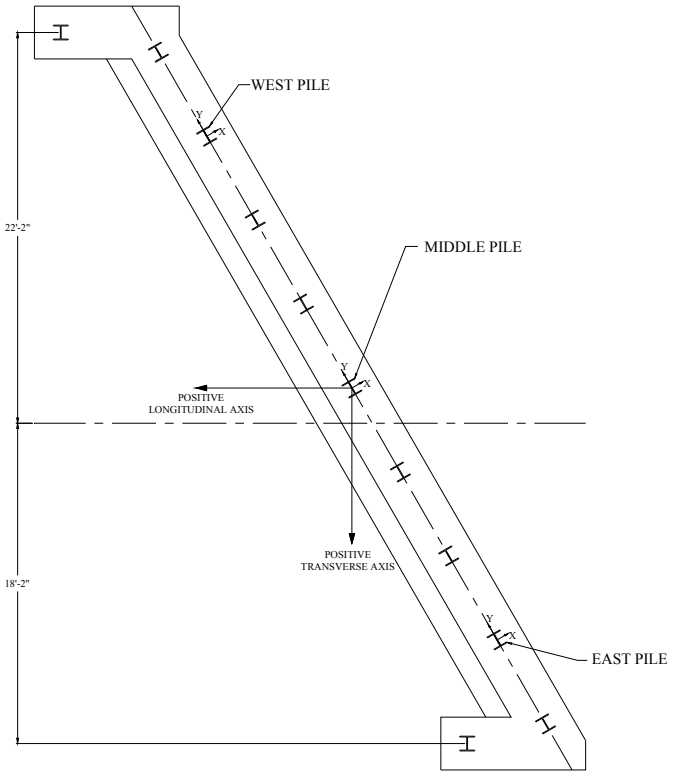


Figure 4.57. Pile location and global axis orientation

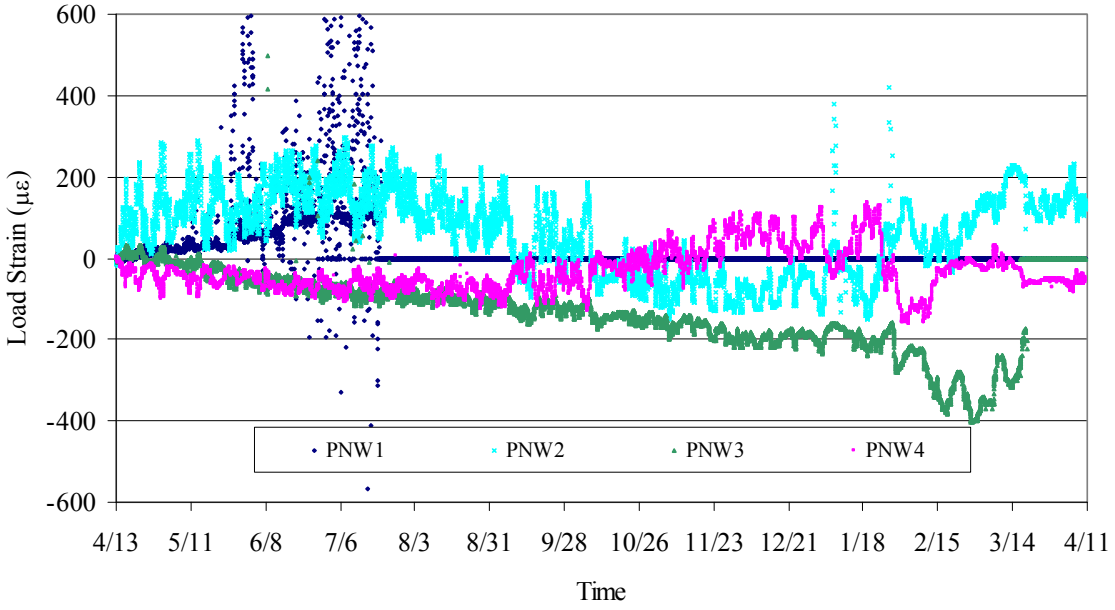


Figure 4.58. Northbound bridge west pile strains obtained at tips of flanges

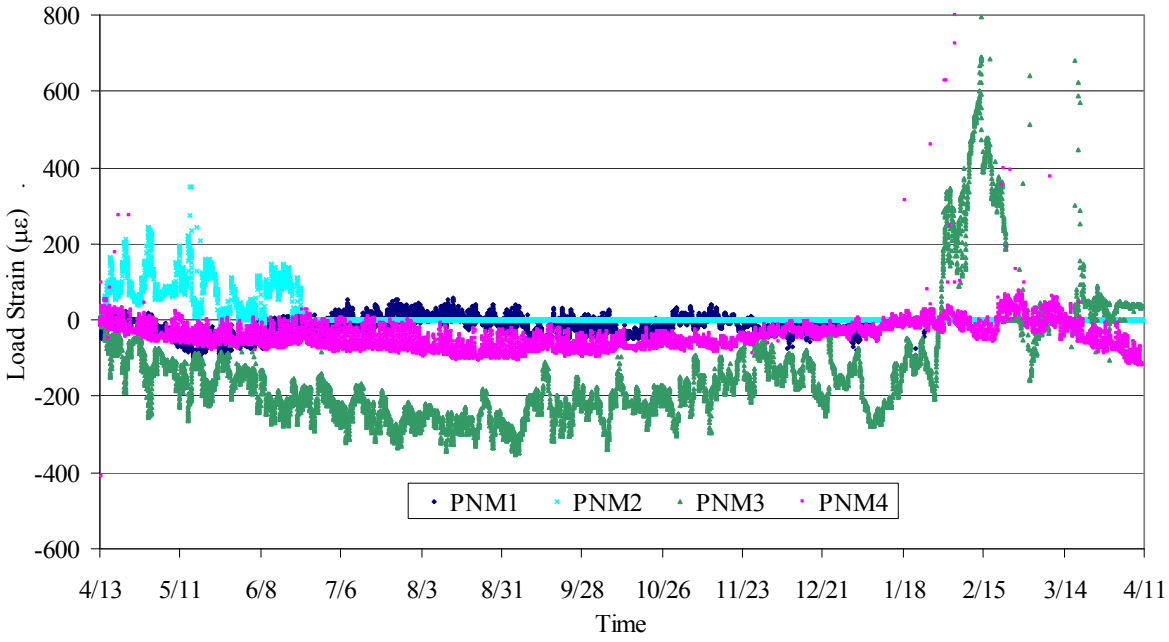


Figure 4.59. Northbound bridge middle pile strains obtained at tips of flanges

The individual strains obtained from the pile gauges are composed of the summation of axial strain, ε_a; x-axis bending strain, ε_x; y-axis bending strain, ε_y; and torsional normal-warpage

strain, ε_t. The relationship relating the four strain measurements and the four strain components are shown in Equation 4.18 through 4.21. These relationships can only be used if the members are doubly symmetric and the gauges are placed doubly symmetrically about the centroid of the member.

$$\Delta\varepsilon_1 = \Delta\varepsilon_a + \Delta\varepsilon_x - \Delta\varepsilon_y + \Delta\varepsilon_t \tag{4.18}$$

$$\Delta\varepsilon_2 = \Delta\varepsilon_a + \Delta\varepsilon_x + \Delta\varepsilon_y - \Delta\varepsilon_t \tag{4.19}$$

$$\Delta\varepsilon_3 = \Delta\varepsilon_a - \Delta\varepsilon_x + \Delta\varepsilon_y + \Delta\varepsilon_t \tag{4.20}$$

$$\Delta\varepsilon_4 = \Delta\varepsilon_a - \Delta\varepsilon_x - \Delta\varepsilon_y - \Delta\varepsilon_t \tag{4.21}$$

Where:
$\Delta\varepsilon$ = change in strain
$_1$ = Longitudinal strain at location #1
$_2$ = Longitudinal strain at location #2
$_3$ = Longitudinal strain at location #3
$_4$ = Longitudinal strain at location #4
$_a$ = Axial strain component
$_x$ = x-axis bending strain
$_y$ = y-axis bending strain
$_t$ = Torsional normal warpage strain

When Equations 4.18 through 4.21 are solved simultaneously the axial strain, torsional strain, x-axis bending strain, and y-axis bending strain can be obtained by the resulting Equations, 4.22 through 4.25 respectively.

$$\Delta\varepsilon_a = \frac{(\Delta\varepsilon_1 + \Delta\varepsilon_2 + \Delta\varepsilon_3 + \Delta\varepsilon_4)}{4} \tag{4.22}$$

$$\Delta\varepsilon_t = \frac{(\Delta\varepsilon_1 - \Delta\varepsilon_2 + \Delta\varepsilon_3 - \Delta\varepsilon_4)}{4} \tag{4.23}$$

$$\Delta\varepsilon_x = \frac{(\Delta\varepsilon_1 + \Delta\varepsilon_2 - \Delta\varepsilon_3 - \Delta\varepsilon_4)}{4} \tag{4.24}$$

$$\Delta\varepsilon_y = \frac{(-\Delta\varepsilon_1 + \Delta\varepsilon_2 + \Delta\varepsilon_3 - \Delta\varepsilon_4)}{4} \tag{4.25}$$

Since the data obtained from the piles is restricted to three operational gauges the torsional normal-warpage strains must be assumed to be negligible in order to solve three simultaneous equations for the three unknown component strains. Equations 4.26 through 4.28 give the combination of longitudinal pile strains that can be used to determine the axial, x-axis, and y-axis bending strains. Of the two equations listed for each force only one was used based on which specific gauges were operational.

$$\Delta\varepsilon_a = \frac{(\Delta\varepsilon_1 + \Delta\varepsilon_3)}{2} \text{ or } \Delta\varepsilon_a = \frac{(\Delta\varepsilon_2 + \Delta\varepsilon_4)}{2} \tag{4.26}$$

$$\Delta\varepsilon_x = \frac{(\Delta\varepsilon_1 - \Delta\varepsilon_4)}{2} \text{ or } \Delta\varepsilon_x = \frac{(\Delta\varepsilon_2 - \Delta\varepsilon_3)}{2} \tag{4.27}$$

$$\Delta\varepsilon_y = \frac{(\Delta\varepsilon_2 - \Delta\varepsilon_1)}{2} \text{ or } \Delta\varepsilon_y = \frac{(\Delta\varepsilon_3 - \Delta\varepsilon_4)}{2} \tag{4.28}$$

The axial, x-axis bending, and y-axis bending strains obtained for the west and middle piles by use of Equations 4.26 through 4.28 are shown in Figure 4.60 and Figure 4.61, respectively. As seen, the west and middle pile showed very different responses during the duration of the testing period.

The pile strains were converted into axial force, P; x-axis moment, M_x; and y-axis moment, M_y; by using Equations 4.29 through 4.31 respectively.

$$\Delta P = \Delta\varepsilon_a * A * E \tag{4.29}$$

$$\Delta M_x = \frac{I_x * E * \Delta\varepsilon_x}{c_y} \tag{4.30}$$

$$\Delta M_y = \frac{I_y * E * \Delta\varepsilon_y}{c_x} \tag{4.31}$$

Where:
ΔP = Change in axial force
ΔM_x = Change in x-axis bending force
ΔM_y = Change in y-axis bending force
A = Area of the steel pile
E = Modulus of elasticity of steel pile (E = 29000ksi)
c_x = distance to the extreme fibers on the x-axis
c_y = distance to the extreme fibers on the y-axis

Figure 4.62 and Figure 4.63 show the forces in the pile for the west and middle pile, respectively. The west pile x-axis moment, y-axis moment, and axial force had ranges of approximately 455 kip*in., 142 kip*in., and 90 kips respectively. The middle pile had a different bending response during the testing period. The range of x-axis bending moment and y-axis bending moment for the middle pile was 215 kip*in. and 300 kip*in. respectively. The response pattern of the middle pile axial force was different from the west piles, however, the ranges of force for both piles were the same

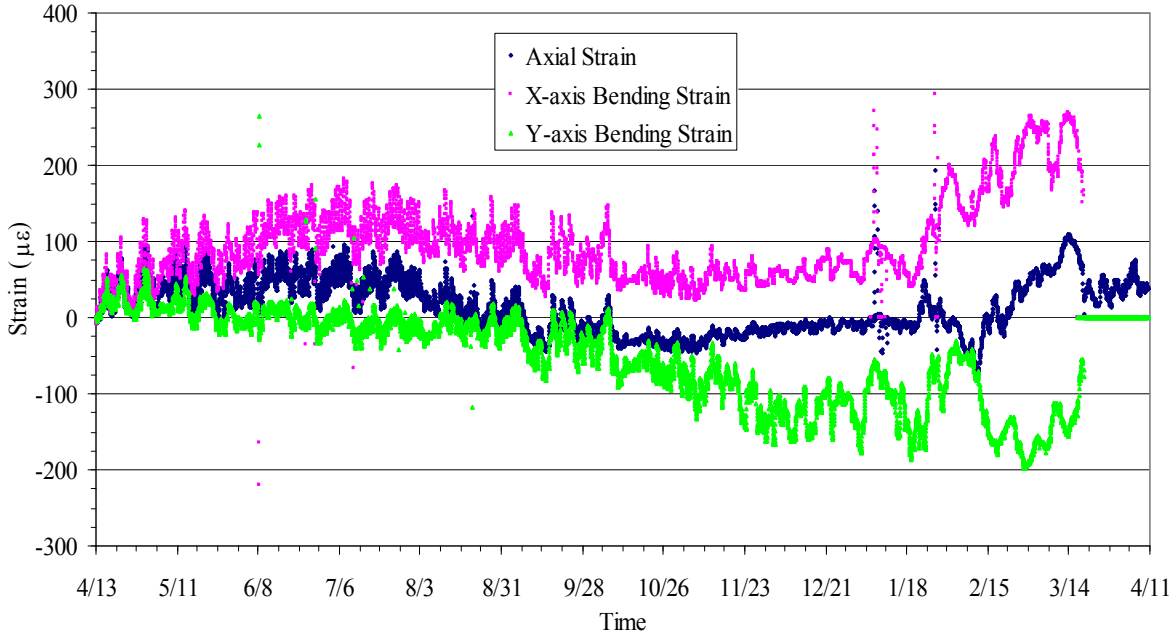


Figure 4.60. Northbound bridge west pile axial and bending strains

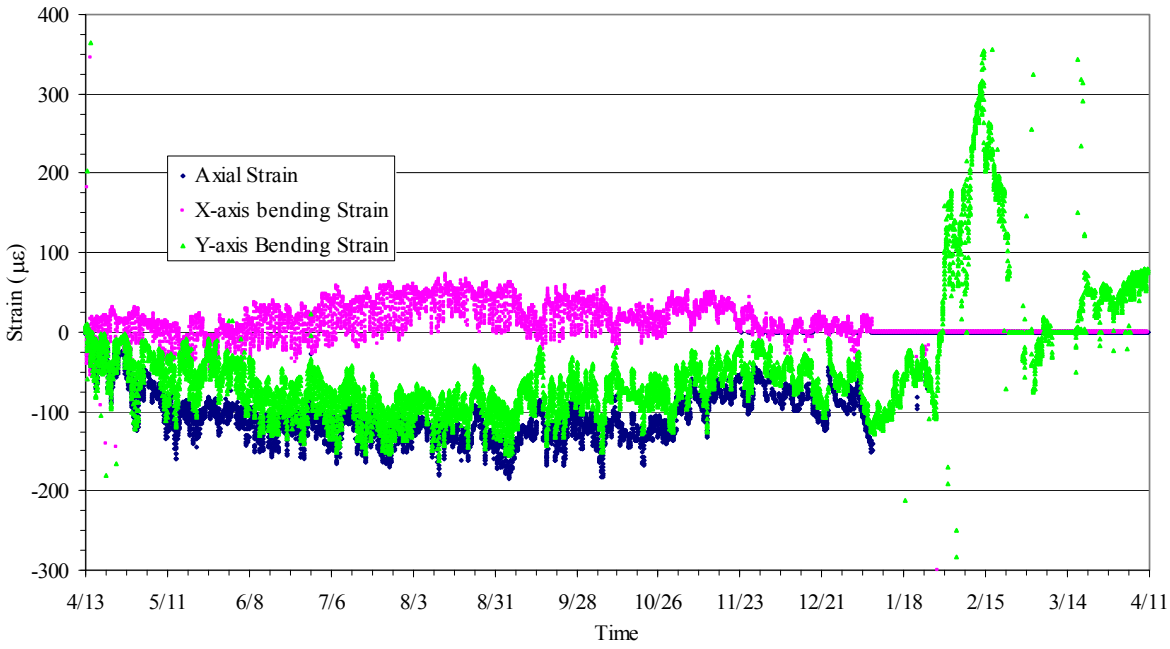


Figure 4.61. Northbound bridge middle pile axial and bending strains

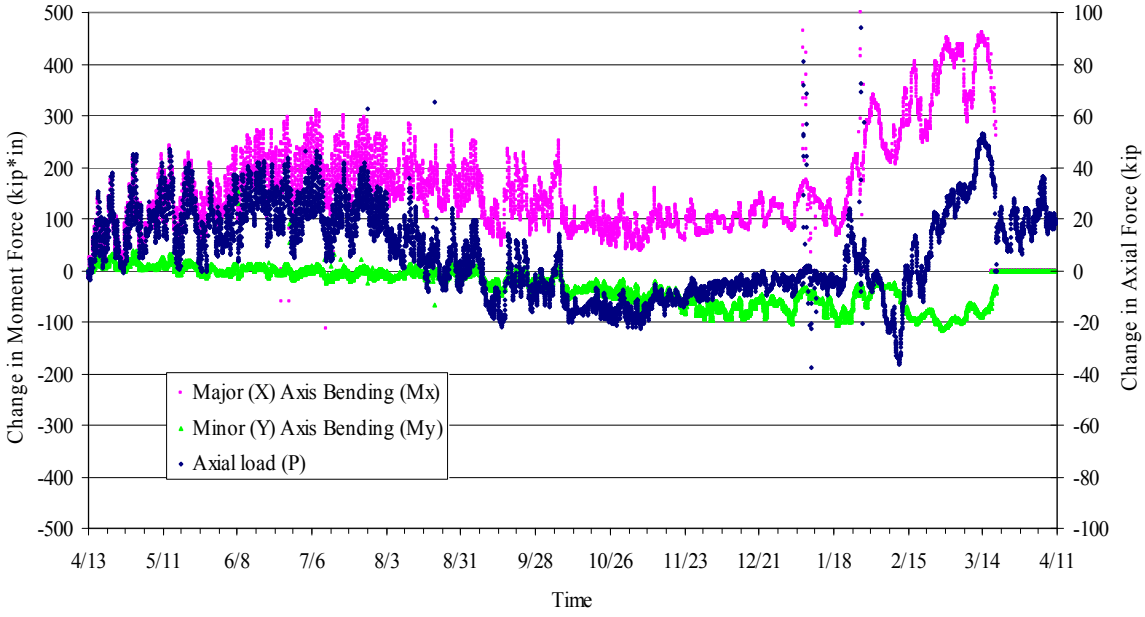


Figure 4.62. Forces in northbound bridge west pile

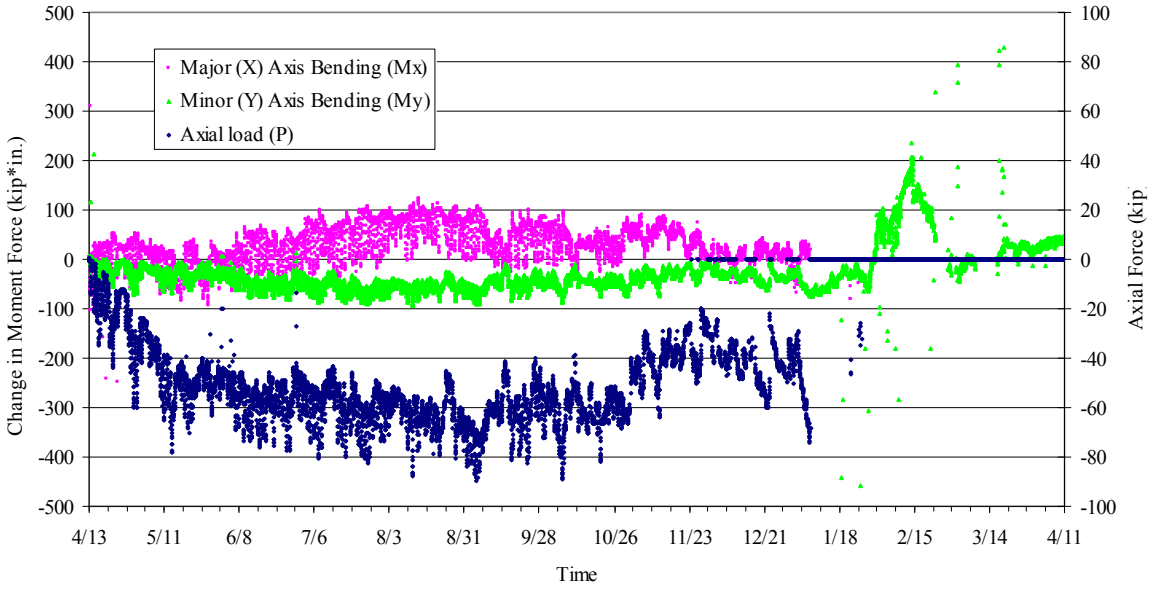


Figure 4.63. Northbound bridge middle pile forces

The forces in the piles were compared with the movements of the abutment presented in Section 4.2.2. To make these comparisons the longitudinal and transverse abutment movements were transformed into local strong (x) and weak (y) axis movements for each pile. Figure 4.64 and Figure 4.65 show the west pile forces with respect to the local x and y movements. From the plotted figures the relationship between the movement of abutment and the corresponding force is not clear though, again, some short term looping trends seem to be evident.

Similar plots were created for comparison of the middle pile movement and forces. Figure 4.66 and Figure 4.67 show the middle pile forces and corresponding movements.

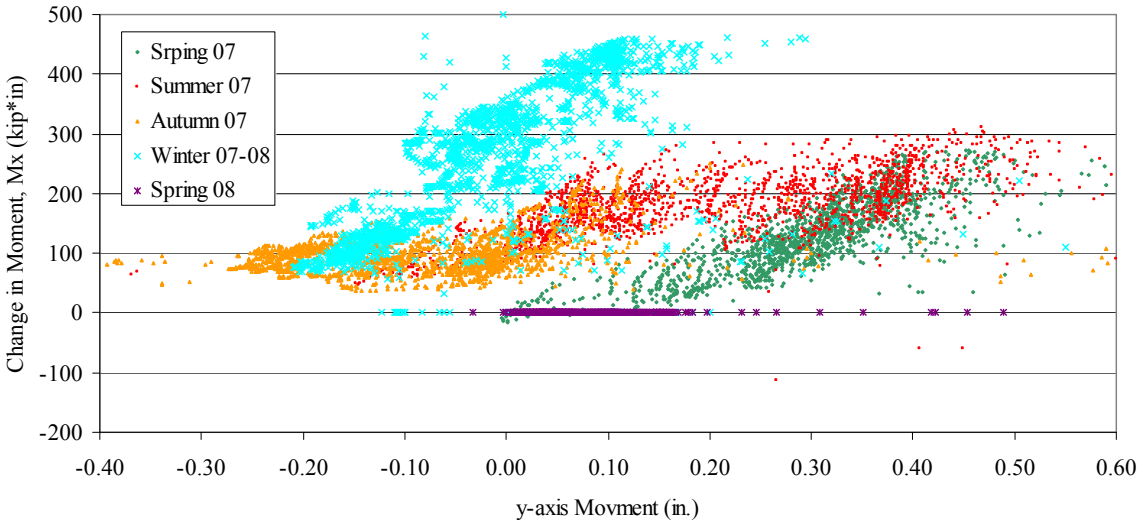


Figure 4.64. Northbound bridge west pile y-axis movement compared to strong axis bending

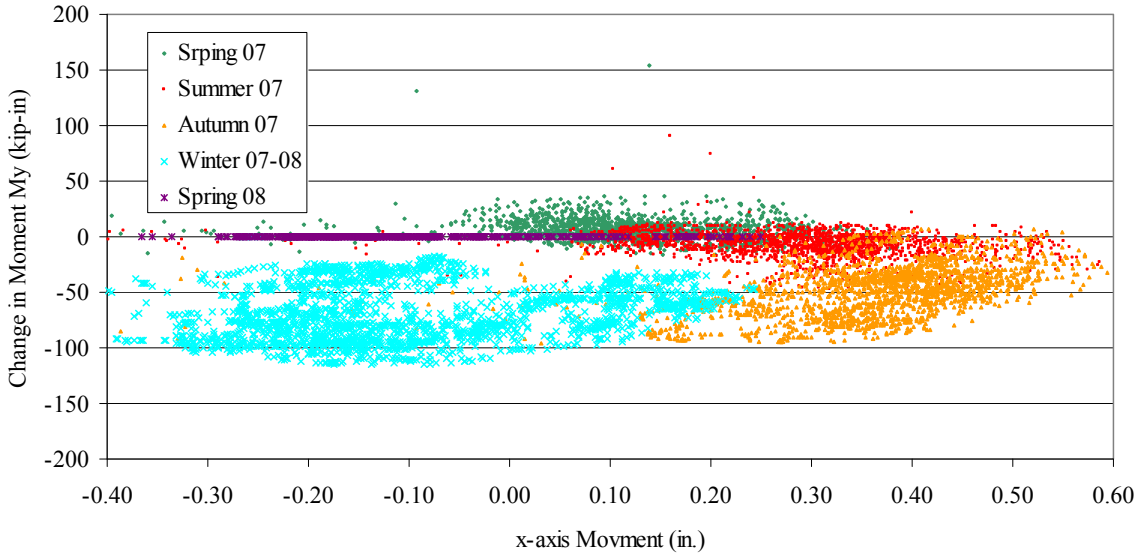


Figure 4.65. Northbound bridge west pile x-axis movement compared to weak axis bending

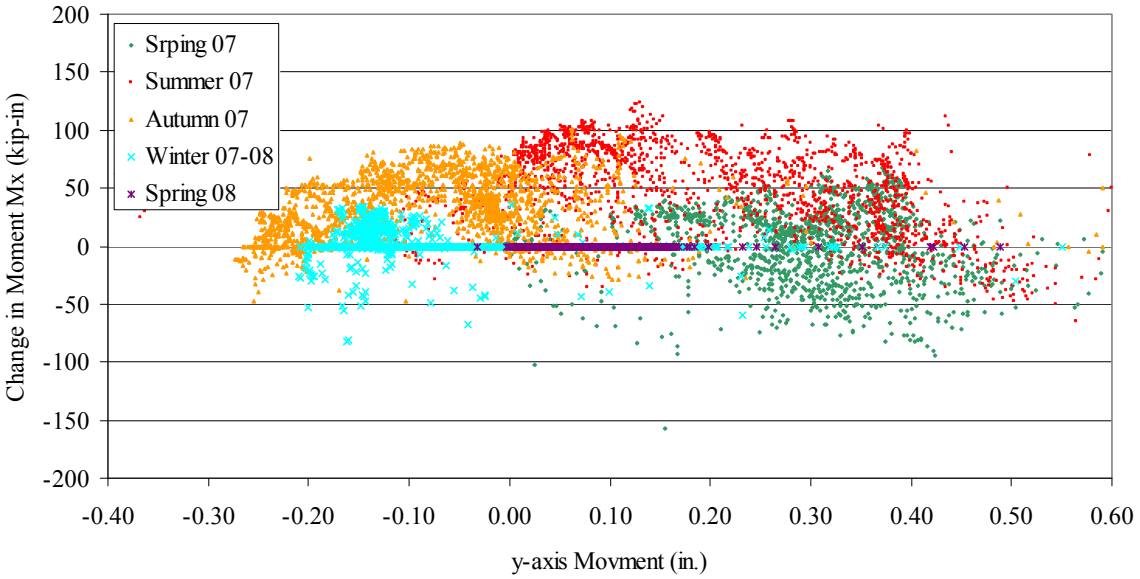


Figure 4.66. Northbound bridge middle pile y-axis movement compared to strong axis bending

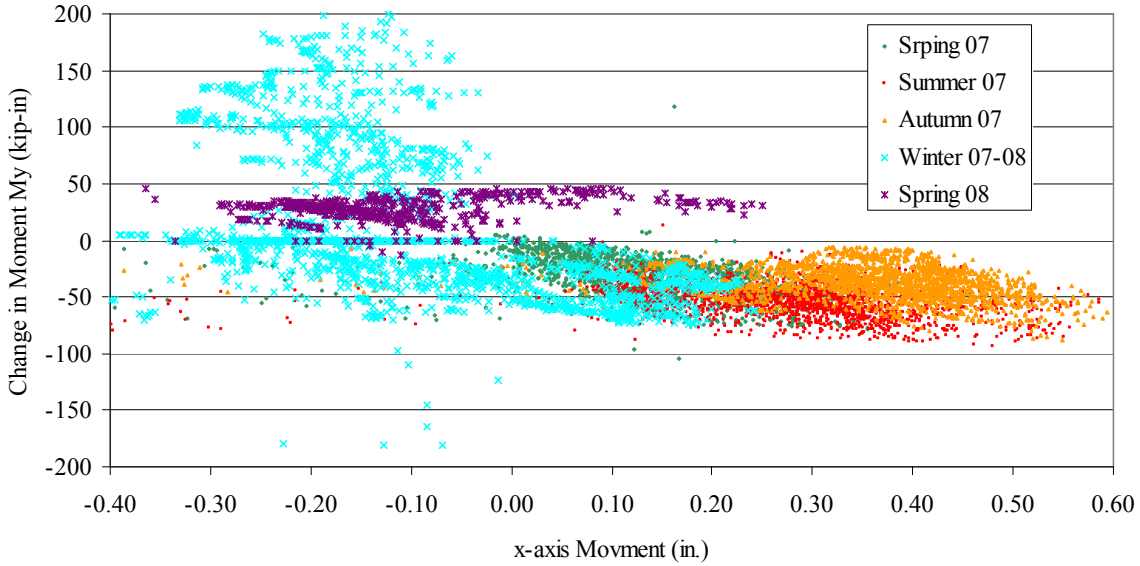


Figure 4.67. Northbound bridge middle pile x-axis movement compared to weak axis bending

4.5. Visual Inspection

During visits to the project site in the Spring of 2008, visual inspections of the bridges and approach slabs were performed. During the visit April 10th, 2008 a transverse crack was found in the middle of panel 2A on the south end (refer to Figure 3.7). The crack ran from the east shoulder and continued across the panel to the grouted longitudinal joint. The end of the crack at the east shoulder is shown in Figure 4.68. No other cracks or other signs of deterioration were found at the either end of the bridge.

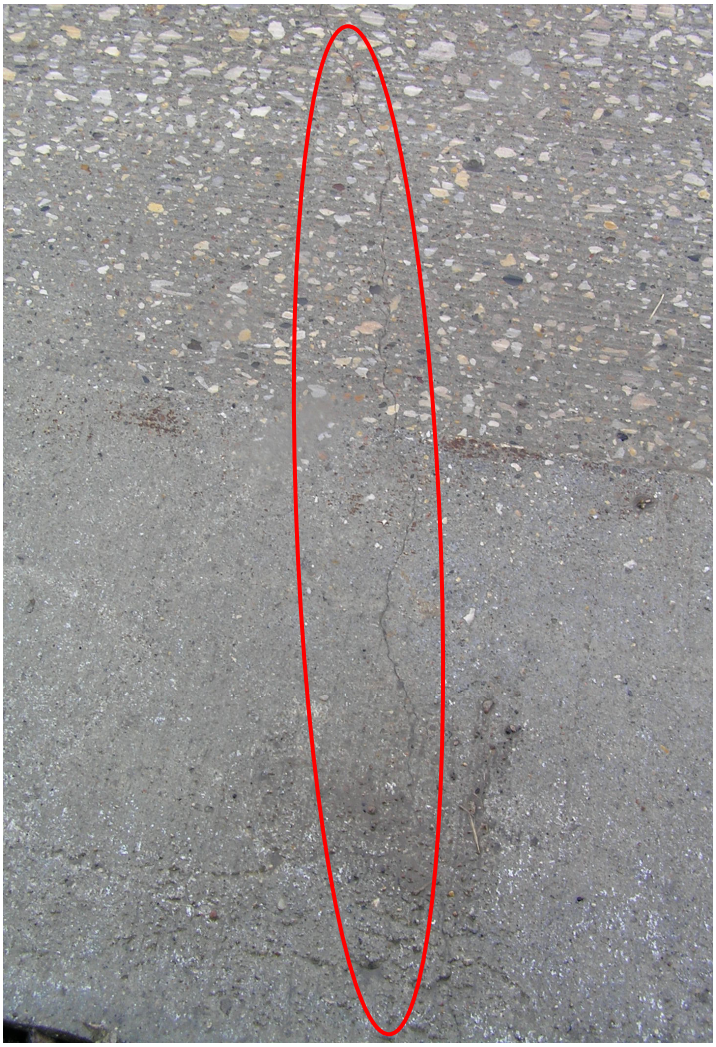


Figure 4.68. Transverse crack in precast approach slab

5. SOUTHBOUND BRIDGE RESULTS

5.1. Temperature

5.1.1. Approach Slab Temperatures

The internal temperature of the cast-in-place approach slab on the southbound bridge was measured in a manner similar to the approach slab for the northbound bridge (refer to Section 4.1.1). The primary difference between the northbound approach slab and the southbound approach slab embedded gauges is that there is only one transverse group of embedded gauges instead of the four installed in the northbound bridge approach (see Figure 3.14). Using the same hot and cold days as was used for the northbound bridge discussion, the temperature recorded by the strain gauge thermistors is shown in Figure 5.1 with respect to the position of the gauge across the slab. Note that gauge ESWE has a malfunctioning thermistor and will not be utilized here. Ignoring gauge ESWE, the measured temperature can be seen in Figure 5.1 to be almost constant across the slab width.

The average temperature of the 5 working gauges of the southbound approach slab plotted against time is shown in Figure 5.2. Unexpectedly warm temperatures (i.e., never colder than 30 °F in January) suggested that there may have been something wrong with the measured temperatures of the southbound bridge. The average southbound approach slab temperature was compared to the average northbound approach slab temperature (Figure 5.2), and was found to compare fairly well from April to September, as would be expected for two similar structures built beside each other. However, after September, the southbound average temperature deviates and unexplainably records a warmer temperature than the northbound bridge for the remaining time.

The disparity in temperatures between the northbound and southbound was not limited to just the approach slabs. Section 5.1.2 discusses the temperatures measured by the girder gauges and the conclusions drawn from this disparity. In Section 5.1 results from the southbound bridge will be compared to the northbound bridge, since the temperatures should be very similar for two similar structures built besides each other. All other comparisons between the two bridges and the resulting conclusions can be found in Chapter 6.

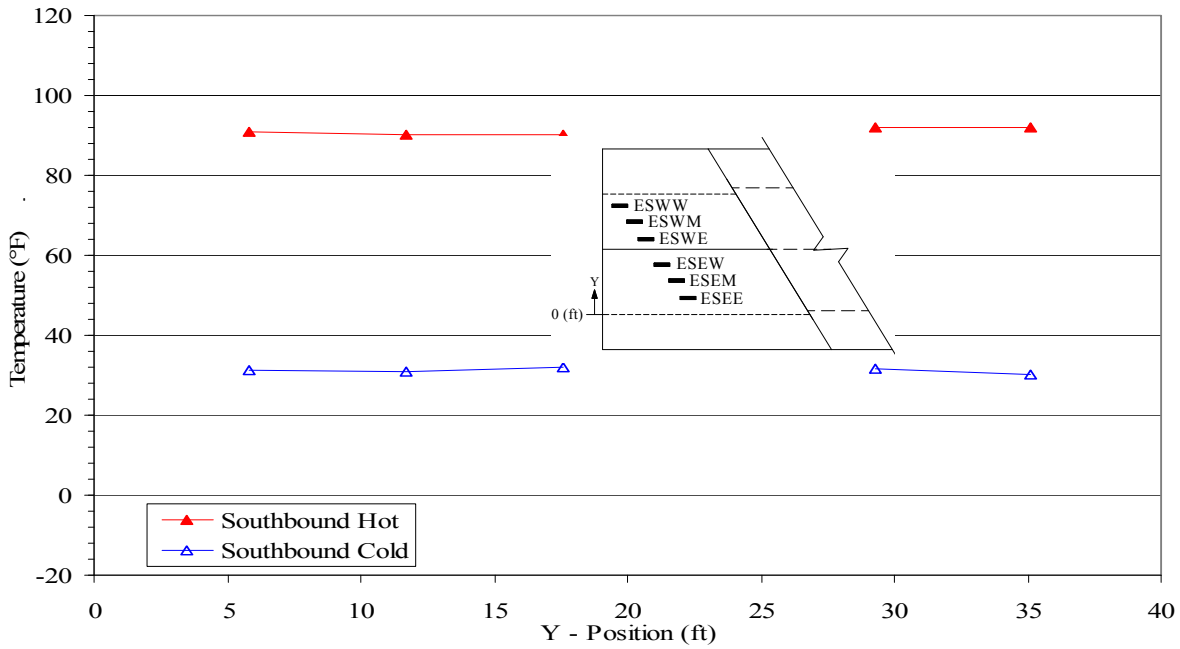


Figure 5.1. Temperature variation across the southbound bridge cast-in-place approach slab

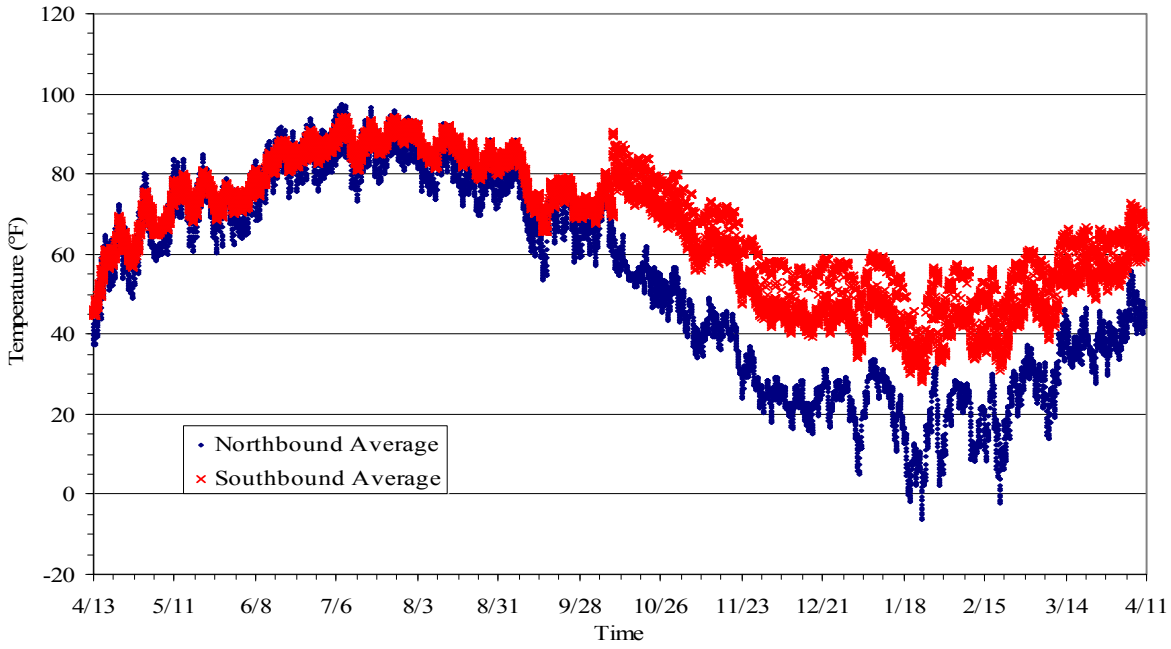


Figure 5.2. Average southbound and northbound bridge approach slab temperatures over time

5.1.2. Bridge Superstructure Temperature

The temperature of the bridge superstructure on the southbound bridge is measured in the same manner as the northbound bridge since they have the same instrumentation plan. See Section 4.1.2 for additional details.

Temperatures recorded by the top and bottom girder strain gauges are shown in Figure 5.3 and Figure 5.4 respectively, relative to the gauge longitudinal position. As can be seen, the temperature remains fairly constant both across the bridge width and along the length of the girders. The same typical hot and cold days were used as in Section 4.1.2.

Because there was almost no variation in the temperature across the bridge, the recorded temperatures at the top and bottom flanges were averaged across the bridge. These averages were then compared relative to the gauge position along the girder (see Figure 5.5).

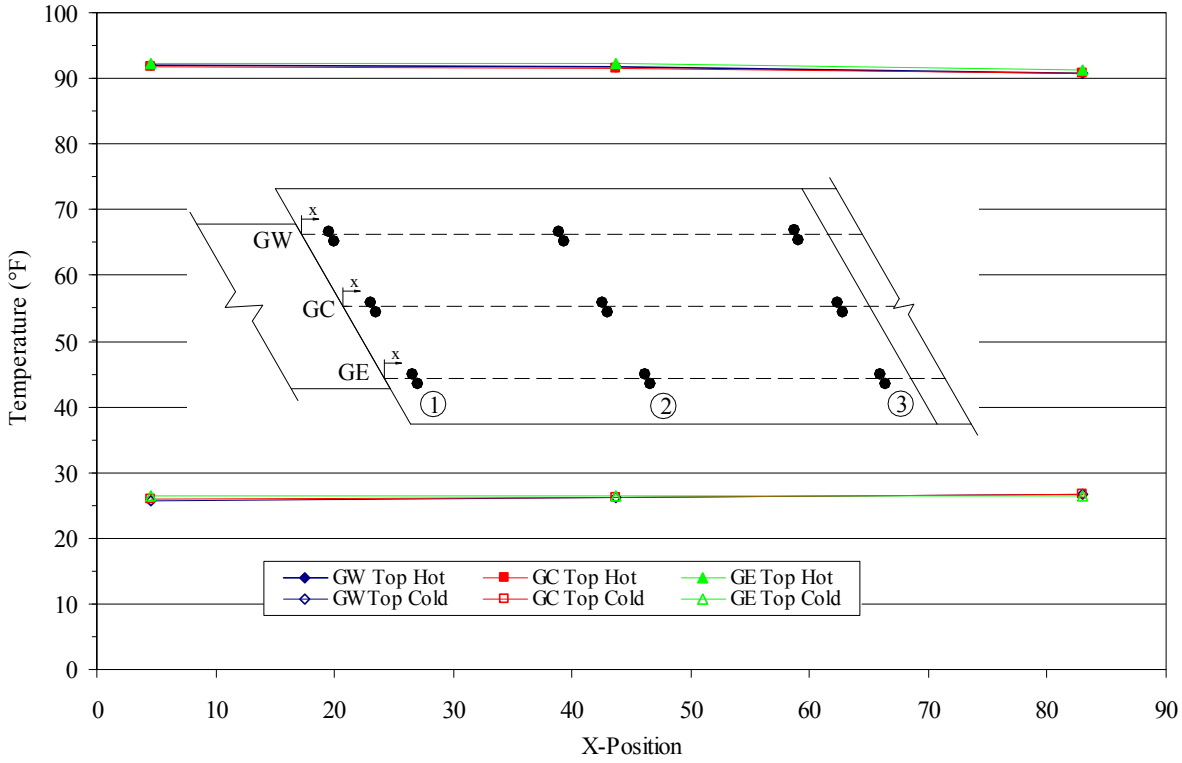


Figure 5.3. Temperature variation of the top of the southbound bridge girders

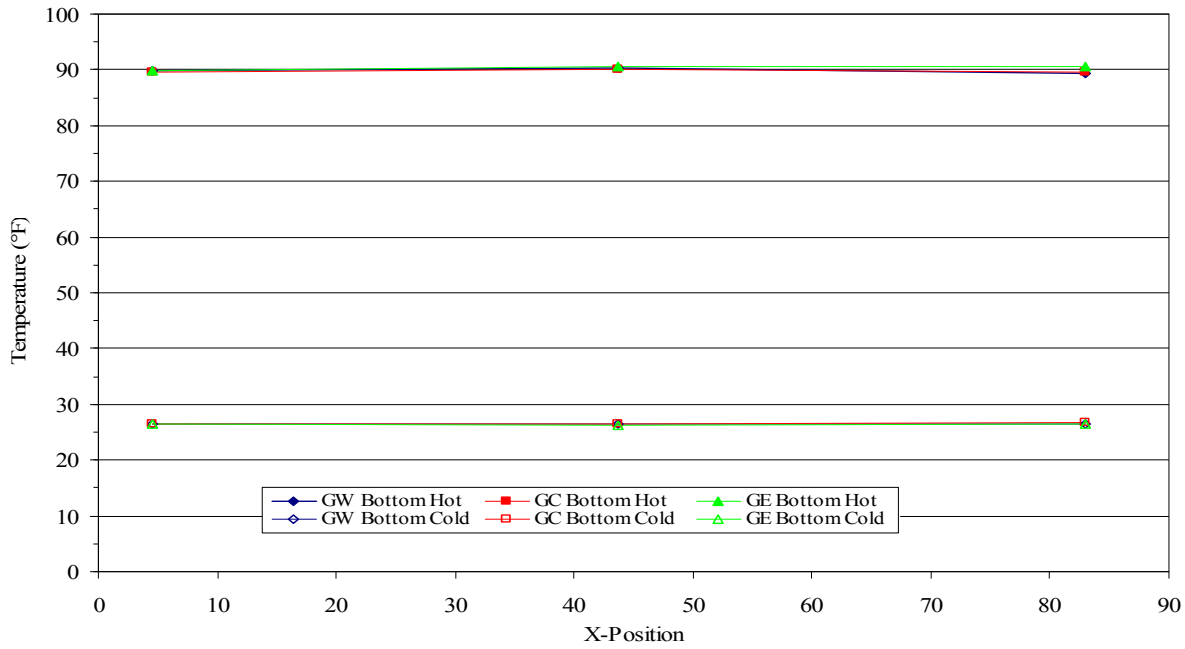


Figure 5.4. Temperature variation of the bottom of the southbound bridge girders

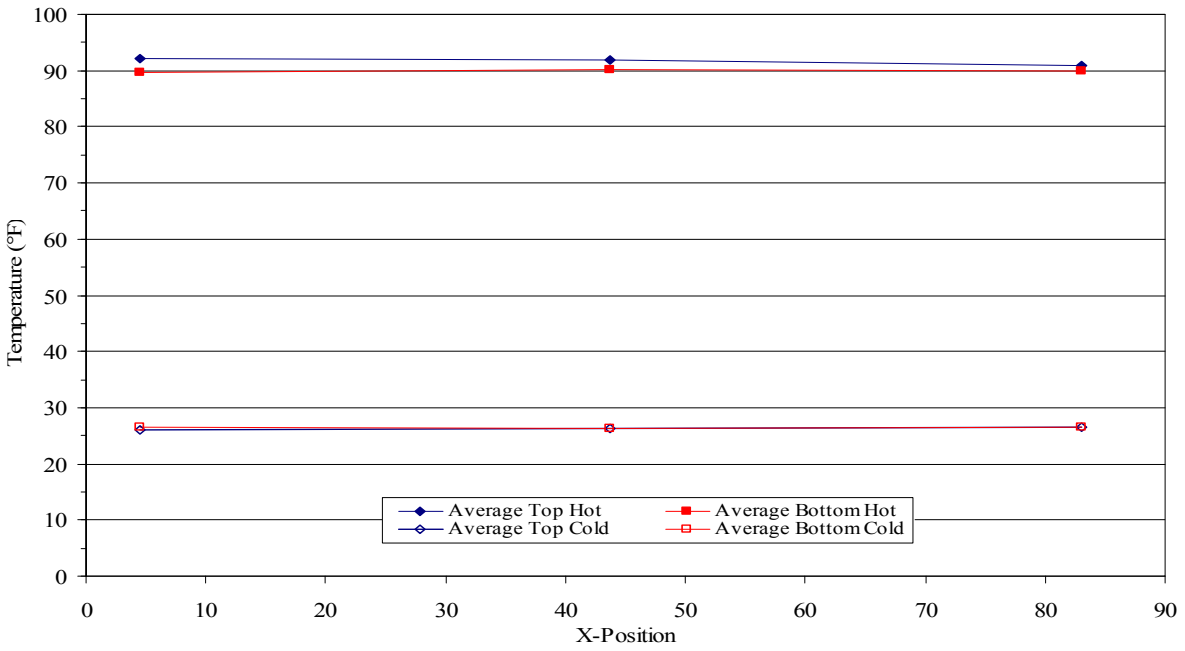


Figure 5.5. Average temperature variation along the southbound bridge girders

Again, like the northbound bridge there was only a slight variation between the temperatures at the top of the girders and at the bottom of the girders. Therefore, the temperatures measured by

the 9 gauges on the top flange and those of the 9 bottom flange gauges were averaged (henceforth referred to as the bridge temperature) and are shown with respect to time in Figure 5.6. The temperature range is from -22 °F to 99 °F

The southbound bridge temperature is compared to the northbound bridge temperature in Figure 5.7. Similar to the approach slabs, the two bridge temperatures do not compare. Specifically, after September the southbound bridge temperatures deviate from the northbound bridge temperatures by approximately 20 °F, which indicates that one of the recorded bridge temperatures is incorrect.

When the southbound bridge temperature is compared to the air temperature from Section 4.1.2 in Figure 5.8 and Figure 5.9 and simultaneously compared to the northbound bridge temperature in Section 4.1.2, the error in the southbound bridge temperature becomes clear. Clearly the southbound bridge temperature deviates from the air temperature after September. As a result, the correlation between the southbound bridge and the air temperature (see Figure 5.9) is also not as good as the correlation between the northbound bridge and the air temperature shown in Section 4.1.2. After this analysis it was decided to use the northbound bridge temperatures for analysis of the southbound bridge.

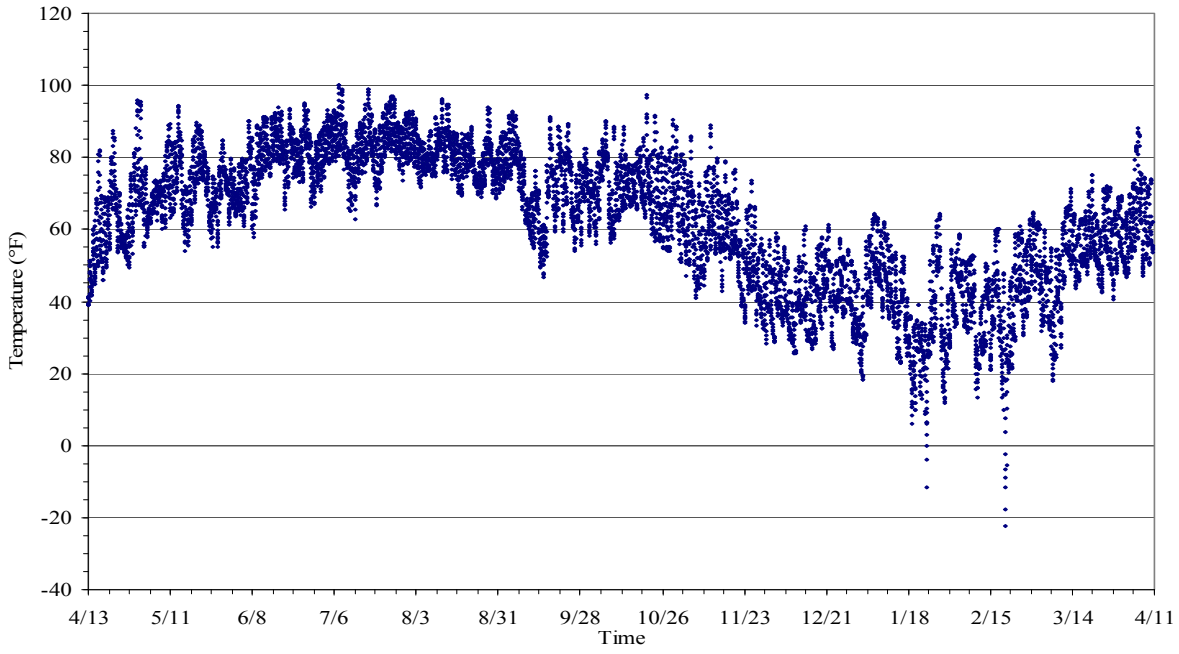


Figure 5.6. Southbound bridge temperature over time

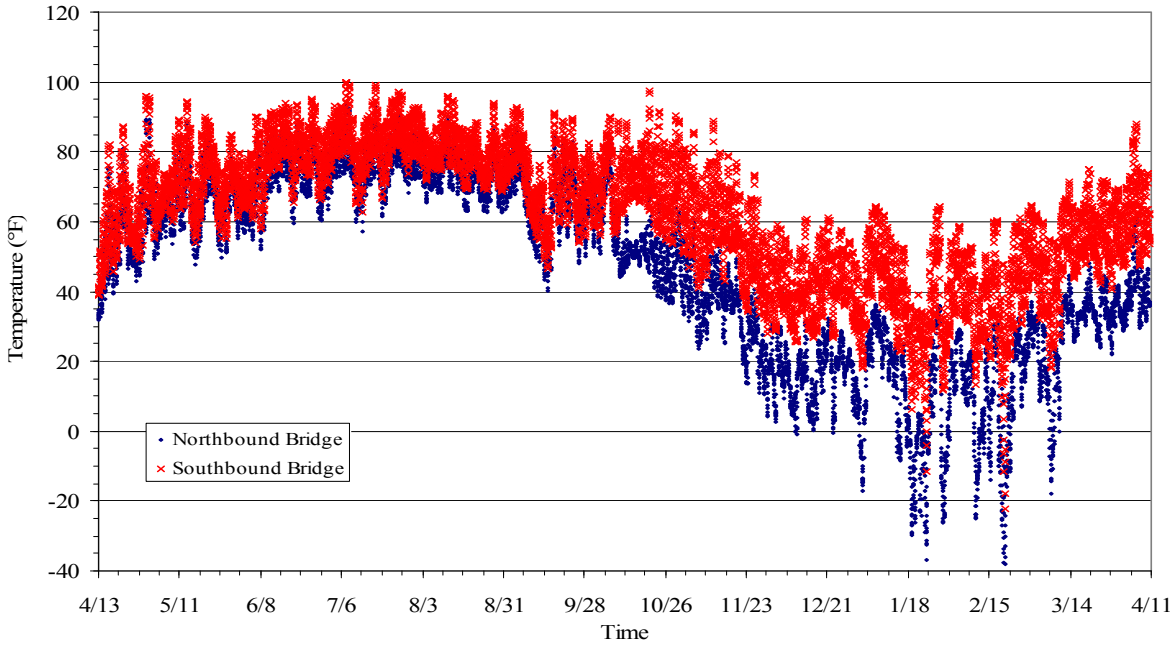


Figure 5.7. Northbound and southbound bridge temperatures over time

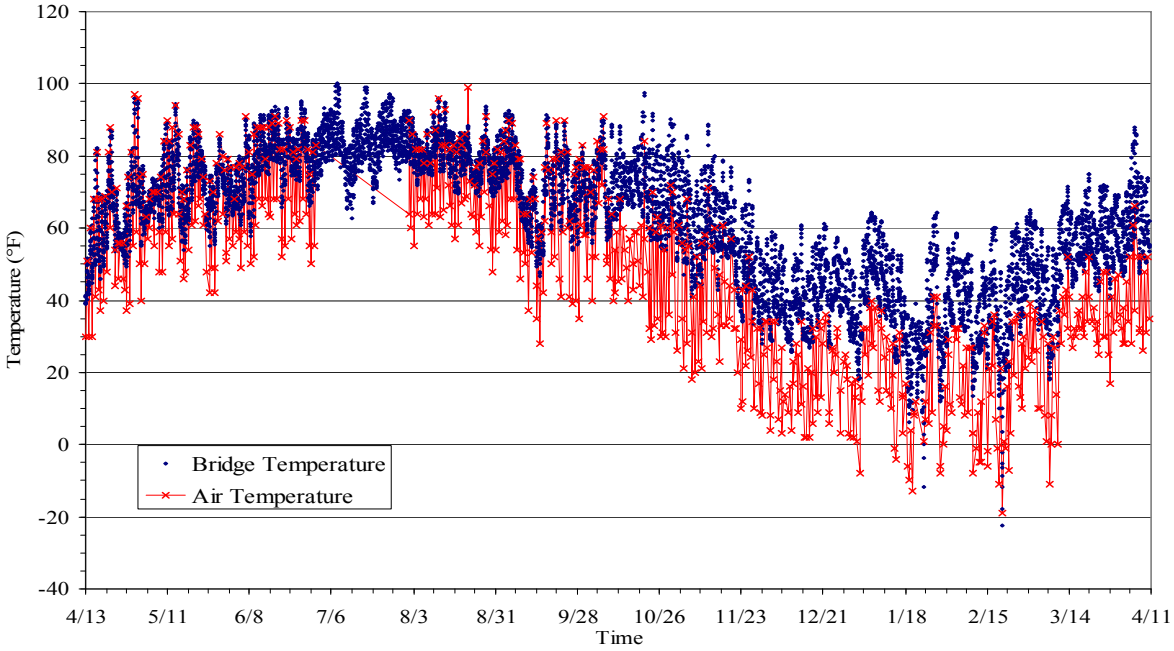


Figure 5.8. Southbound bridge and air temperature over time

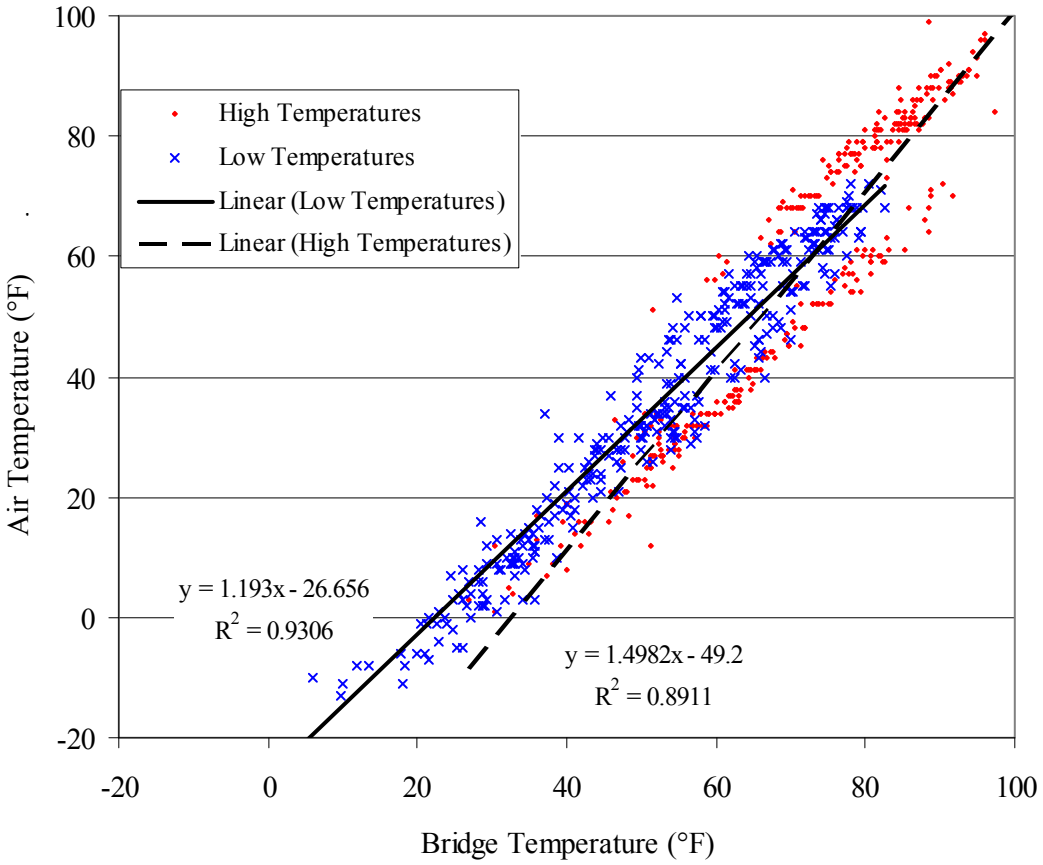


Figure 5.9. Correlation of daily high and low air to southbound bridge temperatures

5.2. Bridge Superstructure

5.2.1. Abutment Displacement

With the exception of the approach slab, the southbound bridge is the same design as the northbound bridge with the same instrumentation. Therefore, the discussion on bridge/gauge orientation, temperature correction of extension wire, and calculation steps to find the total abutment displacement described in Section 4.2.1 were followed for the discussion presented in this section. Refer to Figure 4.9 for an illustration of positive displacement.

Shown in Figure 5.10 is a plot of the typical abutment displacement, Δ_{abut}, after corrections for extension wire thermal elongation. The range of displacements is from -0.5 in. to 0.3 in., or 0.8 in. total range of displacement. Displacement caused by abutment rotation, Δ_{θ}, is shown in Figure 5.11, and is essentially zero.

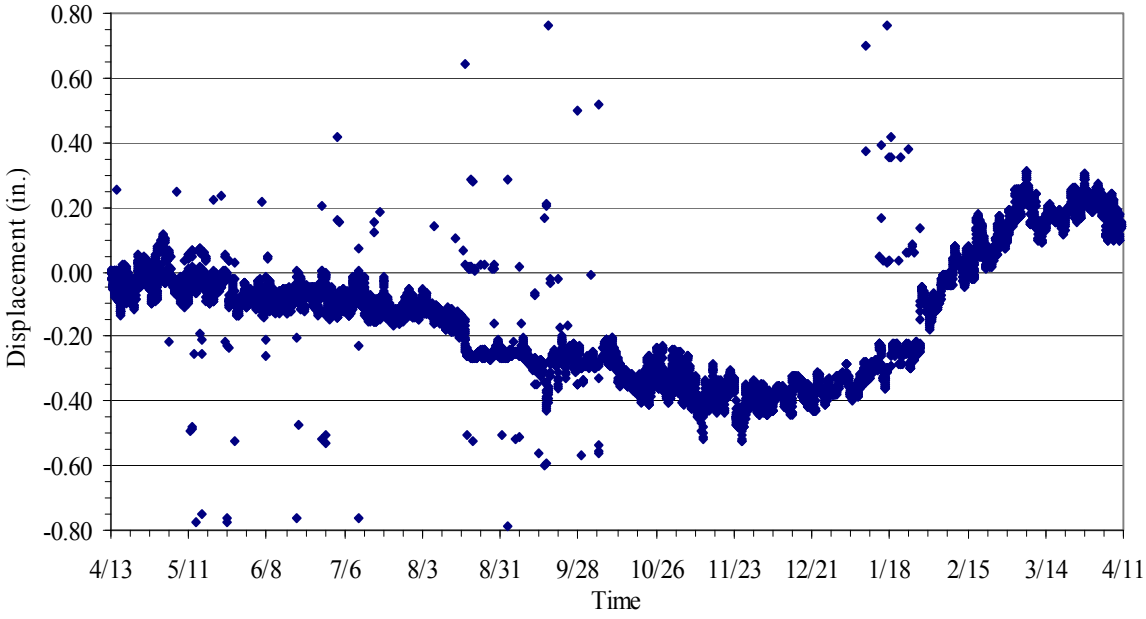


Figure 5.10. Typical southbound bridge abutment displacement at abutment base over time (Δ_{abut})

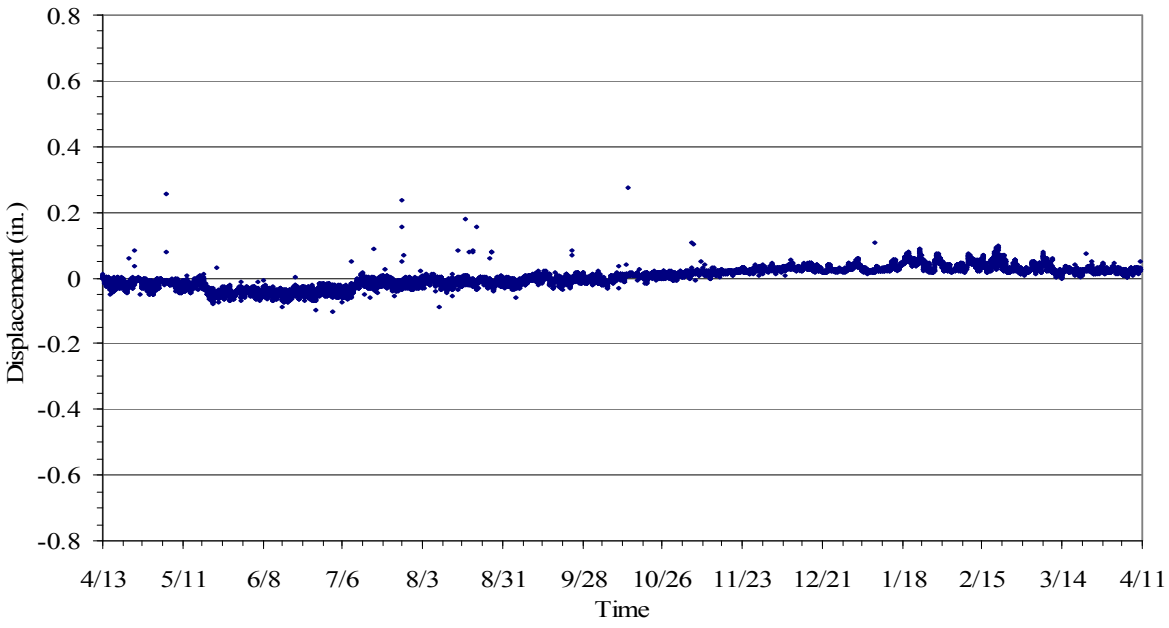


Figure 5.11. Typical displacement of the southbound bridge abutment due to abutment rotation over time

By combining the abutment displacement Δ_{abut}, and the displacement from rotation, Δ_{θ}, (Equation 4.2) the total displacement at the mid-depth of the approach slab was determined and is shown in Figure 5.12 and Figure 5.13 for the west and east ends of the abutment, respectively. At the west end of the abutment, ignoring the scatter, the total displacement ranges from -0.45 in. to 0.30 in.; the east end of the abutment undergoes a total displacement range of -0.65 in. to 0.70 in. By averaging the two abutment ends, the displacement at the center of the abutment at the approach slab mid-depth was estimated and is shown in Figure 5.14. At the center of the abutment the total displacement ranges from approximately -0.5 in. to 0.5 in.

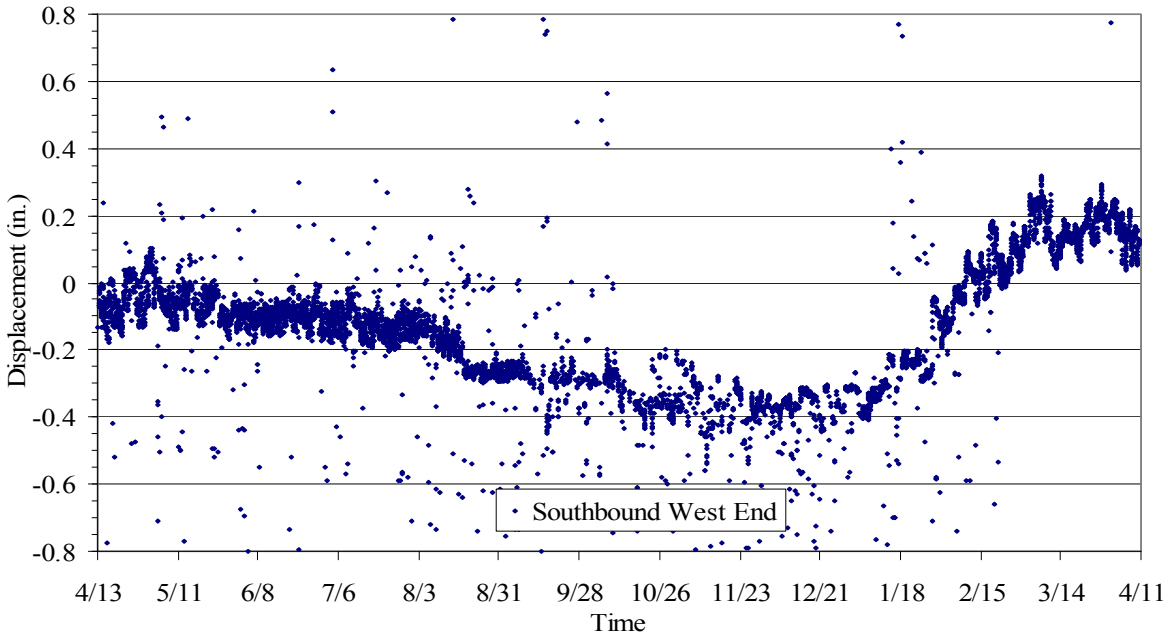


Figure 5.12. Total southbound bridge abutment displacement at the west end at slab mid-depth over time

Because the displacement of the abutment is caused by the thermal expansion and contraction of the bridge superstructure, a theoretical change in length can be calculated using Equation 4.4 and assuming the bridge thermally expands like an unrestrained bar. Refer to Section 4.2.1 for information on the temperatures and coefficient of thermal expansion used. Since the bridges have the same geometric features, the theoretical displacement shown in Figure 4.16 would also be the theoretical displacement for the southbound bridge.

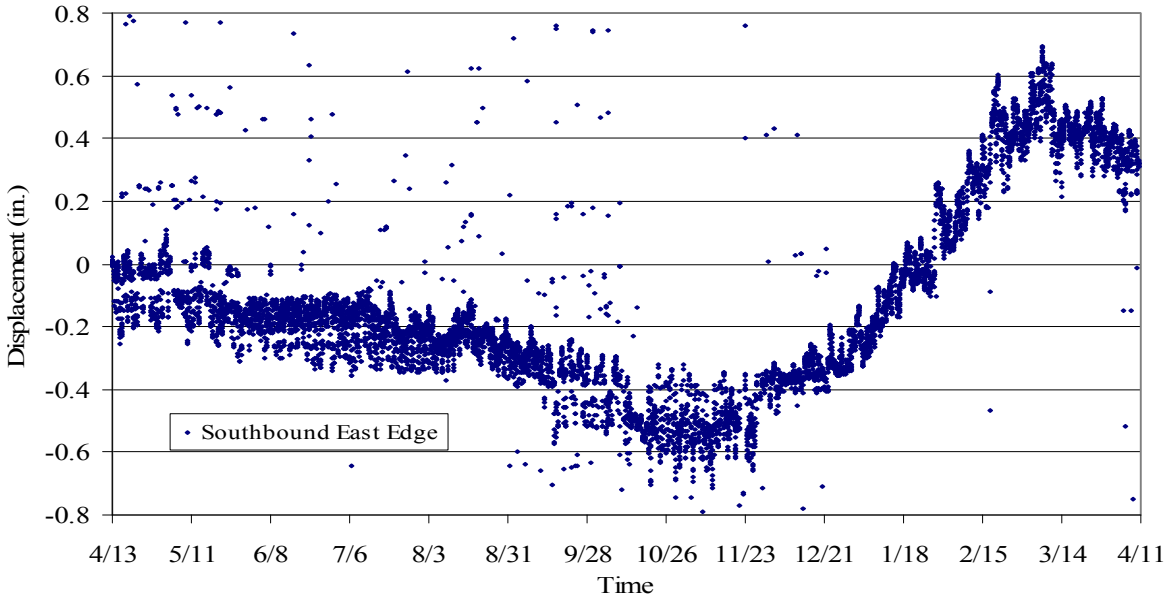


Figure 5.13. Total southbound bridge abutment displacement at the east end at slab mid-depth over time

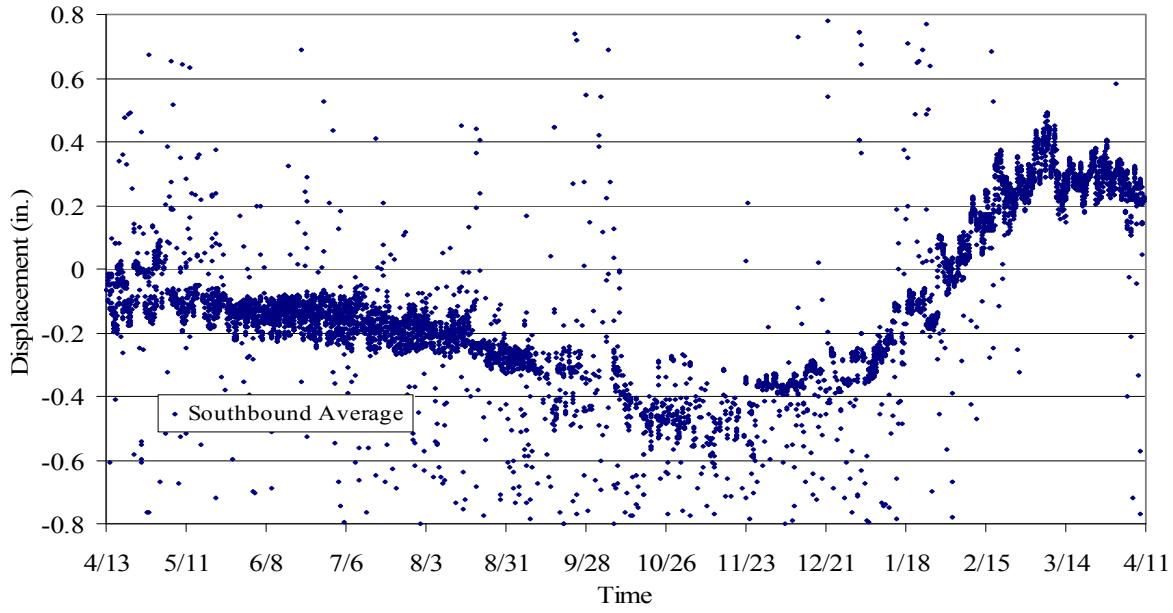


Figure 5.14. Average total southbound bridge abutment displacement at slab mid-depth over time

Comparison of the theoretical and average abutment displacement can be seen in Figure 5.15. From July to the beginning of December the theoretical and actual displacement follow the same

trend (i.e., the abutment displaces to the north as the temperature cools). Beginning in December the abutment displaces to the south while the theoretical displacement predicts continued displacement to the north corresponding to reduced temperatures. Probable causes for this are discussed in Section 4.2.1.

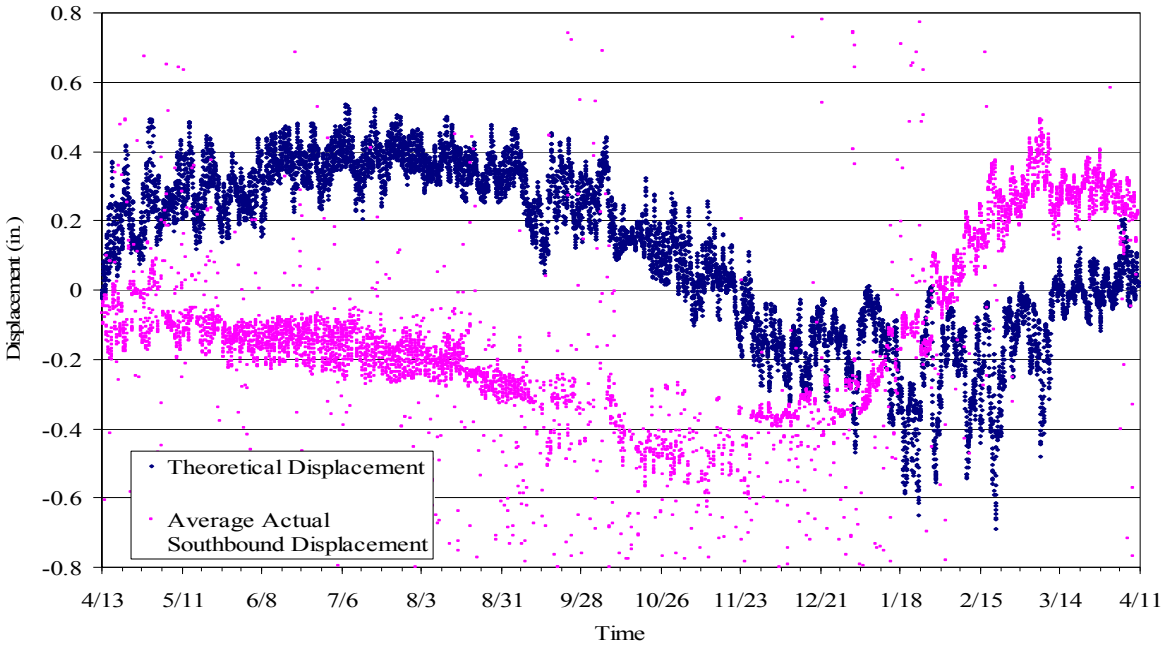


Figure 5.15. Theoretical and average actual abutment displacement of the southbound bridge over time

The abutment mid-slab displacement is plotted against the bridge temperature from Section 4.1.2 (as discussed in Section 5.1.2) in Figure 5.16. There is no clear relationship between the abutment displacement and the bridge temperature. In many regards, this behavior is similar to that observed in Figure 4.18 and again discussed in Section 4.2.1 with short term cycles within an annual cycle.

On the southbound bridge the transverse displacement transducer is located on the east end of the abutment (refer to Figure 3.14) meaning that positive displacement represents a displacement to the west (note that this is opposite of Figure 4.20). Refer to Section 4.2.1 for a discussion on abutment displacement and horizontal rotation.

Transverse abutment displacements over time are plotted in Figure 5.17. As the temperature decreases displacement to the east occurs. The displacement range is from 0.05 in. to -0.5 in.

The transverse displacement is compared to the average longitudinal displacement in Figure 5.18. No annual trend is apparent. However, there appears to be a seasonal and short term linear relationship (dashed lines) with a slope of approximately 1.2, probably caused by friction

ratcheting discussed in Section 4.2.1 and explained in Appendix A. A positive relationship suggests that as the abutment moves south the east end moves to the west.

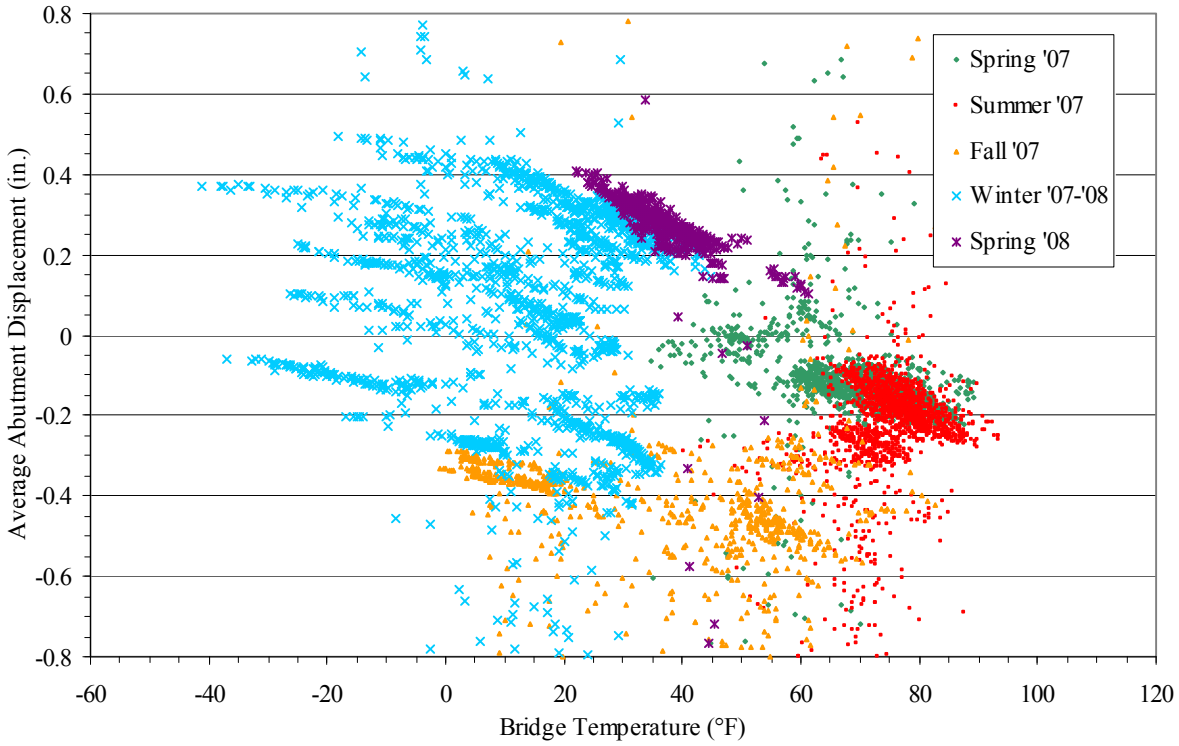


Figure 5.16. Southbound bridge abutment displacement versus change in bridge temperature

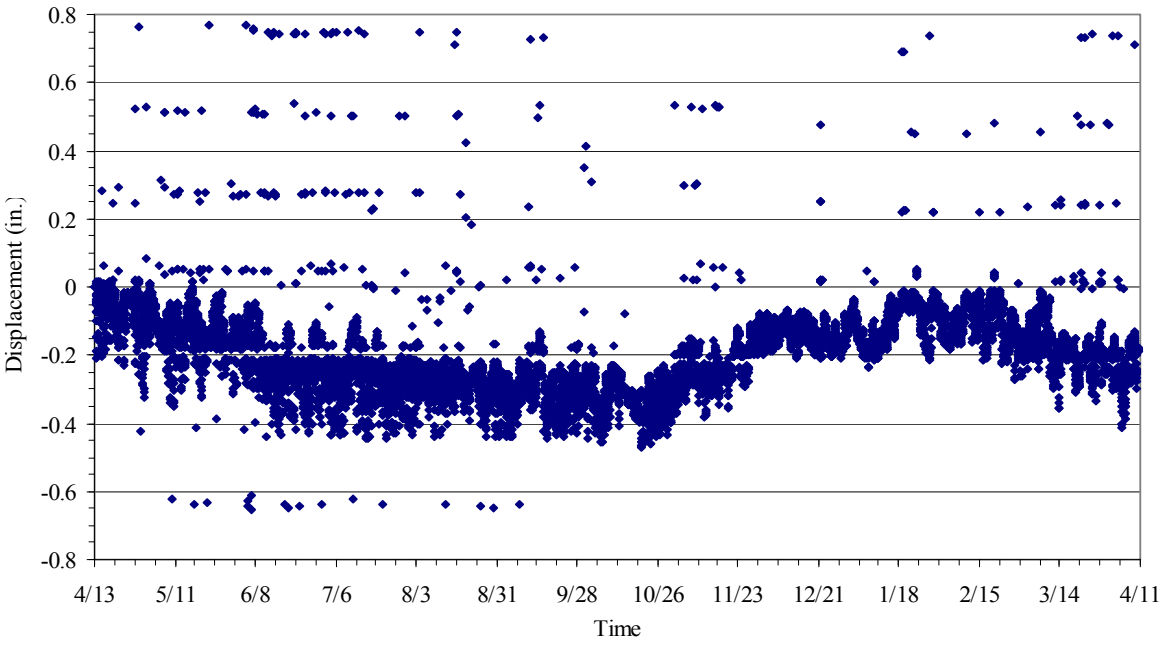


Figure 5.17. Southbound bridge transverse abutment displacement over time

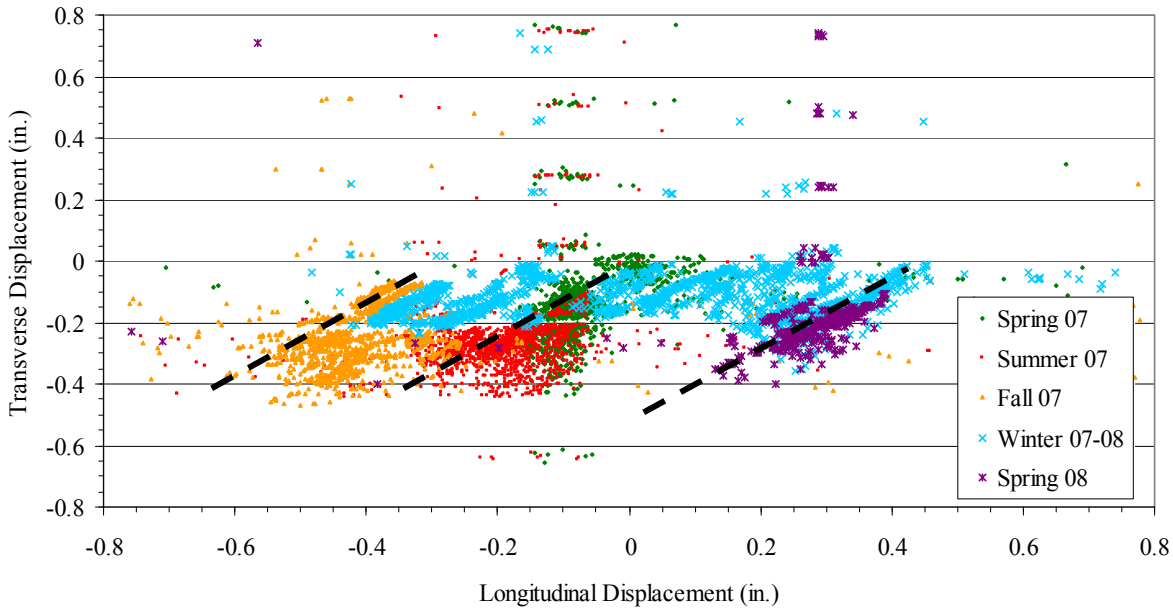


Figure 5.18. Southbound bridge transverse abutment displacement versus average longitudinal abutment displacement

5.2.2. Girder Strain Gauges

The southbound bridge superstructure is identical to the northbound bridge both as a structure and in instrumentation. Refer to Section 3.3 for instrumentation details and Section 4.2.2 for strain calculations.

A typical change in load strain over time is shown in Figure 5.19. As the temperature decreases (July to January) the load strain decreases, which is an increase in compression. In a similar way, as the temperature increases the load strain increases.

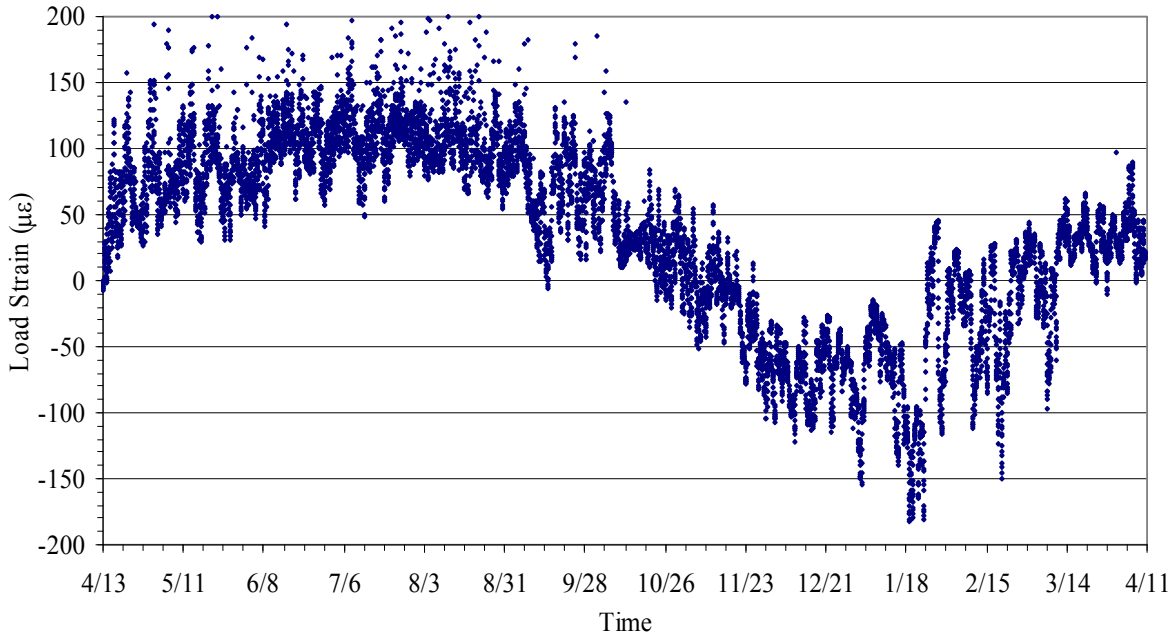


Figure 5.19. Typical southbound bridge girder load strain behavior over time

Note that for analysis in this work two of the gauges where disregarded due to the large amount of scatter and inconsistent readings. Gauge GSWT2, shown in Figure 5.20, has a large amount of scatter and inconsistent readings from the beginning until the end of November. On the other hand, Gauge GSEB3 had consistent readings until November when the readings became very scattered (see Figure 5.21). All the readings from those two gauges were disregarded because the inconsistency of the readings reduced the confidence.

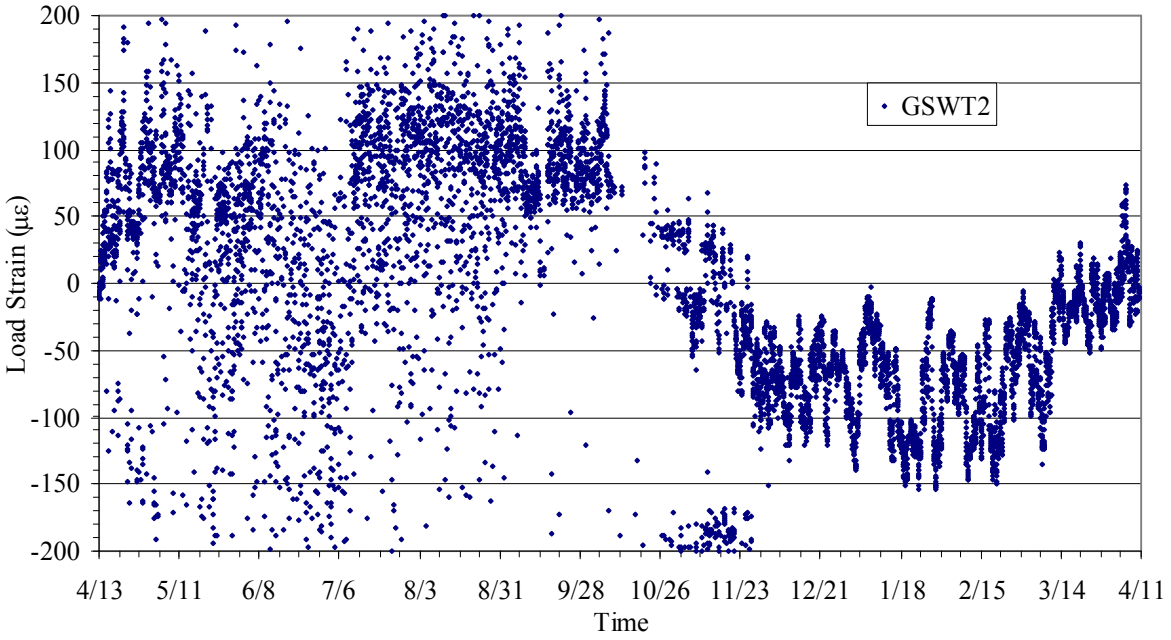


Figure 5.20. Southbound bridge girder load strain over time from gauge GSWT2

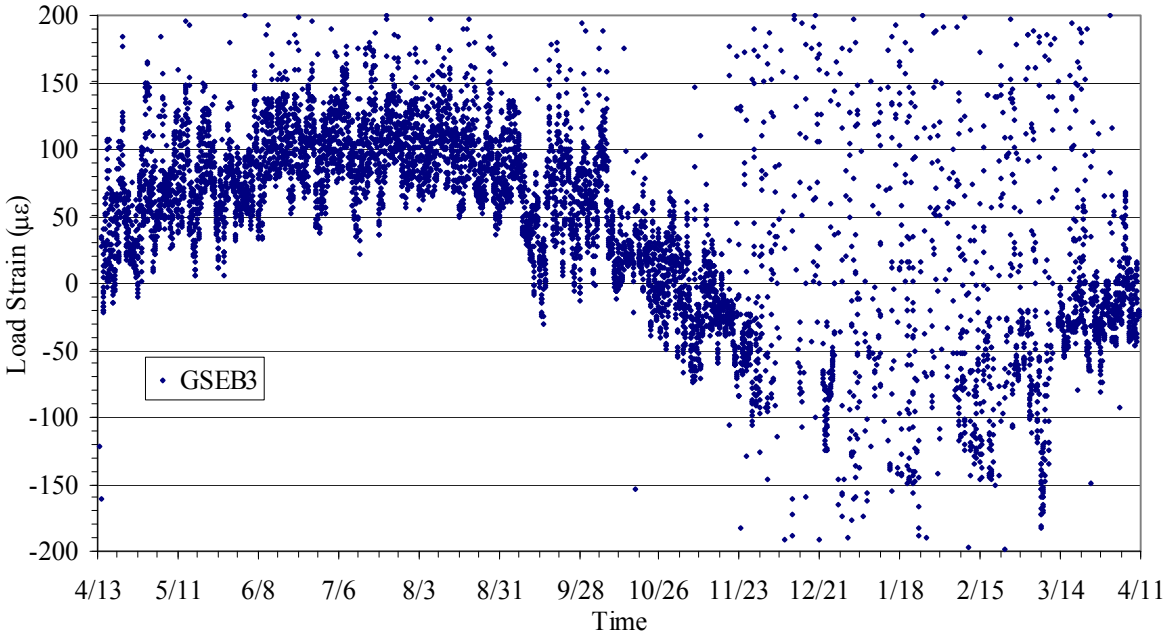


Figure 5.21. Load strain over time from gauge GSEB3

The recorded girder load strains that were not disregarded are shown in Figure 5.22 and Figure 5.23, for the top and bottom flange, respectively, plotted against gauge position for the hot and

cold days identified in Section 4.1.1. Variation across the bridge is shown by the different series for each girder. Similar strains might be expected for each girder for each case (top/bottom, hot/cold), but this is not always the case. On the cold day the load strains of each girder compared fairly well at all 3 positions, but on the hot day the mid-span load strains of the center girder, GC, and east girder, GE, did not compare as well probably due to skew effects. To study the overall, general behavior of the bridge, the load strains were averaged across the bridge as shown in Figure 5.22 and Figure 5.23 for the top and bottom flange, respectively.

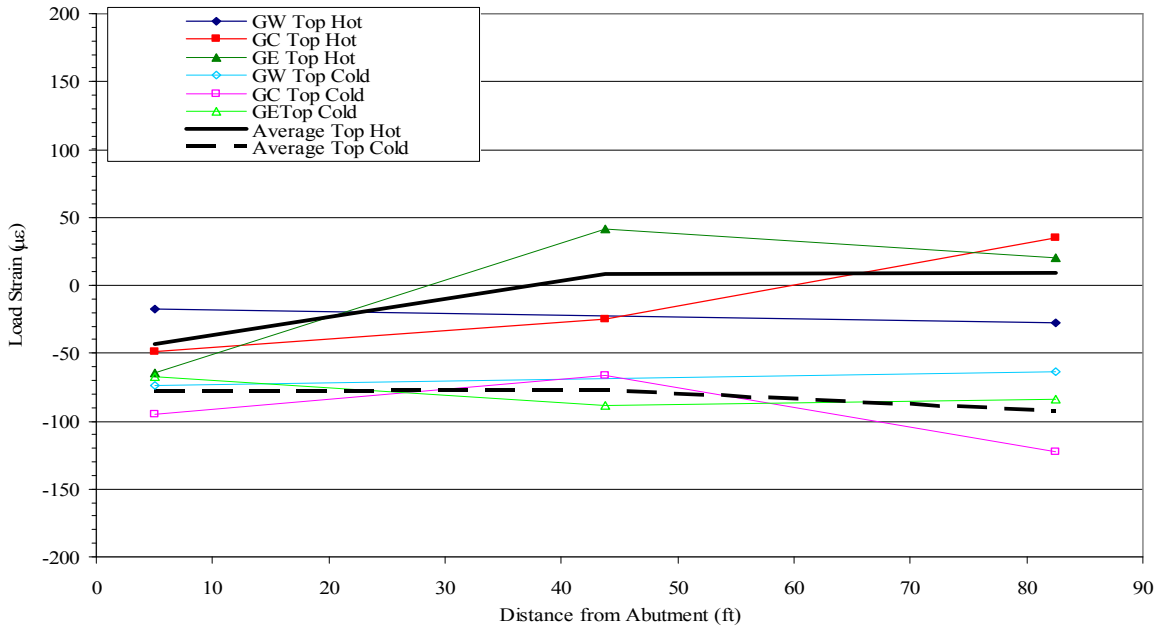


Figure 5.22. Load strain variation at the top of the girders with respect to position

Figure 5.24 is a plot showing the average girder moment relative to position along the girder for the typical hot and cold day. The moments were found by the same method and sign convention presented in Section 4.2.2 and by using the average load strains shown in Figure 5.22 and Figure 5.23 in Equation 4.8. For the typical hot day, which was reported as partly sunny, the moment is positive and increases from either end of the girder to a maximum positive moment of 250 kip*ft. For the typical cold day the moment remains relatively constant at -50 kip*ft, increasing slightly over the length.

As the bridge is heated both by the changing air temperature and solar radiation, it expands longitudinally and the top deck fibers are hotter than the shaded bottom girder fibers. Conceptually, the thermally induced forces at the abutment/girder joint include forces from the approach slab, passive soil on the abutment back wall, piles, and girders (see Figure 4.27). The moment in the girder in Figure 4.27 is arbitrarily drawn as negative (causing tension on top), but is dependent on the magnitudes of the slab force, pile forces, and the soil pressure resultant force. If the slab force is greater than the soil pressure resultant force and pile forces, the reaction moment of the girder could become positive.

In addition, if the girders are viewed as two-dimensional the moments are expected to vary linearly between the girder ends since there is no vertical load applied during heating. Figure 5.24 shows that the calculated moment varies non-uniformly which implies changing shear. The bridge skew, as discussed in Section 4.2.2, could be a cause for the non-uniform moments.

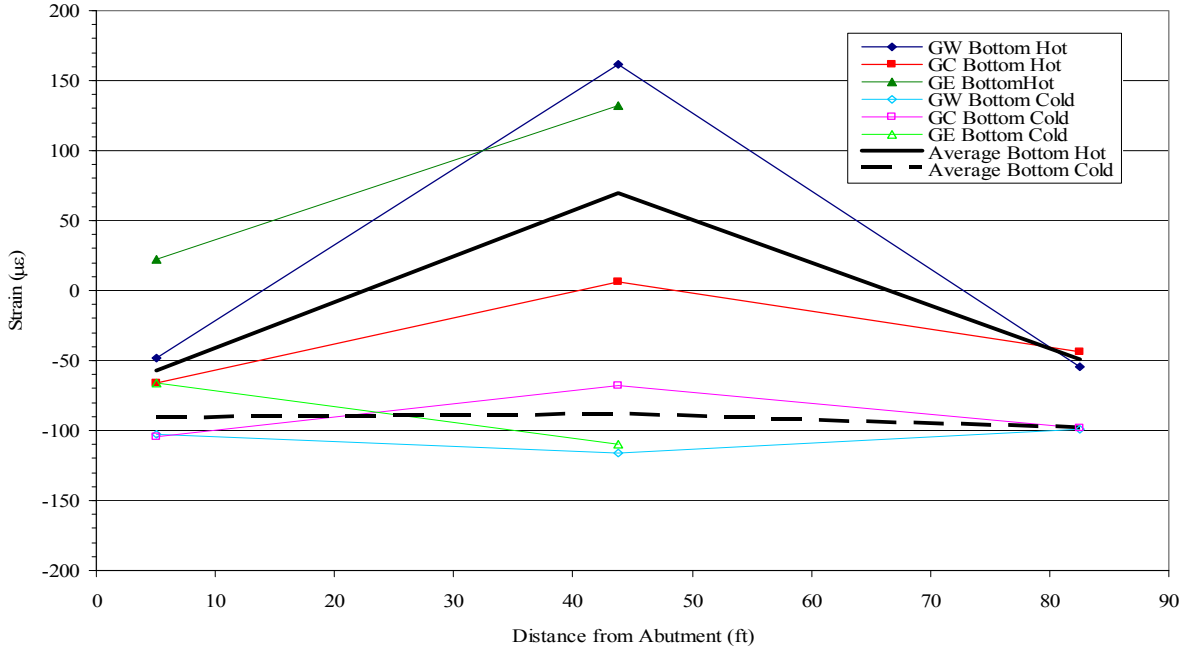


Figure 5.23. Load strain variation at the bottom of the girders with respect to position

The average mid-span moment is plotted against time in Figure 5.25. A cyclic pattern of change from positive to negative to positive moments as the bridge is heated, cooled, and heated is evident. The average mid-span moment ranges from 550 kip*ft to -50 kip*ft.

Figure 5.26 is a plot of the average mid-span moment versus the bridge temperature from Section 4.1.2. Different colors were used to denote the different seasons to highlight the relationship of moment to temperature over time. An annual linear trend of increasing moment with temperature increases is evident which is shown by the bold solid line having a slope of 6.6 kip*ft/°F. A short term linear relationship between the moment and temperature can also be seen in Figure 5.26, highlighted by the dashed lines. Refer to Section 4.2.1 and Appendix A for a discussion of this behavior.

Figure 5.27 is a plot of the average mid-span moment versus the average longitudinal abutment displacement from Section 5.2.1. Like Figure 5.26, different colors were used to highlight the different seasons. No clear annual relationship can be seen between the abutment displacement and the mid-span moment, though some short term cyclic behavior is evident.

The annual moment envelope is obtained by finding the maximum and minimum average at the 3 gauge positions, and is shown in Figure 5.28. The upper bound tends to follow the trend of the average hot day shown in Figure 5.24.

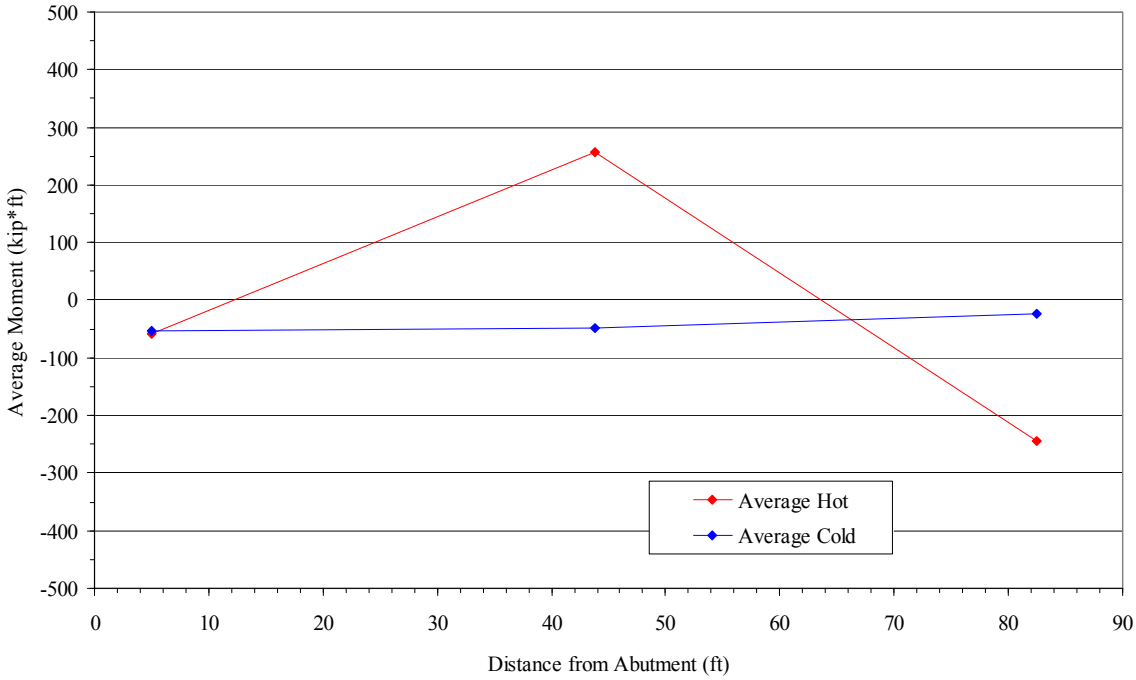


Figure 5.24. Southbound bridge average girder moment with respect to position

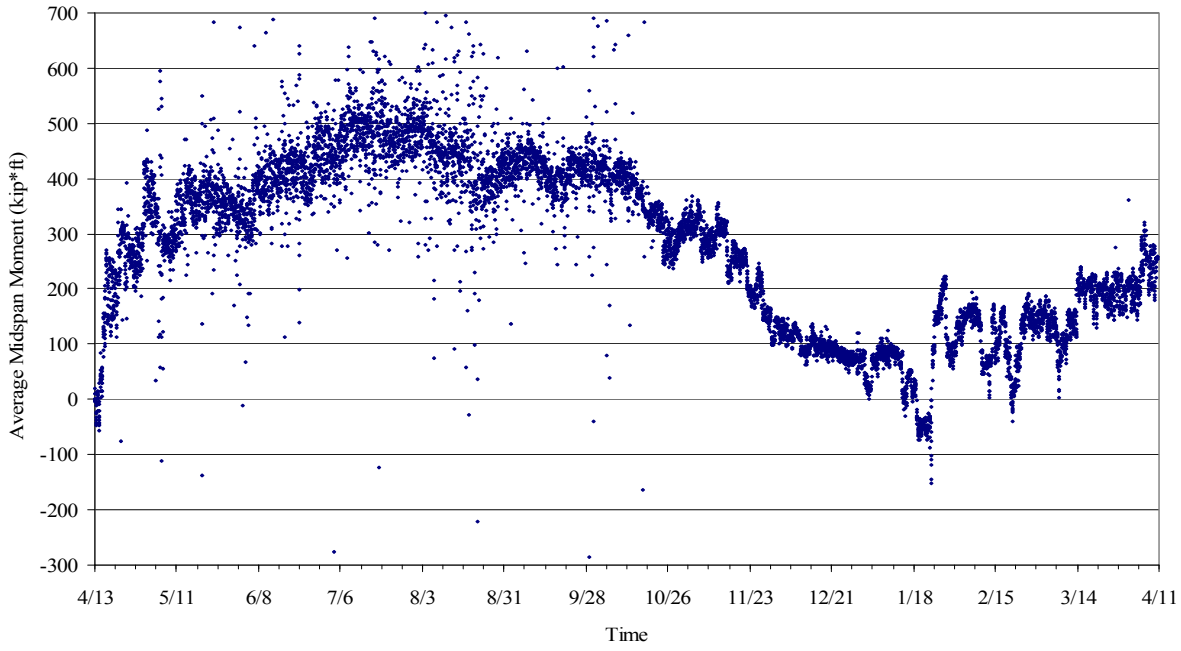


Figure 5.25. Southbound bridge average mid-span moment over time

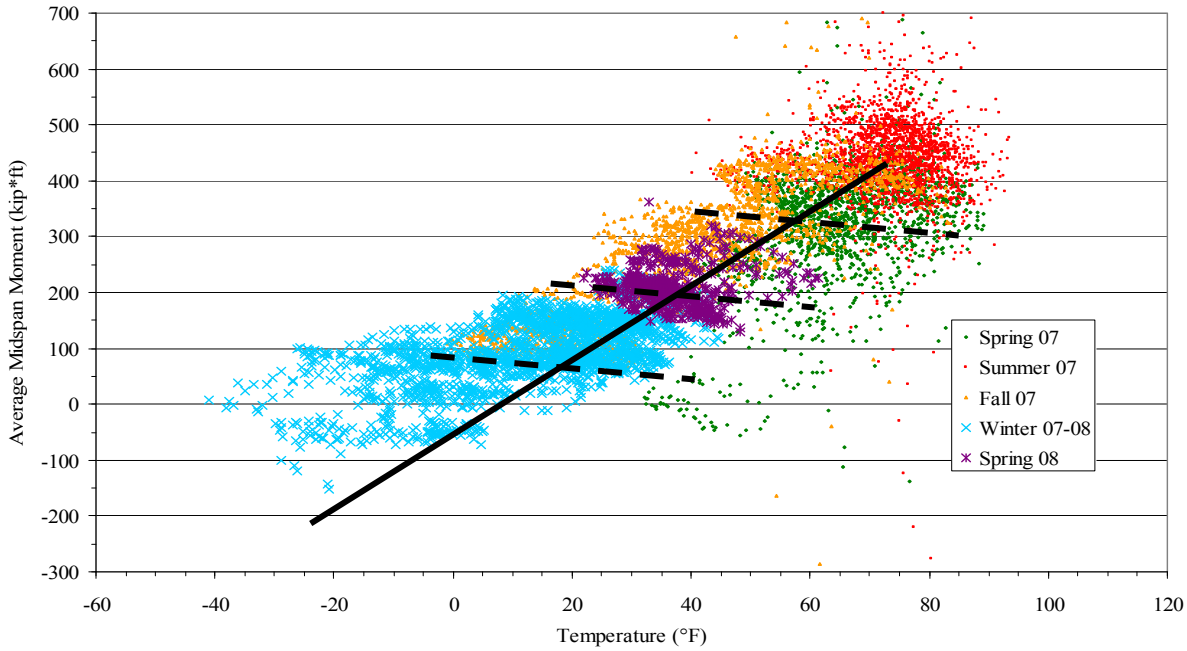


Figure 5.26. Southbound bridge average mid-span moment versus bridge temperature

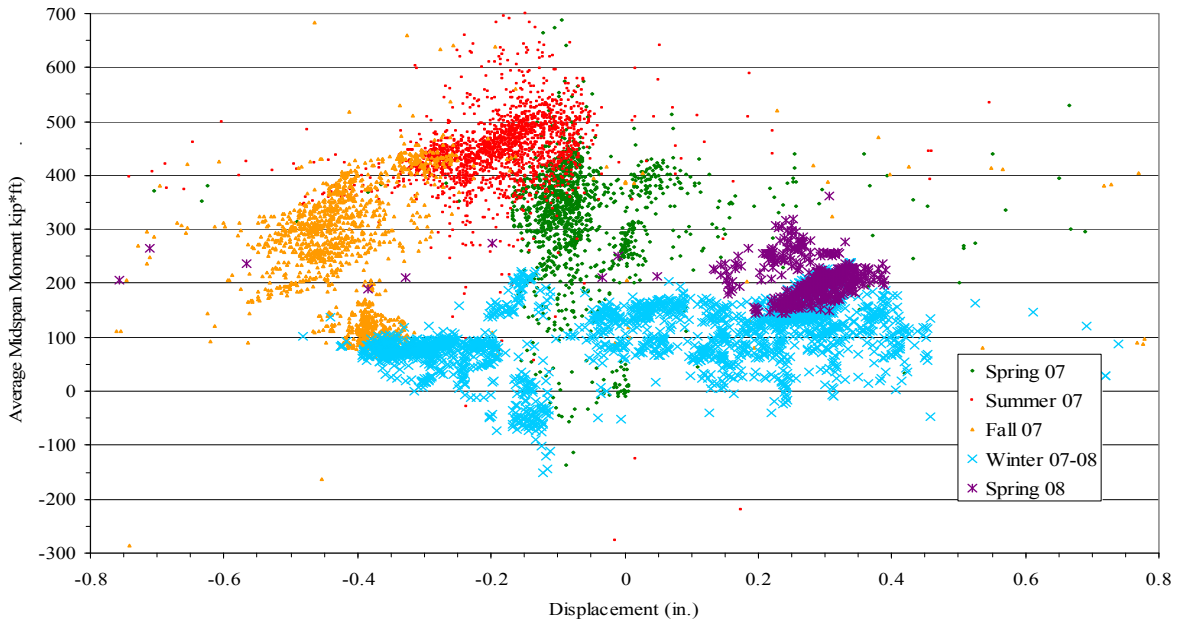


Figure 5.27. Southbound bridge average mid-span moment versus average longitudinal abutment displacement

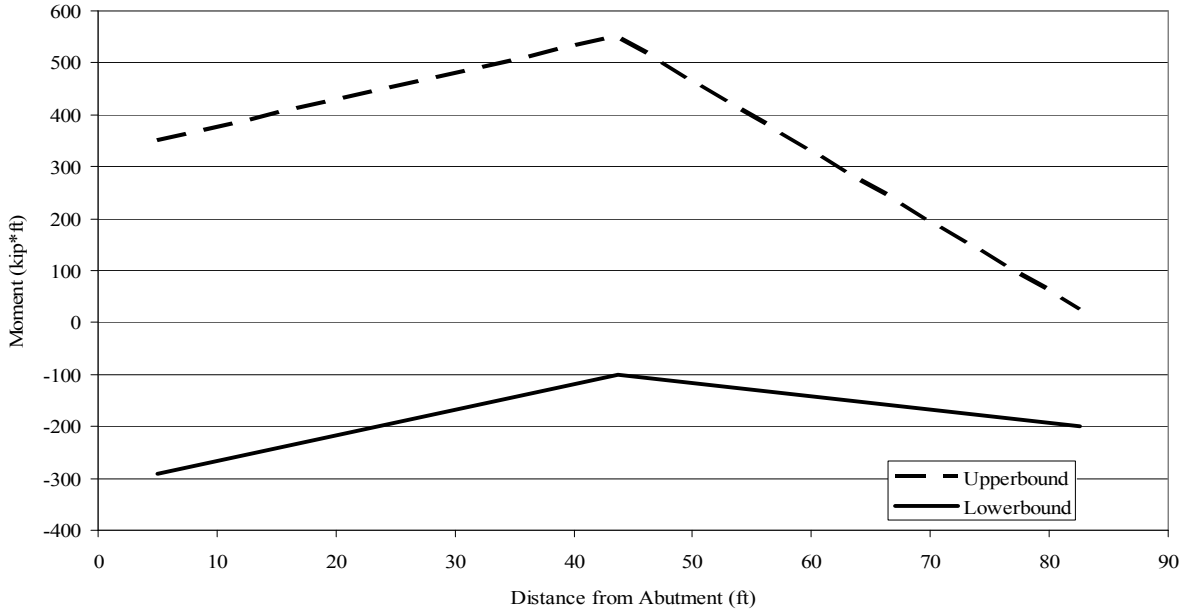


Figure 5.28. Southbound bridge girder moment envelope

Using the average load strains shown in Figure 5.22 and Figure 5.23 in Equation 4.9, the average change in axial loads at hot and cold times were found, and are shown in Figure 5.29. For a two

dimensional bridge the expected axial load distribution is a constant axial force along the length of the girder, but the results in Figure 5.29 show that the axial load on the typical hot day varies from -150 kips near the abutment and pier to 100 kips at mid-span, while on the typical cold day the load varies -425 kips from the abutment to the mid-span and then drops to -500 kips near the pier. The bridge skew does affect axial load distribution.

Averaging the axial load along the girders and plotting versus times results in Figure 5.30. The average axial load ranges from 50 kips to -550 kips. As the temperature decreases (July to January) the relative axial load decreases.

When the average axial load is plotted versus the bridge temperature (found in Section 4.1.2), as it is in Figure 5.31, a linear relation of the axial load to temperature from winter to spring is clear. The bold line highlights the linear relationship of 5.3 kips/°F. As the temperature increases, the relative axial load increases. From spring through the fall the relationship of load to temperature is a "loop", with short term trends evident.

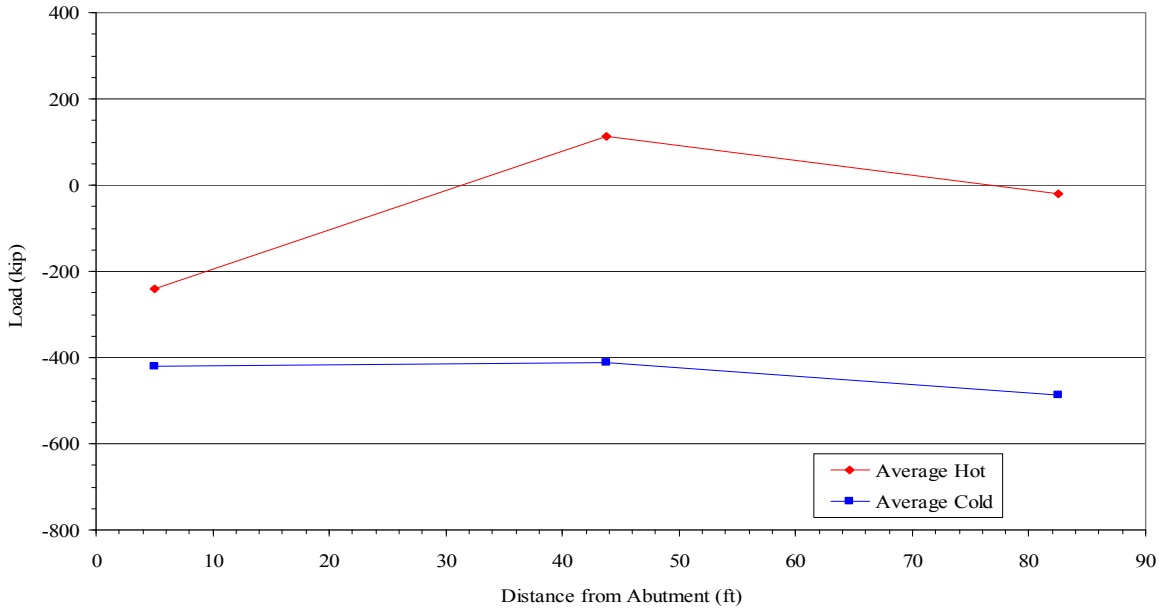


Figure 5.29. Southbound bridge average axial load with respect to position

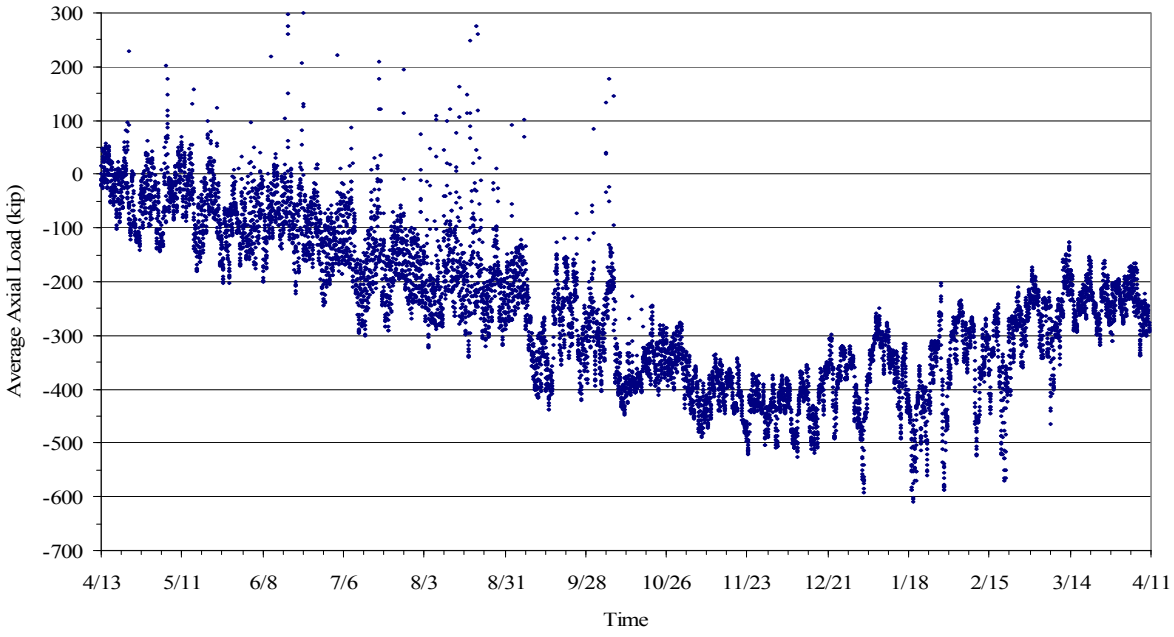


Figure 5.30. Southbound bridge average girder axial load over time

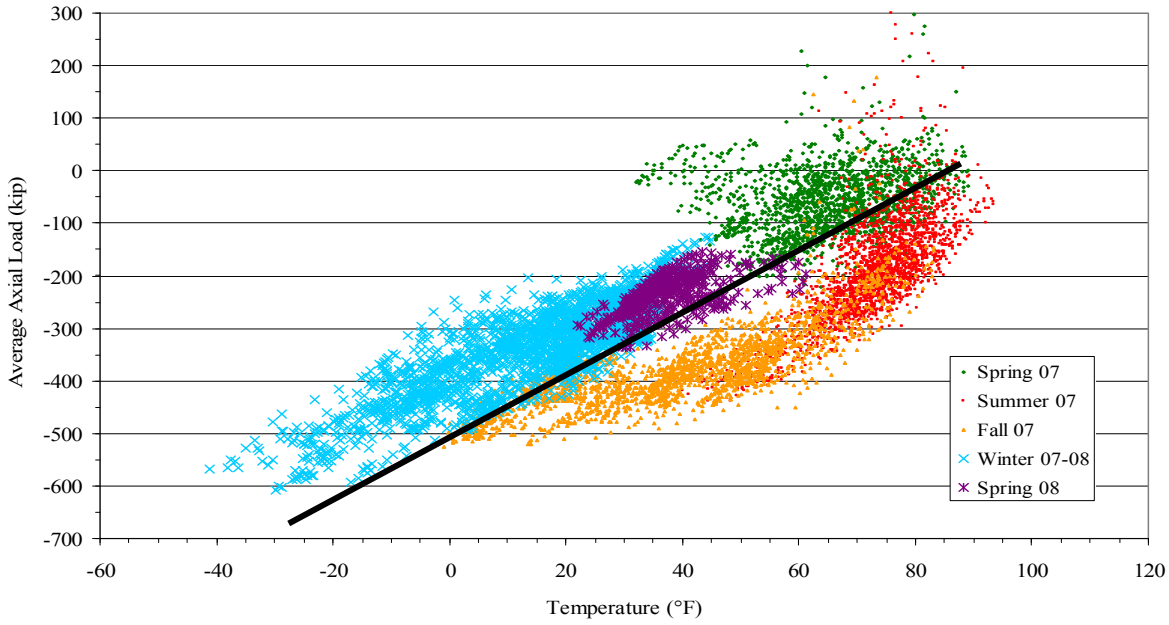


Figure 5.31. Average axial load versus bridge temperature

The average axial load is plotted in Figure 5.32 versus the average longitudinal abutment displacement found in Section 5.2.1. There is no clear relationship between axial load and abutment displacement, although some cyclic short term behavior can be seen.

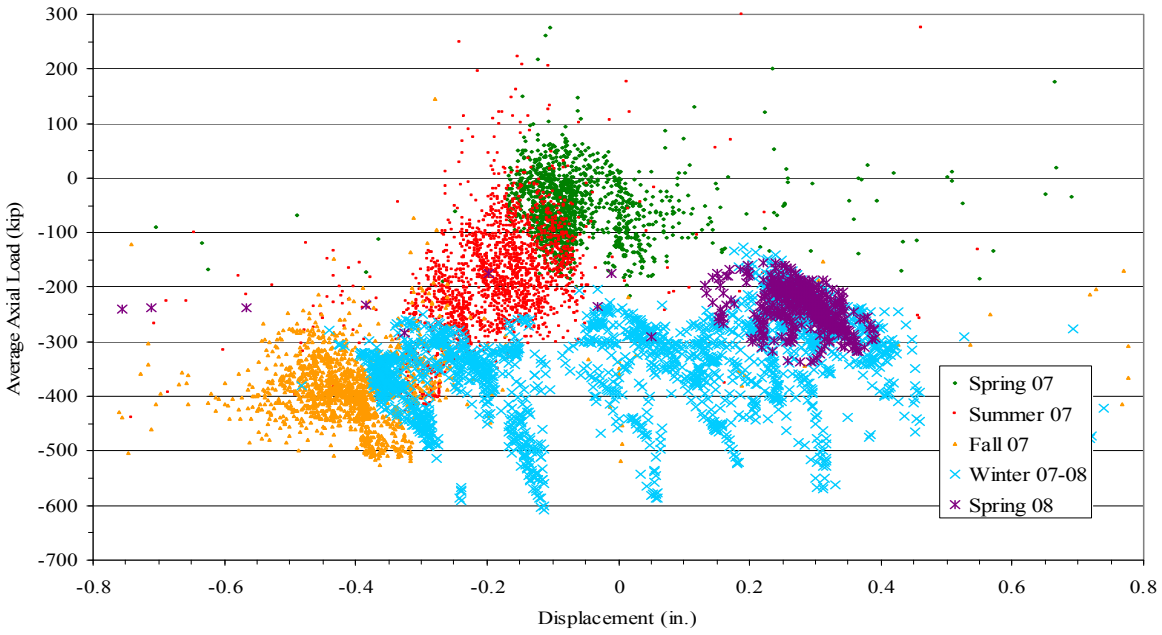


Figure 5.32. Southbound bridge average axial load versus average longitudinal abutment displacement

5.3. Approach Slab

5.3.1. Embedded Strain Gauges

The approach slab was instrumented with six strain gauges as described in Section 3.3. Typical strain readings obtained from an embedded strain transducer are shown in Figure 5.33. In general, the load strain decreased from April 2007 until December 2007 where the load strain then started to increase. The increase in load strain took place from December 2007 until March 2008 when the strain became essentially constant through the end of the monitoring period.

The strains for the 6 gauges are used in Figure 5.34 against transverse position for both the hot and cold days (same days as Section 4.3). The load strain in the west half of the slab varied little between transverse locations. Gauge ESEE (3.5ft location) in the east half consistently showed lower strain readings than the other two gauges located in the same half. The range of strain for the east gauges was approximately 30με for both the hot and cold day. Overall, the strains in the slab were transversely similar and the data from the 6 gauges were averaged to obtain the total average load strain in the slab which is shown in Figure 5.35.

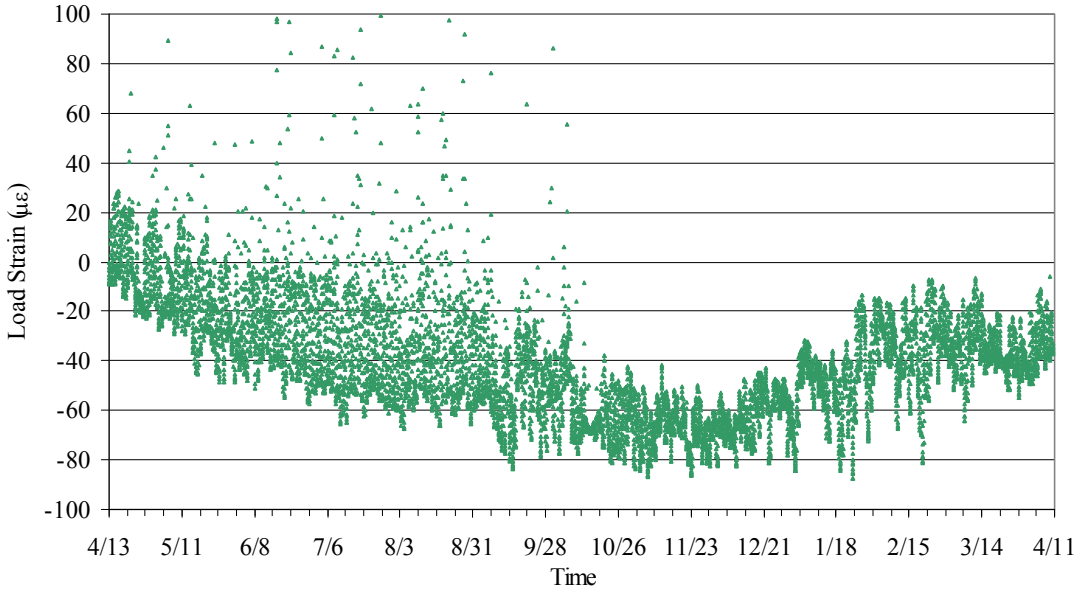


Figure 5.33. Representative strain reading obtained from southbound bridge embedded approach slab strain gauge ESEW

The average load strain is plotted with respect to temperature in Figure 5.36. Different colors are used to illustrate the annual seasonal effects. The winter and summer months have the most strain variation with a small temperature gradient. The fall and spring, however, have the least variation in strain but the largest temperature gradient. An annual cyclic pattern is clearly seen with the strain magnitude beginning and ending in the spring. The overall slope of the data is nearly zero with a total range of 100 με. The relationship between the strain in the slab and temperature form a cyclical oval shape pattern for a short term set of data (see section 4.2.1 and Appendix A).

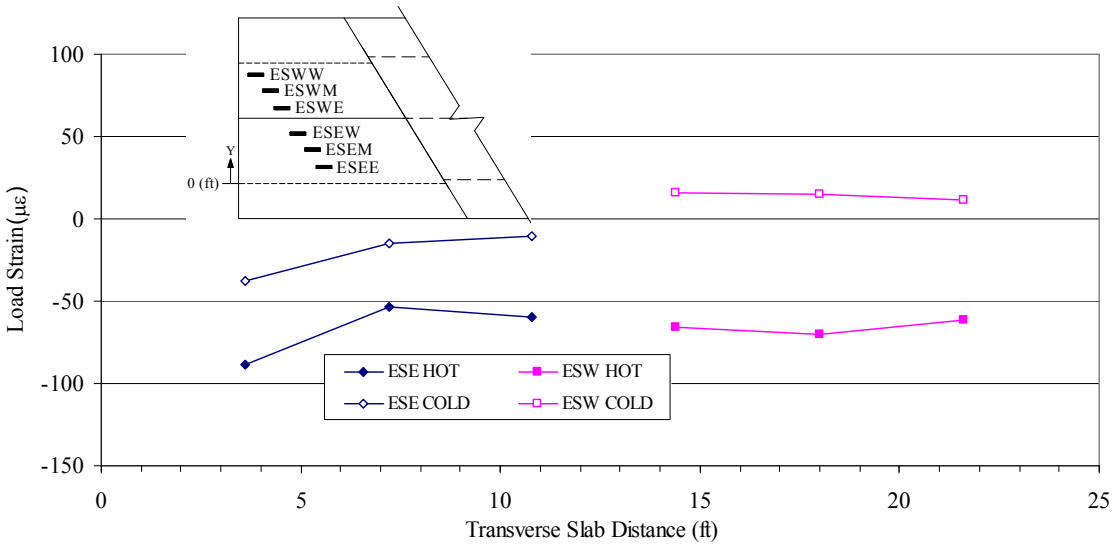


Figure 5.34. Southbound bridge hot and cold day load strain comparison with respect to location

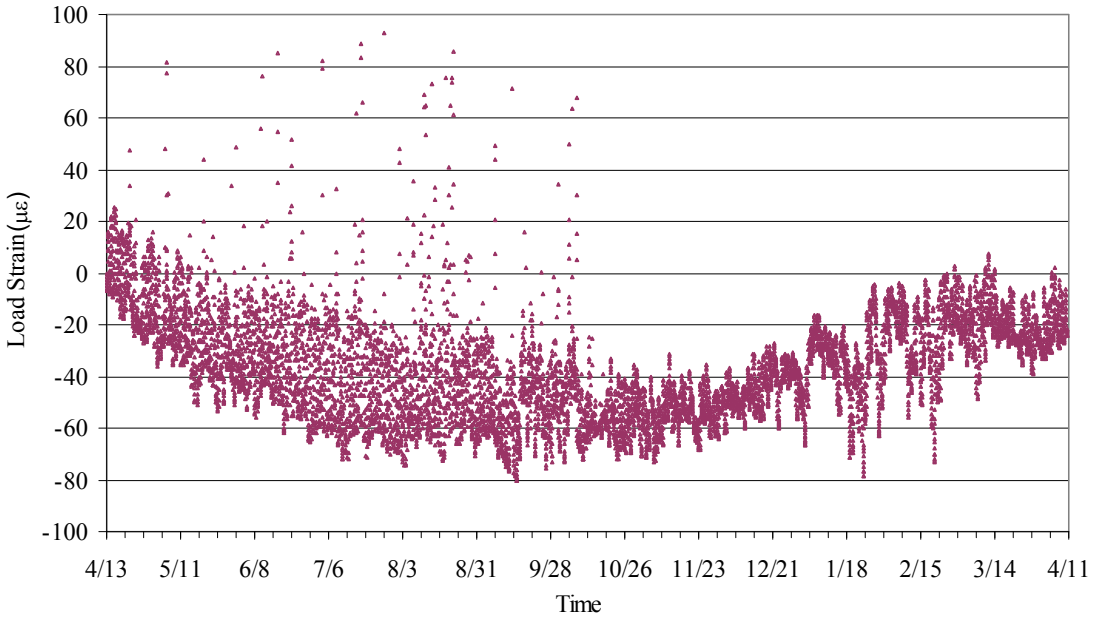


Figure 5.35. Average load strain of the southbound bridge embedded gauges

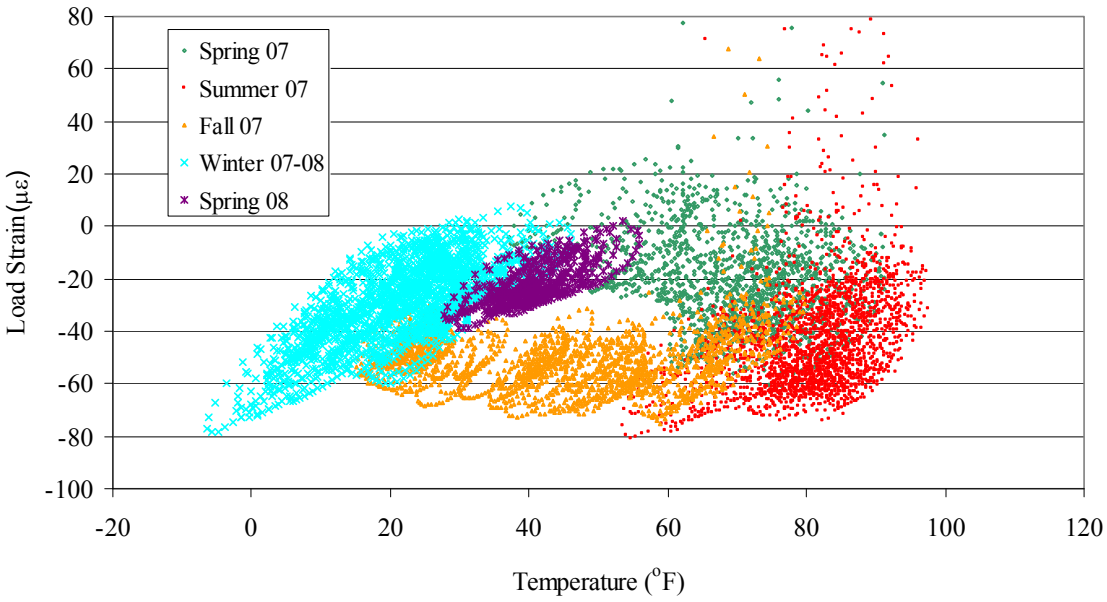


Figure 5.36. Southbound bridge approach slab load strain with respect to temperature

The change in the approach slab longitudinal force was calculated by Equation 4.10 (A = 3684in.^{2}) and is plotted versus the temperature in Figure 5.37. Figure 5.36 and Figure 5.37 yield similar observations. The same oval cyclical pattern was also found during the short term changes over time. The force in the slab ranged from -1400 kips in the summer to 500 kips in the winter. The total range of approximately 1900 kips relates to a 520 psi stress change from winter to summer.

Figure 5.38 shows force versus the change in average abutment movement. No relationship is apparent between the displacement of the abutment and the force in the slab except that the seasons are generally grouped together and short term cycling can be seen.

Figure 5.39 represents the force per unit width of slab versus location on the same hot and cold day as presented in Figure 5.34. In general, the west slab shows very uniform force across the slab, therefore leading one to conclude that the friction is uniform under the west slab. The east slab, however, varies slightly in force between gauges. The variance in force could be from non-uniform friction under the slab, a malfunctioning expansion joint on the east side, or other unknown sources. The slab is physically longest at the location with the largest decrease in force, which could be causing additional frictional effects.

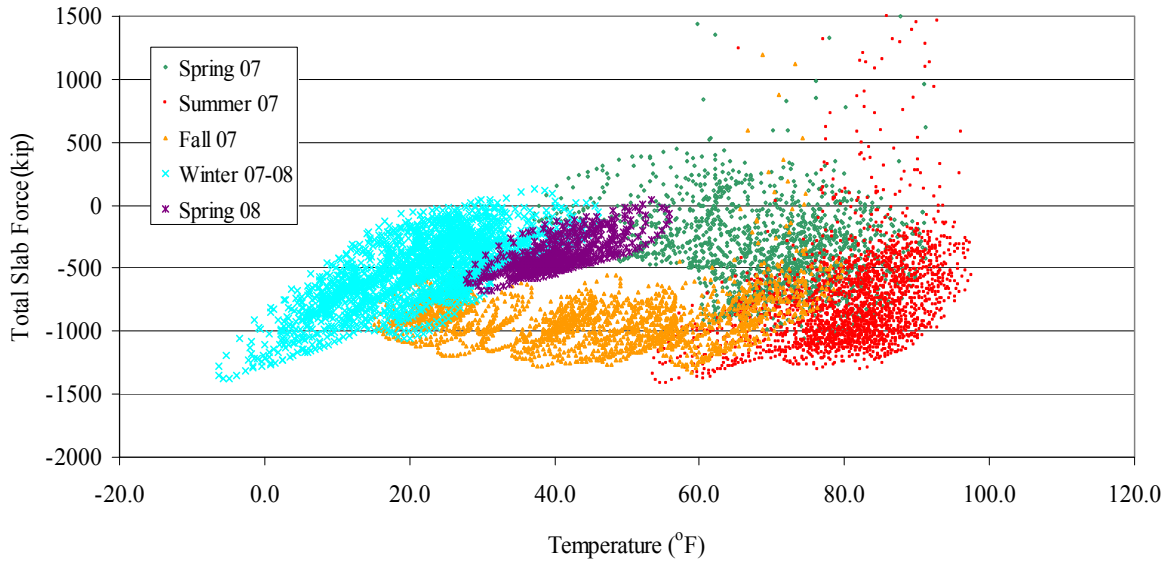


Figure 5.37. Southbound bridge approach slab average force with respect to change in slab temperature

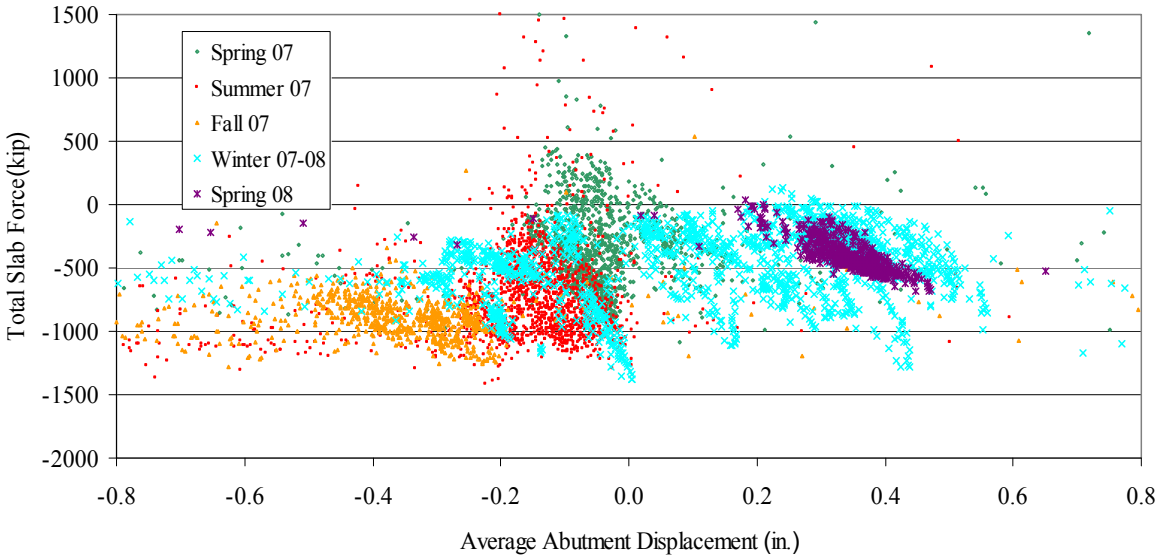


Figure 5.38. Southbound bridge approach slab average force relative to the movement at the abutment

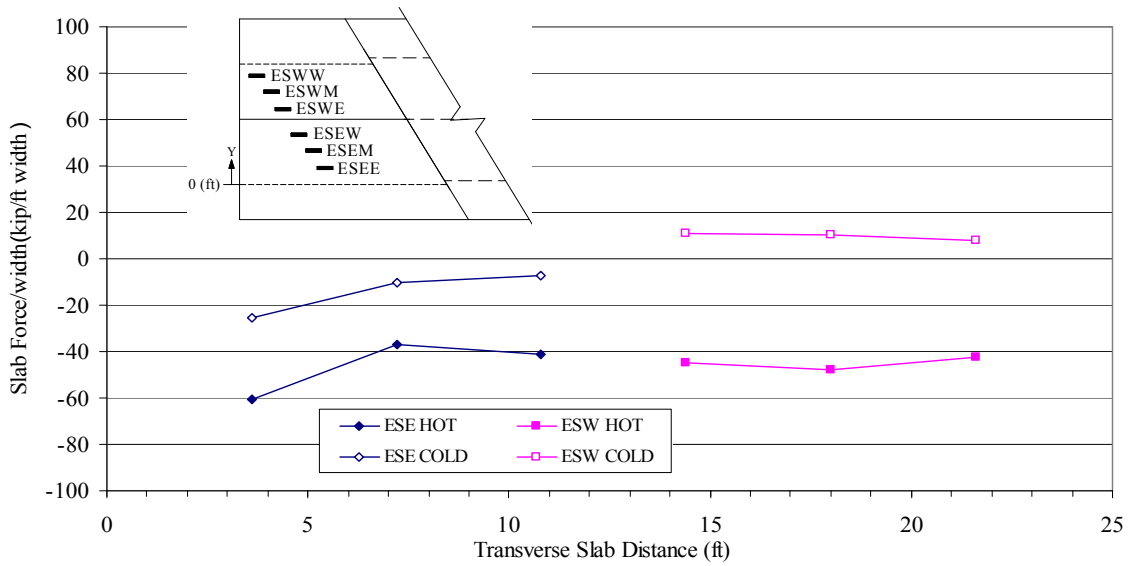


Figure 5.39. Southbound bridge hot and cold day load force comparison with respect to location

5.3.2. Crackmeters

The approach slab joints were equipped with crackmeters along the east and west faces of the slab to monitor joint opening and closing over time. Figure 3.14 shows the location of the three working crackmeters. The relationship between the crackmeter readout and the opening of the joint and expansion joint of the slab can be found in Section 4.3.3.

The crackmeters located on the west side of the slab, denoted CSW1 and CSW2 in Figure 3.14, provided usable data during the duration of the project and the resulting joint changes are shown in Figure 5.40. A positive reading indicates the joint is opening. Joints CSW1 between the bridge and the approach slab, as shown in Figure 5.40, had readings of less than 0.03 in. during the test period. Crackmeter CSW2, which is located at the expansion joint of the approach slab and pavement, had a range of over 1.1 in. Figure 5.41 compares the expansion joint movement at both CSW2 and CSE2. The change was nearly identical at both the east and west edges of the slab.

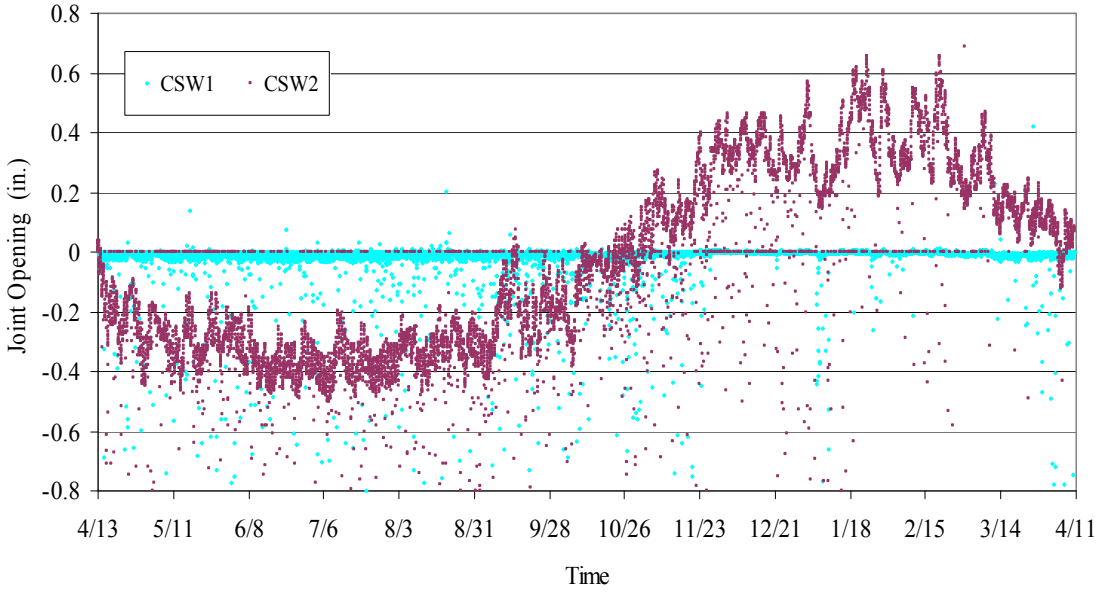


Figure 5.40. Southbound bridge cast in place approach slab joint opening

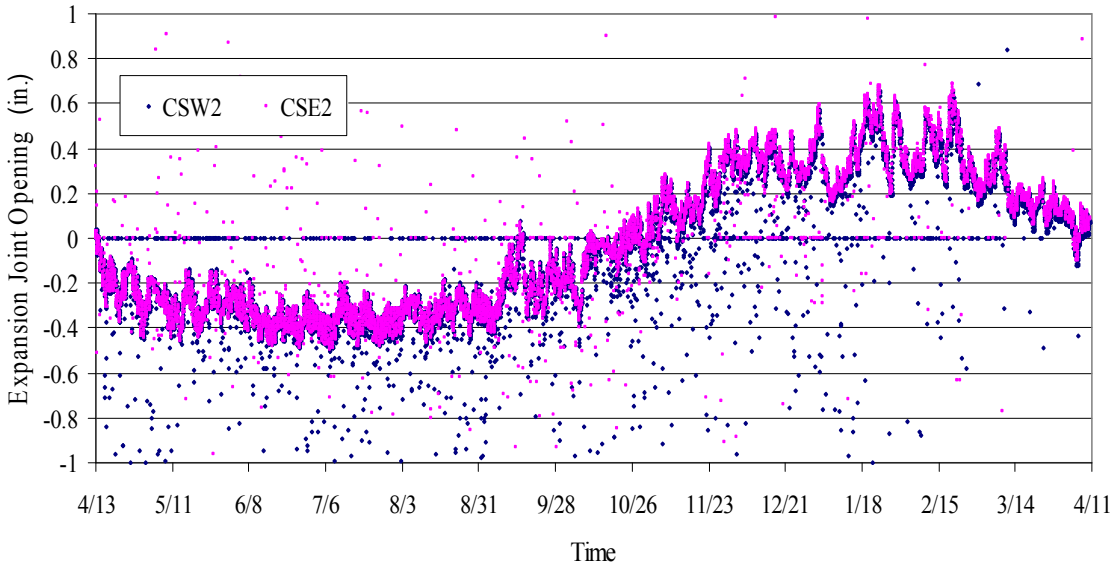


Figure 5.41. Movement of east and west edge of the southbound bridge expansion joint

The crackmeter at the expansion joint was connected to the pavement and to the approach slab. Therefore, the reading obtained from crackmeter CSW2 and CSE2 is the relative movement of the approach slab and the pavement. No instrumentation was installed to monitor the total movement of the pavement. The opening of the expansion joint is seen to have an approximate linear relationship with temperature, as seen in Figure 5.42. As the temperature increases the joint opening size decreases, as expected. Seasonal and short term cycles are evident.

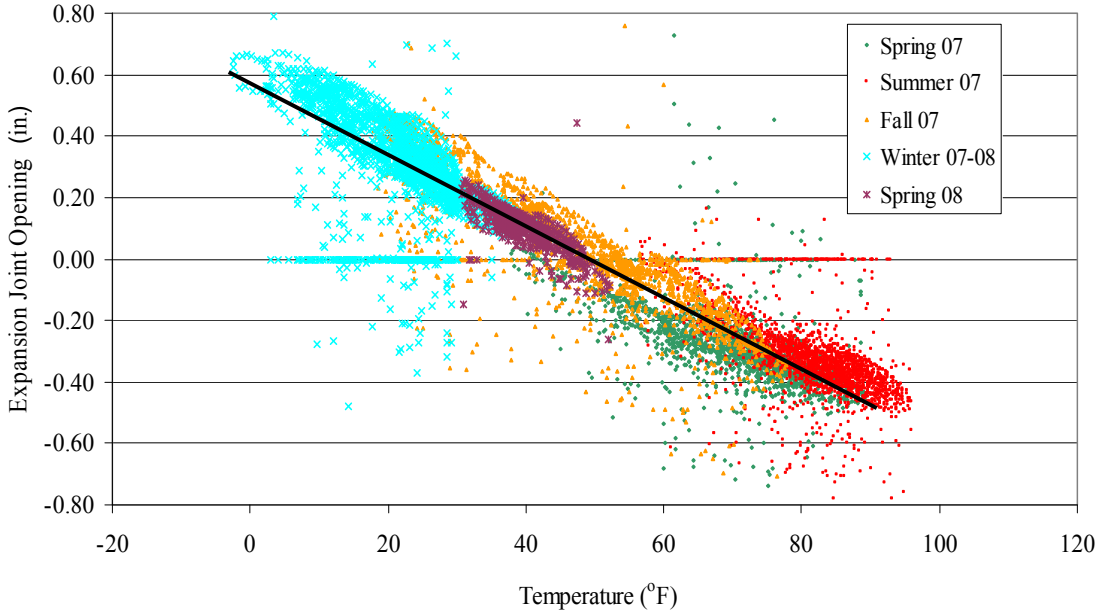


Figure 5.42. Southbound bridge expansion joint opening relative to temperature

5.3.3. Comparison of Expansion Joint Movement and Abutment Movement

The total accumulated movement at the southern edge of the approach slab is shown in Figure 5.43. The south edge movement was calculated by summing the abutment movement (see Section 5.2.1), change in slab length due to temperature and load strains, and joint movement of CSW1. The joint movements, temperature, and stress effects contributed about 10% of the total movement of the slab. Most of the movement of the slab was caused by the movement at the bridge abutment. The maximum movement obtained during the test period was approximately 0.50 in. to the south, which is a 0.05 in. increase from the abutment movement presented in Section 5.2.1. The range of total movement was approximately 0.70 in.

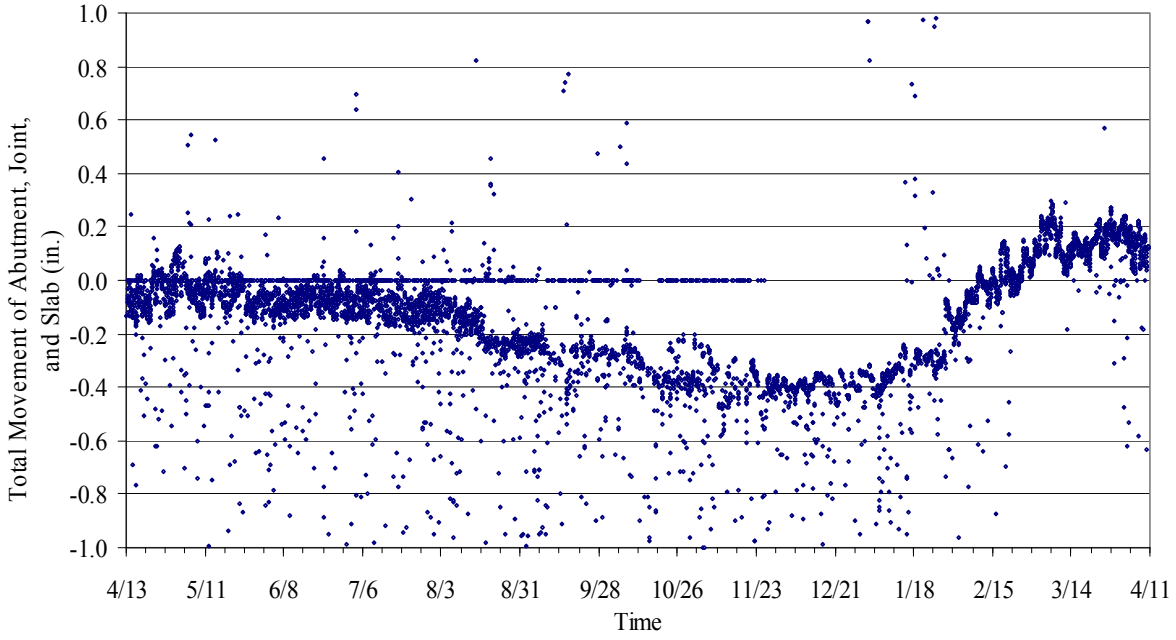


Figure 5.43. Total movement of south end of southbound bridge approach slab

Figure 5.44 shows the abutment movement with respect to the expansion joint opening. During fall the abutment had very little movement while the expansion joint closed 0.7 in. During the winter the abutment moved to the south approximately 0.6 in. while the expansion joint had relatively small movements. The spring and summer season show little movement of either the abutment or the expansion joint. From Figure 5.44 it appears that the abutment and the expansion joint movements are dependent upon one another and have the cyclic behavior seen previously.

The expansion joint opening is compared with the force in the slab, as shown in Figure 5.45. The general shape and pattern of the plot is a mirror image to the strain and force in the slab plotted with respect to temperature as shown in Figure 5.36 and Figure 5.37. Again, similar to Figure 5.36 and Figure 5.37, the slab force saw little change during the fall and spring with a large movement at the expansion joint. The summer appeared to have the largest change in force with the least amount of expansion joint movement.

The expansion joint should allow free movement of the slab relative to the pavement, however, improperly working dowel bars and/or foreign matter within the expansion joint could cause a build up of stress. The general trend during the summer and winter, shown by the dashed lines in Figure 5.45, is that as the expansion joint opens there is an increase in compression. To some extent, the simple analytical model in Appendix A helps to explain this.

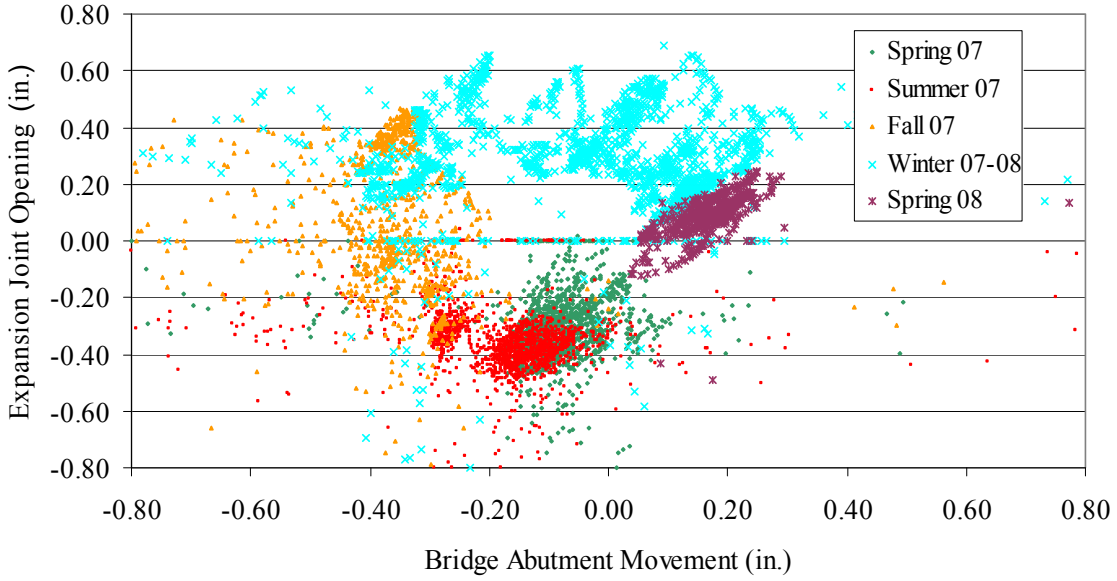


Figure 5.44. Comparison of southbound bridge abutment movement and expansion joint movement

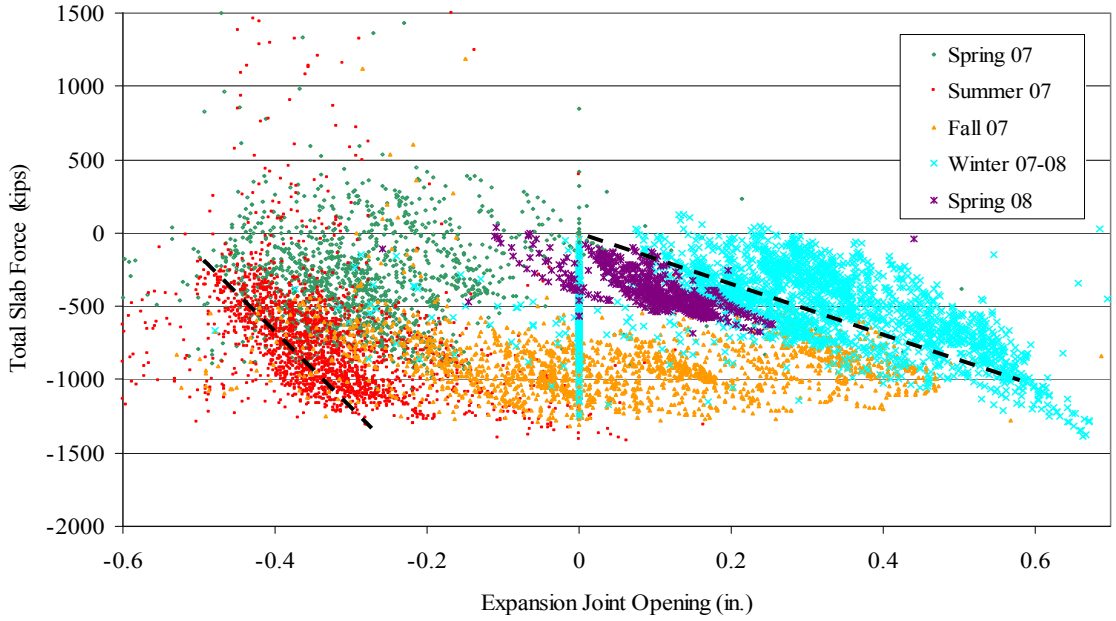


Figure 5.45. Expansion joint opening related to the load force in the southbound bridge approach slab

5.4. Bridge Substructure

5.4.1. Pile Gauges

The behavior of three HP 10x57 piles located in the south abutment of the southbound bridge was monitored with 4 strain gauges located on each of the three piles. The location of the strain gauges, positive local axis orientation is similar to the northbound bridge and is shown in Figure 4.56. The pile orientation and location with respect to the abutment is shown in Figure 4.57.

Of the 12 gauges installed on the three piles, only one gauge recorded usable data for the duration of the testing period, six gauges had limited and/or scattered data, and five of the gauges did not have any recorded data. The seven gauges that gave some type of reading over the test period are plotted for the west, middle, and east piles shown in Figure 5.46, Figure 5.47, and Figure 5.48 respectively.

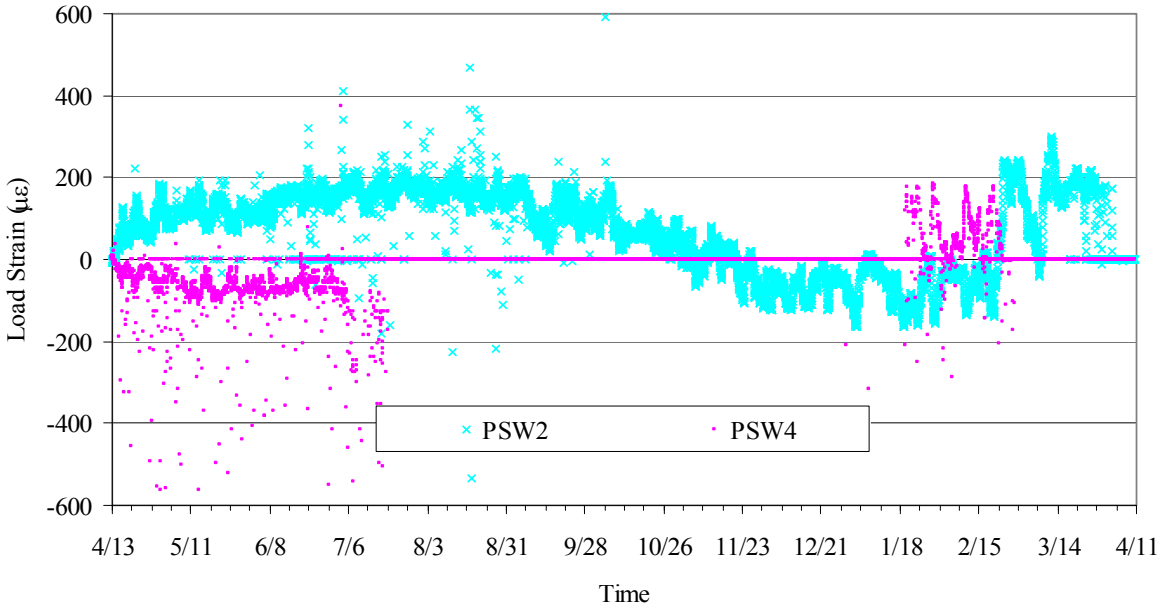


Figure 5.46. Southbound bridge west pile strains obtained at tip of flanges

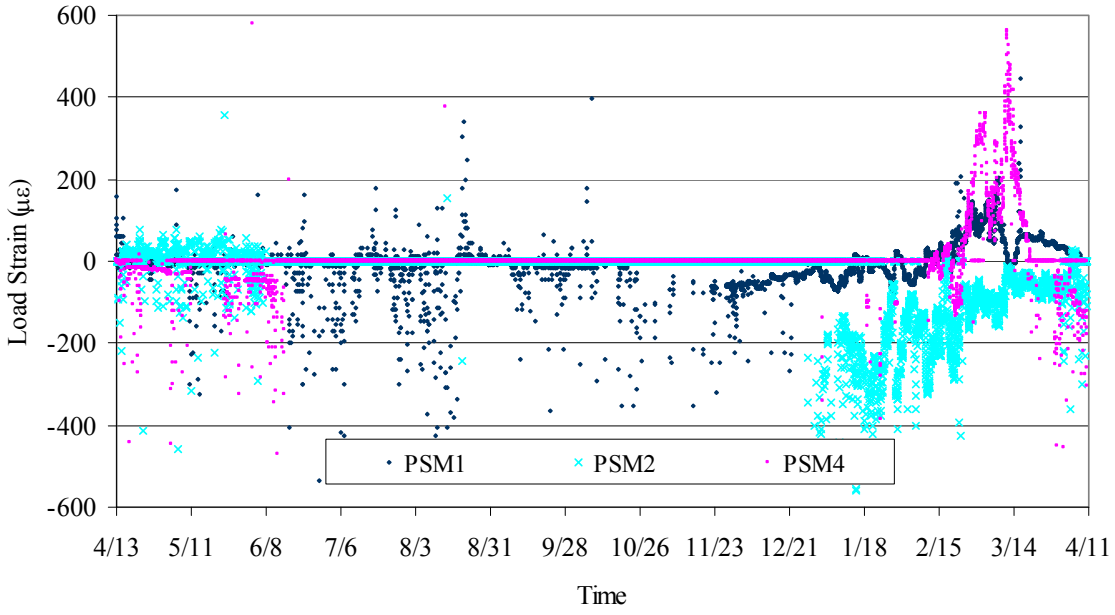


Figure 5.47. Southbound bridge middle pile strains obtained at flange tips

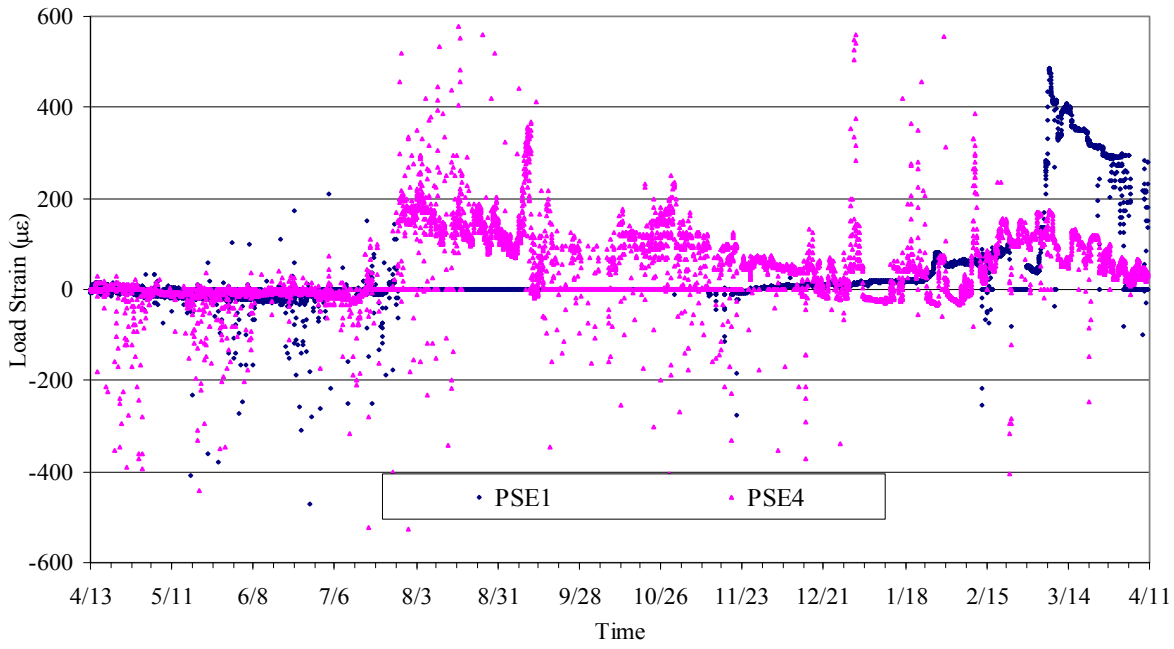


Figure 5.48. Southbound bridge east pile strains obtained at flange tips

The 6 gauges with partial and or scattered readings were not used for further comparison due to a lack of confidence in the data. The one usable gauge was located at PSW2 shown in Figure 5.46. Since only one gauge was fully operationally, the axial strain, x-axis bending strain, y-axis bending strain, and corresponding force could not be calculated. The PSW2 strain, however, was compared to the strain from the corresponding pile gauge located on the northbound bridge, plotted in Figure 5.49. The north and southbound strain responses at the W2 location had very similar responses.

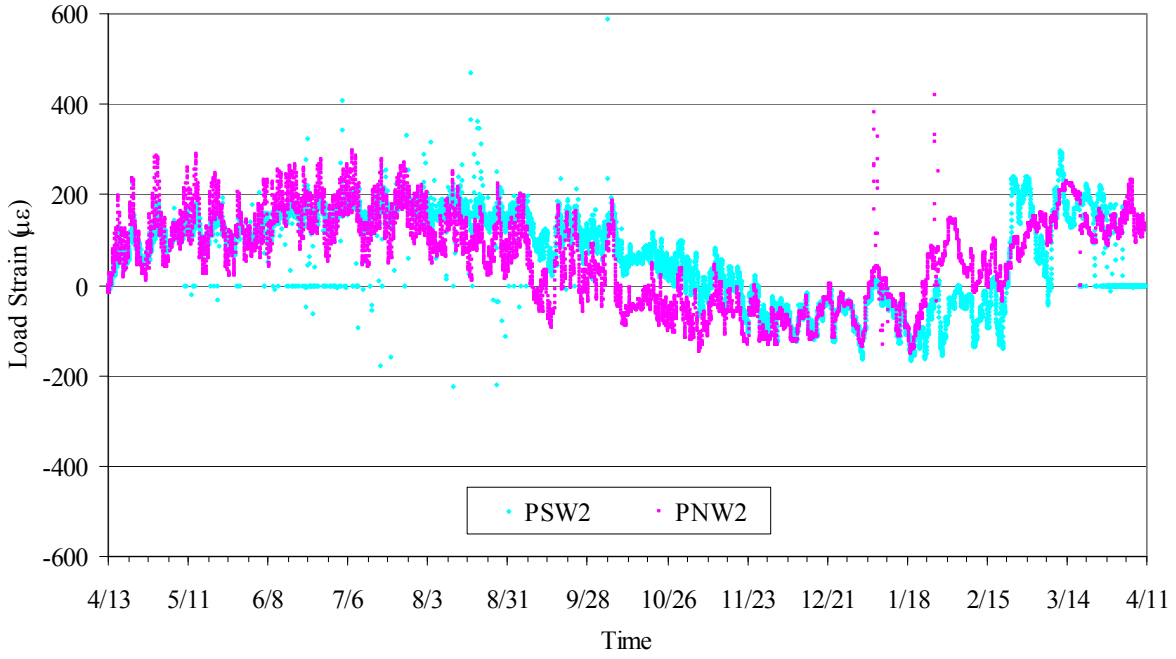


Figure 5.49. Southbound and northbound strain at W2 location

The six gauges that had recorded data but were determined to be unusable were also compared with the corresponding working gauge on the northbound bridge. The southbound gauges show little to no similar responses to the northbound bridge, therefore validating the assumption that the gauges should not be used.

The PSW2 load strain was also compared with the average temperature of the southbound girders, as shown in Figure 5.50. The correlation between the temperature and strain was nearly linear with a positive slope as shown by the bold line in Figure 5.50. From February to the end of the testing period, however, the strain did not follow the linear pattern seen for the previous months.

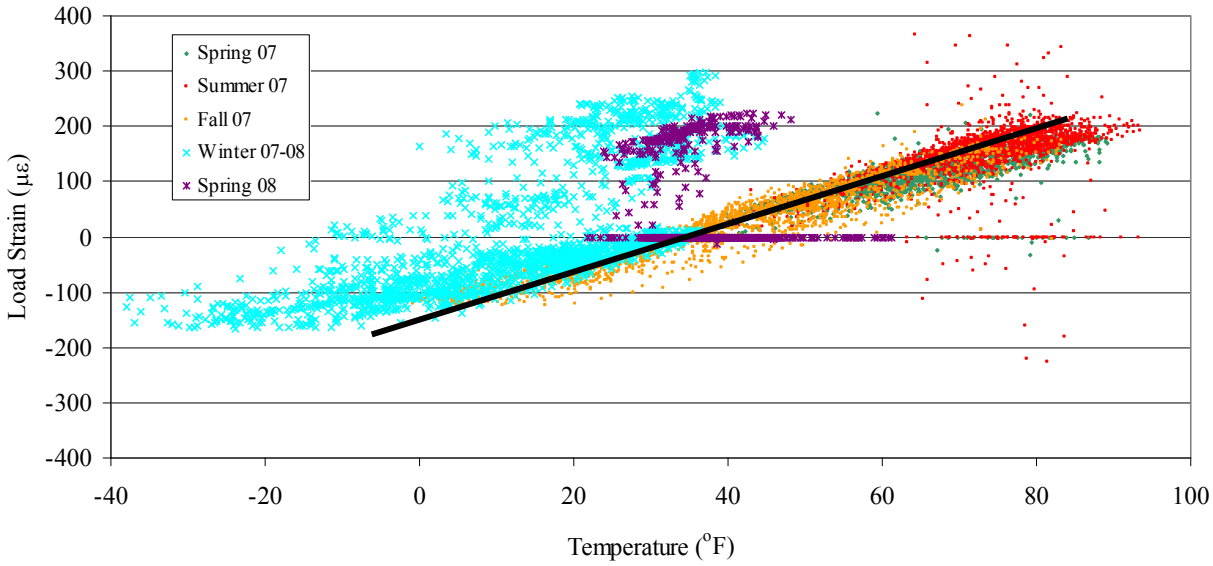


Figure 5.50. PSW2 load strain compared to average bridge temperature

5.5. Visual Inspection

During visits to the project site in the Spring of 2008, visual inspections were performed of the bridge and approach slabs. During the visit May 13th, 2008 several cracks were noticed in the cast-in-place approach slabs. Many tight, 2 to 3 in. long transverse cracks were visible at the north end approach slab along either shoulder of the non-reinforced section (refer to Figure 3.11). A 42 in. long transverse crack was found that started on the east shoulder approximately 28 in. from the north construction joint in the north end singly reinforced approach slab section.

In the doubly reinforced section of the south end approach slab along the east shoulder, a 29 in. long transverse crack (see Figure 5.51) was found 15 ft from the approach slab to bridge joint. Also, a void was found under the approach slab at the south end of the bridge on the west edge where the approach slab and concrete barrier rail meet. The hole was 6 in. wide, 13 in. long, 22 in. deep and extended 20 in. under the slab (see Figure 5.52).



Figure 5.51. Transverse cracking of the doubly reinforced approach slab at the south end starting at the east shoulder



Figure 5.52. Void under the west edge of the approach slab at the bridge abutment

6. COMPARISONS, CONCLUSIONS, AND RECOMMENDATIONS

6.1. Temperatures

For the northbound bridge the measured approach slab temperatures ranged from -6 °F to 96 °F and the measured exterior girder temperatures (bridge temperatures) ranged from -41 °F to 93 °F. The bridge temperatures correlated very well to the ambient air temperature as reported in nearby Sheldon, IA (Figure 4.7 and Figure 4.8). For the southbound bridge the measured temperatures ranged from 28 °F to 93 °F and 5 °F to 100 °F for the approach slab and bridge, respectively. The measured southbound bridge temperatures did not compare well to the northbound temperatures nor the ambient air temperatures. As a result, the measured southbound temperatures were disregarded (refer to Section 5.1).

6.2. Bridge Superstructure

6.2.1. Abutment Displacements

Table 6.1 summarizes the abutment displacement results for both bridges. The west end displacements compare well, having the same minimum values, similar maximum values, and a very similar range. The east end displacements do not compare as well. The minimum displacement values are similar, but the maximum displacement is not. Note that the northbound bridge east end displacement (Figure 4.14) was somewhat discontinuous around the end of December, while the southbound bridge east end displacement (Figure 5.13) shows more continuity. The cause of the discontinuous behavior in the northbound trend is unknown. The maximum east end displacement for the southbound bridge occurs in February, which is after the observed discontinuity in the northbound bridge data.

The longitudinal displacement trends over time for both bridges did not follow the theoretical displacement trend for the entire year (Figure 4.17 and Figure 5.15). Specifically, over a 13 week period in the winter the measured displacement showed abutment displacement to the south while the theoretical model predicted displacement to the north. This displacement is different than results found by Abendroth and Greimann (2005) where the displacements followed the temperature. What can be seen though is that all four longitudinal measurements follow the same trend over time (Figure 6.1). The consistency of all four gauges suggests that the behavior is real and is related to other components of the bridge other than girder expansion alone. The simple analytical model in Appendix A helps to explain some of the friction ratcheting that seems to be present. Some other possible explanations for the displacement behavior are that the soil properties at the north end may be different and the abutment movements are not symmetric, e.g., the north end could be shifting south.

The transverse displacement range of the northbound bridge was found to be almost twice that of the southbound bridge (0.95 in. compared to 0.55 in.). Interestingly, the transverse displacement behavior over time of the northbound bridge abutment was not the same as the southbound bridge abutment (Figure 4.19 and Figure 5.17, respectively). Specifically, the northbound abutment displaced to the East as the temperature decreased (July to January) while the

southbound abutment displacement was relatively constant from July to October before displacement to the West (positive displacement) occurred. The difference in transverse displacement could be attributed to the fact that northbound displacement was measured at the west end of the abutment while the southbound displacement was measured at the east end of the abutment. A skewed bridge and abutment will undergo rotation in the horizontal plane as discussed in Section 4.2.1 and illustrated in Figure 4.20.

Table 6.1. Displacement results

Action	Northbound	Southbound
Abutment Longitudinal Displacement		
West End Max	0.40 in	0.30 in
West End Min	-0.50 in	-0.50 in
West End Range	0.90 in	0.80 in
East End Max	0.10 in	0.70 in
East End Min	-0.80 in	-0.65 in
East End Range	0.90 in	1.35 in
Average Range	0.80 in	1.05 in
Abutment Transverse Displacement		
Transverse Max	0.25 in	0.05 in
Transverse Min	-0.70 in	-0.50 in
Transverse Range	0.95 in	0.55 in

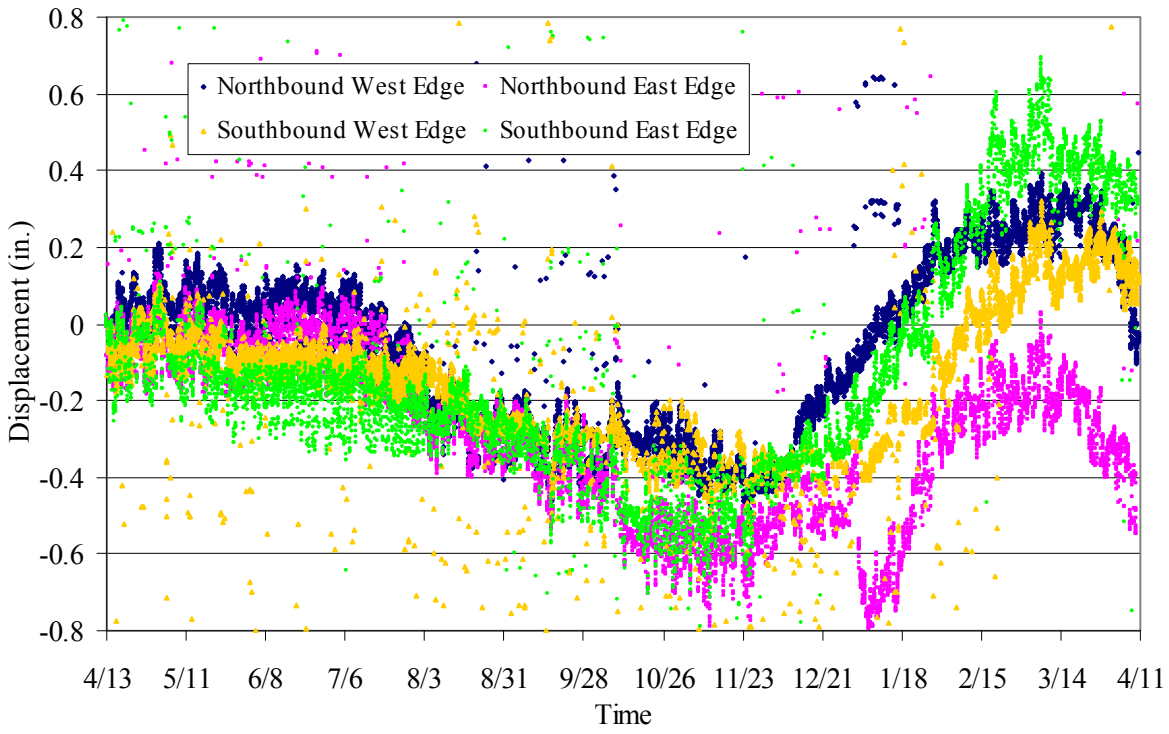


Figure 6.1. Longitudinal abutment displacements (south end) for both bridges

6.2.2. Girder Forces

The average mid-span girder temperature induced moments are listed in

Table 6.2 for each bridge. The moment ranges compare well for the two bridges - 650 kip*ft and 600 kip*ft - for northbound and southbound, respectively. While the ranges are comparable, the specific average minimums and maximums do not. As

Table 6.2 shows, the largest moments for each bridge are opposite in sign. Specifically, the northbound bridge largest moment is a negative moment of 500 kip*ft and the southbound bridge largest moment is a positive 550 kip*ft. By looking at the mid-span moments over time (Figure 4.28 and Figure 5.25) it can be seen that the temporal trends are opposite too. The northbound bridge greatest mid-span moment of -500 kip*ft occurs in July, the same time that the southbound bridge greatest moment of 550 kip*ft occurs. One common trait the two bridges share in regards to moment is that both moment diagrams (Figure 4.31 and Figure 5.28) do not have the expected uniform linear relationship. The varying moment over the length of the bridge may be caused by skew effects. Based on the data obtained from the girders it is inconclusive as to why the moments are opposite signs in the two bridges. A more complete understanding of the forces acting on the free body diagram in Figure 4.27 may help to explain this.

Table 6.2. Girder force results

Action	Northbound	Southbound
Girder Midspan Moment		
Average Min	-500 kip*ft	-50 kip*ft
Average Max	150 kip*ft	550 kip*ft
Range	650 kip*ft	600 kip*ft
Average Girder Axial Load		
Max	100 kips	50 kips
Min	-600 kips	-600 kips
Range	700 kips	650 kips

The average temperature induced axial loads for both bridges compare well (see Table 6.2). Both bridges have a minimum axial load change of -600 kips and the ranges only differ by 50 kips.

An observation of both bridges, however, is that the axial loads are not constant along the girder length, which may be caused by skew effects. On a hot day, both bridges undergo an increase in axial force (tensile force) from the abutment to mid-span of 450 kips (northbound bridge) and 350 kips (southbound bridge) (see Figure 4.32 and Figure 5.29). On the cold day the northbound bridge axial load decreases from the abutment to mid-span by 200 kips, but the southbound bridge axial load remains relatively constant (see Figure 4.32 and Figure 5.29).

6.3. Approach Slab

Results from monitoring the approach slabs are shown in Table 6.3. The load strains in the northbound and southbound approach slabs compare well, having the same average maximum strain value. The load strain ranges are also similar, 120 με and 105 με respectively. With applicable assumptions the strains were converted to force and stress in the pavement (Sections 4.3.1 and 5.3.1) and are listed in Table 6.3. Between the northbound and southbound bridge, the stress ranges in the slabs compare well, 580 psi and 520 psi, respectively. Frictional forces could only be determined for the northbound approach slab (Section 4.3.1) because the southbound slab did not have strain gauges at multiple points along the length of the approach slab. The range of friction force was found to be from -4.0 to 4.0 kip/ft. Using the average approach slab length, the average friction force was found to be 615 kips which is 27% of the total force range in the slab (2300 kips). The friction force was not expected to be large due to the placement of 2 sheets of polyethylene between the slab and the base course (clean ¾ in. gravel). The slab force showed annual and short term cycling behavior. The short term cyclic behavior appears to be caused by friction ratcheting. From the above information one can conclude that 73% of the force in the slab comes from a source other than friction, possibly the expansion joint. If the expansion joint is not perfectly aligned, the dowels bars could create resistance to movement of the slab and an associated build up of force.

Relative movement of the approach slab joints was found to only occur at the expansion joint between the approach slab and the mainline pavement. As summarized in Table 6.3, the relative movement between the approach slab and bridge joint was less than 0.03 in. for both bridges. The relative movement between panels of the northbound bridge was also very small. At the expansion joint the ranges of relative movement was 0.9 in. and 1.1 in. for the northbound and southbound bridges, respectively. The expansion joint movement also displayed annual and short term cyclic behavior. The range of relative expansion joint movement for the two bridges compare very well with the abutment movement average range, being approximately 0.1 in. greater than the movements shown in Table 6.1. Because the range of movement at the expansion joint is only slightly greater than that of the abutment, the free expansion and contraction of the approach slab due to changing temperature must be partially restrained, this would account for some of the force in the approach slab.

The post-tensioned longitudinal strands in the northbound approach slab had a force range of 2.1 kips (Figure 4.49) and a loss of 1.1 kips which is equal to about 2.5% of the total initial post-tensioning force. The southbound bridge did not have any post-tensioning.

Table 6.3. Approach slab results

Action	Northbound	Southbound
Slab Load Strain		
Average Min	-95 με	-80 με
Average Max	25 με	25 με
Range	120 με	105 με
Slab Forces		
Min Force	-1860 kips	- 1400 kips
Max Force	480 kips	500 kips
Range of Force/Stress	2300 kips / 580 psi	1900 kips / 520 psi
Friction Range	-4 to 4 kips/ft	Information Not Available
Joint Movement		
Abutment Joint	< 0.03 in	< 0.03 in
Expansion Joint		
- Max Closure	0.6 in	0.45 in
- Max Open	0.3 in	0.65 in
- Range	0.9 in	1.1 in
Post-Tensioning		
Force Range	2.1 kips	Information Not Available
Loses	1.1 kips	Information Not Available

6.4. Bridge Substructure

The northbound bridge most west monitored pile experienced x-axis bending moment, y-axis bending moment, and axial force ranges of approximately 455 kip*in., 142 kip*in., and 90 kips, respectively (Figure 4.62). Interestingly, the middle pile had a different bending response during the testing period (Figure 4.63) with a range of x-axis bending moment, y-axis bending moment, and axial force of 215 kip*in., 300 kip*in., and 90 kips, respectively. Due to instrumentation failure, only piles on the northbound bridge were able to be studied, thus no comparisons can be made.

6.5. Visual Inspection

During the monitoring period cracks were observed in the approach slabs of both the northbound and the southbound bridge. The general crack locations are illustrated in Figure 6.2. Interestingly, cracking was only observed in the south end approaches of either bridge (e.g., the

end where instrumentation was concentrated). The crack in the northbound approach slab occurred 33 ft – 10 in. from the slab-to-bridge joint as measured along the east shoulder. This crack was half the width of the approach slab extending from the east shoulder to the center longitudinal joint. In the southbound approach slab, a small crack, 29 in. long, was observed 15 ft from the bridge-to-slab joint as measured along the east shoulder. Cracking in both approach slabs at the south end of the bridges suggest that at some point both slabs experienced tensile stresses.

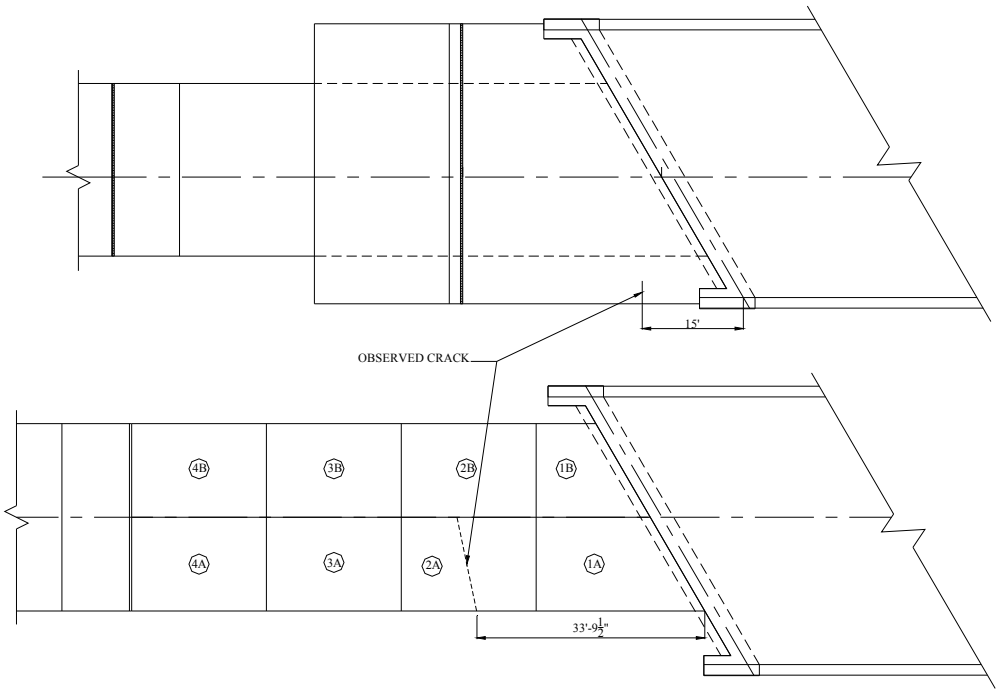


Figure 6.2. Illustration of approach slab crack positions

6.6. General Conclusions

In an effort to reduce the bump experience at the end of bridges, the Iowa DOT is interested in integrally connecting the approach slabs to the bridges. Instrumentation followed by a year long monitoring of two integral abutment bridges, one with cast-in-place approach slabs and one with precast approach slabs, yield the results discussed in this report. From those results the following conclusions have been made:

- The integral connection between the approach slabs and the bridges appear to function well with no observed distress at this location and no relative longitudinal movement measured between the two components.
- Tying the approach slab to the bridge appears to impact the bridge abutment displacements and girder forces. The source of the impact may be the manner in which the approach slab is attached to the main line pavement.
- The two different approach slabs, the longer precast slab and the shorter cast-in-

place slab, appear to impact the bridge differently. This impact was clear in the differences in the mid-span moments and the slab strain patterns over time. It is not clear, however, whether it was the type of approach slab or the size of the approach slab that has the greatest impact.

- The measured strains in the approach slabs indicate a force exists at the expansion joint and should be taken into consideration when designing both the approach slab and the bridge.
- The observed responses generally followed an annual cyclic and/or short term cyclic pattern over time. The annual cyclic pattern had summer responses at one extreme, a transition through the fall to the other extreme response in the winter, followed by a transition in the spring back to the summer responses. A linear relationship of the transitions between the extreme responses was typically observed. Seasonal and short term cycles were evident in most data, probably caused by friction ratcheting.

6.7. Recommendations for Further Study

As a first recommendation, from the data reported herein, the authors recommend that additional bridges be constructed using the approach slabs and connections studied herein and that these new bridges be similarly monitored. At some point, it may be appropriate to consider retro-fitting older bridges.

Further bridge monitoring programs would contribute to better understanding of integral abutment bridges with integral approach slabs and different skew angles, span lengths, slab lengths, horizontal alignments, and girder type (concrete or steel), especially since not all the experimentally measured results compared with previous studies (Abendroth and Greimann (2005)), which reported no friction ratcheting. Future monitoring programs should utilize instrumentation to eliminate the observed uncertainties which have been described herein. This could include measuring displacements at both ends of the bridge, measuring the actual concrete temperature and gradient of members like the girders, measuring the soil pressure on the abutment, and installing the displacement transducer reference posts in a way to increase confidence that the posts do not move. A method to determine the coefficient of thermal expansion for the particular concrete on the project should also be employed since it was found that the coefficient of thermal expansion affects interpolation of results from concrete elements.

In addition, future studies should also monitor if the “bump” is still created at the bridge-to-approach slab connection location, if the bump is moved to the expansion joint location, or if the bump is eliminated altogether. The expansion joint should also be studied in more detail to determine the joint behavior and if modifications to the expansion joint design would change the slab and bridge response.

7. REFERENCES

AASHTO. 2006. LRFD Bridge Design Specifications. Washington, D.C: American Association of State Highway and Transportation Officials.

Abendroth, R. E. and Greimann, L. F. 2005. *Field Testing of Integral Abutments*. Iowa Department of Transportation Project HR-399. Ames, Iowa.

Arsoy, S., Barker, R.M. and Duncan, J.M. 1999. *The behavior of Integral Abutment Bridges (Final Report)*. Virginia Transportation Research Council. Report No. FHWA/VTRC00-CR3.

Brena, S. F., Bonczar, C. H., Civjan, S. A., DeJong, J. T., Crovo, D. S. 2007. Evaluation of Seasonal and Yearly Behavior of an Integral Abutment Bridge. *Journal of Bridge Engineering* Vol. 12. No. 3: 296-305.

Briaud, J .L., James, R. W., and Hoffman, S. B. 1997. *Settlement of Bridge Approaches (The Bump at the End of the Bridge)*. NCHRP Synthesis 234. Washington, D.C: Transportation Research Board, National Research Council.

Burke, M. P. 1993. *Integral Bridges: Attributes and Limitations.* Transportation Research Record, 1393, 1-8.

Cai, C. S., Shi, X. M., Voyiadjis, G. Z., Zhang, Z. J. 2005. Structural Performance of Bridge Approach Slabs Under Given Embankment Settlement. *Journal of Bridge Engineering* Vol. 10. No. 4: 482-489.

Das, M. Braja. 1998. Principals of Geotechnical Engineering Fourth Edition. Boston, MA: PWS Publishing Company.

Girton, D. D., Hawkinson, T. R., Greimann, L. F. 1989. Validation of Design Recommendations for Integral Abutment Piles. Final Report, Iowa DOT Project HR-292, Highway Division, Iowa Department of Transportation, Ames, Iowa.

Greimann, L. F., Abendroth, R.E., Johnson, D.E., Ebner, P.B. 1987. Pile Design and Tests for Integral Abutment Bridges, Iowa State University.

Hassiotis, S., Lopez, J., Bermudez, R. 2005. Full-Scale Testing of an Intergral Abutment Bridge. Paper presented a the FHWA Conference on Integral Abutment and Jointless Bridges, Baltimore, Maryland.

Kunin, J., Alampalli, S. 2000. Integral Abutment Bridges: Current Practice in United States and Canada. *Journal of Performance of Constructed Facilities* Vol. 14. No. 3: 104-111.

Lawver, A., French, C., Shield, C. K. 2000. *Field Performance of Integral Abutment Bridge.* Transportation Research Record, 1740*,* 108-117.

Merrit, D. K., Miron, A.J., Rogers, R. B., Rasmussen, R. O. 2007. Construction of the Iowa Highway 60 Precast Prestressed Concrete Pavement Bridge Approach Slab Demonstration Project. Washington, DC: Federal Highway Administration. Ames, Ia. Iowa Highway Research Board.

Mistry, Vasant C. 2005. Integral Abutment and Jointless Bridges. Paper presented at FHWA Conference: Integral Abutment and Jointless Bridges (IAJB 2005). FHWA. West Virginia University March 16-18, 2005.

Oesterle, R. G., Tabatabai, H., Lawson, T. J., Refai, T. M., Volz, J. S., and Scanlon, A. 1999. *Jointless and Integral Abutment Bridges* Draft Summary Report. Construction Technology Laboratories. Skokie, Illinois

Schaefer, V. R., Koch, J. C. 1992. *Void Development Under Bridge Approaches*. Report No. SD90-03. South Dakota Department of Transportation.

White, D. J., Mekkawy, M. M., Sritharan, S., Sulieman, M. T. 2007. Underlying Causes for Settlement of Bridge Approach Pavement Systems. *Journal of Performances of Constructed Facilities* Vol. 21. No. 4: 273-282.

White, D., Sritharan, S., Suleimann, M., Mohammed, M., and Chetlur, S. 2005 *Identification of the Best Practices for Design, Construction, and Repair of Bridge Approaches.* CTRE Project 02-118, Iowa DOT Project TR-481, Iowa State University

Zhang, H. L., Hu, Change-Shun. 2007. Determination of Allowable Differential Settlement in Bridge Approach due to Vehicle Vibrations. *Journal of Bridge Engineering* Vol. 12. No. 2: 154-163.

APPENDIX A

FRICTIONAL RATCHETING: A SIMPLE MODEL

A.1. A Simple Model

Some insight into the experimentally observed behavior of the bridge/approach slab system can be gained by analyzing a fairly simple analytical model. Consider the bridge and approach pavement illustrated in Figure A.1. A very simple analytical model of the bridge consists of the two axial force elements shown in Figure A.2 (a) and (b). Element 1 represents the approach slab with displacements D_1 and D_2 on the left and right ends, respectively. It is acted upon by a spring on the left which represents the resistance of the pavement at the expansion joint, an axial force, P, on the right, and a friction force, F, acting, at the expansion joint. Element 2 displaces an amount D_2 on its left and is fixed at the right end. It also has an axial force, P.

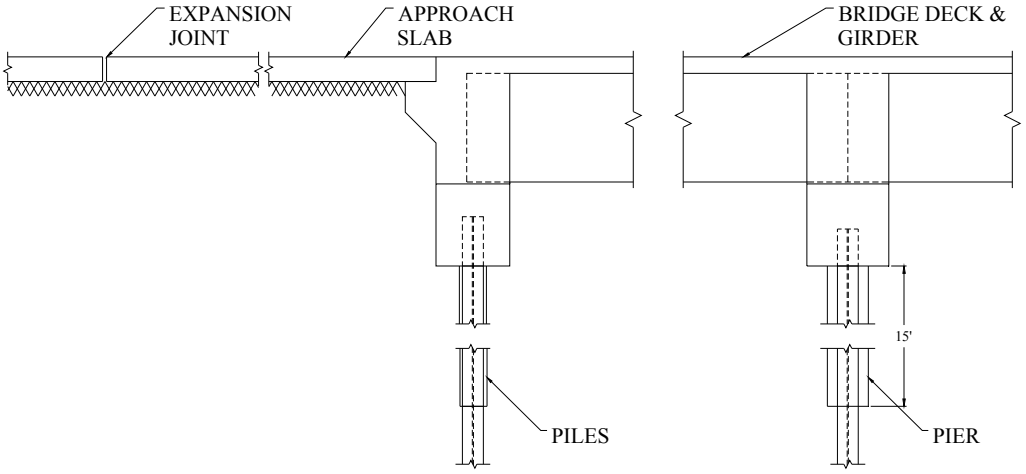
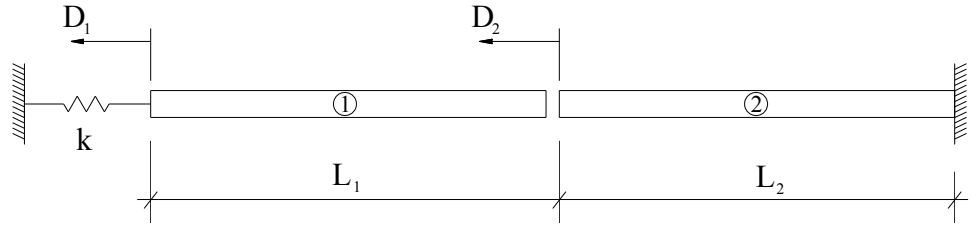
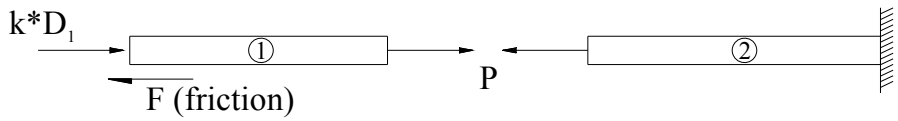


Figure A.1. Elevation view of northbound bridge



(a) Displacements



(b) Forces

Figure A.2. Simple analytical model

Several assumptions are inherent in this simple model. Each element is assumed to carry only axial force. Element 2 is assumed fixed at the bridge centerline, i.e., the bridge centerline is assumed to be a line of symmetry. The stiffness of the piles and piers is neglected. As discussed in Section 6.3 most of the slab force is the result of resisting forces at the expansion joint. Soil resistance behind the abutment is neglected.

The equations governing the behavior of the two elements and the expansion joint spring are

$$D_1 - D_2 = \frac{P}{K_1} + \alpha * \Delta T * L_1 \qquad \text{(A.1)}$$

$$D_2 = \frac{P}{K_2} + \alpha * \Delta T * L_2 \qquad \text{(A.2)}$$

in which

α = coefficient of linear thermal expansion
ΔT = temperature increase
K_i = stiffness of element i
= A_iE_i/L_i for an axial force member

and, by equilibrium

$$P = F - k * D_1 \qquad \text{(A.3)}$$

in which

k = stiffness of the expansion joint spring

and F, P, D_1, D_2, L_1, and L_2 are illustrated in Figure A.2. In this simple model, α and ΔT are assumed to be the same for both elements.

The friction force, F, is limited to F_s, the static friction value, if the slab is not sliding, i.e.,

$$-F_s \le F \le F_s \qquad \text{if } dD_1/dt = 0 \qquad \text{(A.4)}$$

in which dD_1/dt is the velocity at the left end of Element 1. Once the approach slab begins to move, the friction force reduces to the kinetic value and acts in the direction opposite to the direction of motion, i.e., opposite to dD_1/dt, or

$$F = -F_k * \delta \text{ if } dD_1/dt \text{ is not } = 0 \qquad \text{(A.5)}$$

in which

$$\delta = sign\left(\frac{dD_1}{dt}\right) \text{ or}$$

$$= \begin{cases} -1 & \text{if moving right} \\ 0 & \text{if stopped} \\ 1 & \text{if moving left} \end{cases} \tag{A.6}$$

Combining Equation A.1, A.2, and A.3 and solving for D_1 and D_2 yields

$$D_1 = \frac{P}{K} + \alpha * \Delta T * L \tag{A.7}$$

$$D_2 = \frac{P}{K_2} + \alpha * \Delta T * L_2 \tag{A.8}$$

in which

$$\frac{1}{K} = \frac{1}{K_1} + \frac{1}{K_2}$$

$$L = L_1 + L_2$$

If δ is equal to zero (not sliding), D_1 remains constant and from Equation A.7

$$P = K\left(D_1 - \alpha * \Delta T * L\right) \tag{A.9}$$

$$F = P + k * D_1 \tag{A.10}$$

If δ is not equal to zero (sliding), F remains constant at F_k

$$F = -F_k * \delta \tag{A.11}$$

and, from Equation A.3 and A.7

$$D_1 = \frac{\left(\frac{F}{K} + \alpha * \Delta T * L\right)}{\left(1 + \frac{k}{K}\right)} \tag{A.12}$$

$$P = F - k * D_1 \tag{A.13}$$

The above equations were programmed using Visual Basic in Microsoft Excel.

A.2. Some Numerical Results with Bridge Parameters

To begin, the approximate parameters for the approach slab/bridge in the project were input into the software. Figures 3.2 and 4.25 summarize some of these properties.

$$\left.\begin{aligned} K_1 &= \frac{A_1 * E_1}{L_1} = \frac{(1)(28)(144)(4700)}{923} = 20500 kip/in. \\ K_2 &= \frac{A_2 * E_2}{L_2} = \frac{(7)(1230)(4700)}{1818} = 22300 kip/in. \\ L_1 &= 923 in. \\ L_2 &= \frac{3636}{2} = 1818 in. \\ \alpha &= \frac{5(10^{-6})}{^\circ F} \\ F_s &= 750 kip \\ F_k &= 700 kip \\ k &= 2000 kip/in. \end{aligned}\right\} \tag{A.14}$$

The frictional forces F_s and F_k were taken to be approximately equal to about one-half the annual range of the slab forces presented in Figure 4.55. The expansion joint spring stiffness, k, was selected to match the data in Figure 4.55.

The temperature input into the software was a simplified version of the experimental data for the average bridge temperature in Figure 4.6 during a year starting on April 13 and is illustrated graphically in Figure A.3. Schematically, it consists of an annual spring/summer/autumn/winter/spring cycle with six simulated short term cycles superimposed on the annual cycle, as illustrated.

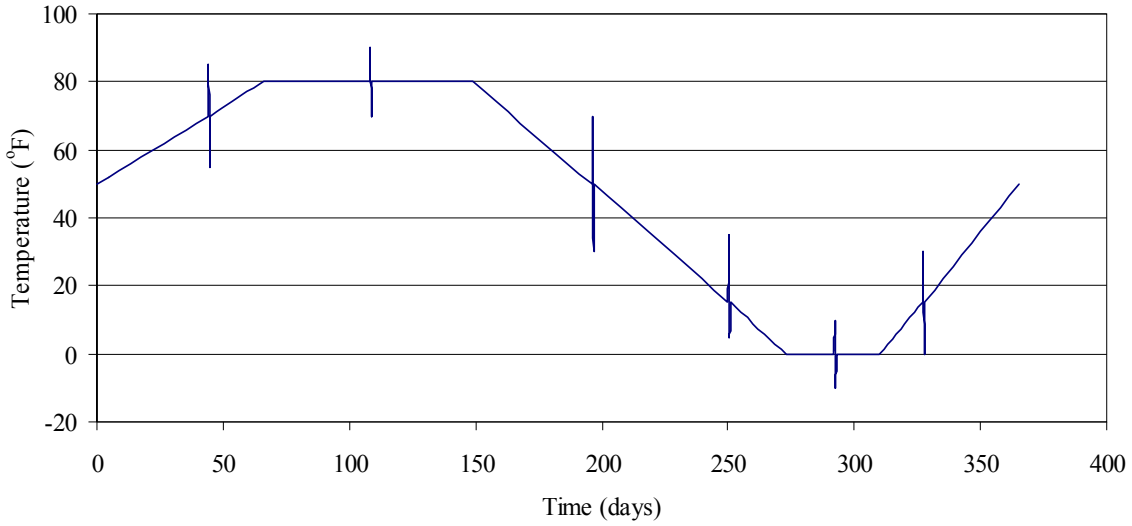


Figure A.3. Simulated annual temperature variation for sample model

The analytical results are illustrated in Figure A.4, A.5, and A.6 with D_1, D_2, and F plotted versus time. All three figures illustrate that, at certain times during the year, the static friction resistance, F_s, is overcome and the slab slides with a resisting friction force equal to the kinetic value, F_k.

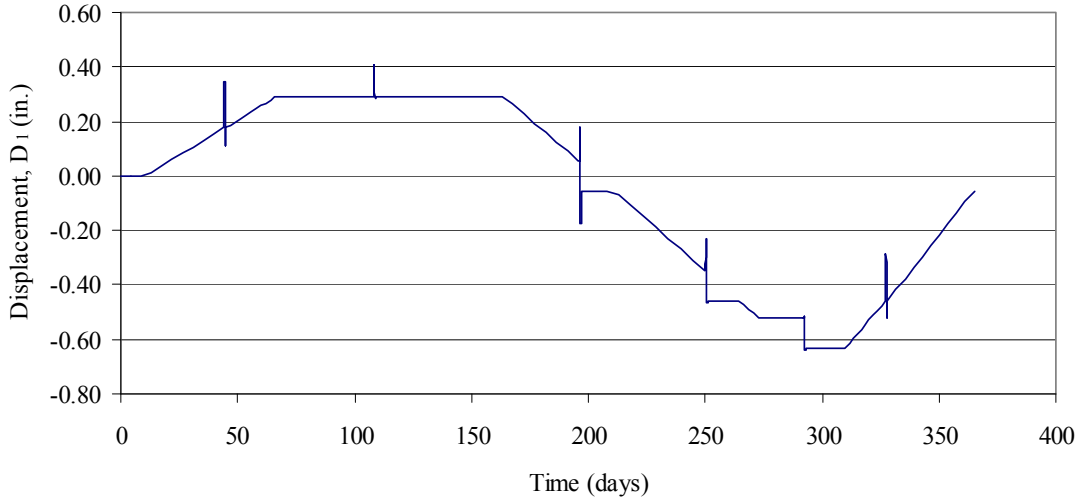


Figure A.4. Annual Movement at expansion joint from simple model

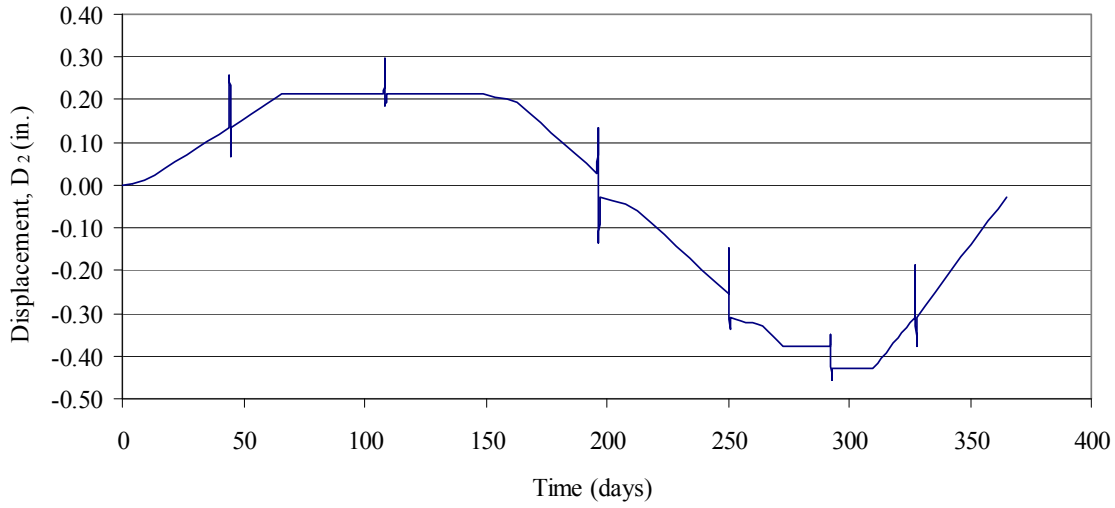


Figure A.5. Annual movement at abutment from simple model

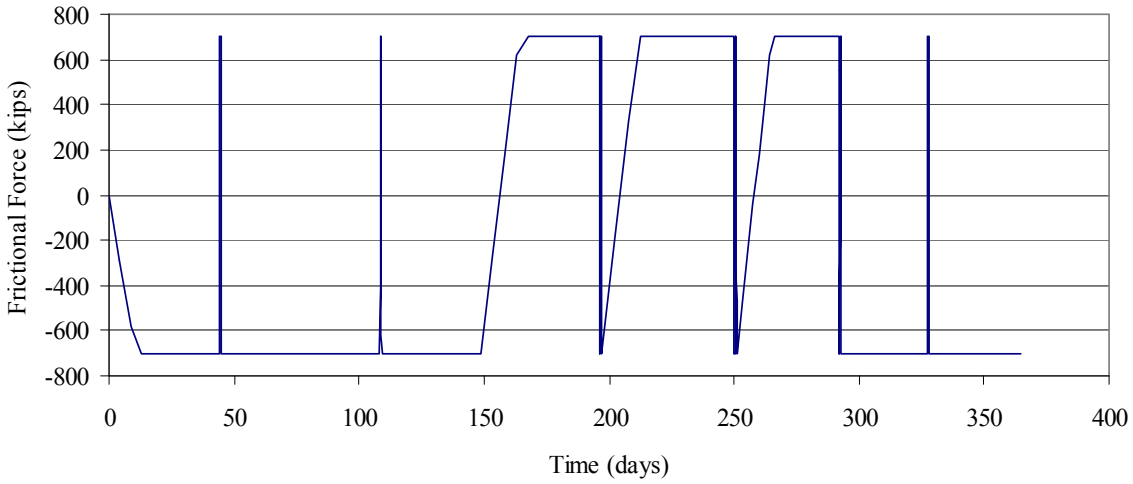


Figure A.6. Annual frictional force from simple model

Figure A.7 is a plot of the displacement D_2 (red) versus the temperature that can be compared to the experimental results in Figure 4.18. (The straight lines in Figure 4.18 are repeated in Figure A.7.) In both figures, a similarity in the annual cycle and the short term cycles can be observed, particularly during the autumn. Within the longer annual cycle there is a series of loops when the slab is either not sliding, sliding left, or sliding right.

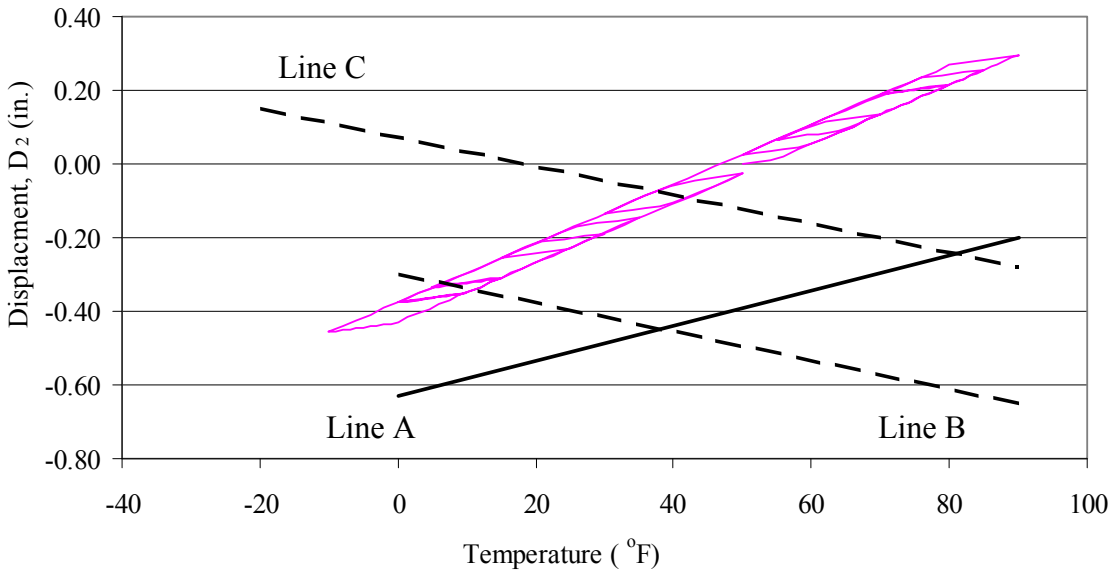


Figure A.7. Abutment Displacement versus temperature from simple model

A typical loop from Figure A.7 is illustrated in Figure A.8. To help study this loop, the governing equations of the previous section can be written in rate form as

$$\frac{\Delta D_1}{\Delta T} = \frac{1}{K} * \frac{\Delta P}{\Delta T} + \alpha * L \qquad \text{(A.15)}$$

$$\frac{\Delta D_2}{\Delta T} = \frac{1}{K_2} * \frac{\Delta P}{\Delta T} + \alpha * L_2 \qquad \text{(A.16)}$$

$$\frac{\Delta F}{\Delta T} = \frac{\Delta P}{\Delta T} + k * \frac{\Delta D_1}{\Delta T} \qquad \text{(A.17)}$$

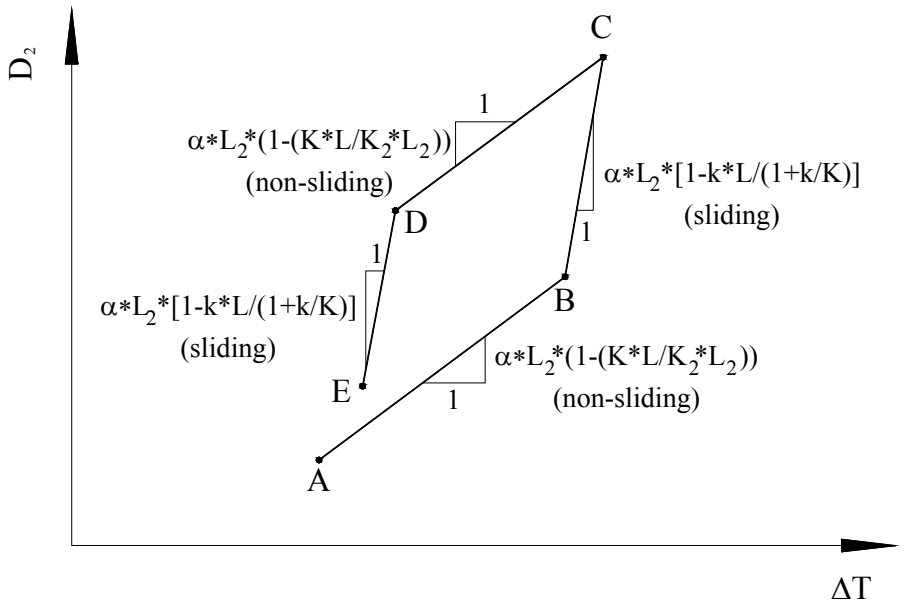


Figure A.8. Typical temperature loop

If the slab is not sliding, $\Delta D_1/\Delta T$ is zero and Equation A.12, A.13, and A.14 can be solved for the force rate per temperature change as

$$\frac{\Delta P}{\Delta T} = -\alpha * K * L \qquad \text{(A.18)}$$

so that Equation A.16 becomes

$$\frac{\Delta D_2}{\Delta T} = \alpha * L_2 \left(1 - \frac{K * L}{K_2 * L_2}\right) \qquad \text{(A. 19)}$$

which is the slope of the non-sliding portions of the loop in Figure A.8. If the slab is sliding, $\Delta D_1/\Delta T$ is non-zero and

$$\frac{\Delta F}{\Delta T} = 0 \qquad \text{(A. 20)}$$

so that, by Equation A. 15, A.16, and A.17

$$\frac{\Delta D_2}{\Delta T} = \alpha * L_2 * \left[\frac{1 - k * L}{\left(1 + \frac{k}{K}\right)} \right] \qquad \text{(A.21)}$$

The typical loop in Figure A.8 represents a typical temperature cycle with the temperature increasing from A to C and decreasing from C to E. Along the path AB, the slab is not sliding and D_2 increases at a rate give by Equation. A.19. At Point B, the slab starts to slide as the friction force overcomes the frictional resistance, F_s, and Equation. A.21 gives the rate of change of D_2.

As the temperature decreases, D2 moves in the negative direction, again, not sliding for the segment CD until the friction resistance is overcome and sliding begins at Point D ending this temperature cycle at E. The rate of change of D_2 is again given by Equation A.19 from C to D and Equation A.21 from D to E.

The first few lines of Table A.1 summarize some of the information discussed above. The Table also presents some other observations. For example, along the path AB the temperature increases, the slab is not sliding, and the bridge and slab are in compression. As the slab starts to slide, i.e., B to C, both elements remain in compression.

Note that, if

$$1 - \frac{K * L}{K_2 * L_2} < 0 \qquad \text{(A.22)}$$

i.e., the slab is quite stiff relative to the bridge, the slope of the non-sliding portion (AB and CD) would be negative, in which case the slab is dominating the behavior. The data in Figure 4.18 has this characteristic.

Comparison of Fig. 4.18, A.7, and the loops in Fig. A.8 help to explain some of the cyclic looping behavior observed in the experimental data, e.g., the sliding/non-sliding phenomenon with distinctly different slopes of the D_2 (abutment) displacement versus temperatures plots. However, the simple model does not explain all of the observed behavior. For example, the slopes of the loops in Fig 4.18 do not match those in Fig A.7. During the autumn, the sliding portions of the loops are positive in both the experimental data and the analytical model results, though with somewhat different numerical values. However, in the winter/spring, the slope of the sliding portion of the experimental data is essentially flat, but not for the analytical results. Additionally, the slope of the non-sliding portion of the experimental loops is negative for all seasons in Fig. 4.18 but positive in Figure A.7.

Additional results of the analytical model are presented in Figures A.9 (green) and A.10 (blue), which are plots of the slab force versus the movement at the expansion joint and of

the slab force versus temperature, respectively. These figures compare to Figures 4.41 and 4.55, respectively. The black lines in Figures A.9 and A.10 represent the data trend in Figures 4.41 and 4.55, respectively. Again, in spite of its simplicity and major assumptions, the model does reproduce some of the behavioral characteristics observed in the experimental data, e.g., the looping phenomena and the resistance at the expansion joint.

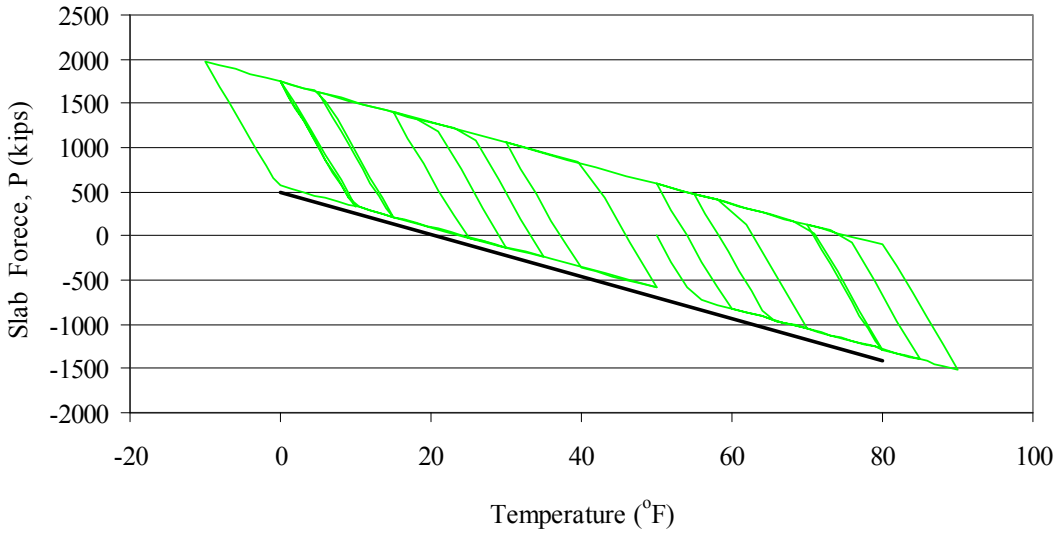


Figure A.9. Slab force versus temperature from simple model

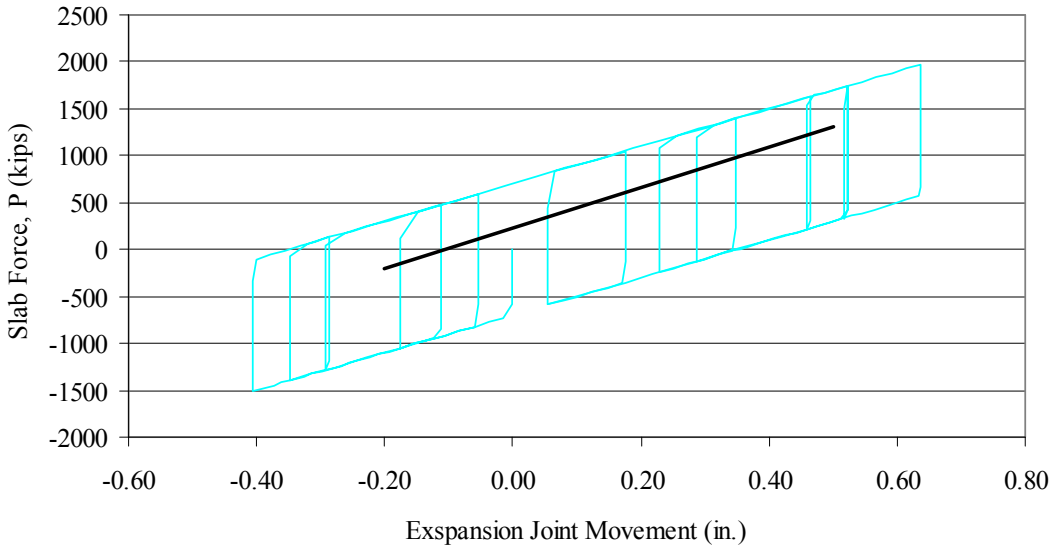


Figure A.10. Slab force versus movement at expansion joint from simple model

Table A.1 Behavior of slab analytical model along various paths

Behavior	Paths			
	AB	**BC**	**CD**	**DE**
Temperature	Increasing Heating	Increasing Heating	Decreasing Cooling	Decreasing Cooling
Slope, $\Delta D_2/\Delta T$	$\alpha*L_2*(1-K*L/K_2*L_2)$	$\alpha*L_2*[1-k*L/(1+k/K)]$	$\alpha*L_2*(1-K*L/K_2*L_2)$	$\alpha*L_2*[1-k*L/(1+k/K)]$
D_2	Increasing	Increasing	Decreasing	Decreasing
D_1	Stopped	Sliding	Stopped	Sliding
δ	0	1	0	-1
F(friction)	$-F_s<F<0$	$-F_k$	$0<F<F_s$	F_k
P (bridge & slab)	Compression	Compression	Tension	Tension